NACA TN No. 1703

8153

TECH LIBRARY KAFB, NM
0144964

NATIONAL ADVISORY COMMITTEE FOR AERONAUTICS

TECHNICAL NOTE

No. 1703

DOWNWASH AND WAKE BEHIND UNTAPERED WINGS OF VARIOUS ASPECT RATIOS AND ANGLES OF SWEEP

By H. Page Hoggard, Jr., and John R. Hagerman

Langley Aeronautical Laboratory
Langley Field, Va.

Washington
October 1948

AFMDC
TECHNICAL LIBRARY
AFL 2811

319.98/41

TECH LIBRARY KAFB, NM

0144964

NATIONAL ADVISORY COMMITTEE FOR AERONAUTICS

TECHNICAL NOTE NO. 1703

DOWNWASH AND WAKE BEHIND UNTAPERED WINGS OF VARIOUS ASPECT RATIOS AND ANGLES OF SWEEP

By H. Page Hoggard, Jr., and John R. Hagerman

SUMMARY

An investigation has been made in the Langley 7- by 10-foot tunnel to determine the downwash angles and the dynamic-pressure ratios behind wings of various sweep angles and aspect ratios, and the aerodynamic force characteristics of the wings. A brief discussion of some of the effects of the more important variables is presented.

The wake center line behind sweptforward wings was found to be located higher than the wake center line behind sweptback wings. A low tail position appears to be most stabilizing for all configurations investigated with the exception of the short tail length behind the unswept wing at an angle of attack of 16°. At low tail positions and low angles of attack the rate of change of downwash angle with angle of attack increases as sweepback decreases. At high tail positions and high angles of attack the reverse tends to be true.

INTRODUCTION

The analysis of reference 1 has shown that the use of sweptback wings for high-speed aircraft can greatly extend the range of flight Mach number attainable before the onset of serious compressibility effects on the wings. The resulting realization by designers of the possibility of attaining supersonic speeds in flight without serious compressibility effects has caused great interest in the use of sweptback wings and a great demand for data on their aerodynamic characteristics throughout the speed range. In response to this demand, the National Advisory Committee for Aeronautics has supplied data on the stability and control characteristics of swept wings at low speeds in reference 2 and another NACA paper of limited distribution. Also a collection and analysis of static longitudinal stability characteristics are given in reference 3.

Data presented in reference 3 indicated that the addition of a horizontal tail behind a sweptback wing may be destabilizing for some values of the rate of change of downwash angle with angle of attack at the tail location. Because the need for data relative to downwash

behind swept wings was urgent, a preliminary investigation was made. These preliminary results are given in reference 4.

The present paper presents the results of an extensive survey of downwash behind swept wings. Data concerning downwash behind sweptforward as well as sweptback wings are included. This paper also presents surveys of dynamic-pressure ratio behind the sweptforward and sweptback wings. The wings used for this investigation vary in sweep from 60° to -60°. The survey encompasses a region extending from the plane of symmetry to beyond the tip in the spanwise direction and extending chordwise seven normal chords behind the quarter-chord line of the wing. The surveys were made in a low-speed tunnel at a speed of approximately 80 miles per hour.

The aerodynamic characteristics of the wings, as determined by force measurements, are also presented.

COEFFICIENTS AND SYMBOLS

C_L	lift coefficient (Lift/qS)
C_D	drag coefficient (Drag/qS)
C_m	pitching-moment coefficient about quarter chord of wing mean aerodynamic chord (Pitching moment/$qS\bar{c}$)
q_o	free-stream dynamic pressure, pounds per square foot $\left(\frac{\rho V^2}{2}\right)$
q	dynamic pressure in region behind wing, pounds per square foot
ρ	mass density of air, slugs per cubic foot
V	air velocity, feet per second
S	wing area, square feet
$\bar{c}$	wing mean aerodynamic chord, feet (same as c for each respective model since models have constant chord)
c	chord of model, feet (chord measured parallel to air stream)
Λ	angle of sweep of leading edge, degrees (positive when wing is sweptback)
A	wing aspect ratio $\left(\frac{b^2}{S}\right)$
b	wing span, feet

h horizontal-tail position with respect to wing chord plane extended, positive upward, semispans

α angle of attack of wing chord line, degrees

ϵ angle of downwash, positive in down direction with respect to relative wind, degrees

$\Delta\epsilon$ jet-boundary correction to downwash

Lift and pitching-moment parameters:

C_{L_α} variation of lift coefficient with angle of attack $\left(\frac{dC_L}{d\alpha}\right)$.

$\frac{dC_m}{dC_L}$ variation of pitching-moment coefficient with lift coefficient

MODELS AND APPARATUS

Models

Details of the models are shown in figure 1. Their principal geometric characteristics are presented in table I. The models were made to the NACA 0015 airfoil contour, perpendicular to the leading edge. The models were made of laminated mahogany bonded and screwed to a heavy steel spar. This spar was necessary to minimize deflection under load. No geometric twist was present in any of the models.

Dynamic-Pressure-Survey Apparatus

All the downwash and dynamic-pressure data presented in this paper were obtained by the use of a multiple-tube rake. (See fig. 2.) The pitch heads of this rake were designed to have the pitch-measuring openings of each head as close together as possible, so that the detrimental effect of a steep pressure gradient on the correct angle reading would be minimized. Details of one of the pitch heads are shown in figure 2(c). Because a large part of the region surveyed was in the tip vortex behind the wing, it was necessary to make the rake sensitive to angles of air flow in the pitch direction but insensitive to air flow in the yaw direction. By using the slats shown in figures 2(a) and 2(b) to form a nozzle with a 2:1 convergence, the rake was made insensitive to yaw flow at small angles of yaw. The maximum angle-of-pitch error caused by air flows yawed 20° is believed to be approximately 1°. Any detrimental effects on total-pressure, static-pressure, and angle-of-downwash readings resulting from the presence of the slats were taken care of by the calibration of the rake under known conditions of total pressure and dynamic pressure.

TESTS AND RESULTS

Test Conditions

The following table summarizes the test conditions for the various models; dynamic pressure is constant at a value of 16.37 and the turbulence factor is constant at a value of 1.6:

Span (in.)	Sweep of leading edge (deg)	Aspect ratio	Chord (M.A.C.) (in.)	Test Reynolds number (a)
60	0	6.0	10.000	0.620×10^6
60	30	5.2	11.547	.720
60	-30	5.2	11.547	.720
60	60	3.0	20.000	1.240
60	-60	3.0	20.000	1.240
30	0	3.0	10.000	.620
52	30	4.5	11.547	.720
52	-30	4.5	11.547	.720
30	60	1.5	20.000	1.240
30	-60	1.5	20.000	1.240

[a]Reynolds number based on mean aerodynamic chord.

The models were mounted so that the strut supported the model 8 inches to the left of the model center line. (See figs. 1 and 3.) This off-center mounting was used to reduce the strut interference in the center-line surveys, and also to allow the weight and air loads of the model to be supported nearer the center of the fore-and-aft dimension of the model and thus reduce deflections of the strut in pitch.

Test Procedure

Force tests.- Force tests of the models were made from an angle of attack of 0° to stalling angle of attack.

Downwash surveys.- The downwash surveys were made behind each model with the rake held normal to the chord plane of the model. (See fig. 3.) The survey-rake positions are shown for each model in a figure preceding the downwash and dynamic-pressure-ratio contour figures for that model. (See figs. 10, 13, 16, 19, 22, 25, 28, 31, 34, and 37.) The survey for each model included 25 positions of the rake except when the model or the structure of the tunnel interfered, as for the highly swept high-aspect-ratio models. The rake was located to give a survey coverage from 12 inches above to 2 inches below the chord plane in order to cover the region of expected tail locations. After the surveys were made for the various angles of attack of the wing, the same process was repeated with wing removed and mounting strut in place so that the change in flow resulting from the presence of the wing itself could be found by subtraction. All surveys were made by changing the angle of attack of the survey rake to agree with that of the model. All survey data were recorded by photographing a multitube inclined manometer.

In the presentation of the data the survey planes are shown located with respect to the chord plane at all angles of attack. The abscissa of each contour plot is laid out with respect to the quarter-chord point of the wing at the spanwise station being considered and not with respect to the quarter-chord point of the mean aerodynamic chord of the wing. For the 60° swept wings the first line of the spanwise survey stations fell within the model and could not be used. The distance from the quarter-chord point of the mean aerodynamic chord to any point given on the contour plots can be found by the use of the values in table I.

Corrections

Tares.- The force-test data have not been corrected for tares. The "wing-in - wing-out" method of obtaining the contour data by subtraction should partly correct for strut interference, leaving only the mutual interference of wing and strut uncorrected. This mutual interference has been found in the past to be small.

Jet boundary.- The jet-boundary corrections applied to the force-test data are presented in table II. The values of C_L and α shown on the contour plots of downwash angle and dynamic-pressure ratio are values read from the corrected force-test data. These jet-boundary corrections for each swept wing were calculated by assuming a straight rectangular wing with the same span and aspect ratio as the swept wing.

Jet-boundary corrections were not applied to the downwash values given in the contour plots. For the information of the user of the downwash data, however, figure 4 is presented. The curves of figure 4 were computed from reference 5, taking into account the effect of sweep, and give $\frac{\Delta\epsilon\sqrt{q/q_o}}{C_L}$ along the wing center line in the chord plane

for each of the ten wings tested for 0° angle of attack. An analysis of some unpublished boundary-induced-upwash calculations indicated that the correction factor presented in figure 4 will be constant over tail spans up to 1 wing semispan and will vary less than 5 percent at the tip of a tail of span equal to 2 wing semispans. The correction factor will probably be within 10 percent for all the wings at all angles of attack and tail heights presented except the 60-inch-span, 60° swept wings at angles of attack greater than 17°. (See reference 5.) The correction should be calculated by using the dynamic-pressure ratio from the contours for the desired tail location and then added to the value of ϵ found on the contour plot.

Accuracy

It was realized that high dynamic-pressure-ratio slopes would influence the accuracy of the downwash data. The slopes were computed to find the values which would cause errors of $1/2^{\circ}$ and of 1° (determined from calibration curves and geometry of the rake pitch heads). By comparison of the dynamic-pressure-ratio cross plots with these calculated slopes, it was found that for the highest slopes in the wing wake the error was less than $\pm 1^{\circ}$. In other regions the error is believed to be smaller.

The dynamic-pressure-ratio contours are believed to be accurate within ± 2 percent since the ratio is determined by division of "wing-in" readings by "wing-out" readings so that errors of rake indication should be minimized.

Presentation of Results

The data are presented in figures 5 to 44 in three general groups: force-test data, survey data, and analysis plots. Force-test data and survey data are indexed in table III.

DISCUSSION

Force Data

The pitching-moment data (figs. 6, 7, 8, and 9) reveal changes in the pitching-moment curves at a value of C_L of about 0.6, especially for the highly swept wings of high aspect ratio, caused by a shift of lift load toward the root section on sweptback wings and a shift of lift load toward the tip section on sweptforward wings. Reference 4 indicates that this shift of lift load has a pronounced effect on the variation of downwash angle with angle of attack resulting in large changes of $\frac{d\epsilon}{d\alpha}$.

All straight and sweptback wings presented in this paper have pitching-moment characteristics in accordance with the chart of aspect ratio against sweepback found in reference 3. The possible application of the chart to sweptforward wings was not discussed in reference 3. A study of figures 7 and 9, however, reveals that the chart of reference 3 would apply to both sweptback and sweptforward wings without any change except for the sign of the angle of sweep.

The following table shows the variation of C_{L_α} and $\frac{dC_m}{dC_L}$ with sweep as determined by the force data presented in this paper. The slopes were measured through a small angle-of-attack range near zero lift.

Sweep (deg)	Span (in.)	Aspect ratio	C_{L_α} (per deg)	$\frac{dC_m}{dC_L}$
-60	60	3.0	0.034	-0.204
-60	30	1.5	.028	-.105
-30	60	5.2	.058	-.070
-30	52	4.5	.052	-.047
0	60	6.0	.063	.036
0	30	3.0	.046	.020
30	60	5.2	.061	.075
30	52	4.5	.059	.080
60	60	3.0	.036	.030
60	30	1.5	.032	.003

From the table of values of $\frac{dC_m}{dC_L}$ it appears that sweepforward causes a pronounced rearward shift of the aerodynamic center. Sweptback wings show only a slight forward shift of the aerodynamic center.

The values of C_{L_α} as obtained from figures 6 to 9 for swept wings are in some cases in good agreement with the theoretical values in figure 4 of reference 6; however, several of the values do not agree. It is believed that the tares resulting from the strut mounting on the left wing panel, if applied, would lead to closer agreement.

The table of values of C_{L_α} shows that sweep, regardless of direction, reduces C_{L_α}. Sweptforward wings are shown to have slightly lower values of C_{L_α} than sweptback wings.

Surveys

Downwash.– Figures 40 and 41 give the spanwise contours of downwash and wake in a vertical plane through an arbitrary tail location behind the swept and unswept wings. This tail was assumed to have the same sweep as the wing and to be located the same actual distance behind all of the wings. This distance was 2 semispans behind the quarter-chord line of the 30-inch-span wings and 1 semispan behind the quarter-chord line of the 60-inch-span wings. The effect of sweep at constant lift on the spanwise distribution of downwash at this assumed tail location for wings of aspect ratio 3 may be found in figure 40(a). The spanwise contours of downwash show the expected maximum downwash angle behind the root of the sweptforward wing and behind the tip of the sweptback wing. The unswept and 60° sweptback wings have large downwash angles behind the tip, and a somewhat higher location of the wake center line with respect to the chord plane than the 60° sweptforward wing. These large downwash angles near the tip of the unswept and sweptback wings are probably a result of the high relative tip loading encountered on these wings.

Figure 41(a) gives the effect of sweep on the spanwise distribution of downwash behind wings of the same basic panel unswept and swept forward and back 60°. The basic panel concept gives an aspect-ratio variation of from 6 for the unswept to 1.5 for the same panel swept 60° either forward or back. This low value of aspect ratio is believed to be the cause of the fact that there are high angles of downwash near the tip of the sweptforward wing as well as at the root where high downwash angles are expected. The sweptback wing gives the anticipated high downwash angles behind the tip, but the region of highest angles occurs nearer the tip than for the sweptback wing of aspect ratio 3 shown in figure 40(a). It appears that both sweptforward and sweptback wings of low aspect ratio have more pronounced tip loading than those of higher aspect ratio.

Wake.– The location, measured from the chord plane, of the wake center line in the plane of symmetry behind sweptforward wings is found to be high at medium angles of attack, and this vertical location increases rapidly with angle of attack. (See figs. 18(a), 24(a), 33(a), and 39(a).) On the other hand, the location of the wake behind sweptback wings was in the chord plane or just below the chord plane in the plane of symmetry and showed only a slight upward shift in location with angle of attack. (See figs. 15(a), 21(a), 30(a), and 36(a).)

In the wake behind sweptforward wings values of q/q_o are low in the plane of symmetry but increase rapidly toward the tip. Sweptback

wings, however, produce values of q/q_o which are fairly high in the wake at the plane of symmetry and decrease toward the tip.

The comparison of the wake behind unswept and 60° swept wings at constant lift and aspect ratio presented in figure 40(b) shows the same trends as discussed previously, that is, high location of low energy wake behind center of sweptforward wings, and the same behind tips of wings swept back 60°. Figure 41(b) does not present as clear a picture as figure 40(b); however, the trend is the same. This low-energy region behind the center section of sweptforward wings and behind the tip section of sweptback wings is probably caused by the transverse flow of air inboard for the sweptforward wing and outboard for the sweptback wing.

Stability.- Some available data on sweptback wings (reference 4) indicate that radical changes in $\frac{d\epsilon}{d\alpha}$ occur in certain regions behind the wing. It was found from the data shown in the present paper that sweptforward wings as well as sweptback wings produced radical changes in $\frac{d\epsilon}{d\alpha}$. Figure 42 shows $\frac{d\epsilon}{d\alpha}$ plotted against the distance of an assumed horizontal-tail position from the wing chord plane extended. Two values of tail length were used, measured from the quarter-chord point of the mean aerodynamic chord, which are believed to bracket the tail positions of modern swept-wing airplanes for which geometric data are now available. Only unswept and 60° sweptforward and sweptback wings with aspect ratio of 3 were considered. The data, presented at two angles of attack and for two spanwise stations (in plane of symmetry and 1/3 semispan from plane of symmetry), have been corrected for jet-boundary effects as presented in figure 4 and reference 5. The data indicate that the lowest tail position tends to give the lowest, that is, most stable, value of $\frac{d\epsilon}{d\alpha}$. A notable exception to the trend is evident for the short tail length behind the unswept wing, particularly at the angle of attack of 16°. For the short tail length behind the unswept wing the highest tail position gave the lowest value of $\frac{d\epsilon}{d\alpha}$. In general $\frac{d\epsilon}{d\alpha}$ increases as sweep decreases. Exceptions to this trend are most numerous for the longer tail length coupled with the high angle of attack. There is also a slight tendency toward violation of this trend for the higher tail positions. In general, the low tail position appears to be the most stable for both unswept and 60° swept wings.

Pictorial Representation

Isometric representations of angles of downwash behind the 30-inch-span wings are given in figures 43 and 44 for the straight rectangular wing and the 60° sweptback wing, respectively. Only the downwash sheets

behind the right half of the wing are shown as the downwash pattern behind the wing is assumed to be symmetrical. Also, the data presented in these figures cover only about 0.8 of the semispan since the downwash angle becomes negative from there to beyond the tip. The data presented were obtained with the wing at an angle of attack of about 8.1° as that seemed to be a compromise between presenting too simple a picture or too confusing a picture. Only downwash angles of 2.0°, 4.0°, and 6.0° are shown. The heavy dotted lines show the shape of the upper surface of the downwash sheets at each of the chordwise stations indicated. The light dotted lines show the shape of the lower surface.

CONCLUSIONS

The data obtained from force tests and dynamic-pressure wake surveys for ten models having various angles of sweep in low-speed three-dimensional air flow indicate the following conclusions:

1. The wake-center-line location (measured from the chord plane) behind sweptforward wings was found to be high whereas behind sweptback wings it was found to be in the chord plane or just below the chord plane.

2. The sweptforward and sweptback wings show their greatest wake energy loss at the plane of symmetry and at the tip, respectively.

3. A low tail position appears to be most stabilizing for all wings investigated except for the short tail length behind the unswept wing at an angle of attack of 16°. The high tail position was most stabilizing for this condition.

4. At short tail lengths and low angles of attack the rate of change of downwash angle with angle of attack generally increases as sweep decreases. At long tail lengths and high angles of attack the reverse tends to be true.

Langley Aeronautical Laboratory
National Advisory Committee for Aeronautics
Langley Field, Va., June 3, 1948

REFERENCES

1. Jones, Robert T.: Wing Plan Forms for High-Speed Flight. NACA TN No. 1033, 1946.

2. Letko, William, and Goodman, Alex: Preliminary Wind-Tunnel Investigation at Low Speed of Stability and Control Characteristics of Swept-Back Wings. NACA TN No. 1046, 1946.

3. Shortal, Joseph A., and Maggin, Bernard: Effect of Sweepback and Aspect Ratio on Longitudinal Stability Characteristics of Wings at Low Speeds. NACA TN No. 1093, 1946.

4. Purser, Paul E., Spearman, M. Leroy, and Bates, William R.: Preliminary Investigation at Low Speed of Downwash Characteristics of Small-Scale Sweptback Wings. NACA TN No. 1378, 1947.

5. Gillis, Clarence L., Polhamus, Edward C., and Gray, Joseph L., Jr.: Charts for Determining Jet-Boundary Corrections for Complete Models in 7- by 10-Foot Closed Rectangular Wind Tunnels. NACA ARR No. L5G31, 1945.

6. Toll, Thomas A., and Queijo, M. J.: Approximate Relations and Charts for Low-Speed Stability Derivatives of Swept Wings. NACA TN No. 1581, 1948.

TABLE I.– GEOMETRY OF THE MODELS

[NACA 0015 airfoil section in plane perpendicular to wing leading edge for all models]

Span (in.)	Sweep (deg)	Aspect ratio	Chord (M.A.C.) (in.)	Area (sq in.)	Distance from c/4 of M.A.C. to L.E. at center line
60	0	6.0	10.00	600.0	2.50
60	30	5.2	11.55	692.8	11.55
60	–30	5.2	11.55	692.8	5.77
60	60	3.0	20.00	1200.0	20.96
60	–60	3.0	20.00	1200.0	20.96
30	0	3.0	10.00	300.0	2.50
52	30	4.5	11.55	600.0	10.39
52	–30	4.5	11.55	600.0	4.62
30	60	1.5	20.00	600.0	17.99
30	–60	1.5	20.00	600.0	7.99

NACA

TABLE II.– JET-BOUNDARY CORRECTIONS

[All corrections are additive]

Span (in.)	Sweep, Λ (deg)	Aspect ratio	$\frac{\Delta\alpha}{C_L}$	$\frac{\Delta C_D}{C_L^2}$	$\frac{\Delta C_m}{C_L}$
60	0	6.0	0.420	0.0070	Negligible
60	30	5.2	.500	.0080	
60	–30	5.2	.500	.0080	
60	60	3.0	.900	.0138	
60	–60	3.0	.900	.0138	
30	0	3.0	.200	.0035	
52	30	4.5	.390	.0067	
52	–30	4.5	.390	.0067	
30	60	1.5	.400	.0070	
30	–60	1.5	.400	.0070	

NACA

TABLE III.– INDEX OF FIGURES SHOWING FORCE TEST AND SURVEY DATA

Sweep angle, Λ (deg)	Span, b (in.)	Figure			
		Force data	Stations surveyed	Downwash contours	Dynamic-pressure-ratio contours
0	60	5	10	11	12
	30		25	26	27
30	60	6	13	14	15
	52		28	29	30
–30	60	7	16	17	18
	52		31	32	33
60	60	8	19	20	21
	30		34	35	36
–60	60	9	22	23	24
	30		37	38	39

NACA

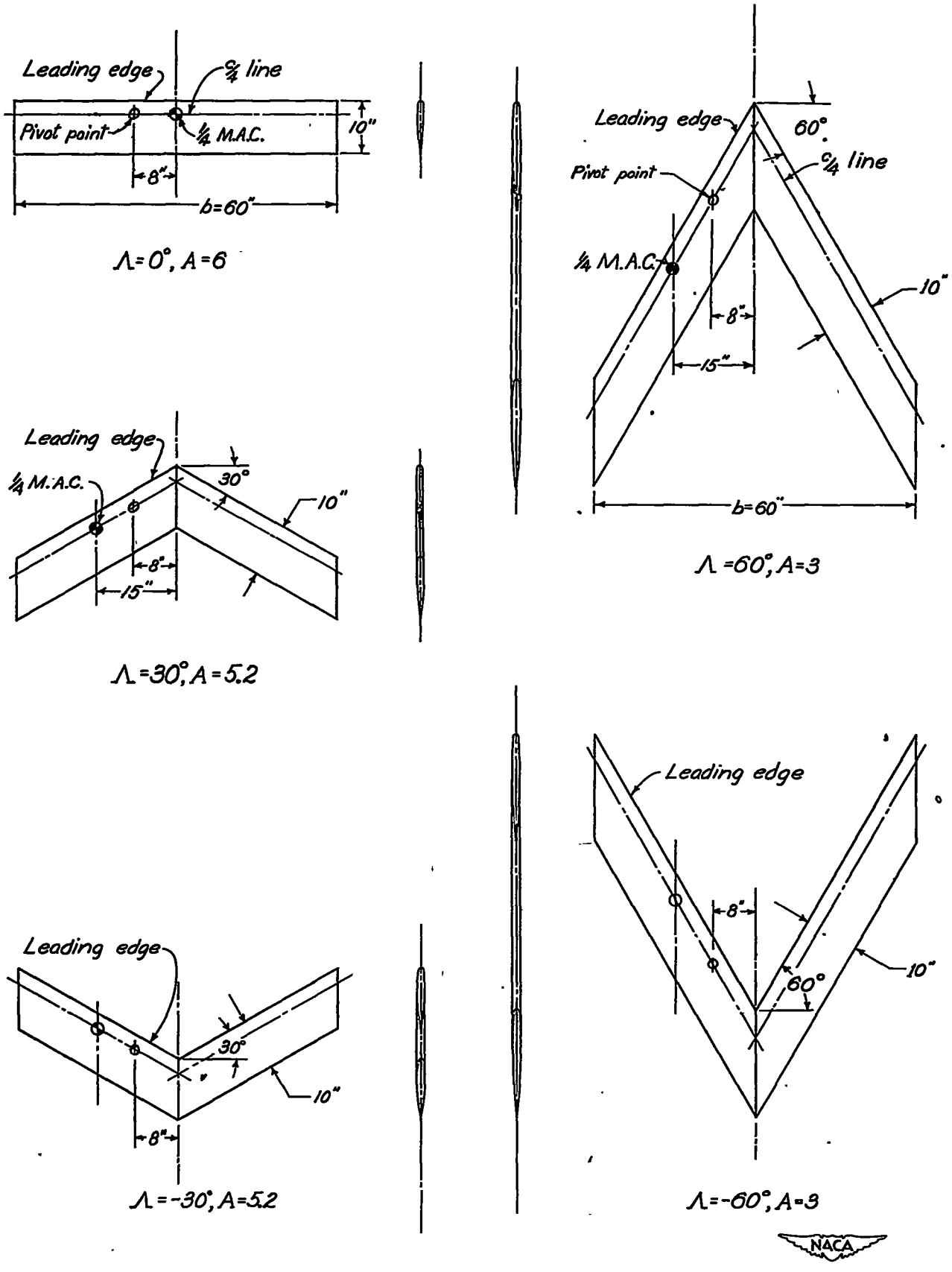

Figure 1.- Details of the ten untapered wings of varying aspect ratio and angle of sweep used for the downwash and dynamic-pressure surveys.

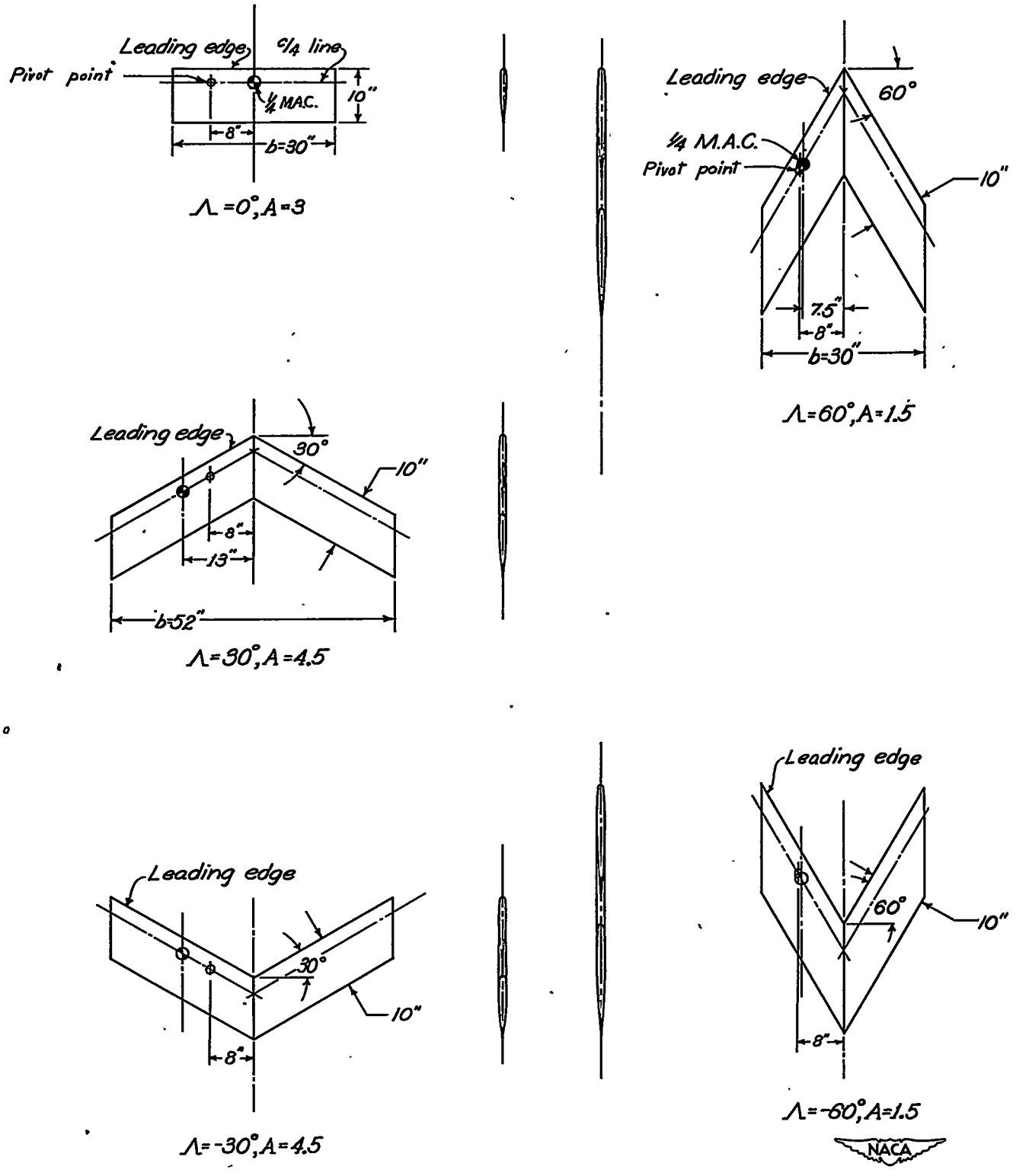

Figure 1.- Concluded.

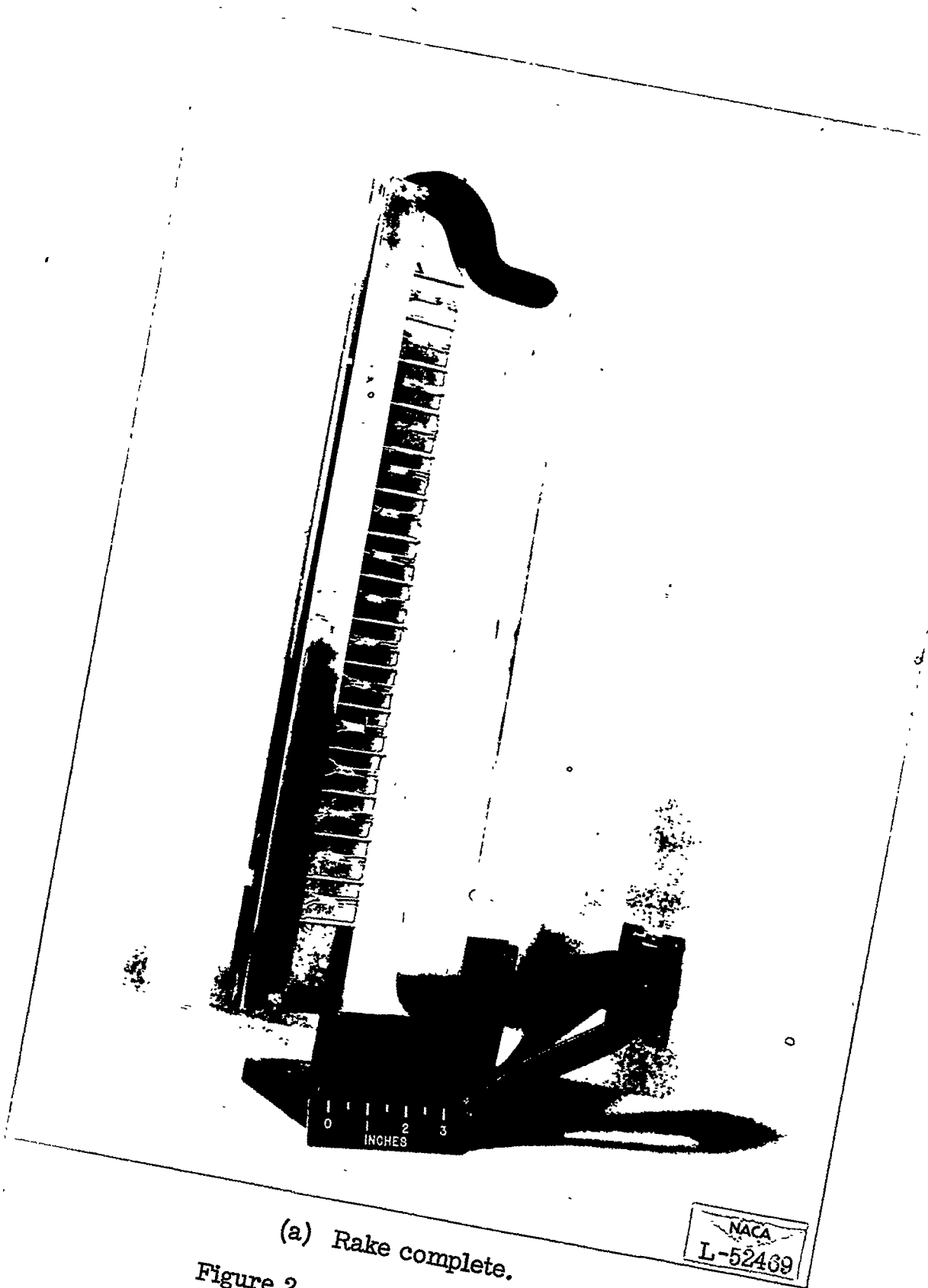

(a) Rake complete.

Figure 2.- Details of survey rake.

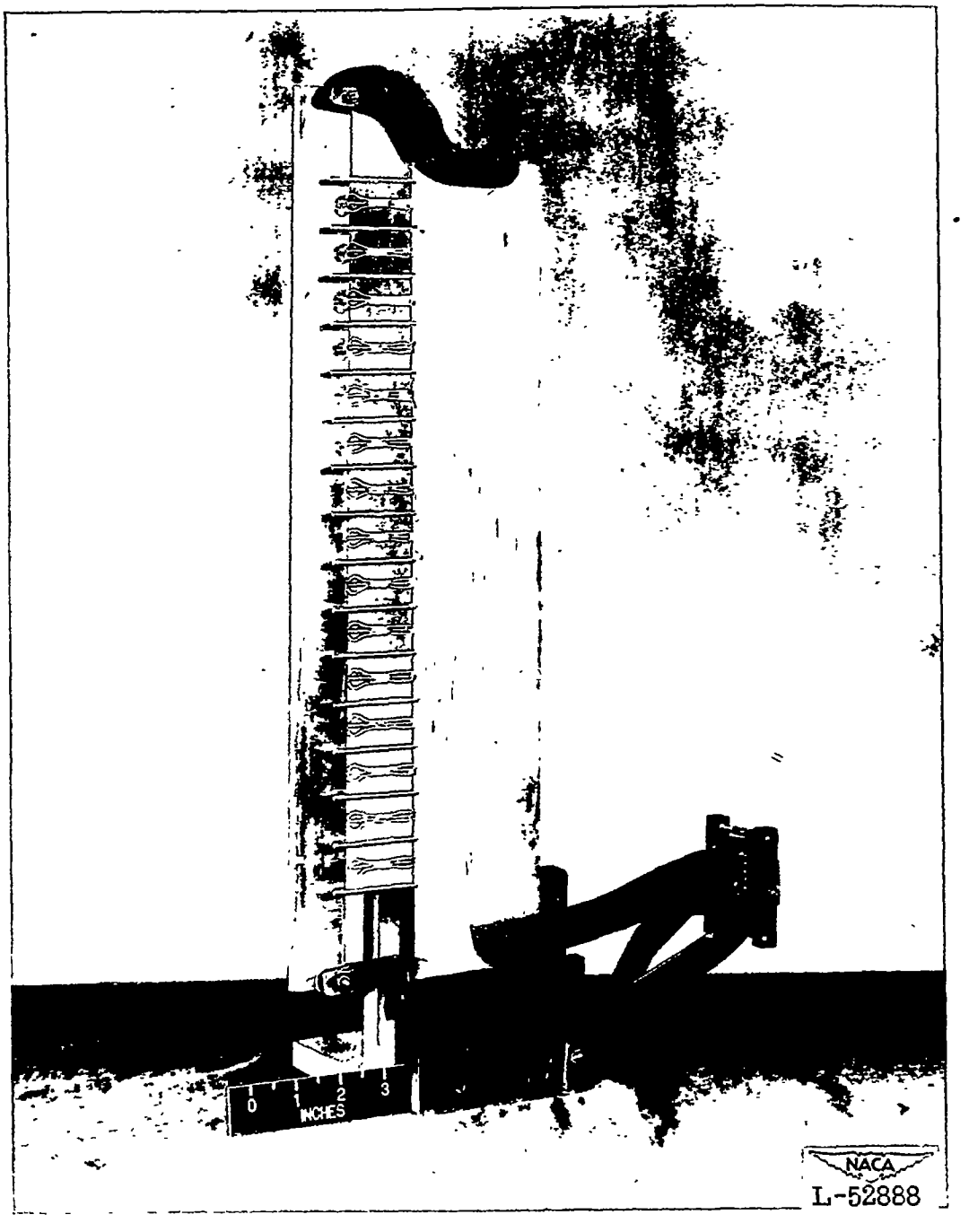

(b) Slat removed showing arrangement of pressure tubes.

Figure 2.- Continued.

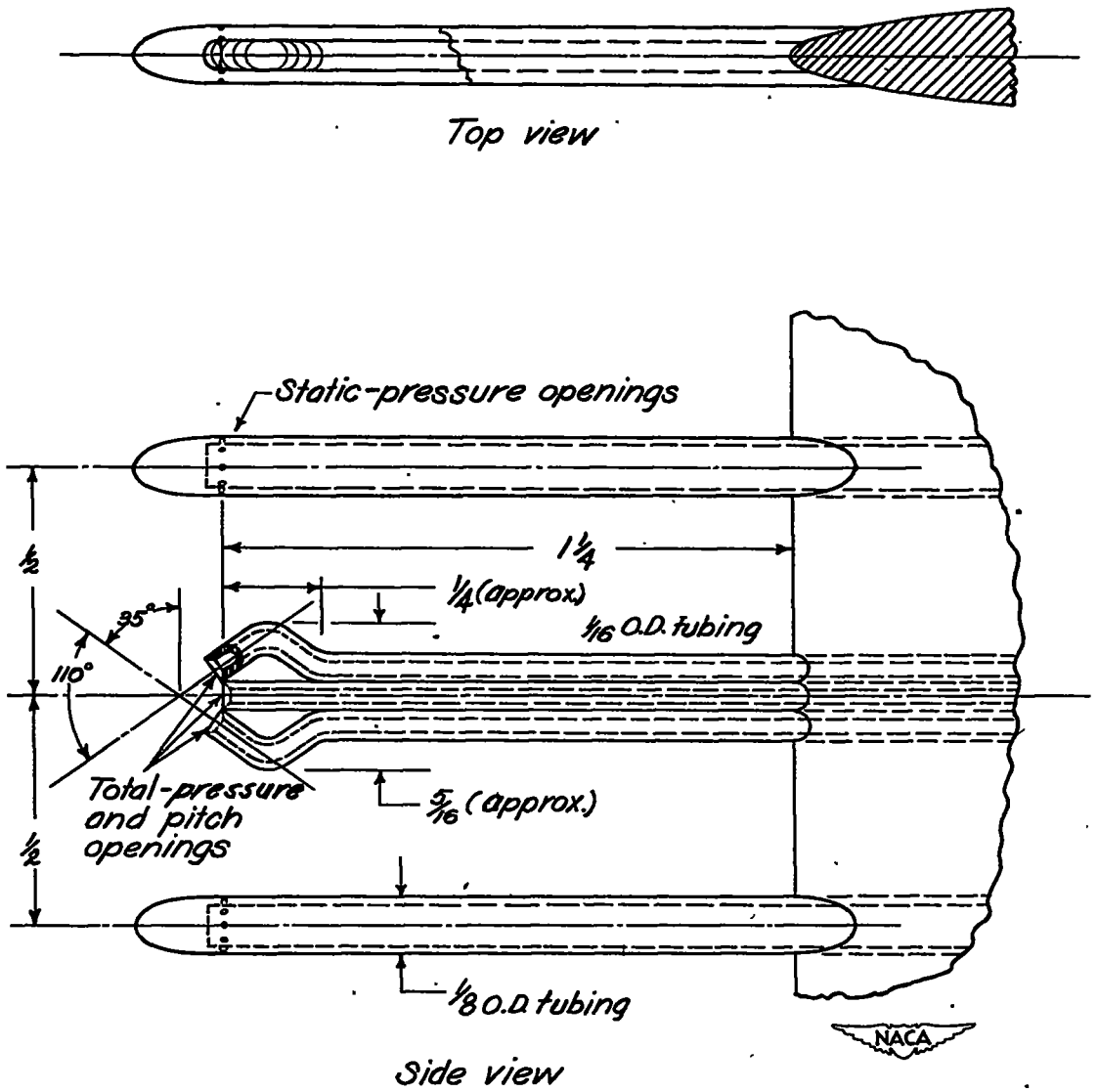

(c) Details of one pitch head of survey rake showing location of the various pressure openings. (All dimensions are in inches.)

Figure 2.-Concluded.

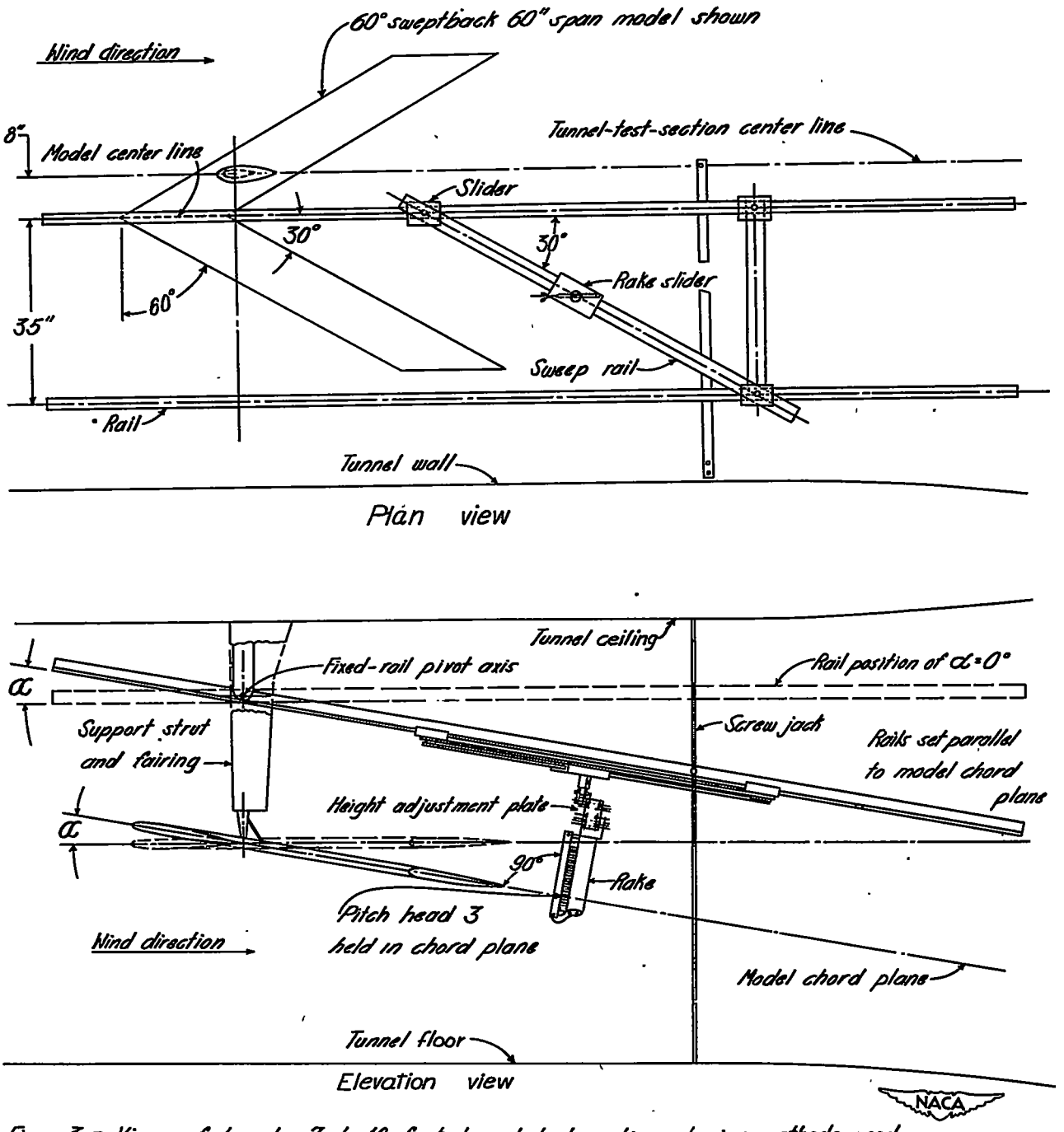

Figure 3.- Views of Langley 7-by 10-foot-tunnel test section showing methods used for supporting model and survey rake.

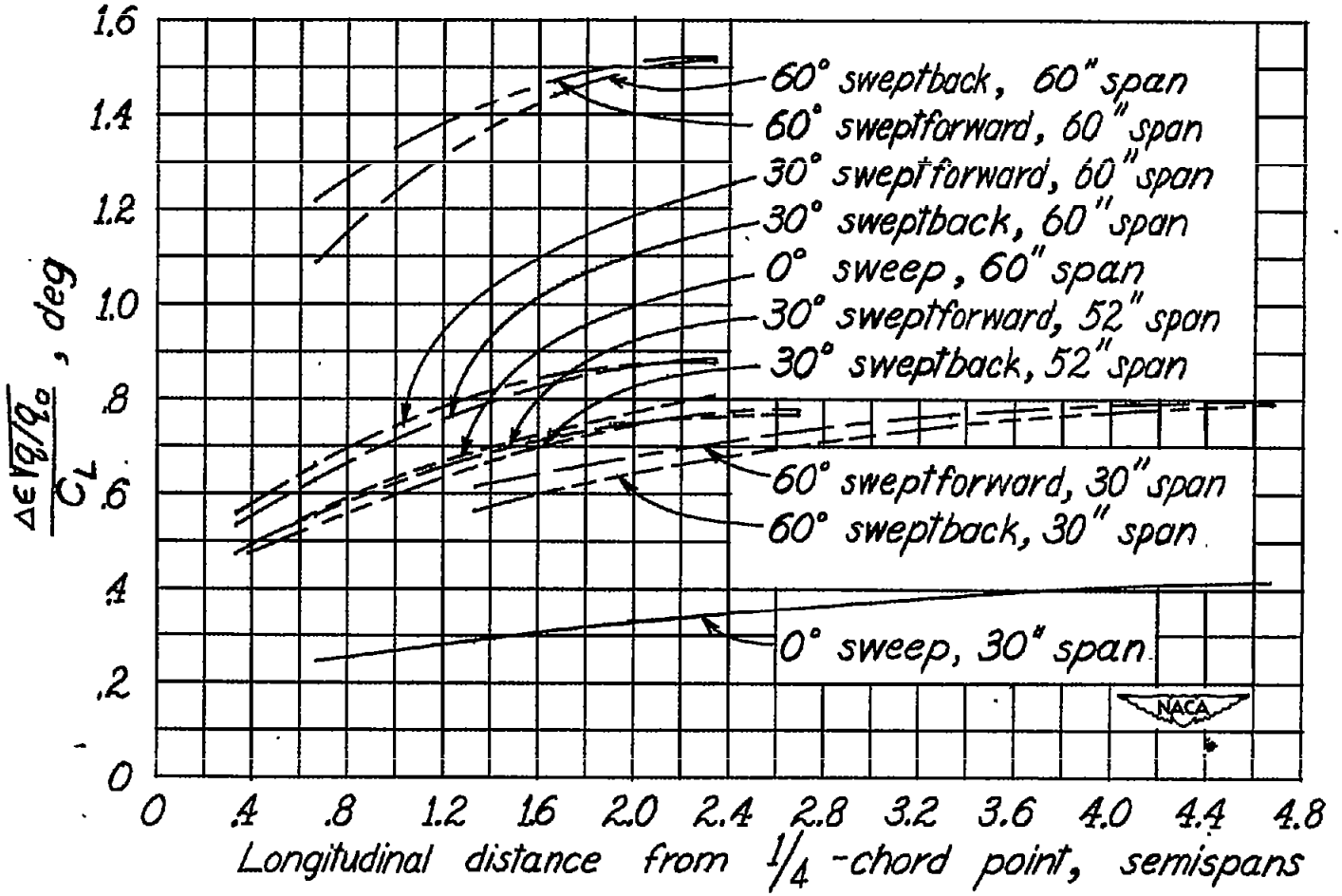

Figure 4.– Jet-boundary corrections along the intersection of the plane of symmetry and the chord plane of the wing as computed from reference 6 for $\alpha = 0°$.

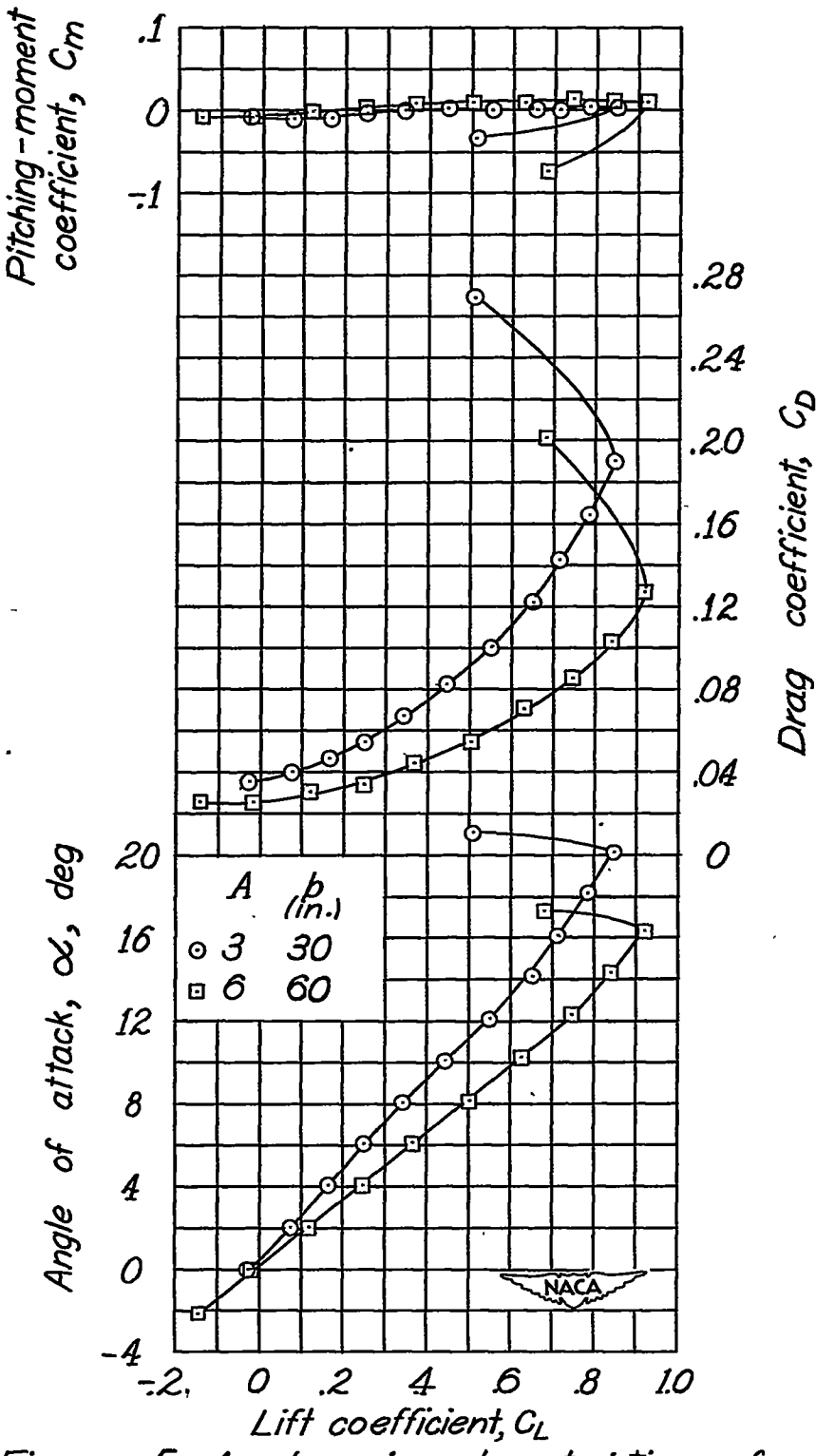

Figure 5.-Aerodynamic characteristics of straight rectangular wings.

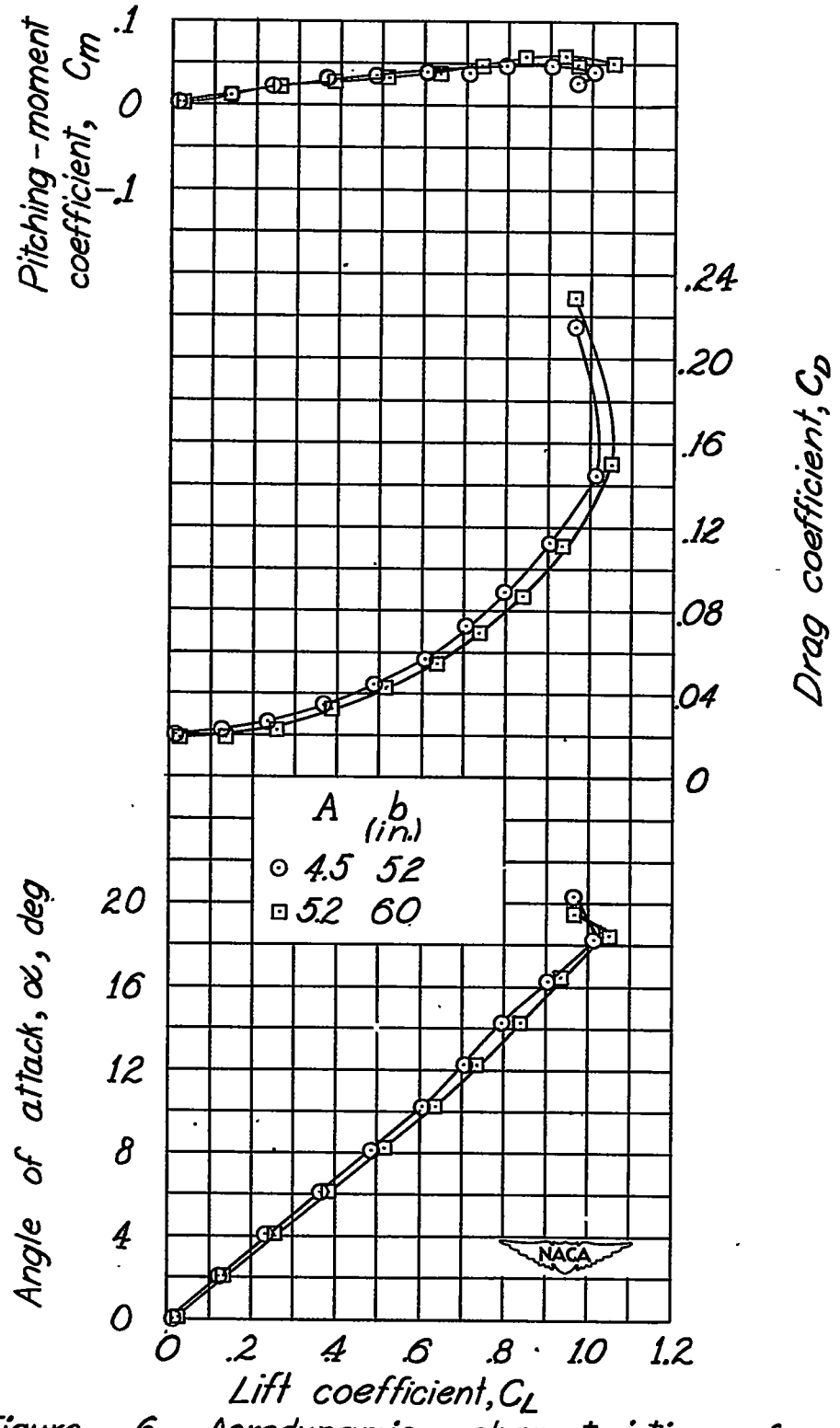

Figure 6.- Aerodynamic characteristics of 30° sweptback wings.

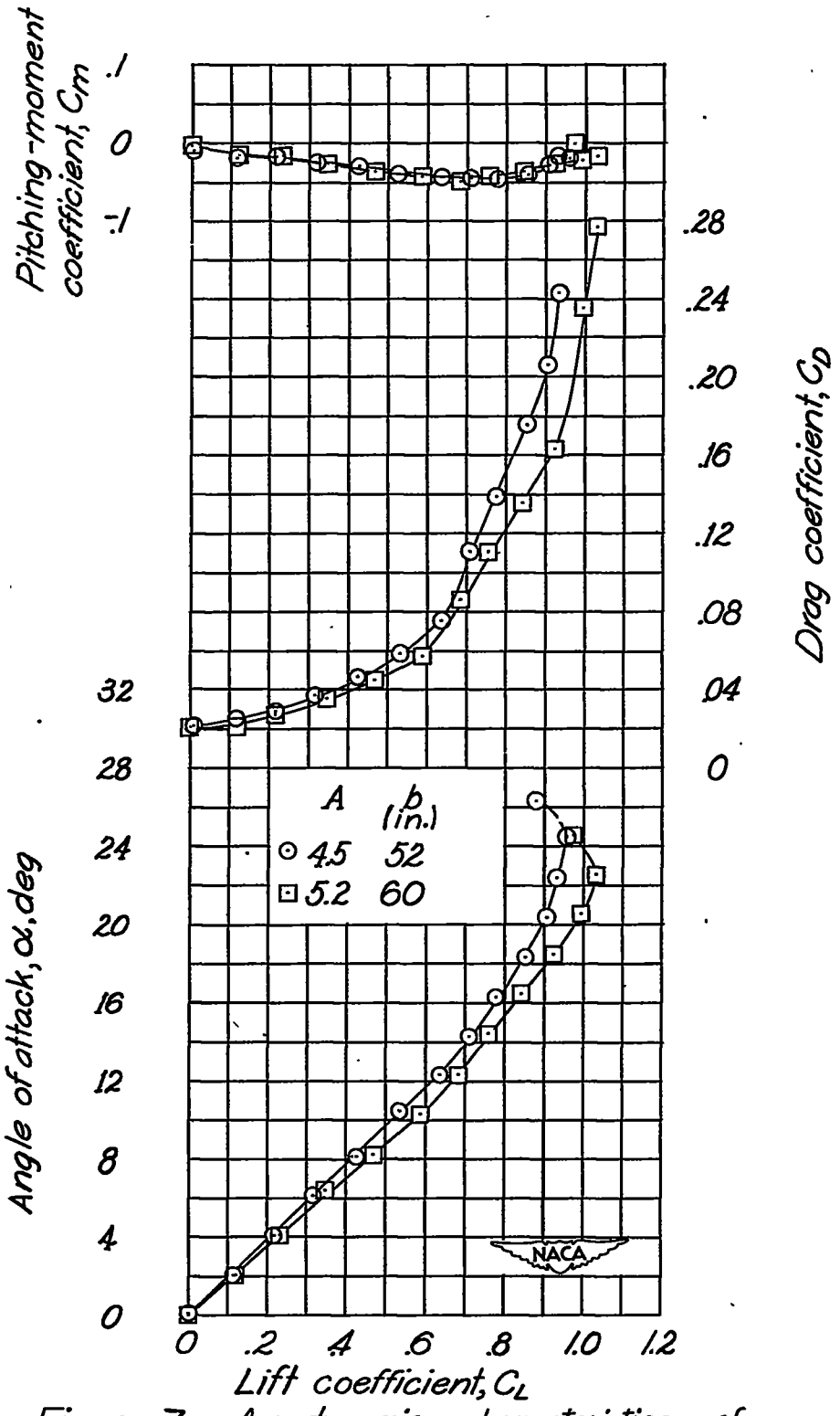

Figure 7.- Aerodynamic characteristics of 30° sweptforward wings.

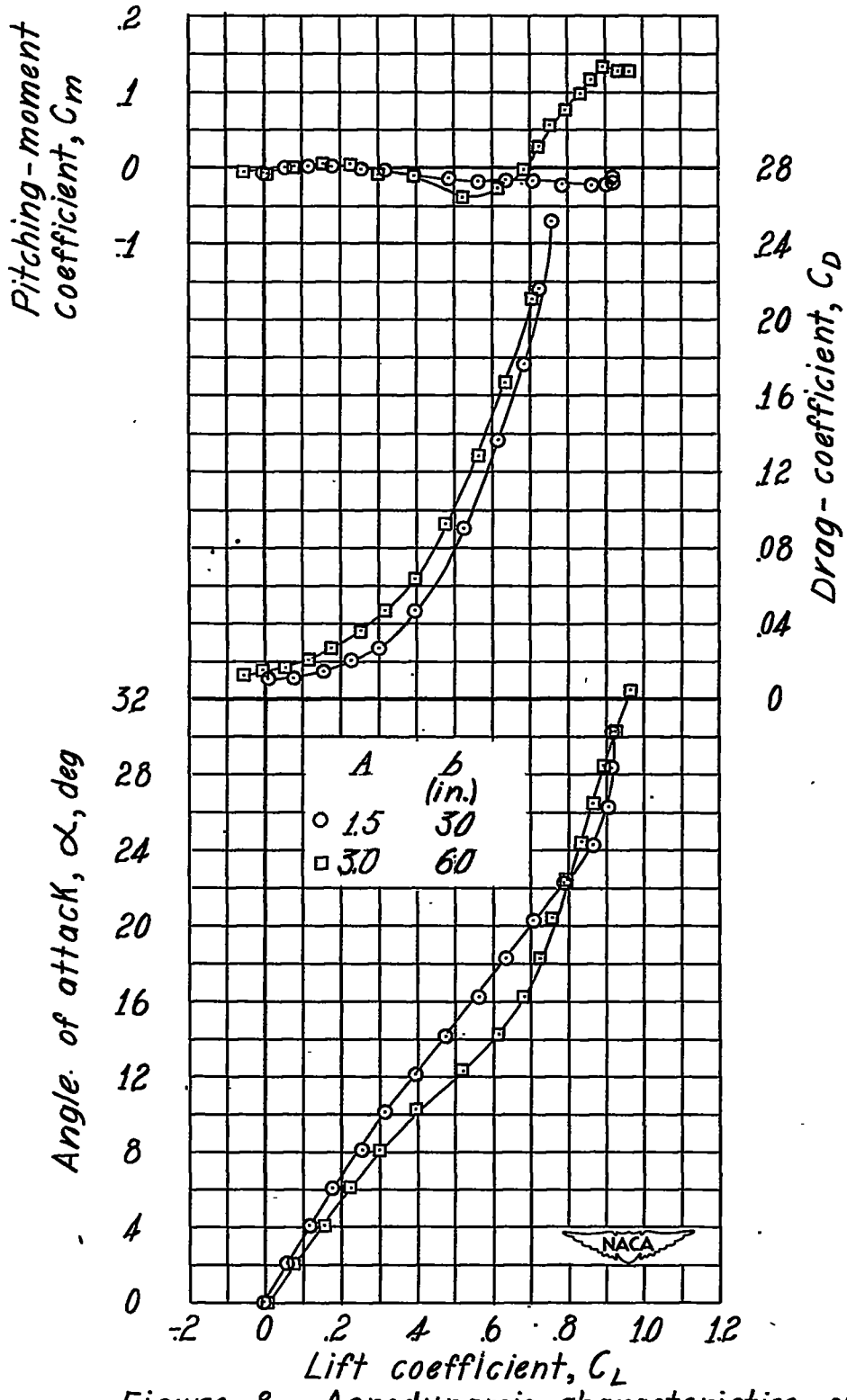

Figure 8.- Aerodynamic characteristics of 60° sweptback wings.

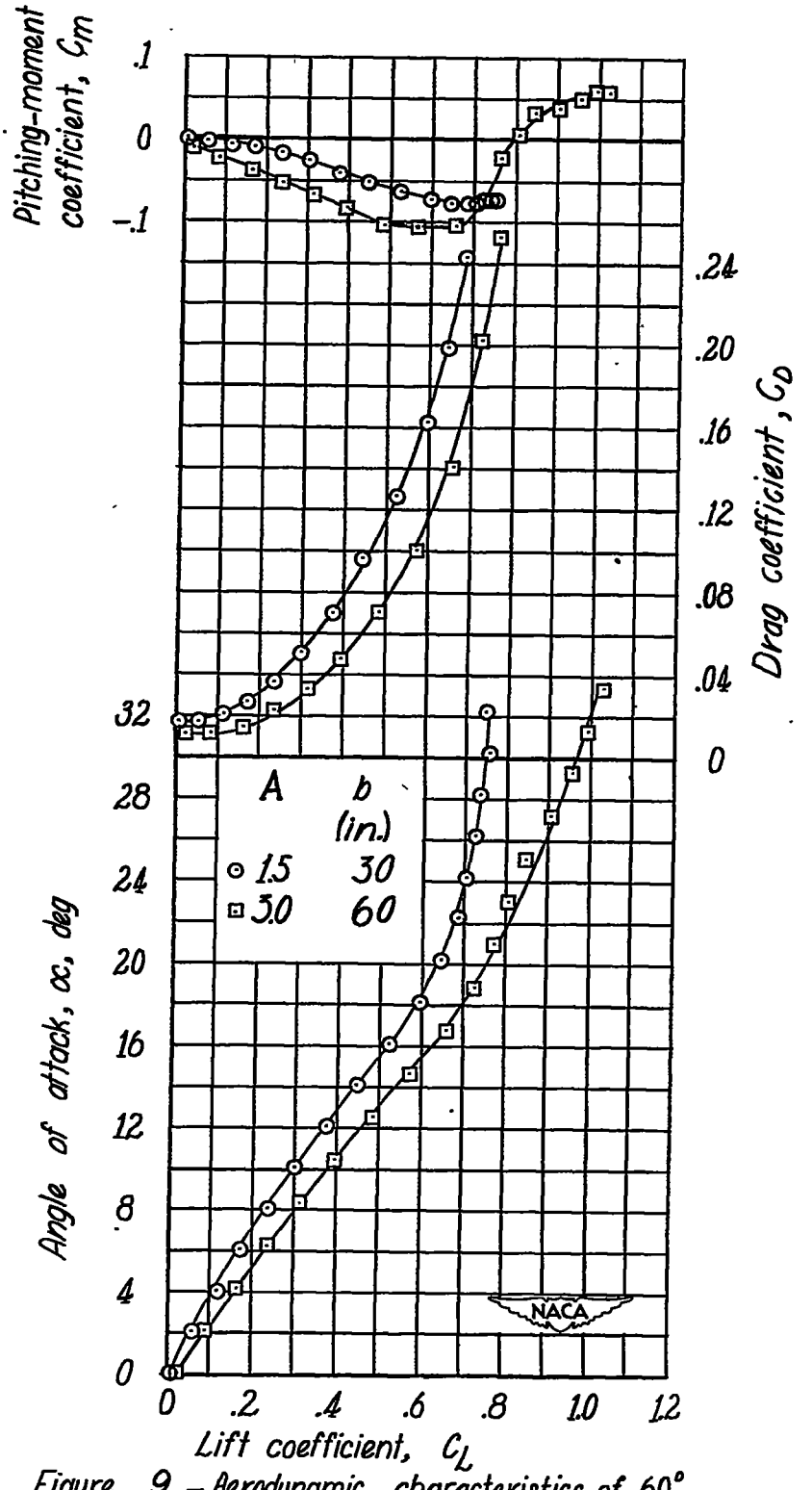

Figure 9.- Aerodynamic characteristics of 60° sweptforward wings.

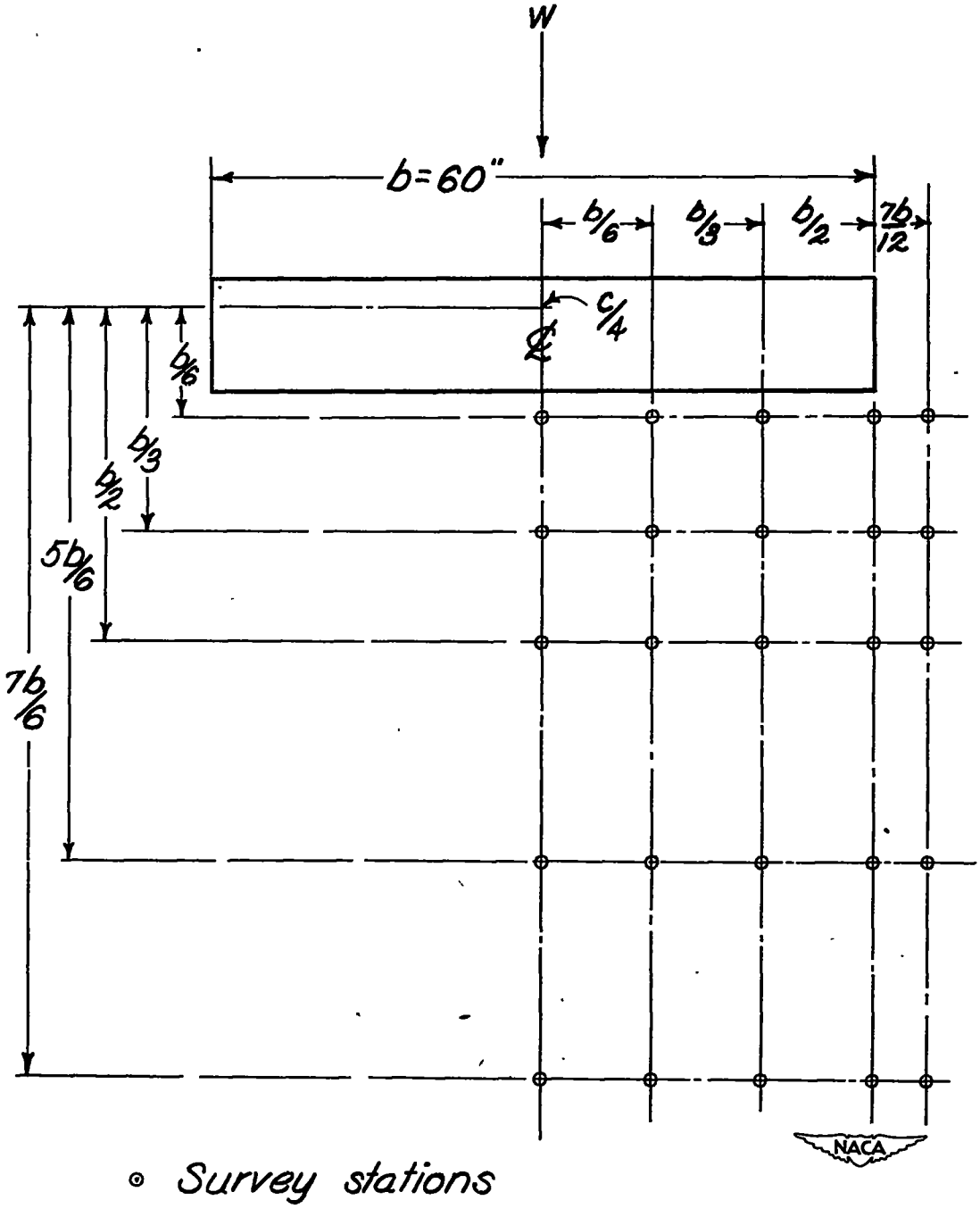

Figure 10.- Survey stations behind straight rectangular wing of 60-inch span. A=6.

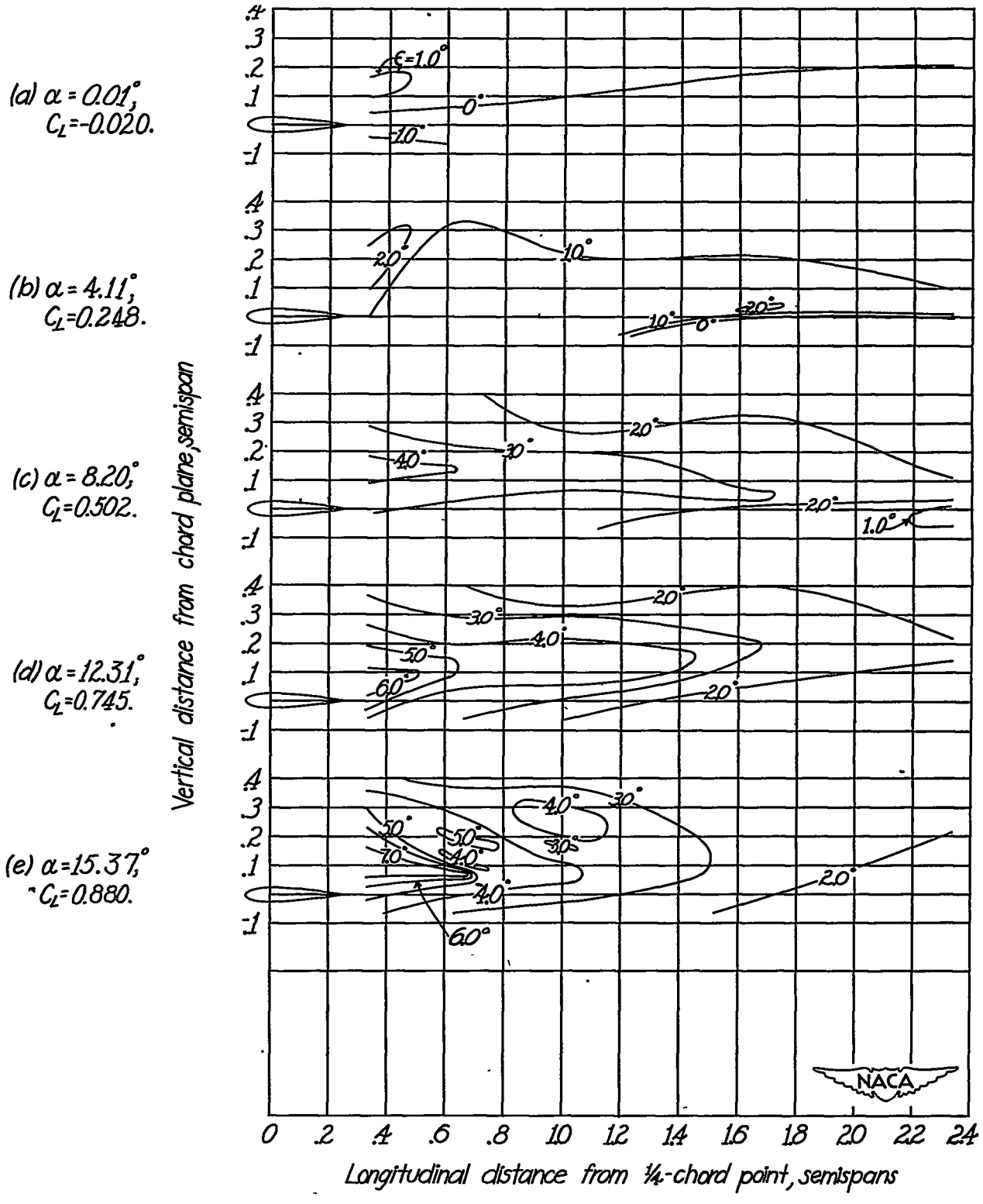

(a) Plane of symmetry.

Figure 11.- Downwash contours behind straight rectangular wing of 60-inch span. A=6.

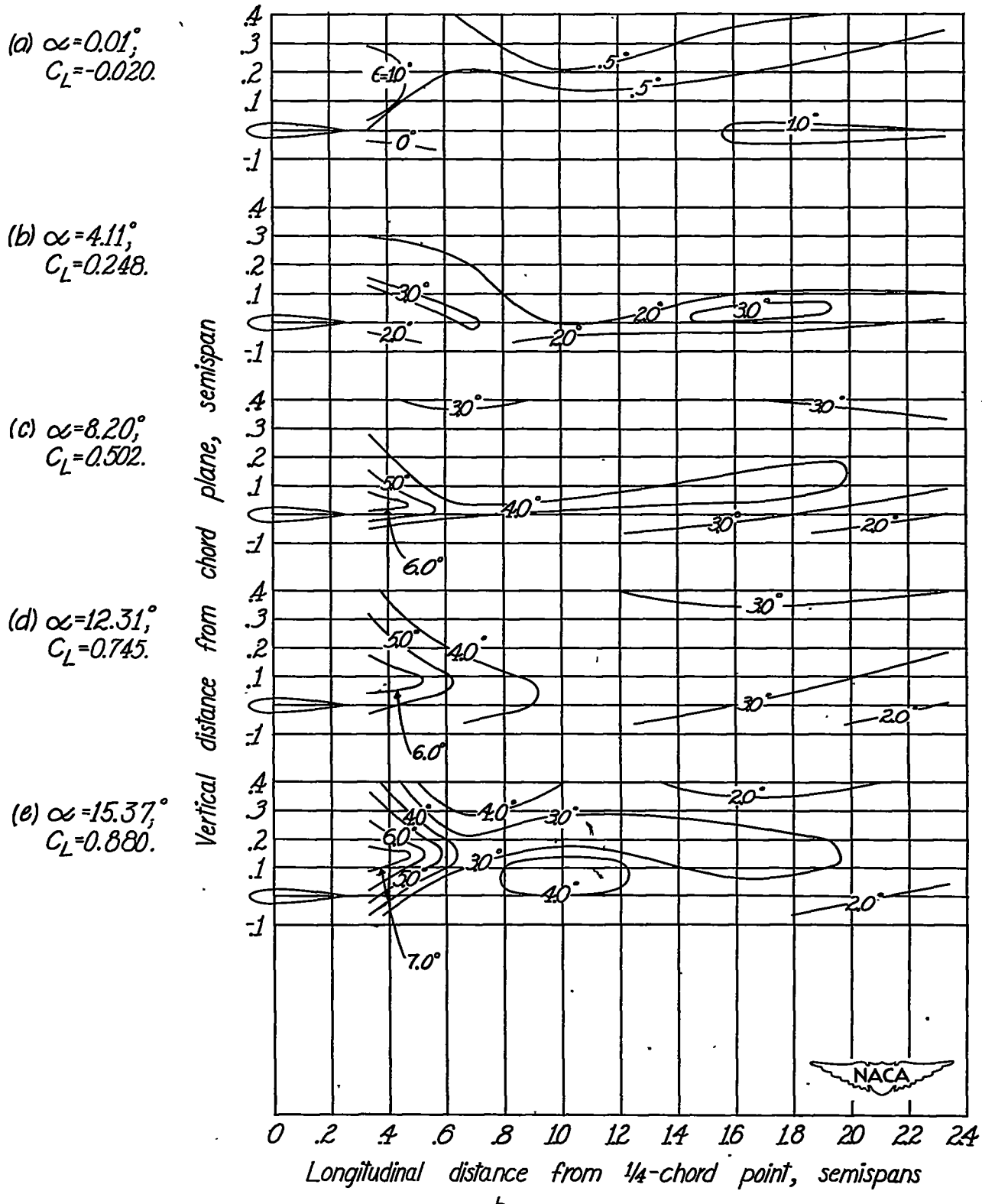

(b) $\frac{b}{6}$ spanwise station.

Figure 11.- Continued.

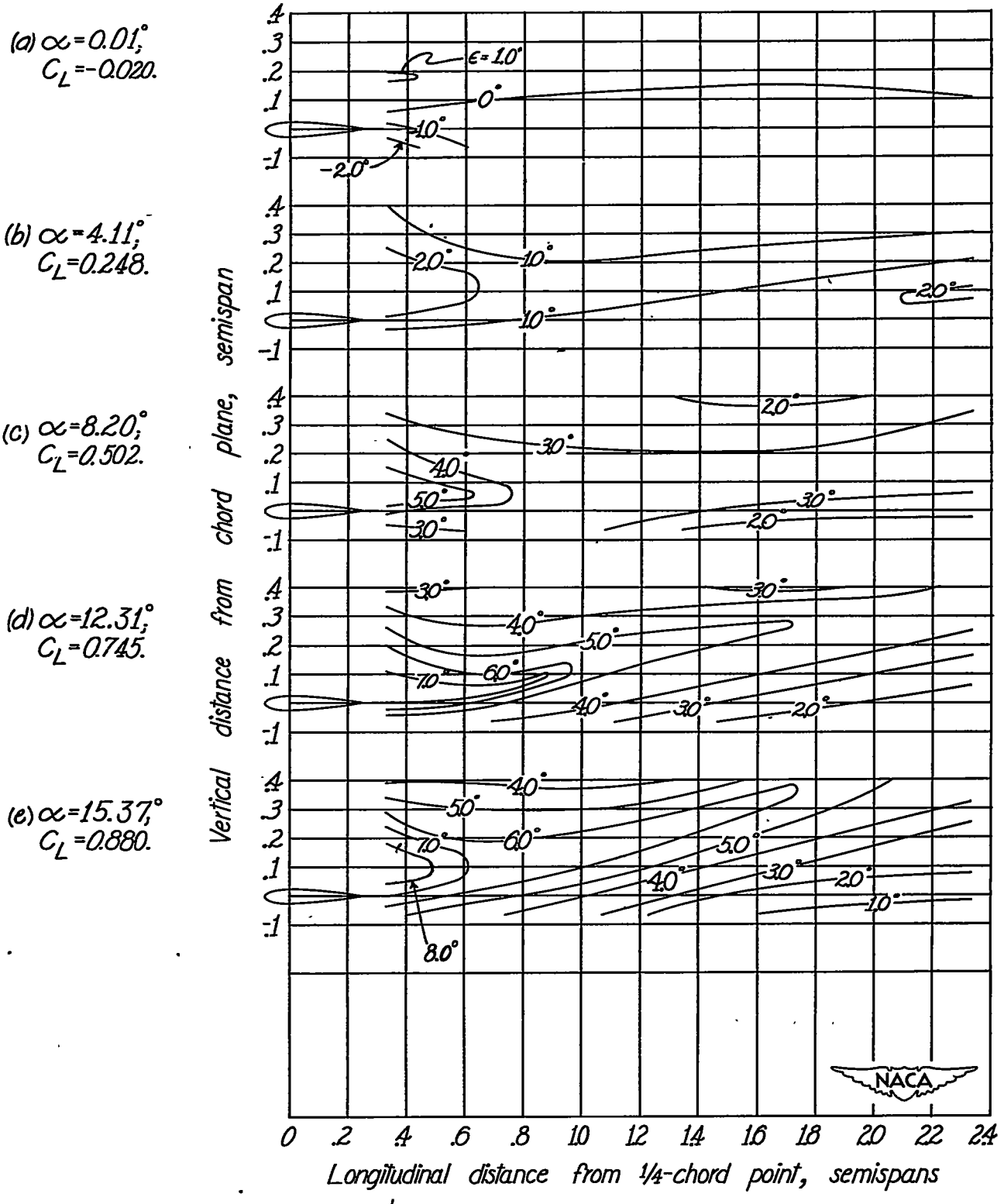

(c) $\frac{b}{3}$ spanwise station.

Figure 11.- Continued.

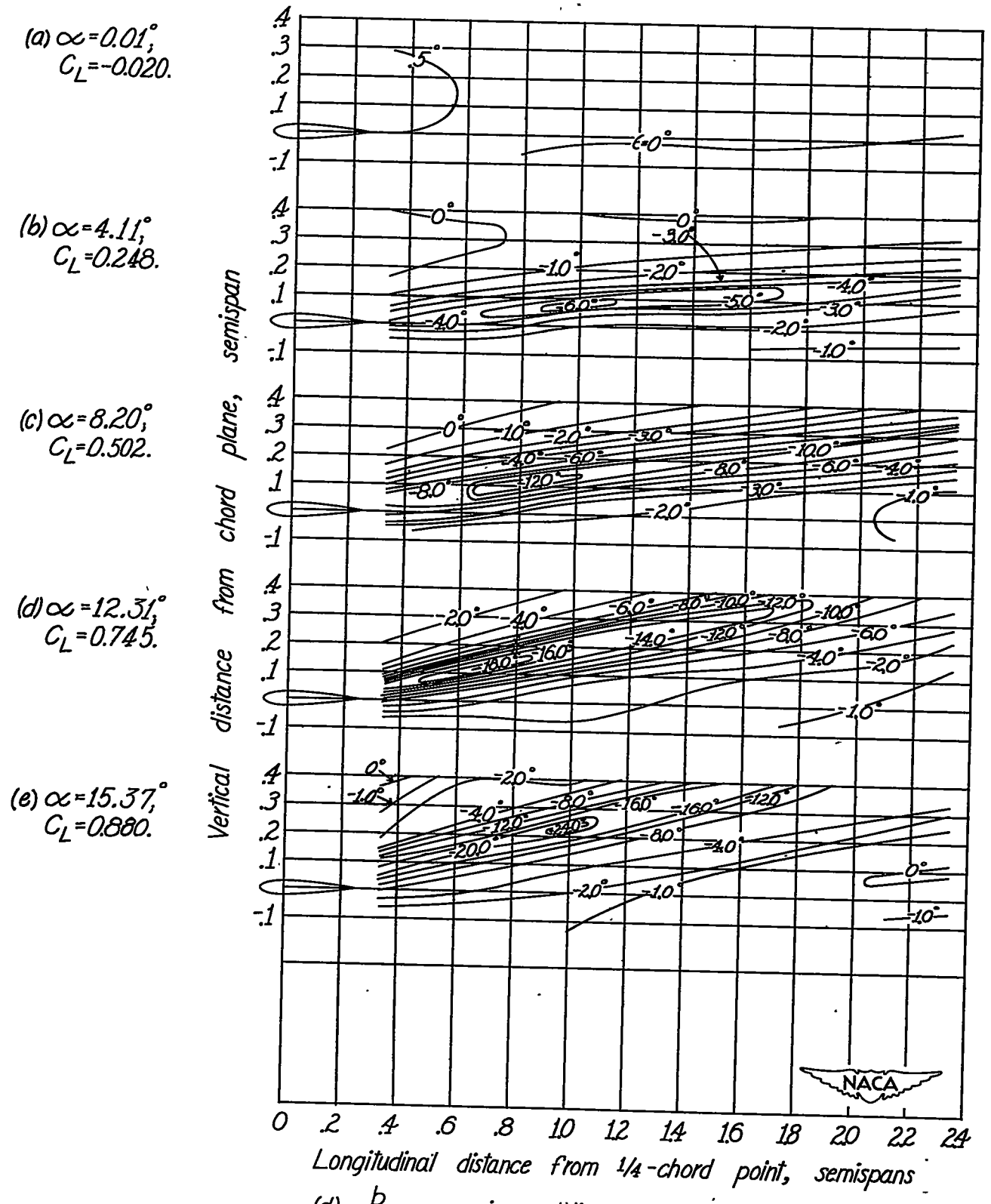

(d) $\frac{b}{2}$ spanwise station.

Figure 11.- Continued.

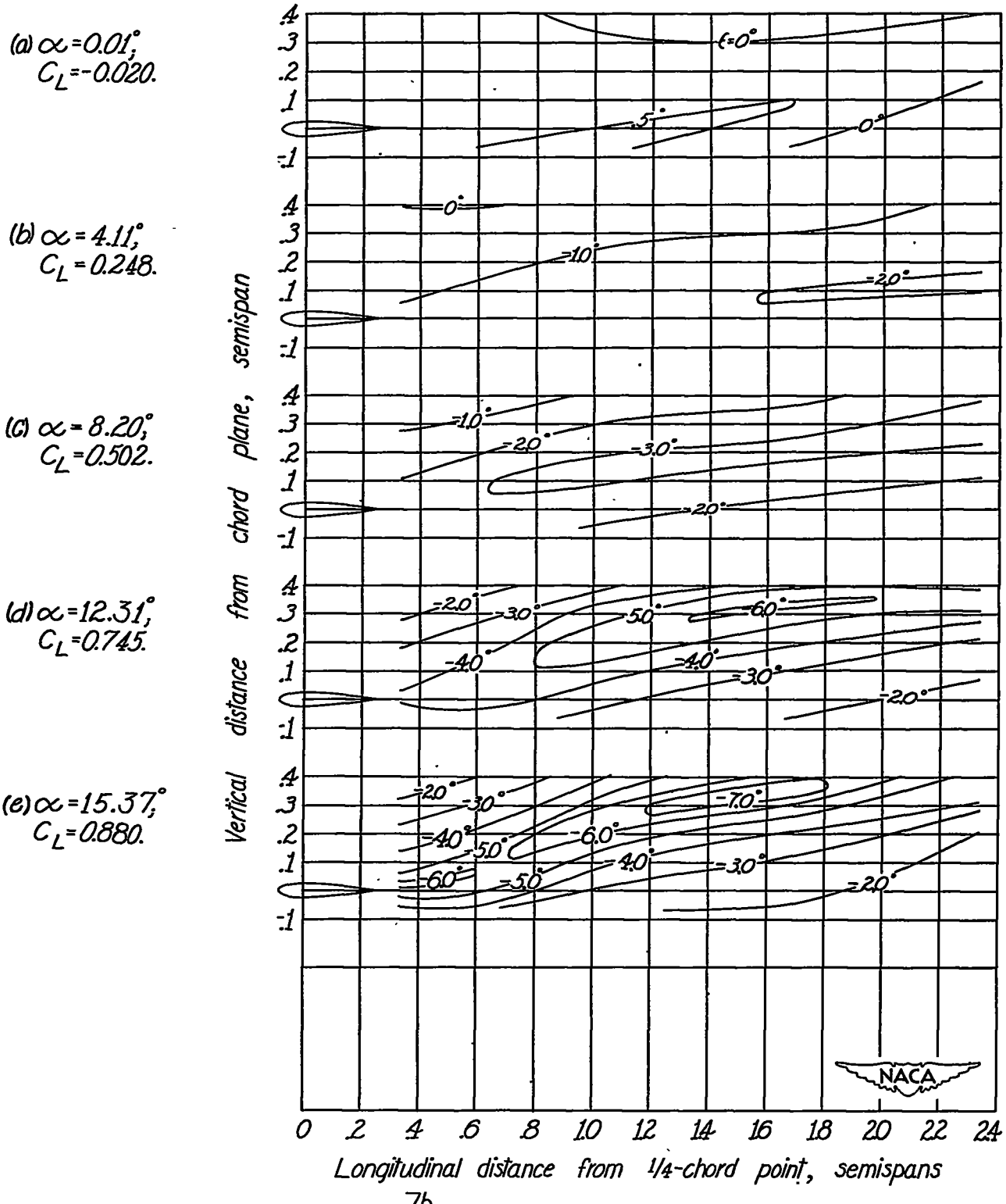

(e) $\frac{7b}{12}$ spanwise station.

Figure 11.–Concluded.

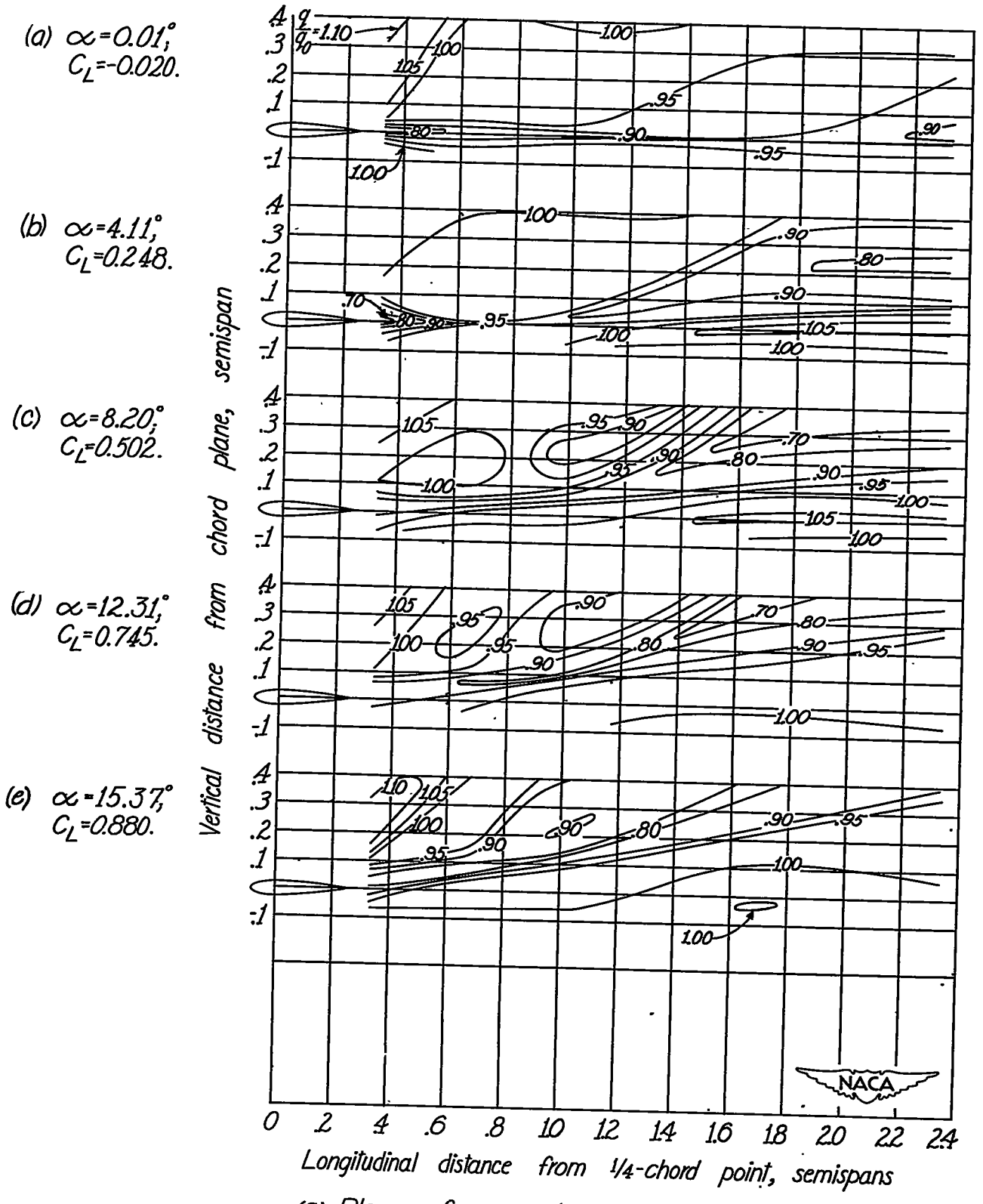

(a) Plane of symmetry.

Figure 12.– Dynamic-pressure-ratio contours behind straight rectangular wing of 60-inch span. A=6.

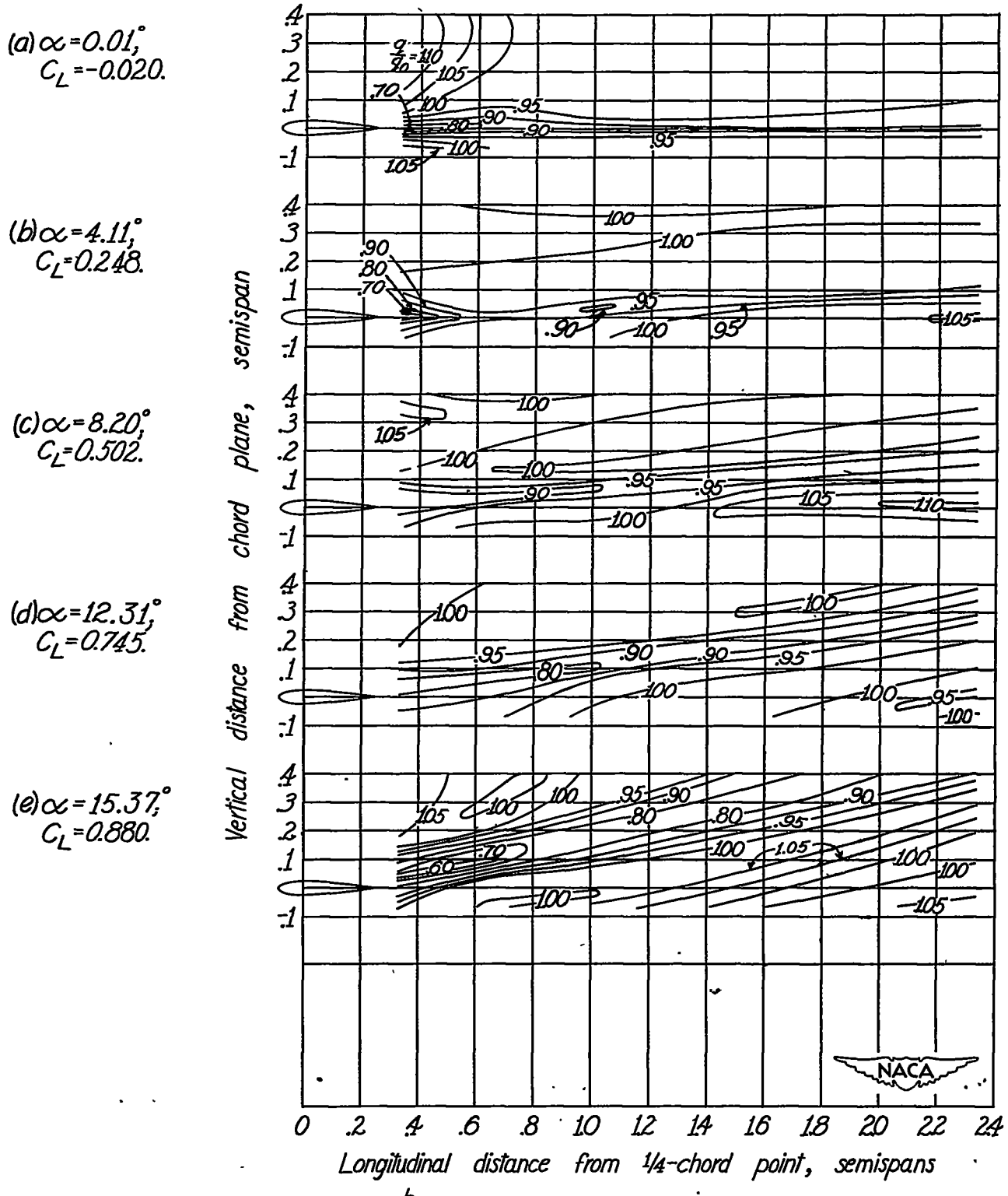

(b) $\frac{b}{6}$ spanwise station.

Figure 12.- Continued.

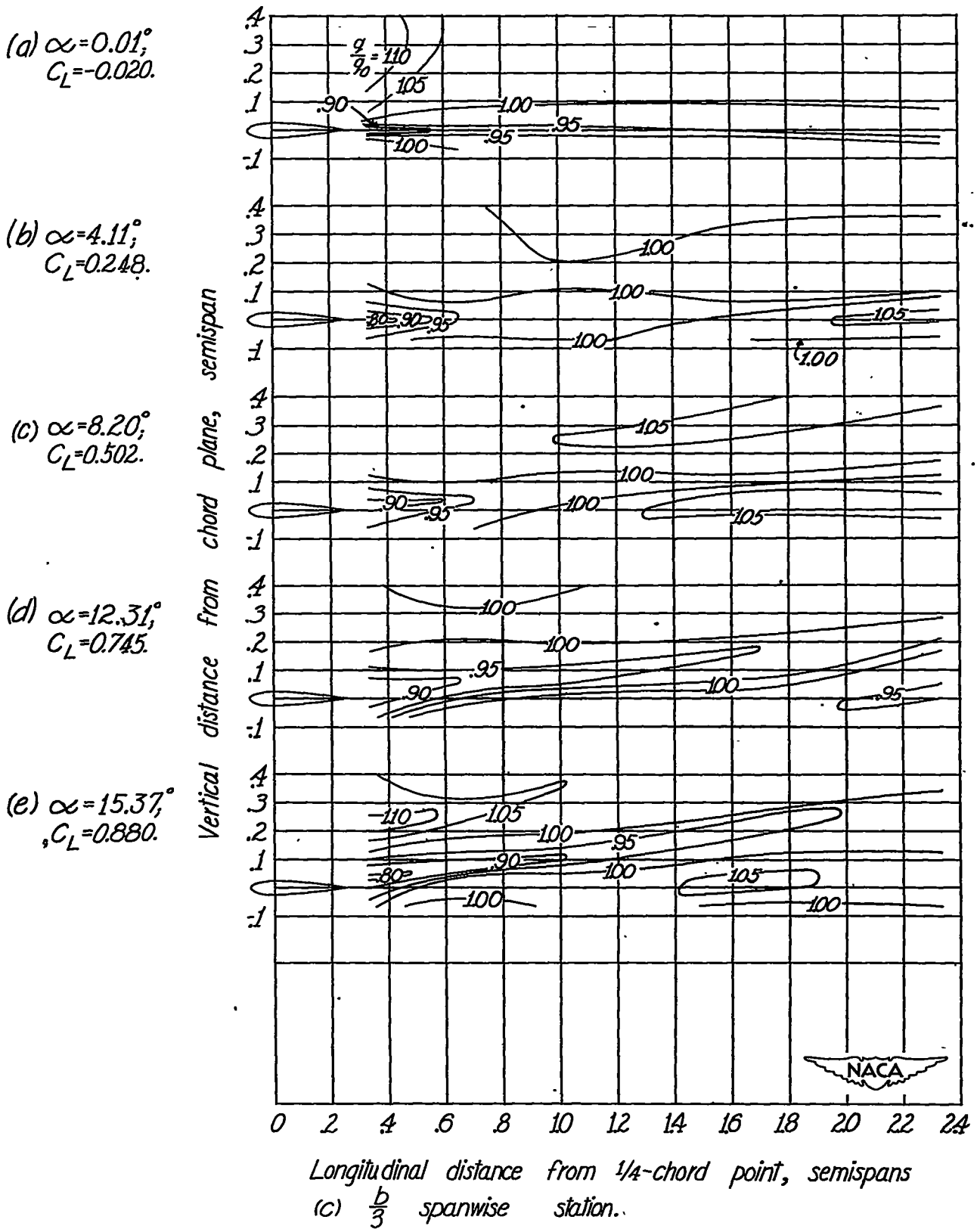

(c) $\frac{b}{3}$ spanwise station.

Figure 12.- Continued.

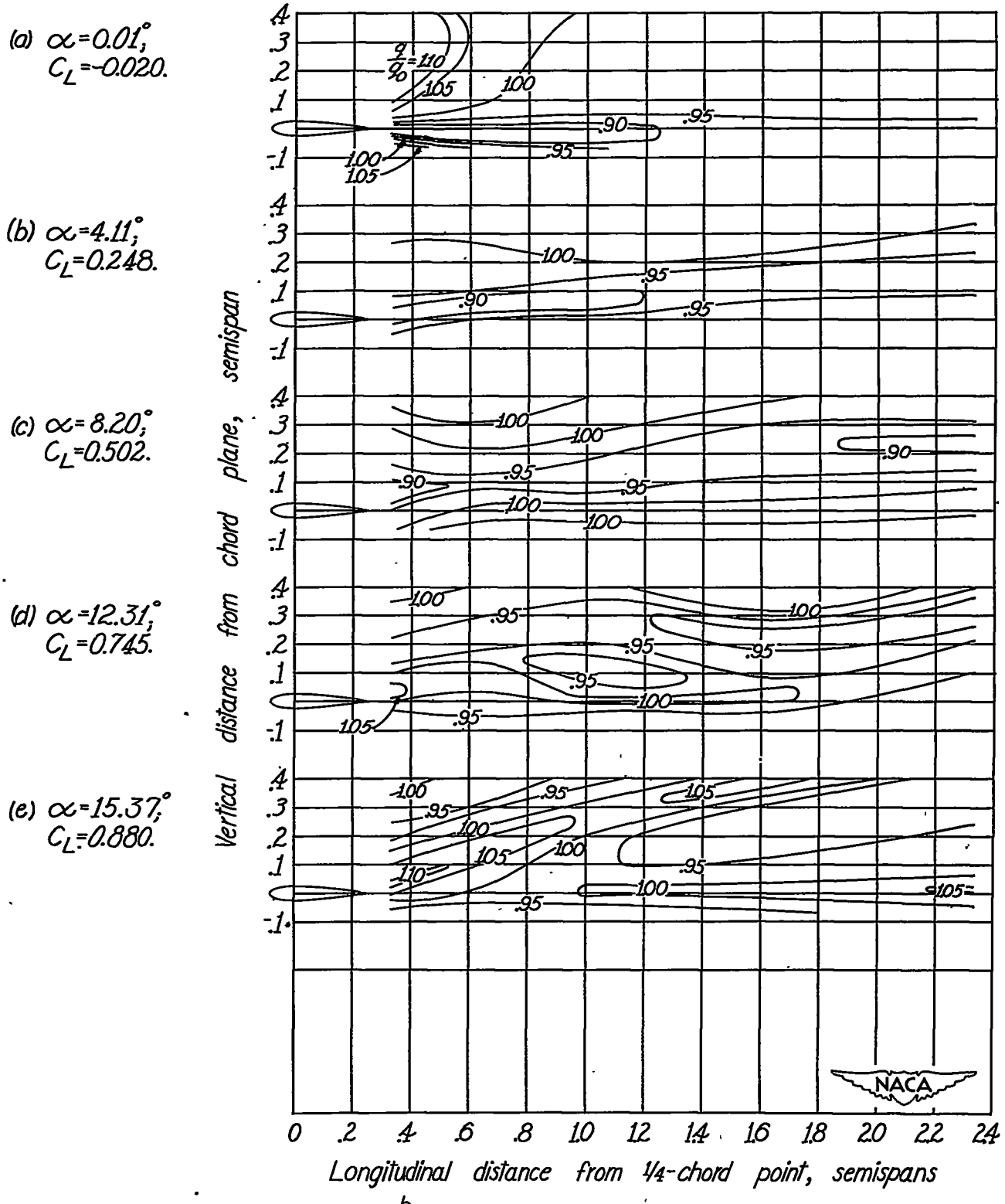

(d) $\frac{b}{2}$ spanwise station.

Figure 12.—Continued.

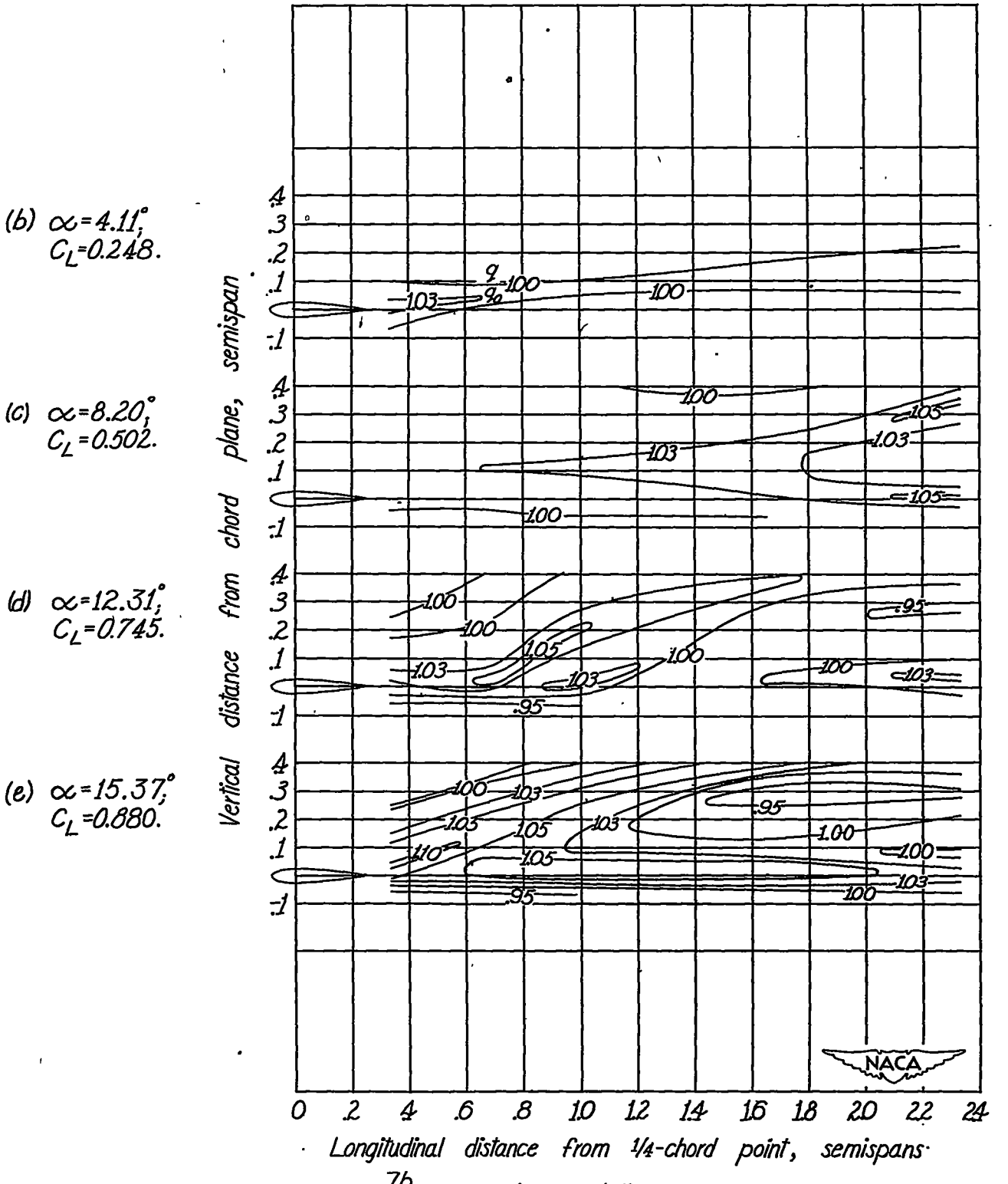

(e) $\frac{7b}{12}$ spanwise station.

Figure 12.-Concluded.

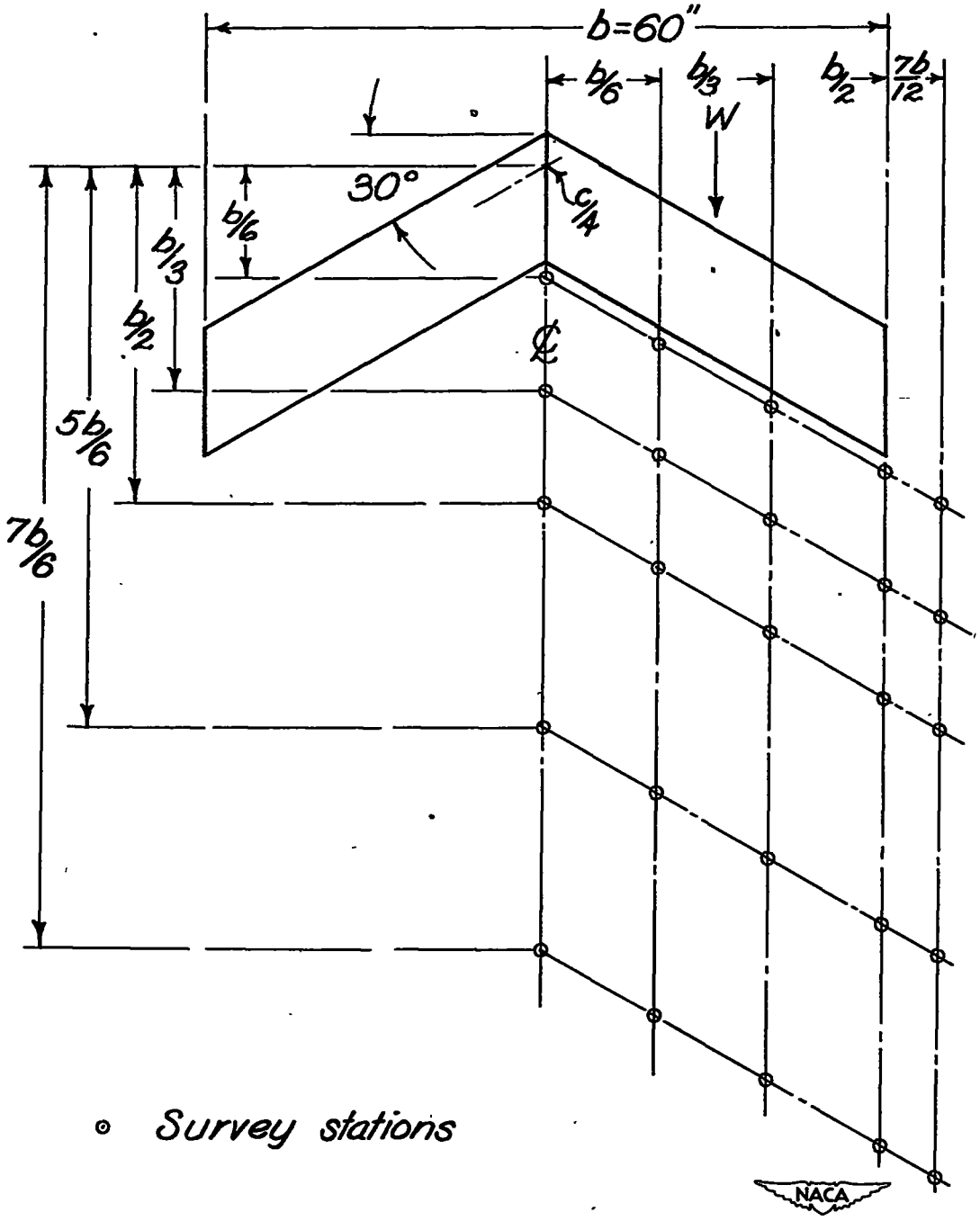

Figure 13.- Survey stations behind 30° sweptback wing of 60-inch span. A=5.2.

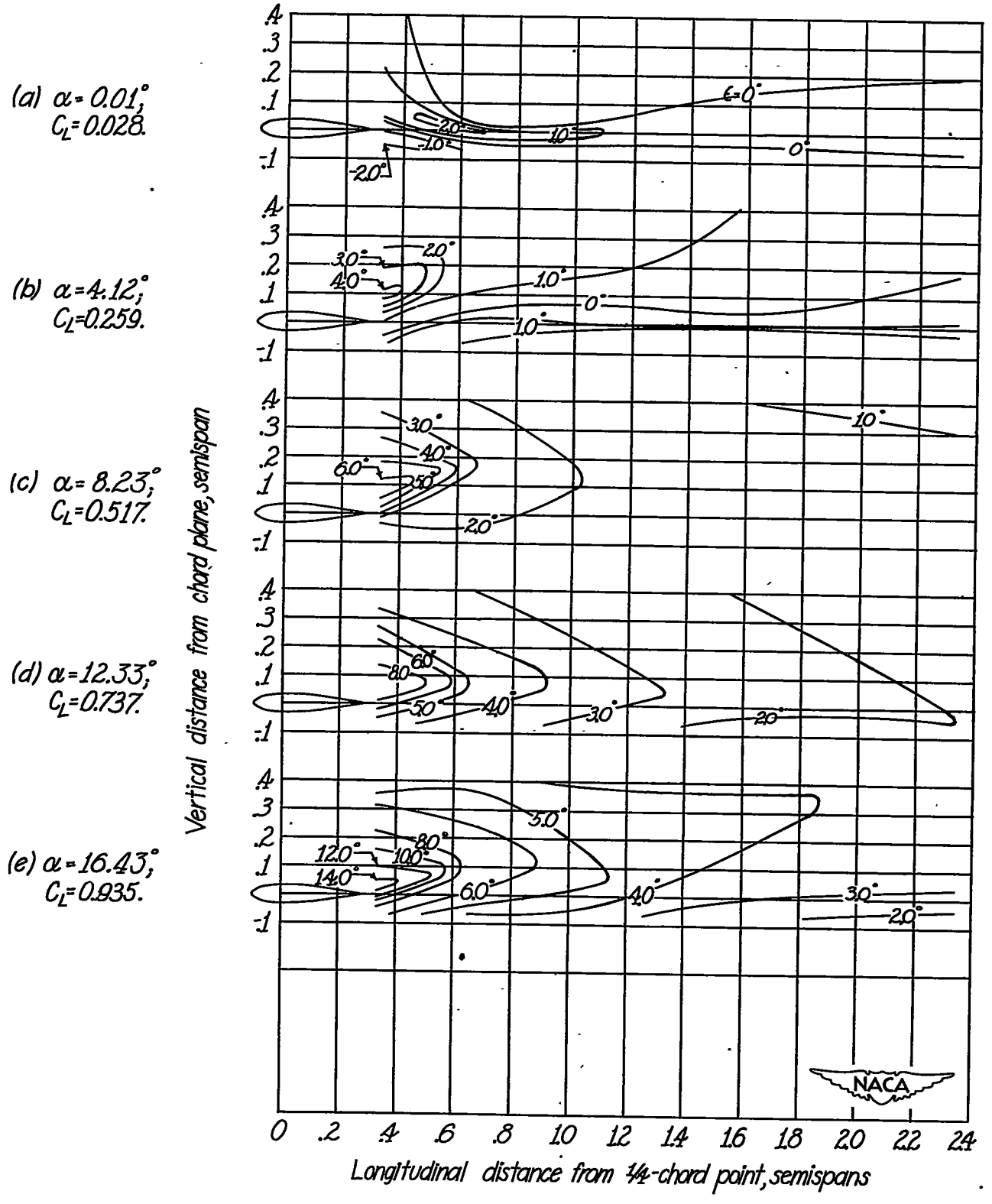

(a) Plane of symmetry.

Figure 14.- Downwash contours behind 30° sweptback wing of 60-inch span. A = 5.2.

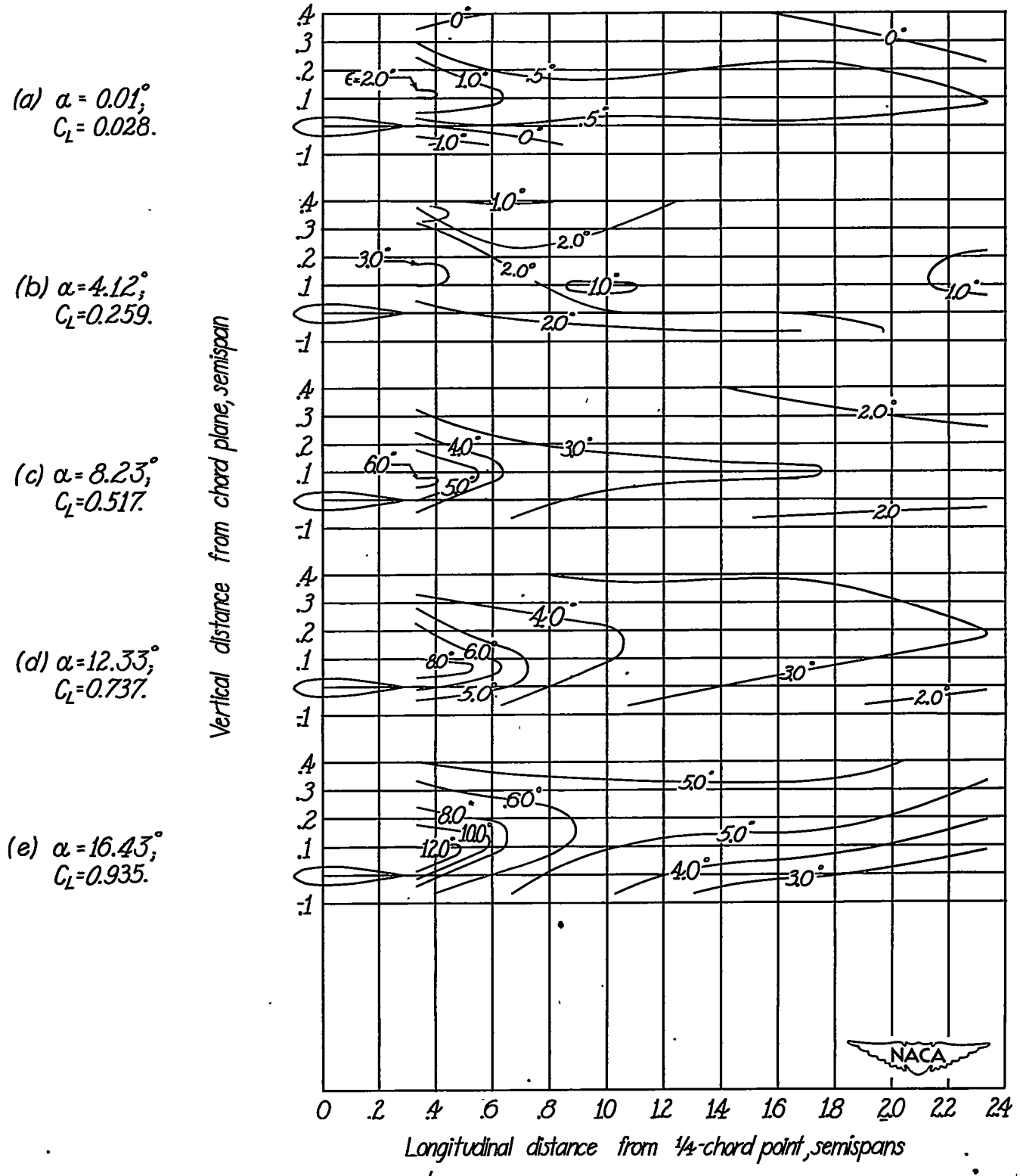

(b) $\frac{b}{6}$ spanwise station.

Figure 14.–Continued.

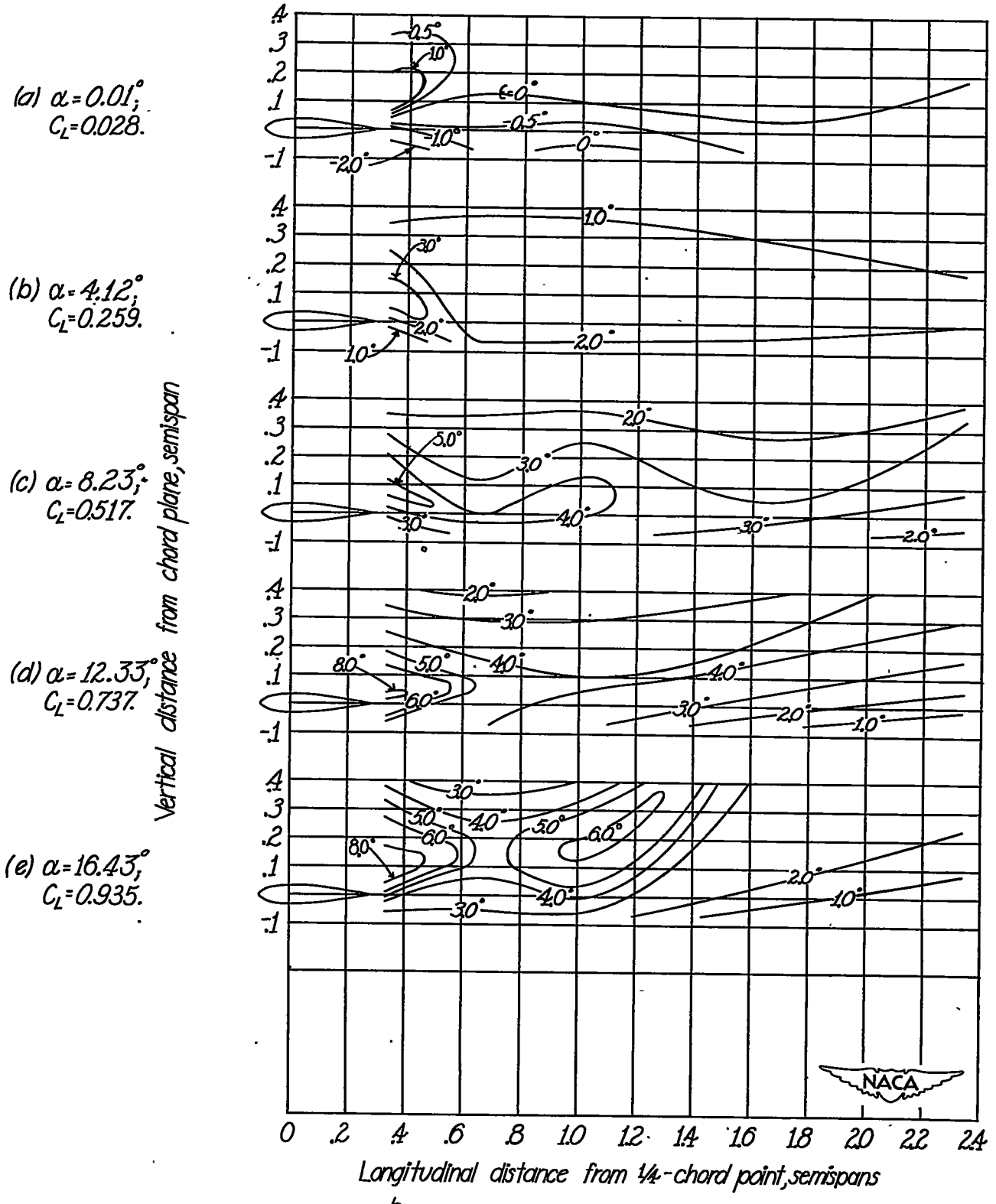

(c) $\frac{b}{3}$ spanwise station.

Figure 14.– Continued.

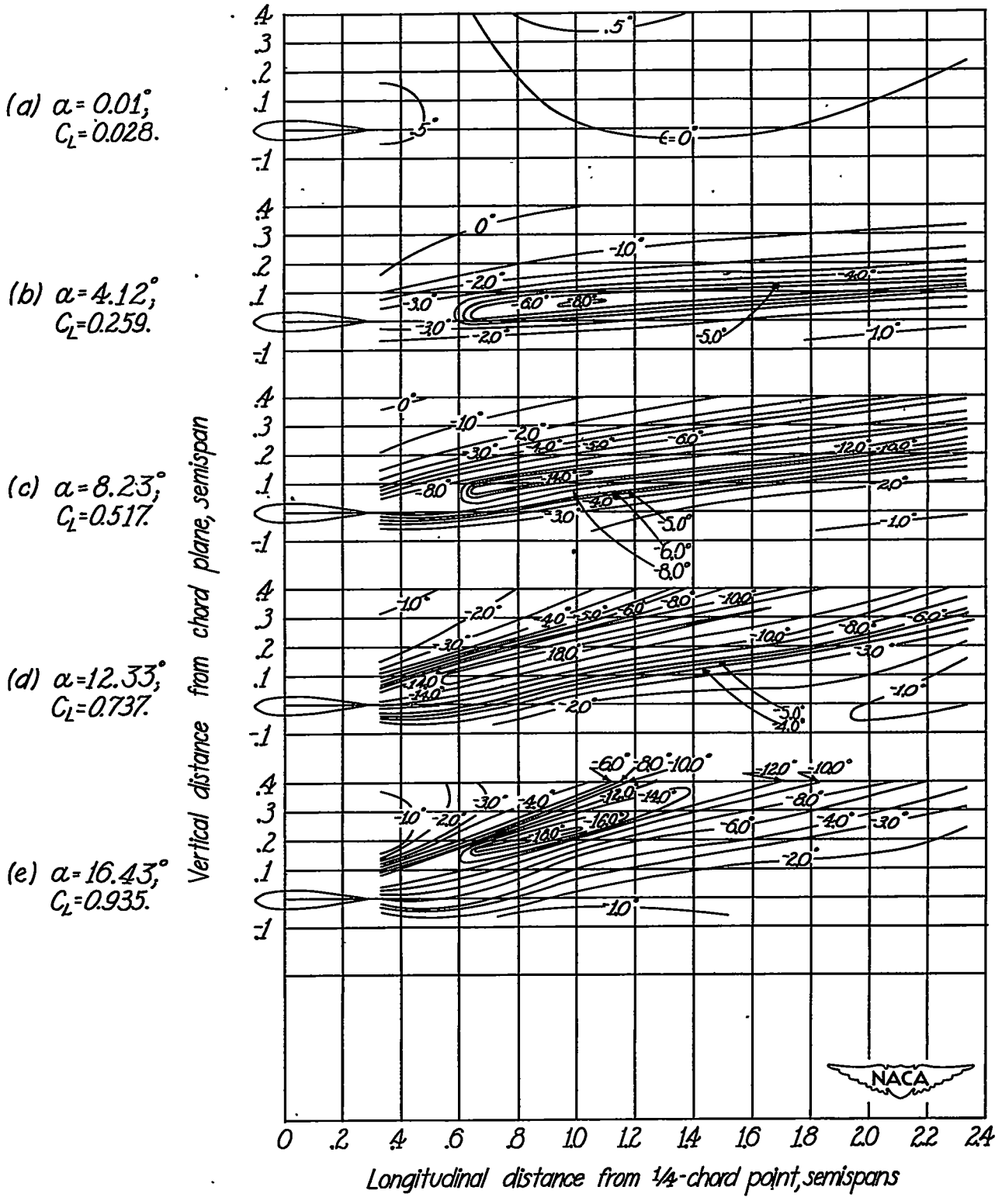

(d) $\frac{b}{2}$ spanwise station.

Figure 14.– Continued.

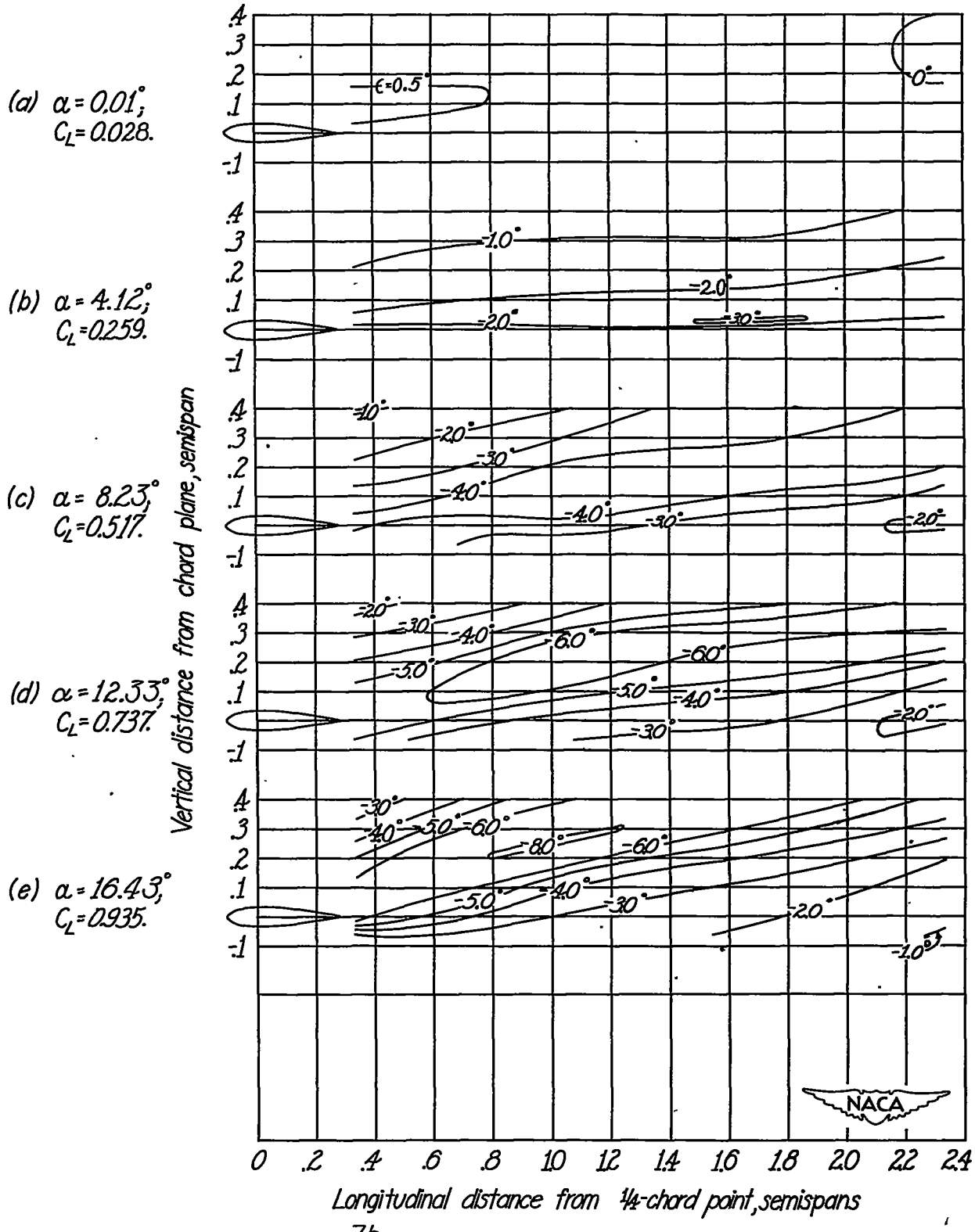

(e) $\frac{7b}{12}$ spanwise station.

Figure 14.-Concluded.

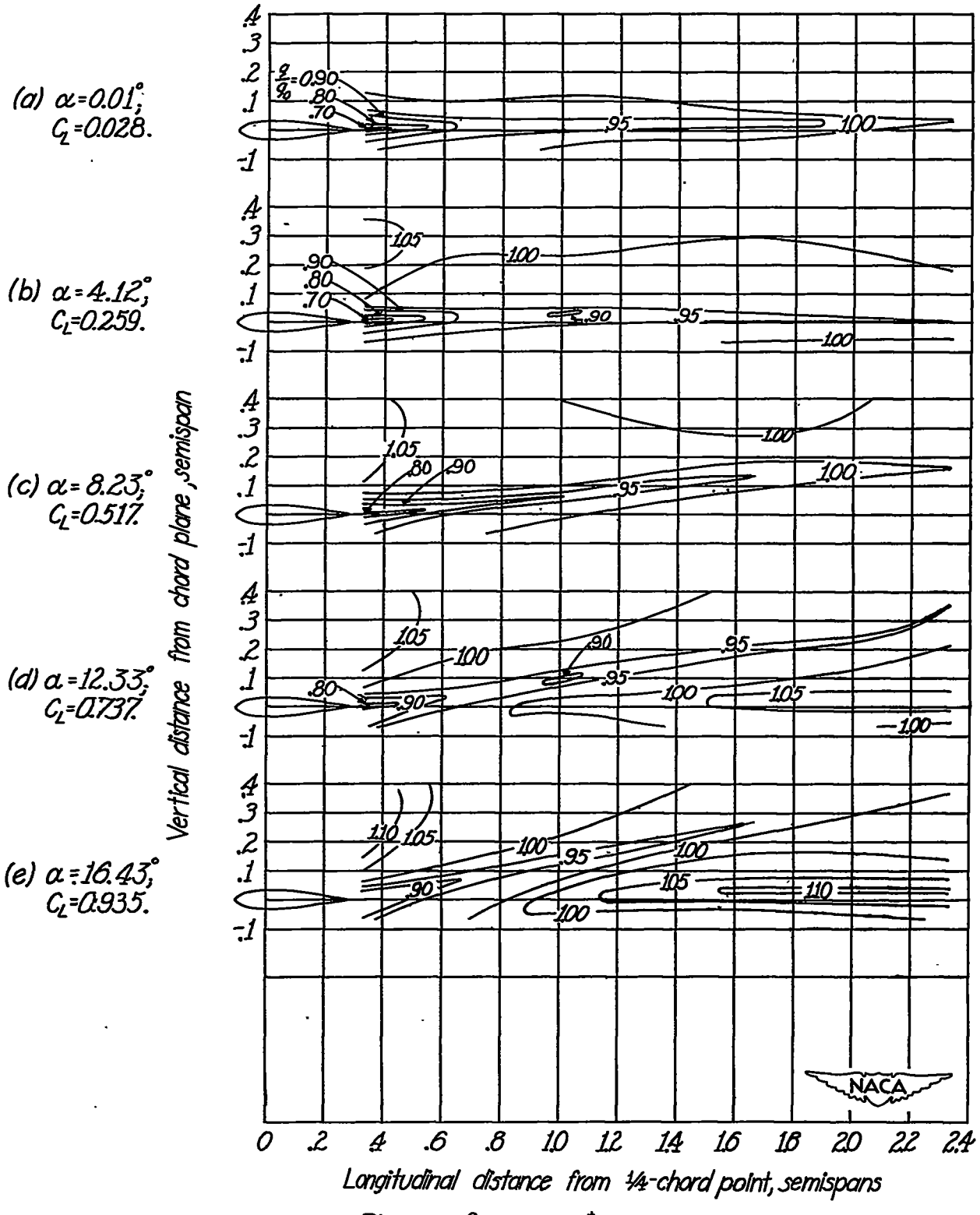

(a) Plane of symmetry.

Figure 15.-Dynamic-pressure-ratio contours behind 30° sweptback wing of 60-inch span. A= 5.2.

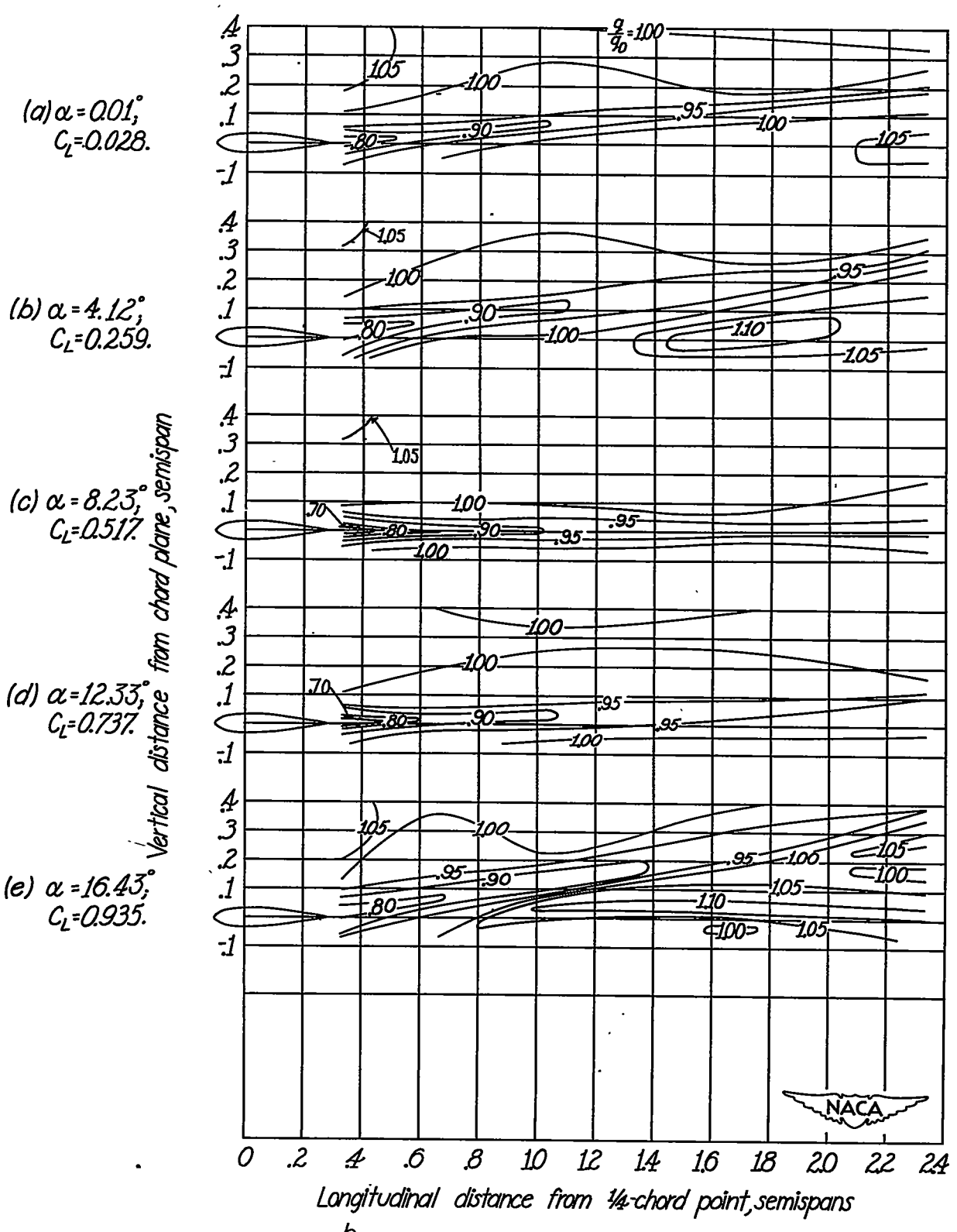

(b) $\frac{b}{6}$ spanwise station.

Figure 15.–Continued.

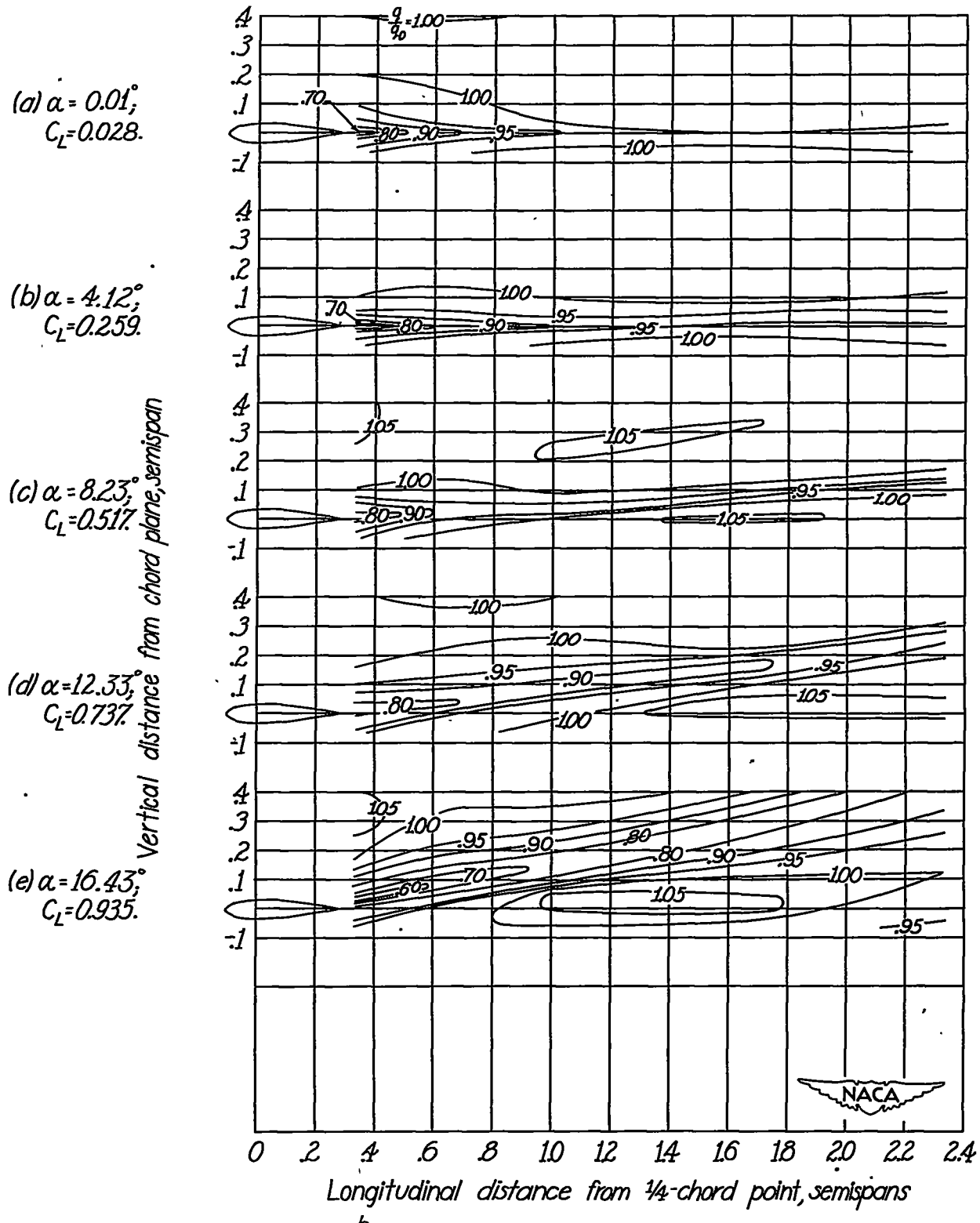

(c) $\frac{b}{3}$ spanwise station.

Figure 15.–Continued.

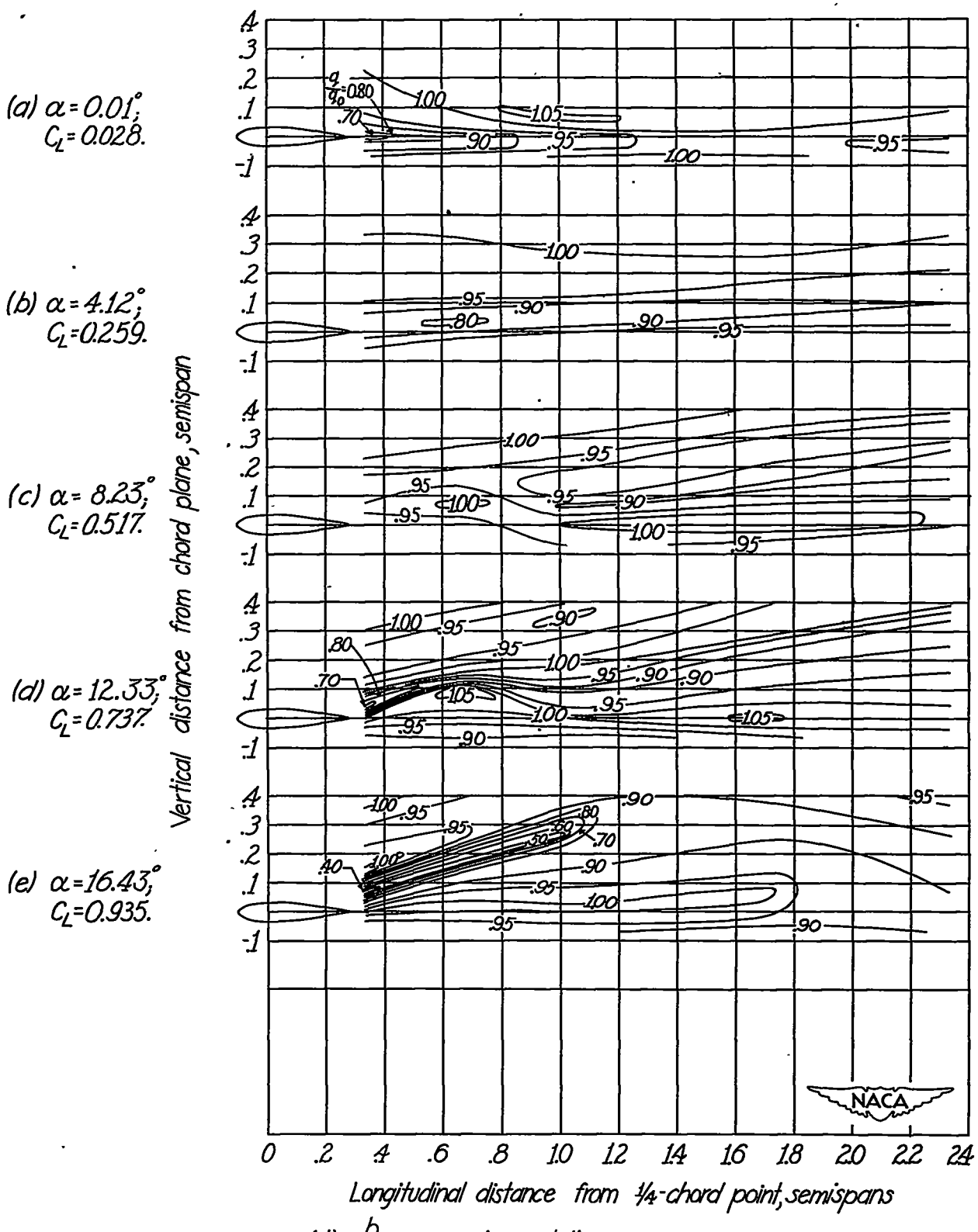

(d) $\frac{b}{2}$ spanwise station.

Figure 15.-Continued.

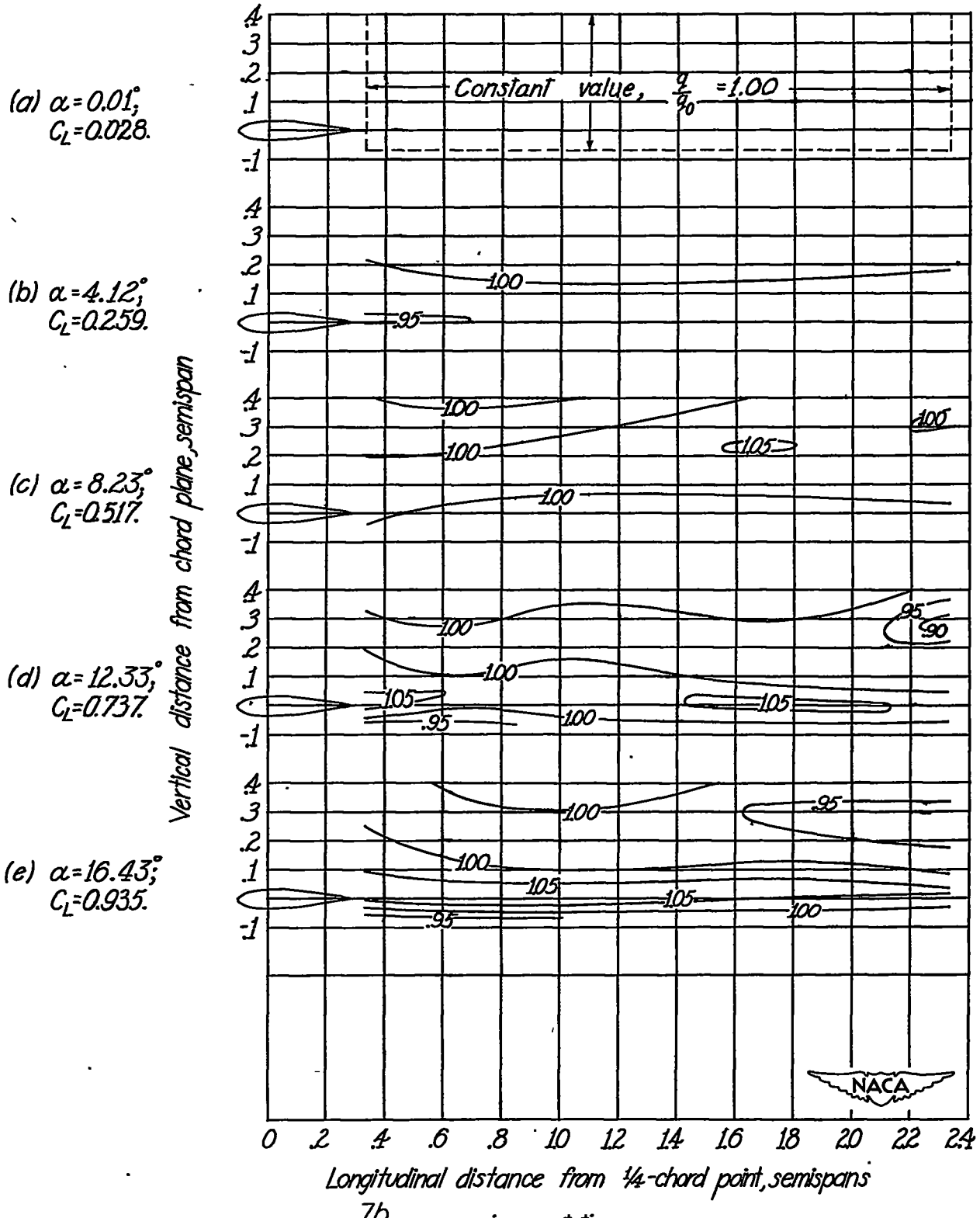

(e) $\frac{7b}{12}$ spanwise station.

Figure 15.- Concluded.

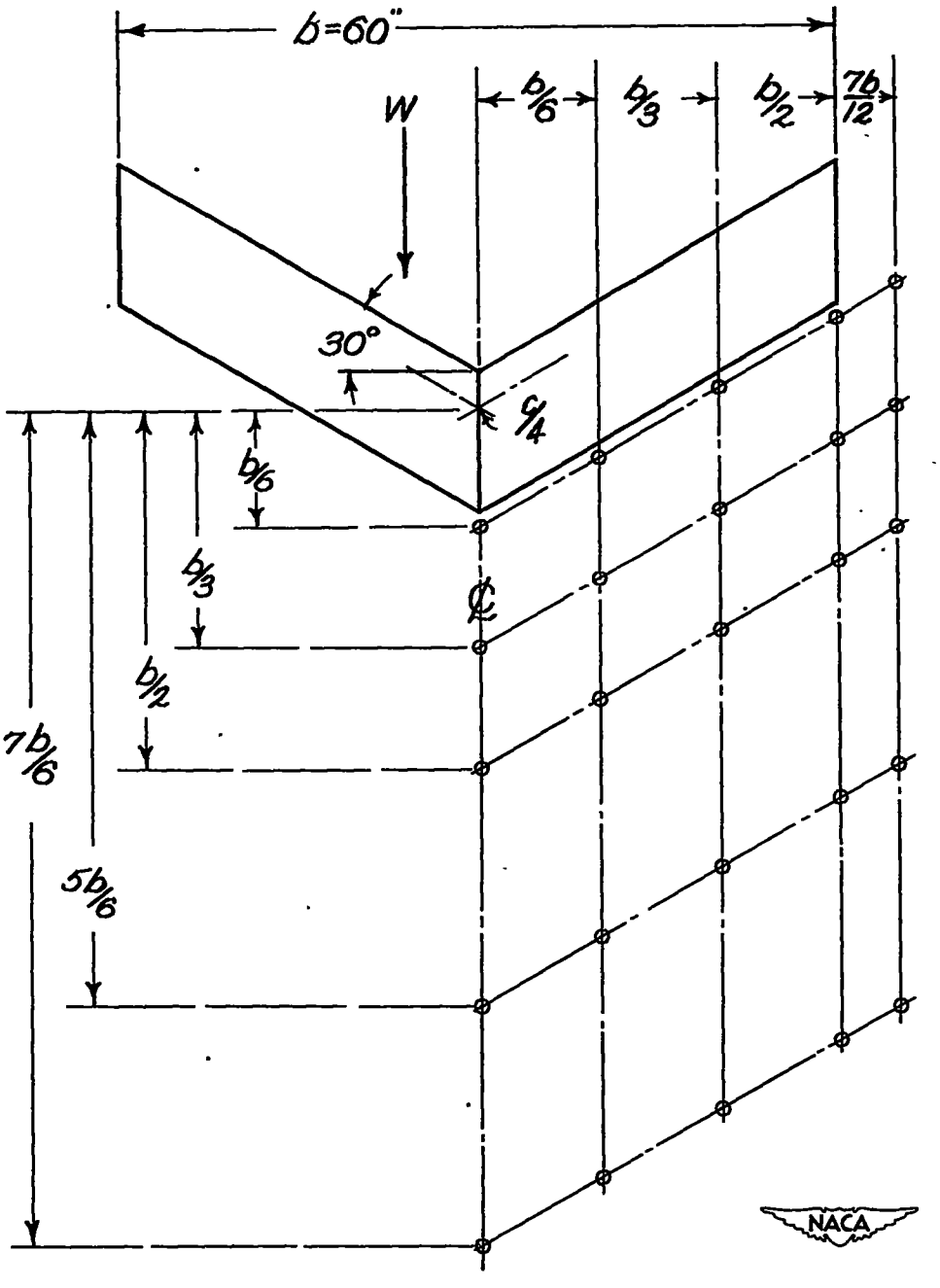

∘ Survey stations

Figure 16.-Survey stations behind 30° sweptforward wing of 60-inch span. A=5.2.

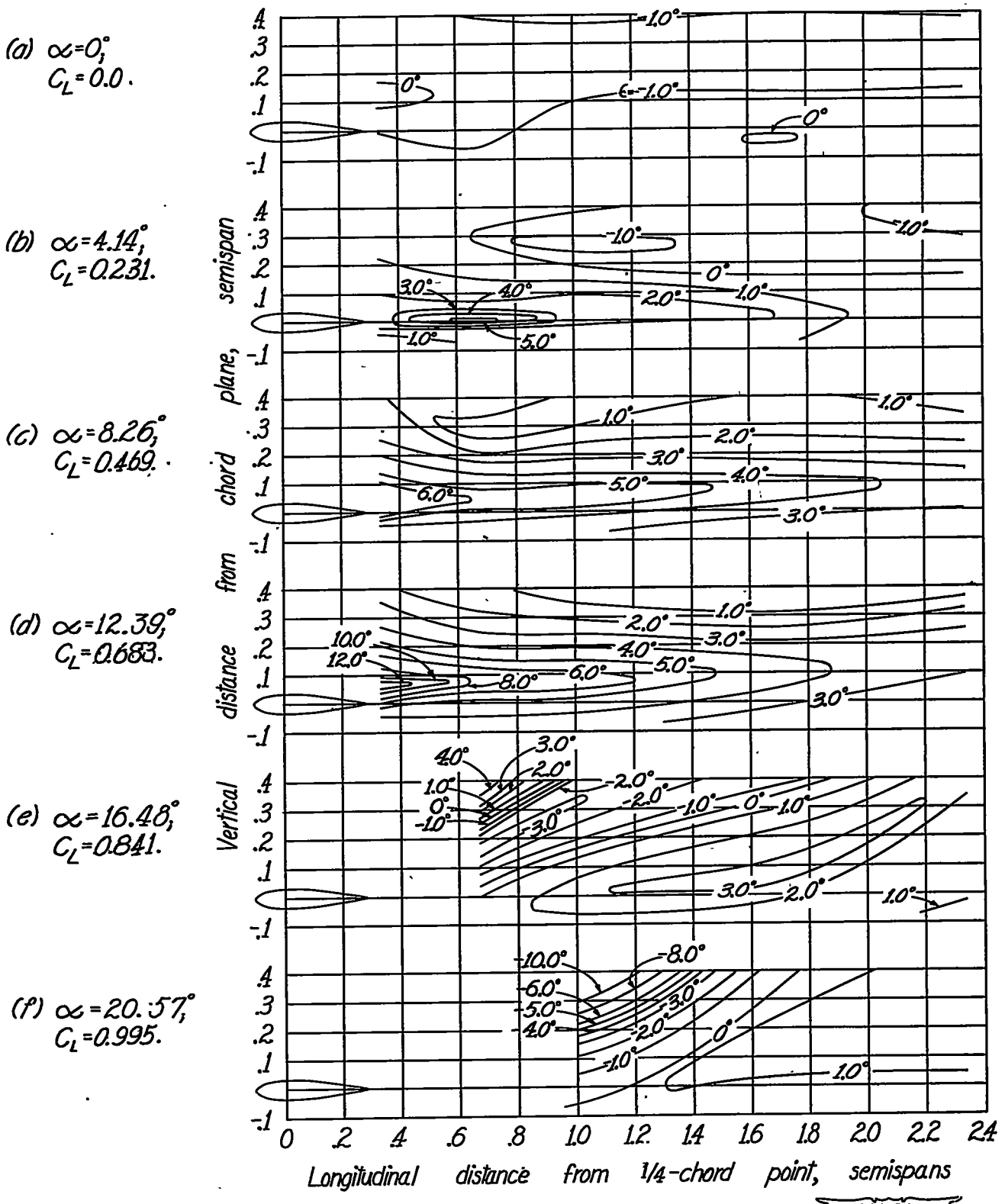

(a) Plane of symmetry.

Figure 17.-Downwash contours behind 30° sweptforward wing of 60-inch span. A=5.2.

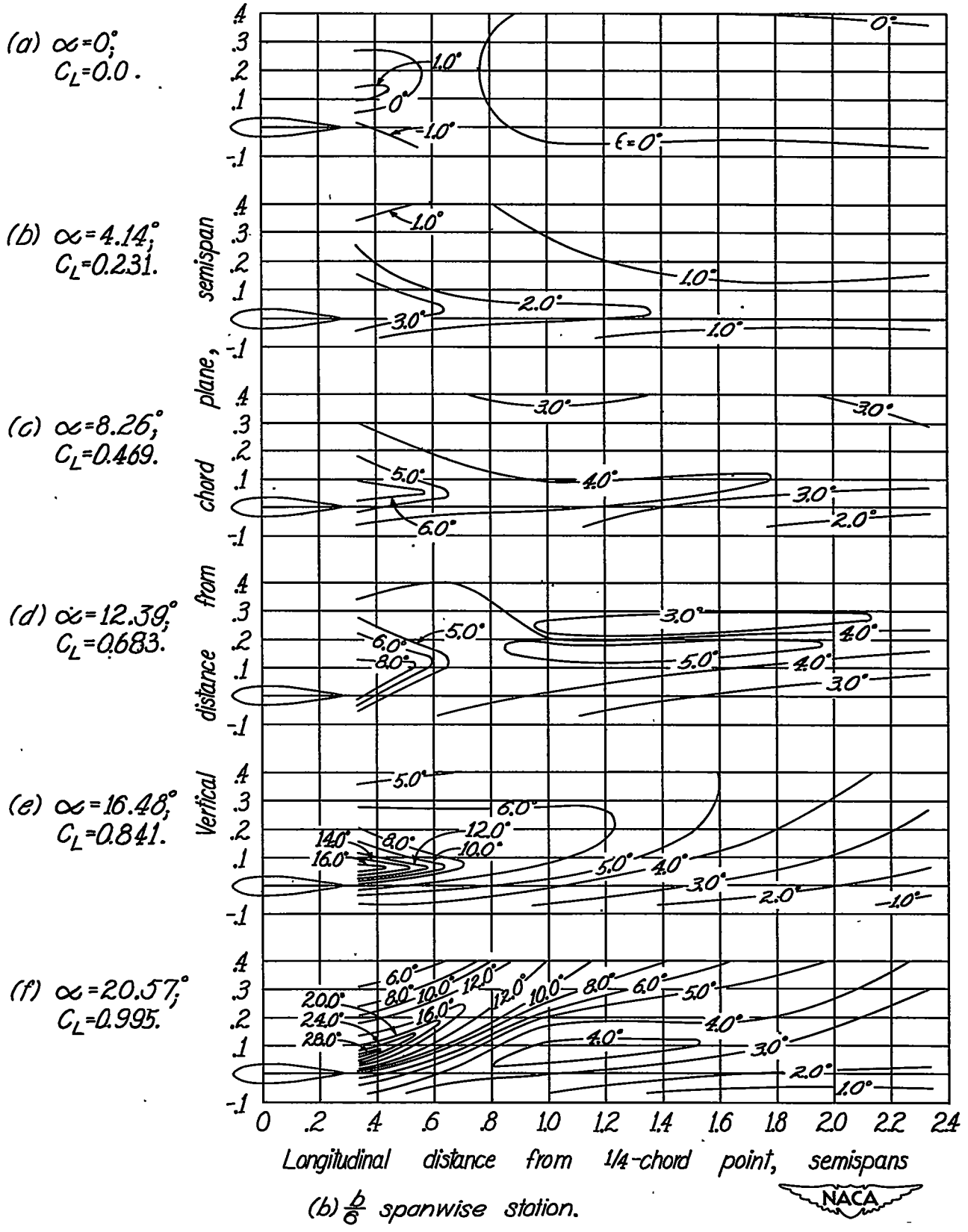

Figure 17.-Continued.

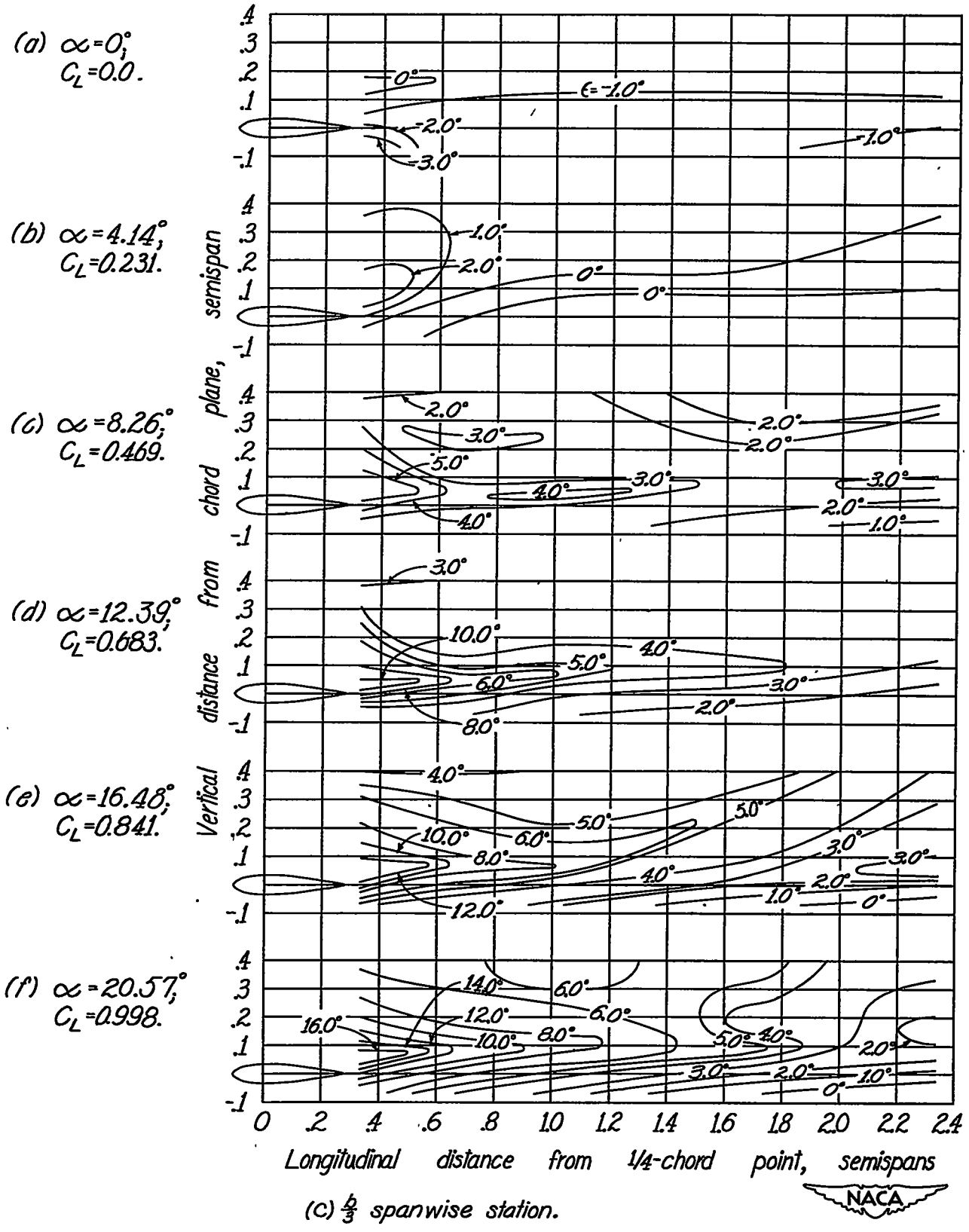

(c) $\frac{b}{3}$ spanwise station.

Figure 17.-Continued.

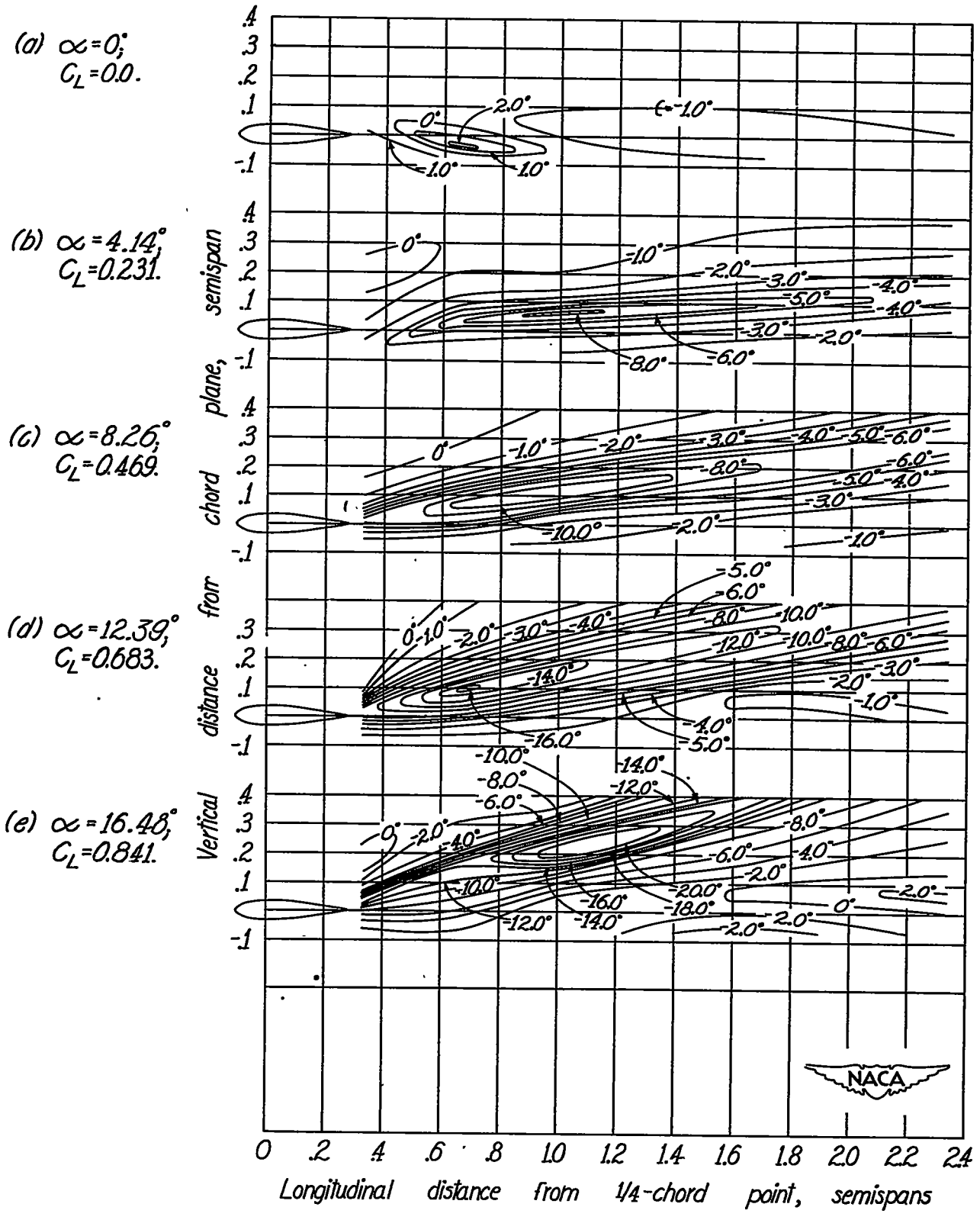

(d) $\frac{b}{2}$ spanwise station.

Figure 17.-Continued.

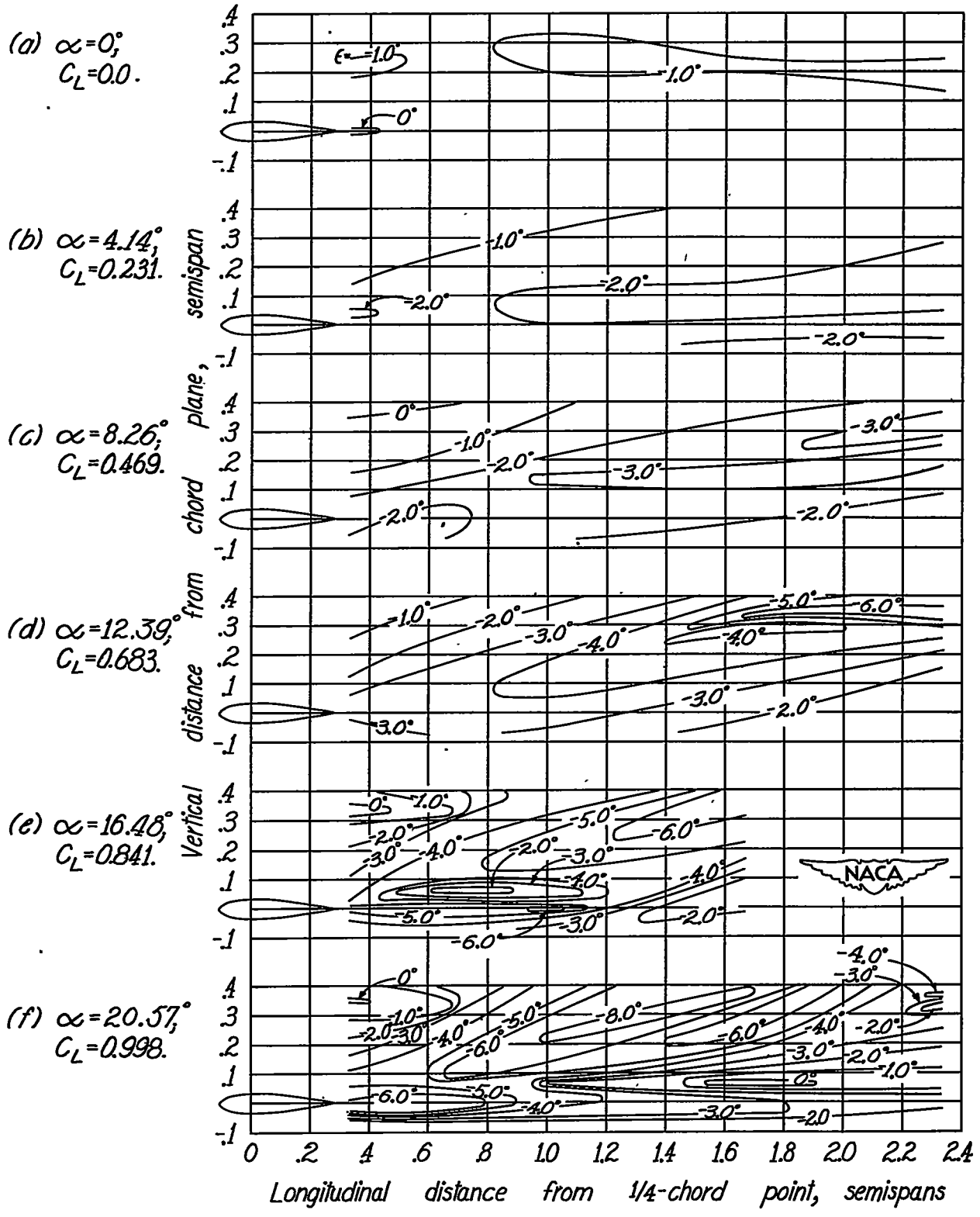

(e) $\frac{7b}{12}$ spanwise station.

Figure 17.- Concluded.

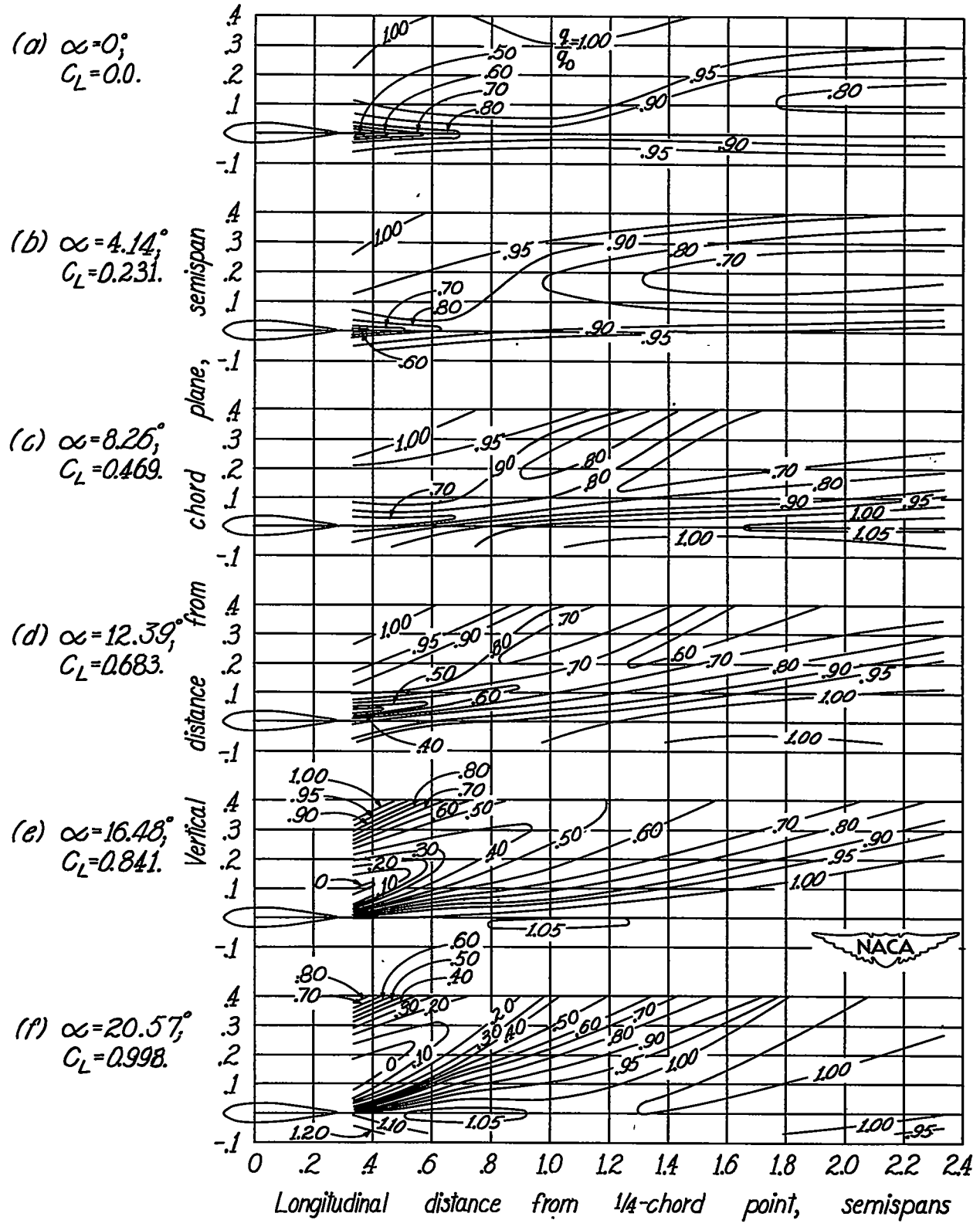

(a) Plane of symmetry.

Figure 18.-Dynamic-pressure-ratio contours behind 30° sweptforward wing of 60-inch span. A=5.2.

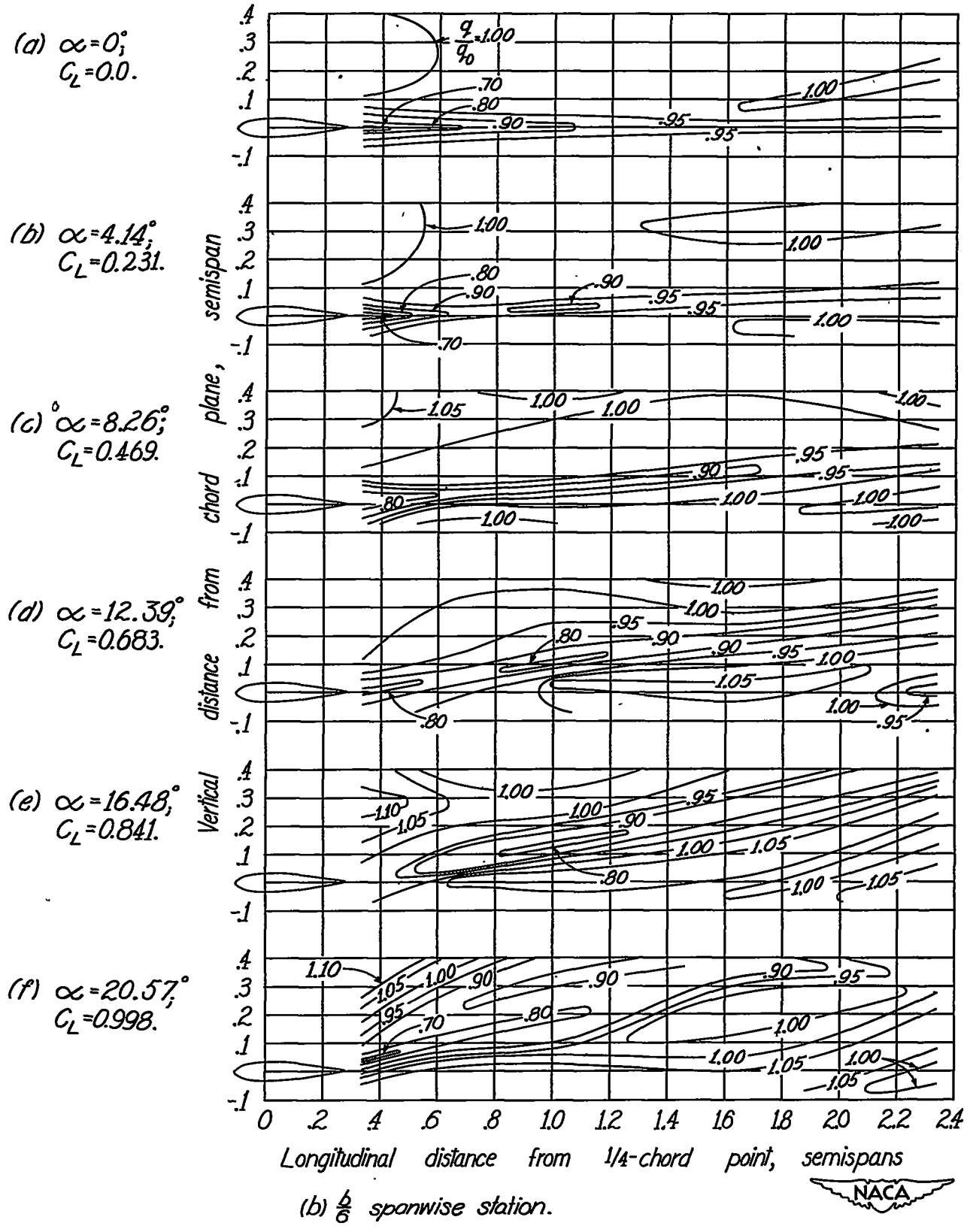

(b) $\frac{b}{6}$ spanwise station.

Figure 18.- Continued.

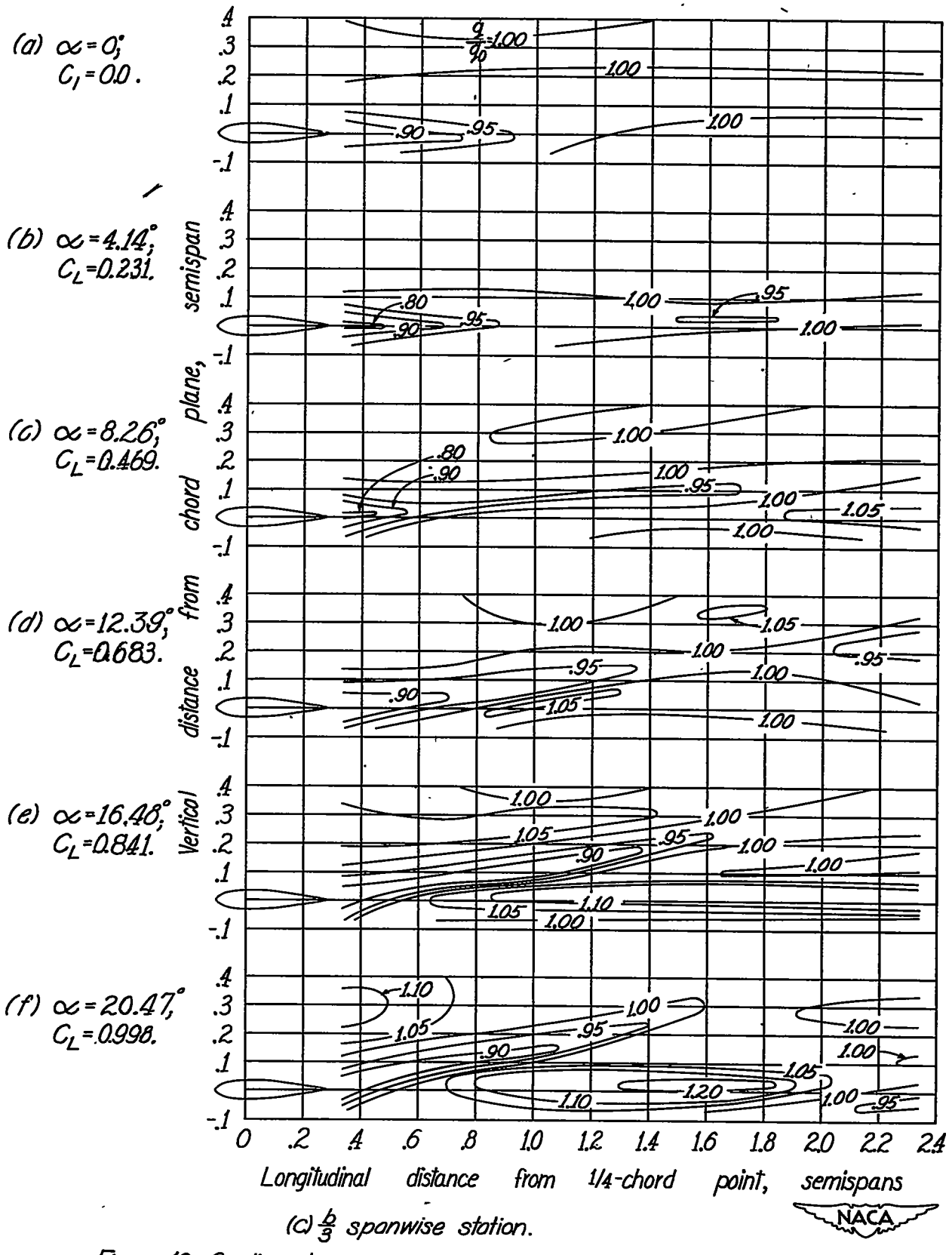

(c) $\frac{b}{3}$ spanwise station.

Figure 18.-Continued.

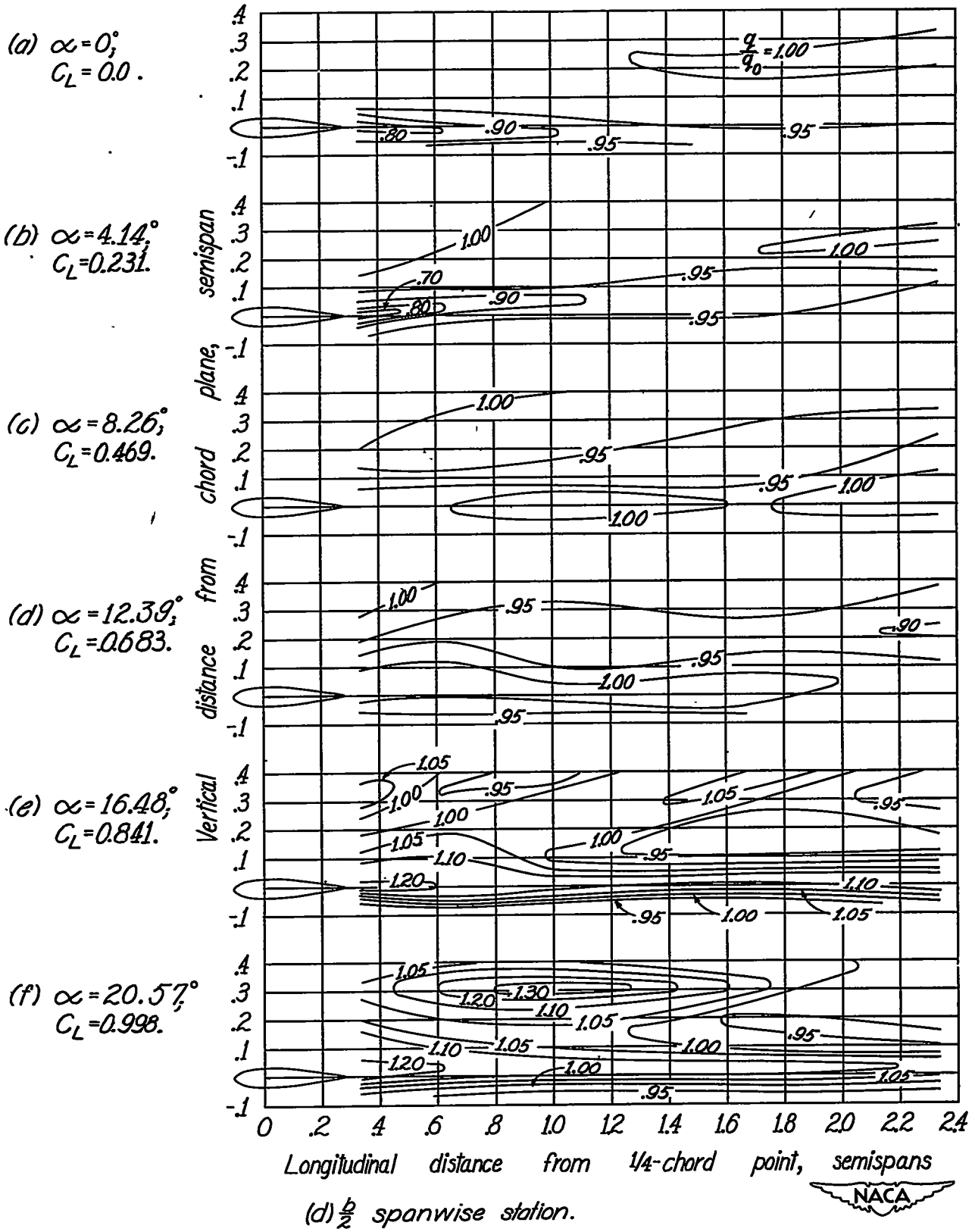

(d) $\frac{b}{2}$ spanwise station.

Figure 18.-Continued.

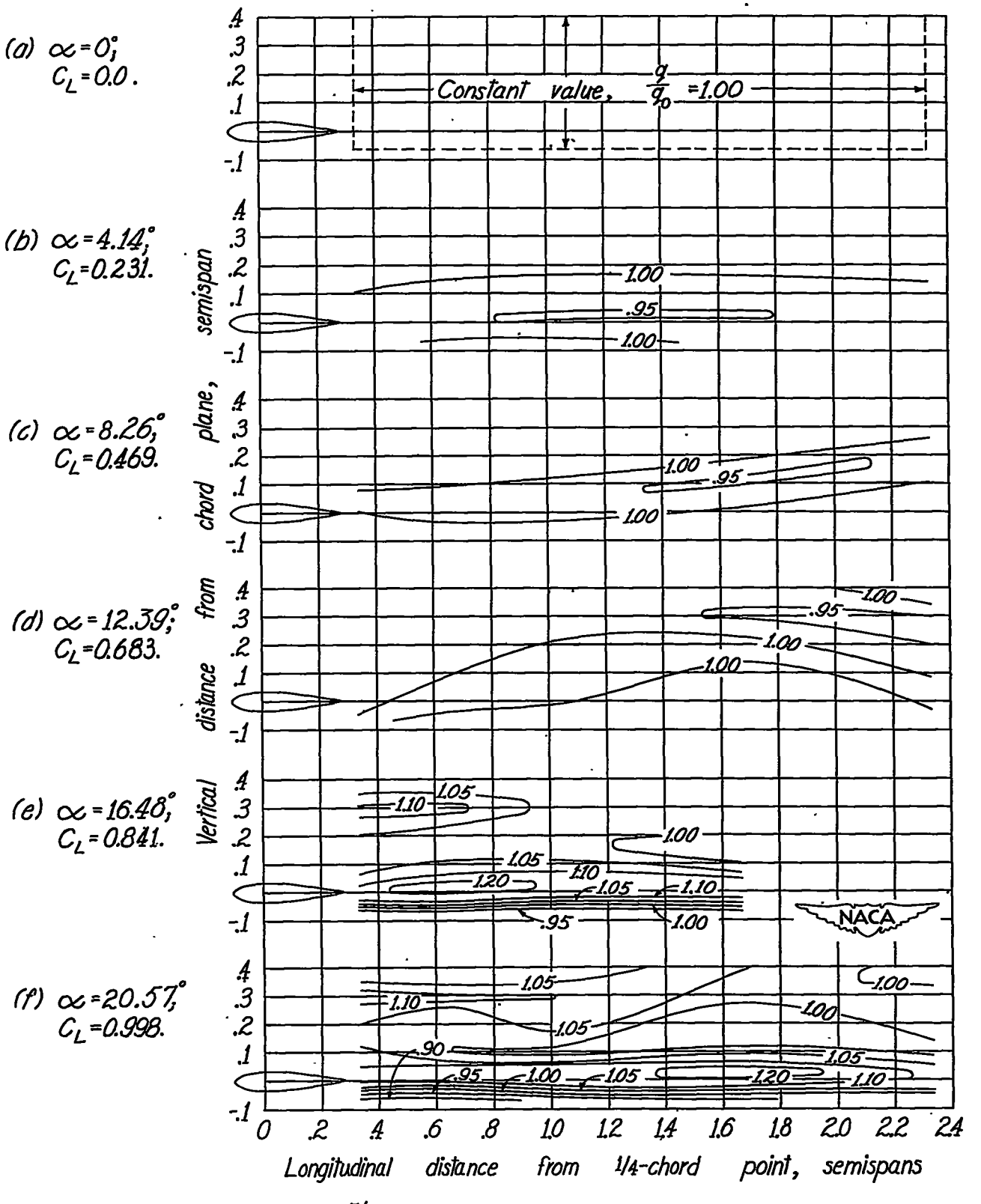

(e) $\frac{7b}{12}$ spanwise station.

Figure 18.-Concluded.

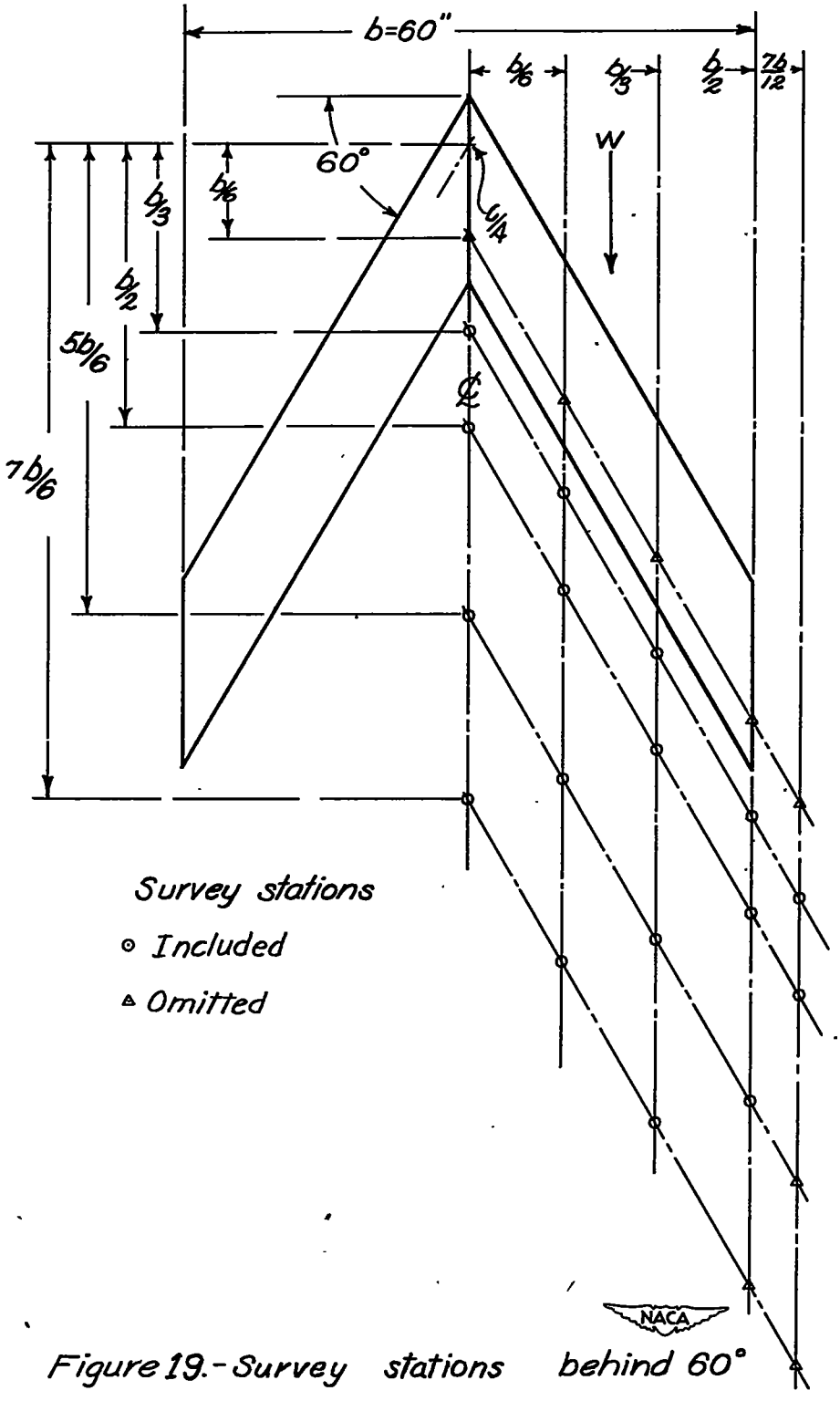

Figure 19.- Survey stations behind 60° sweptback wing of 60-inch span. A=3.

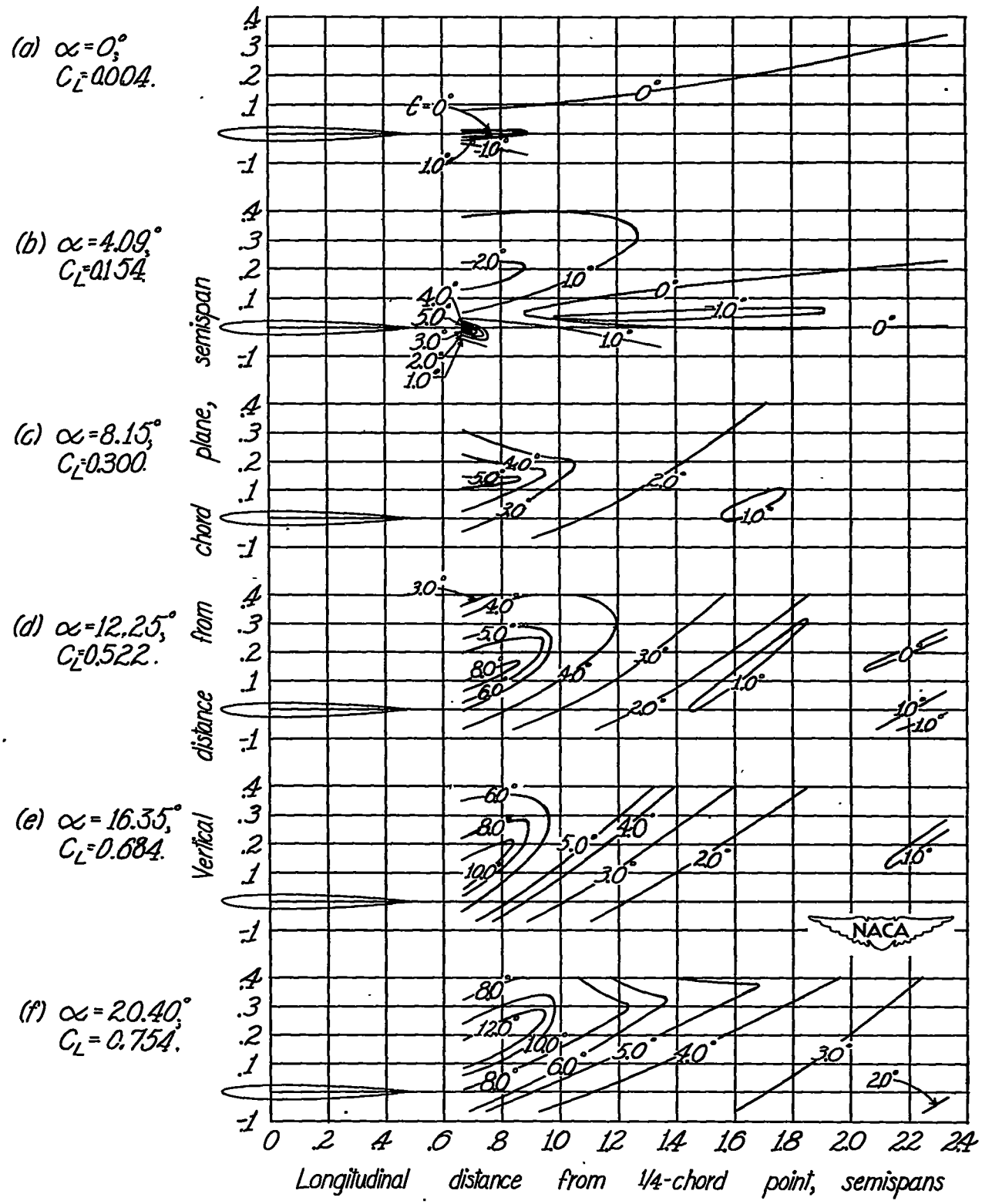

(a) Plane of symmetry.

Figure 20.—Downwash contours behind 60° sweptback wing of 60-inch span. A=3.

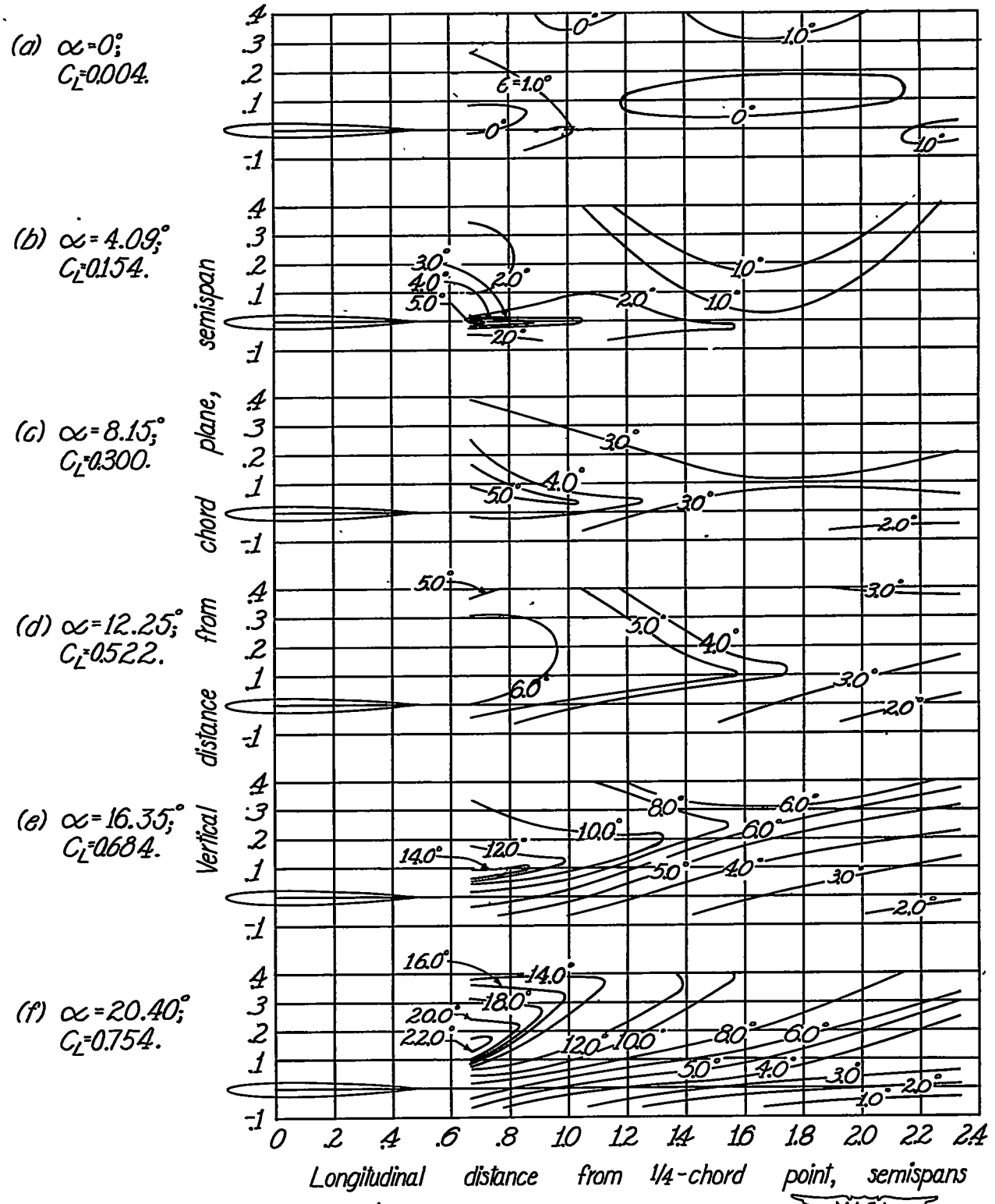

(b) $\frac{b}{6}$ spanwise station.

Figure 20.- Continued.

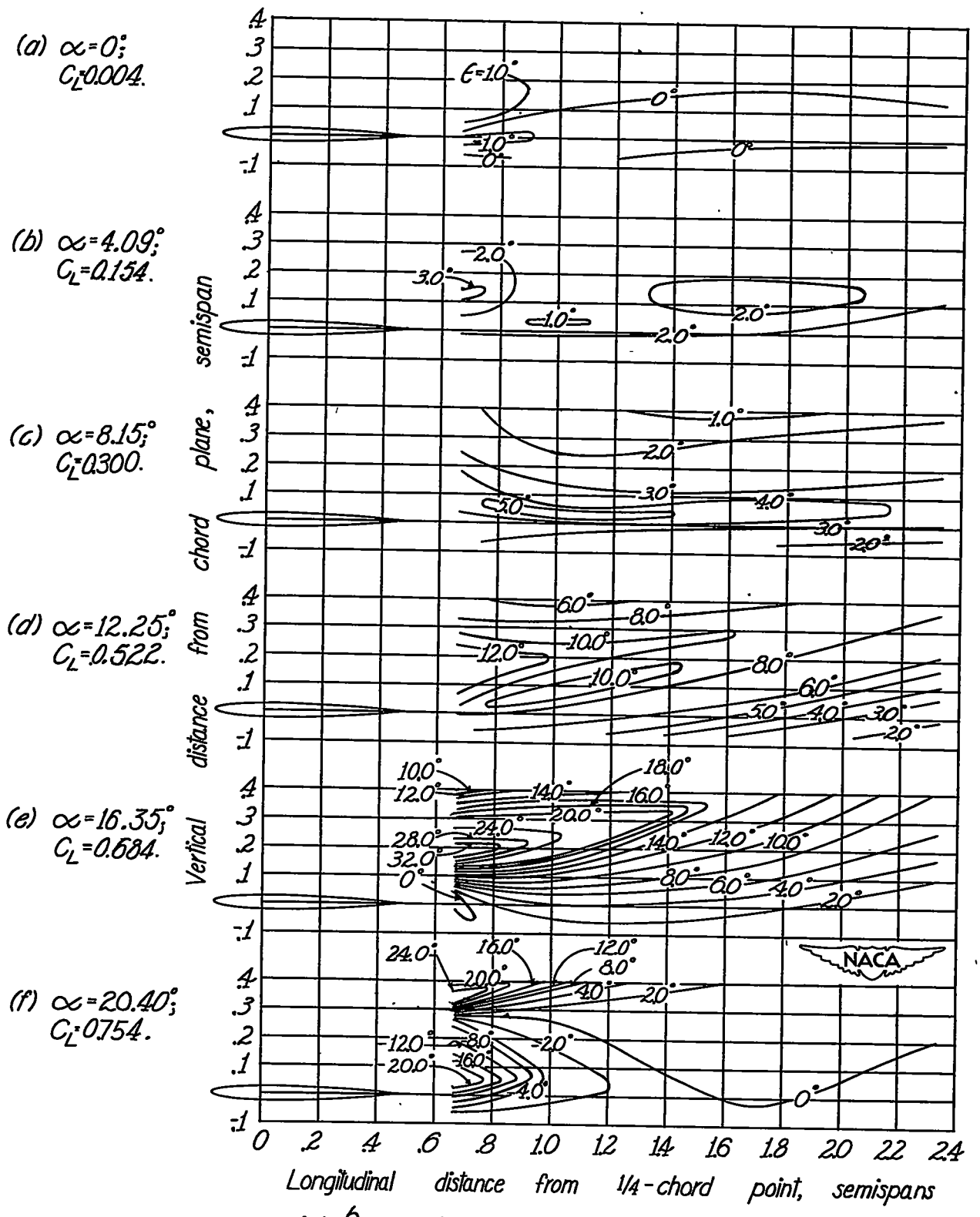

(c) $\frac{b}{3}$ spanwise station.

Figure 20.- Continued.

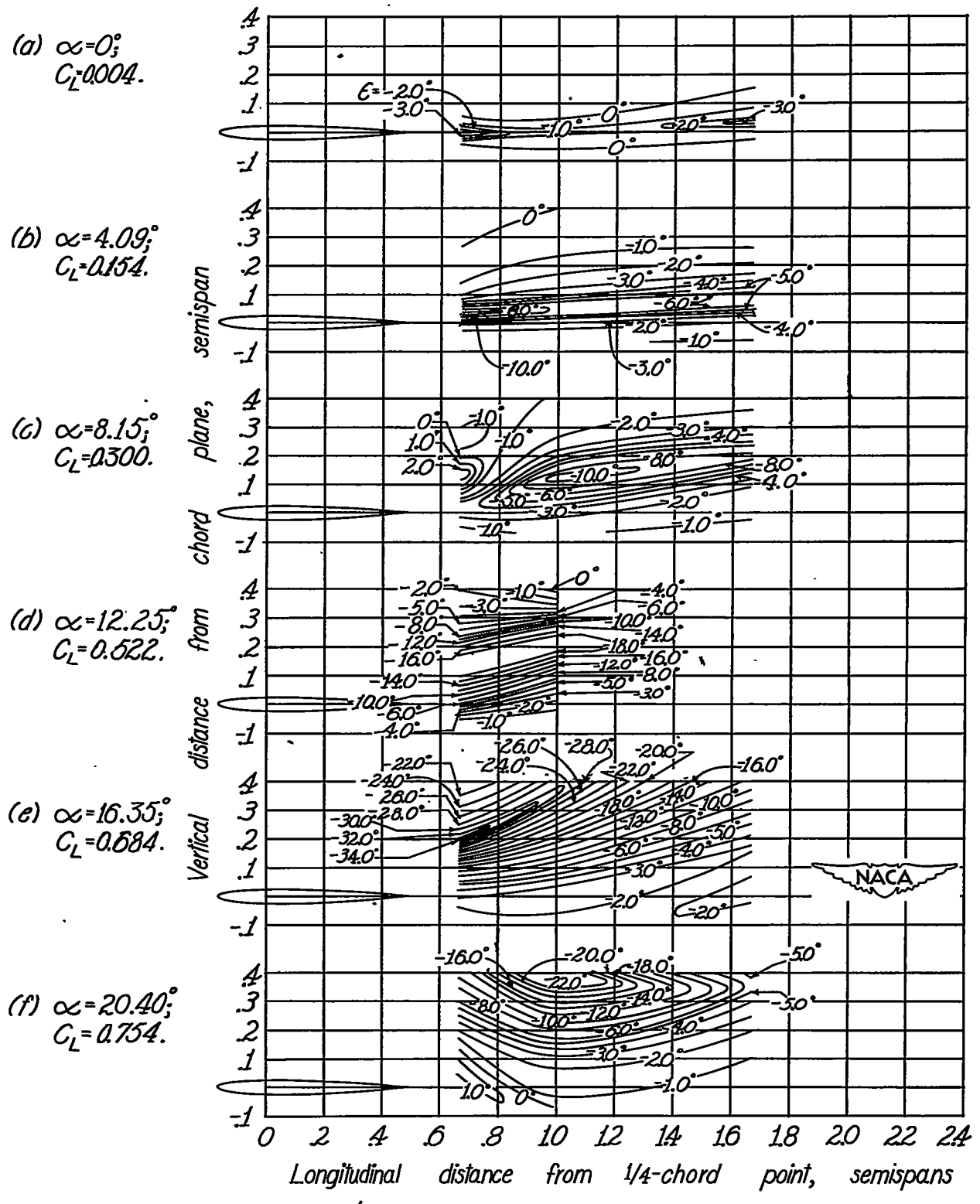

(d) $\frac{b}{2}$ spanwise station.

Figure 20.- Continued.

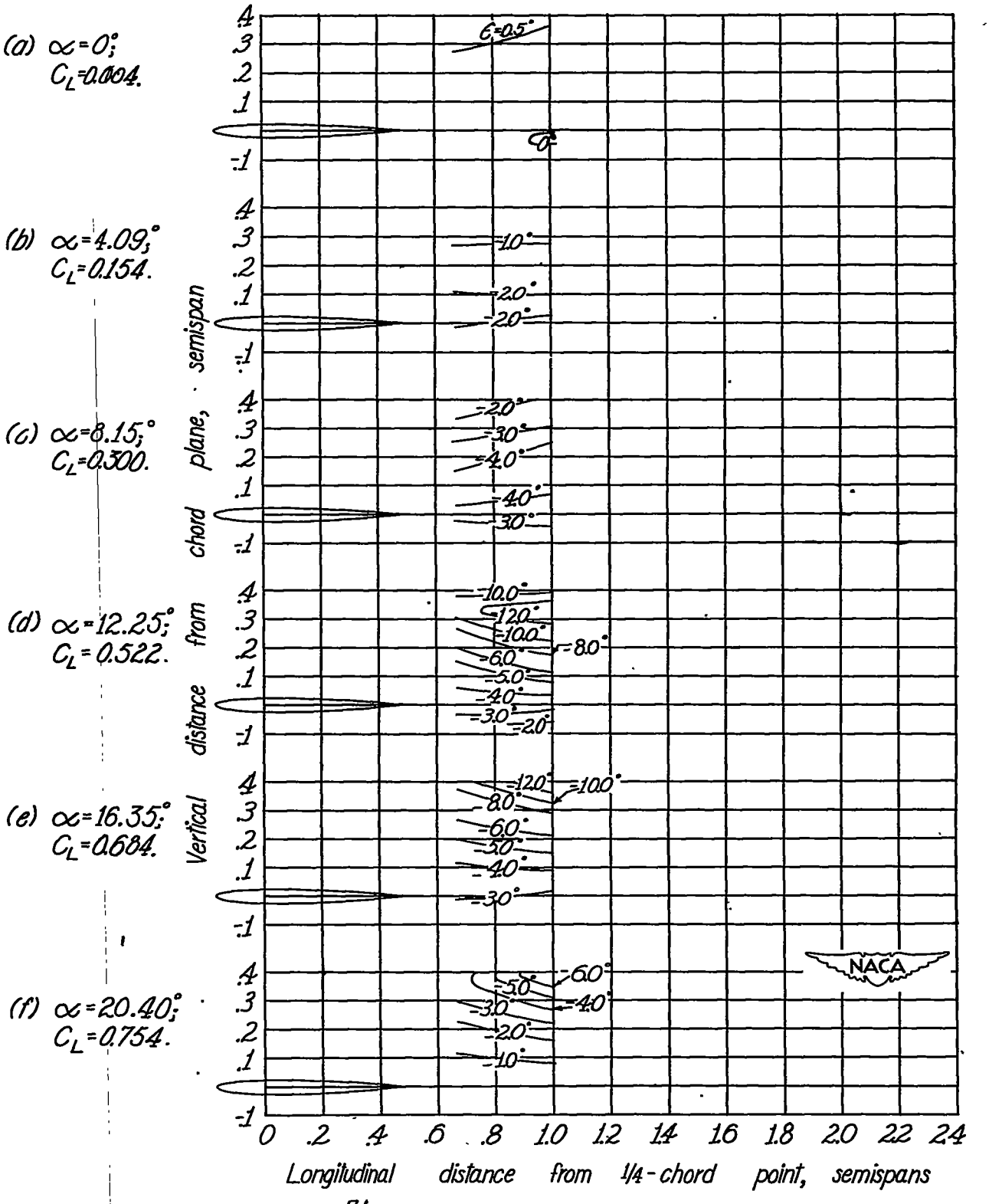

(e) $\frac{7b}{12}$ spanwise station.

Figure 20.- Concluded.

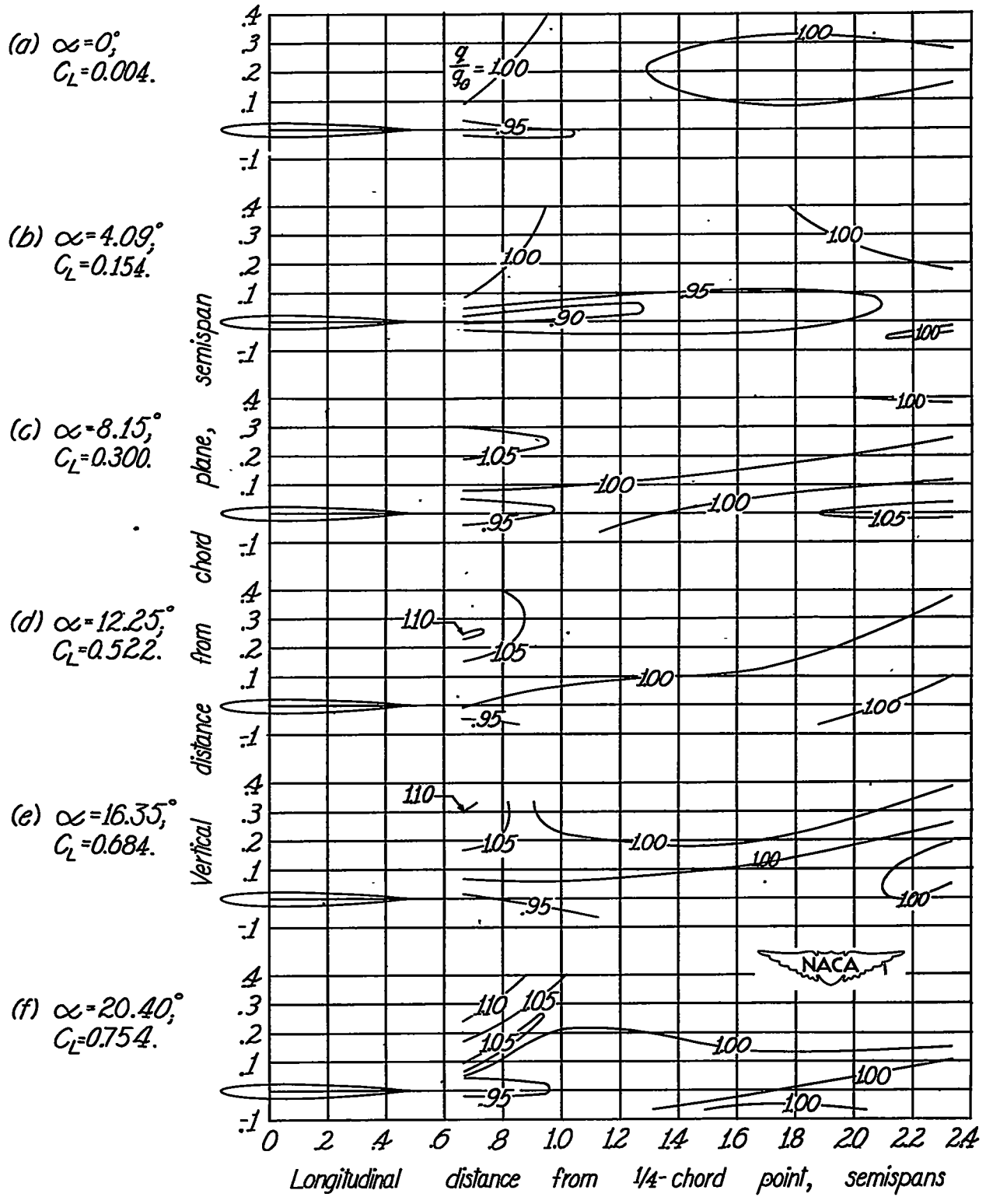

(a) Plane of symmetry.

Figure 21.- Dynamic-pressure-ratio contours behind 60° sweptback wing of 60-inch span. A=3.

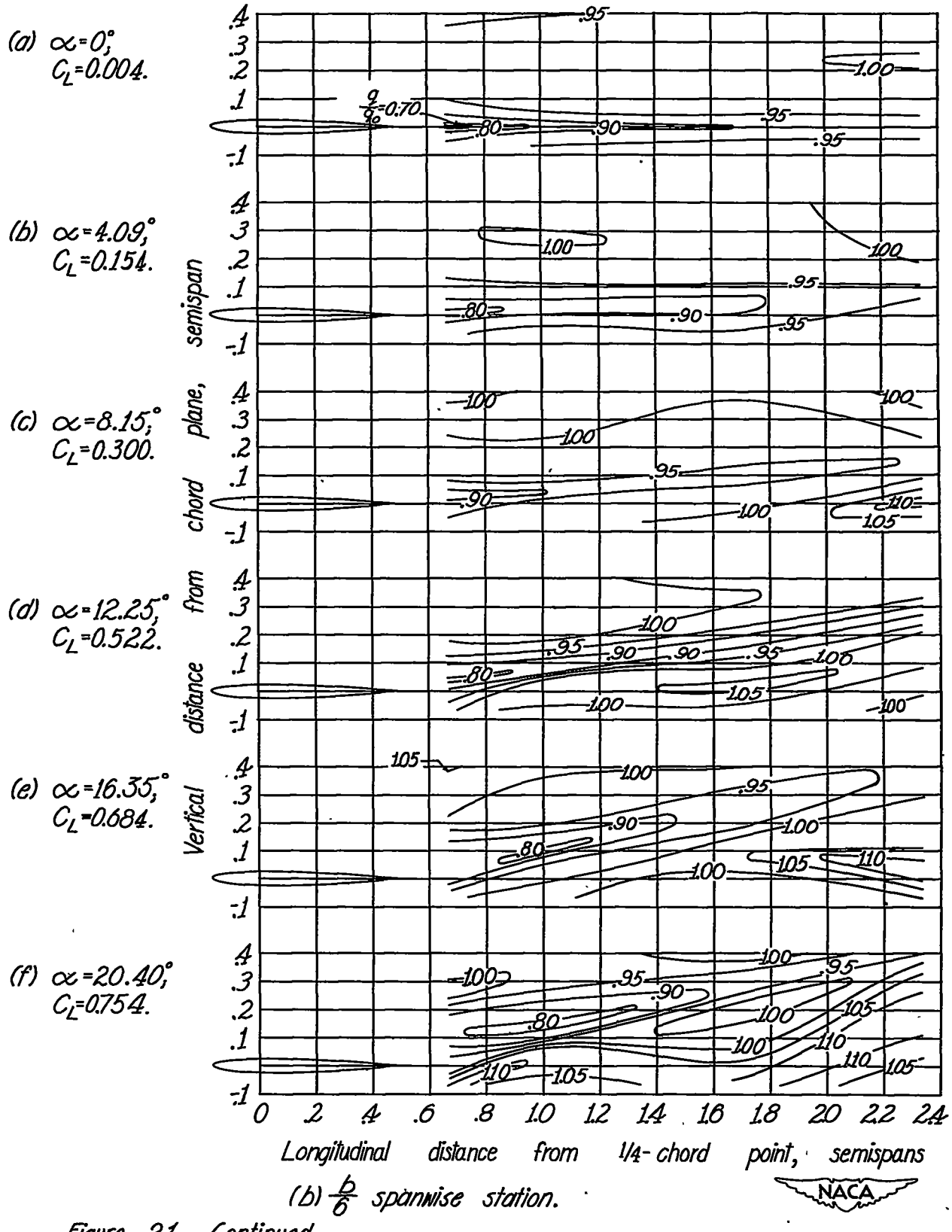

(b) $\frac{b}{6}$ spanwise station.

Figure 21.- Continued.

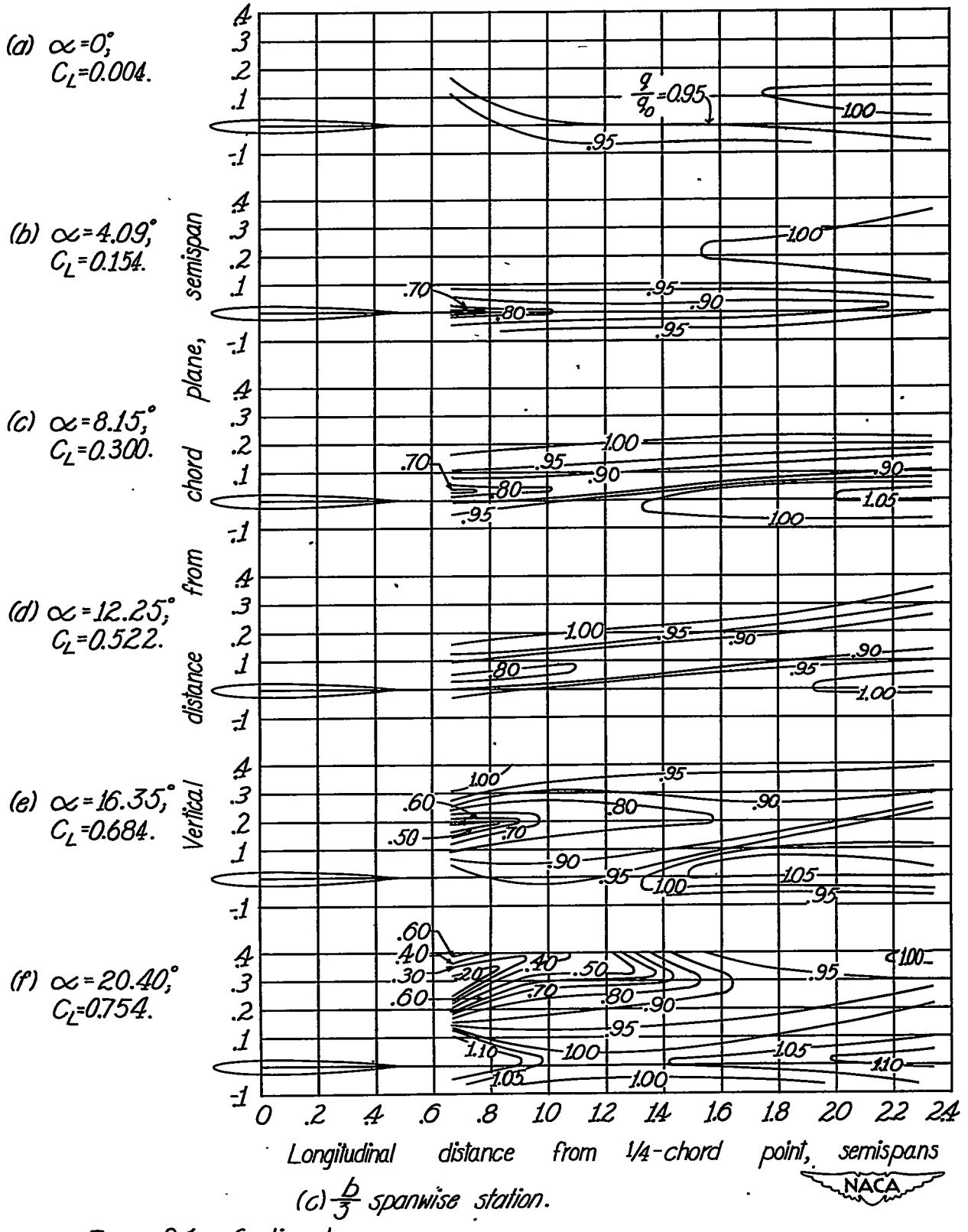

(c) $\frac{b}{3}$ spanwise station.

Figure 21.- Continued.

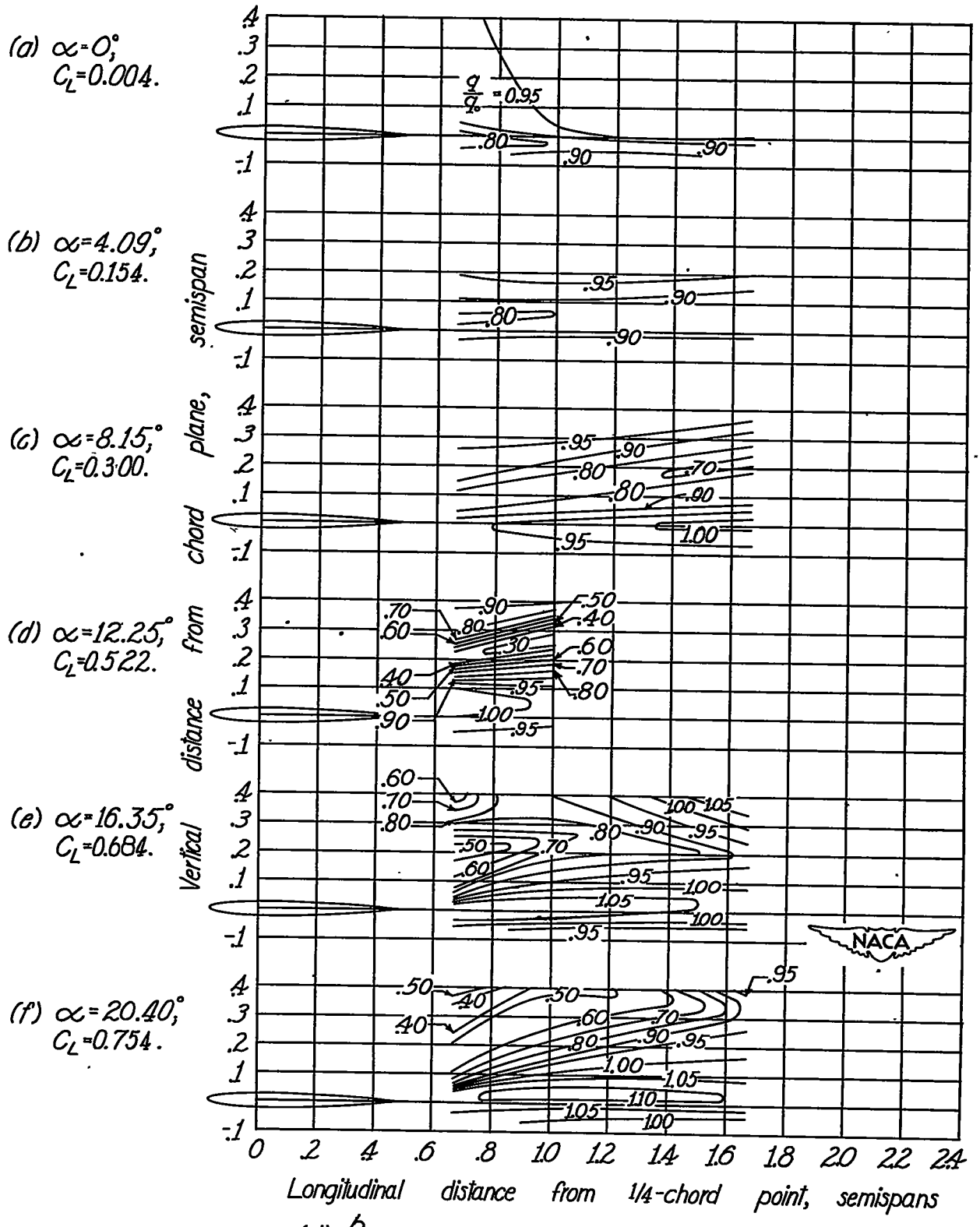

(d) $\frac{b}{2}$ spanwise station.

Figure 21.- Continued.

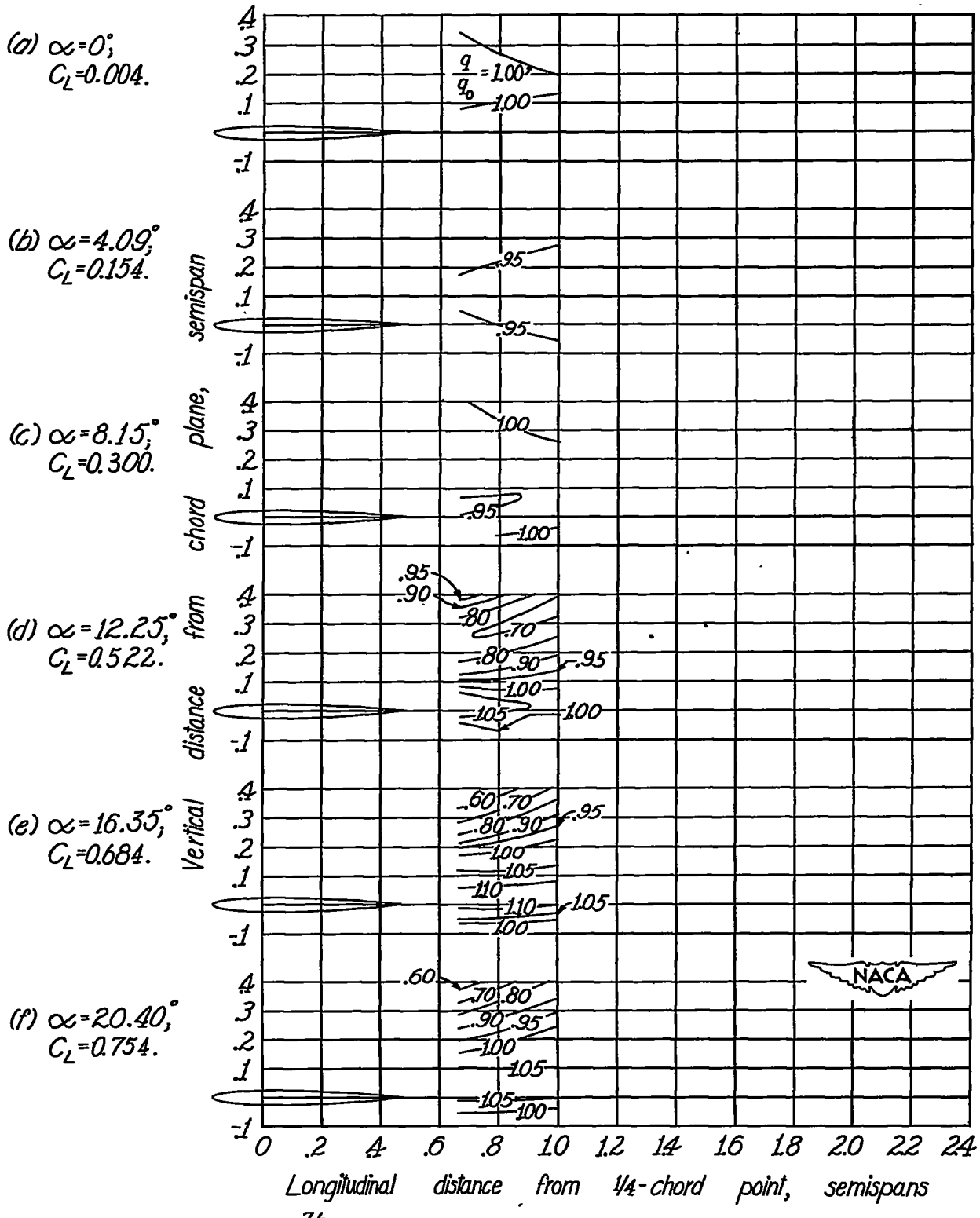

(e) $\frac{7b}{12}$ spanwise station.

Figure 21.- Concluded.

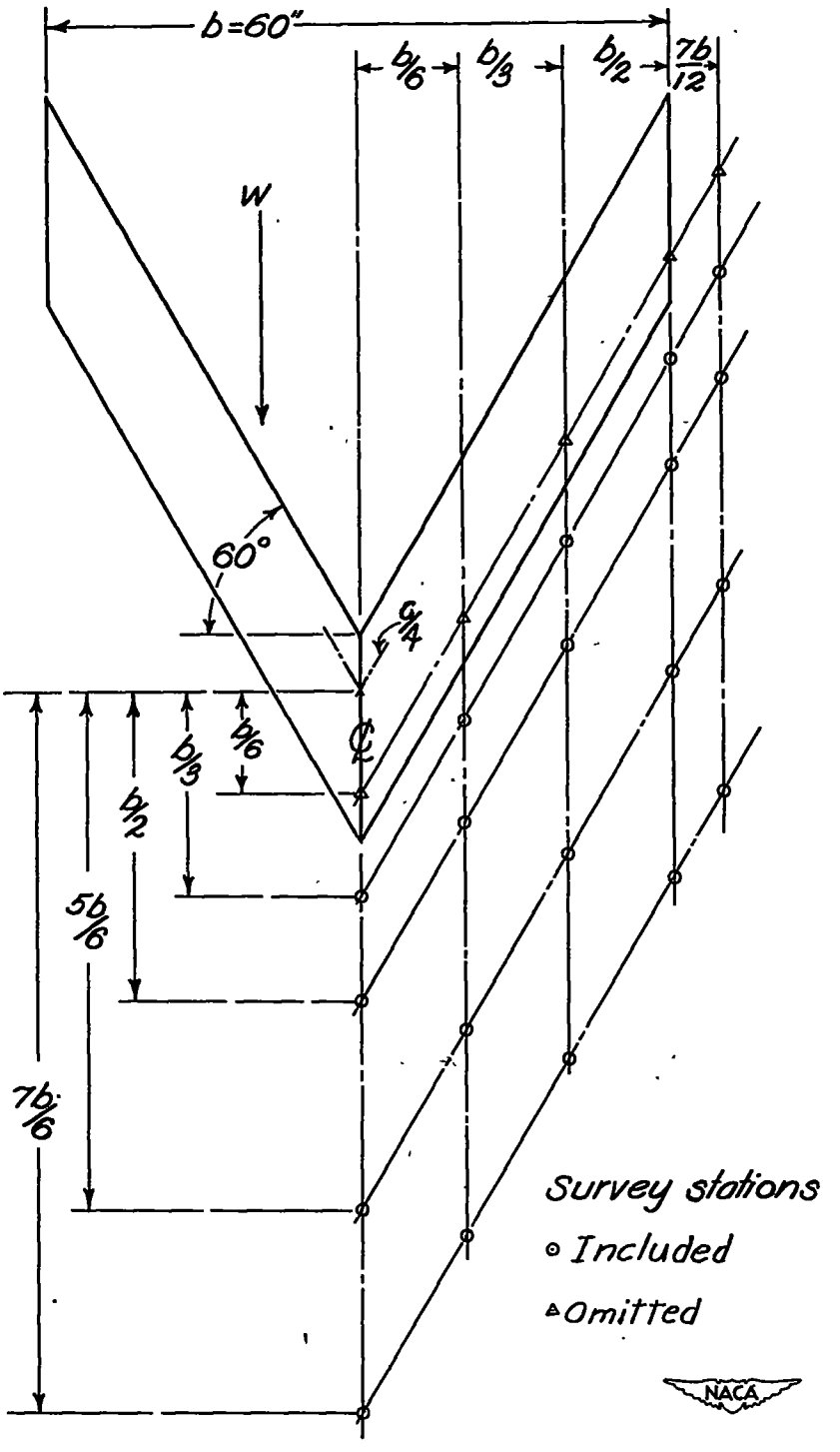

Figure 22.-Survey stations behind 60° sweptforward wing of 60-inch span. A=3.

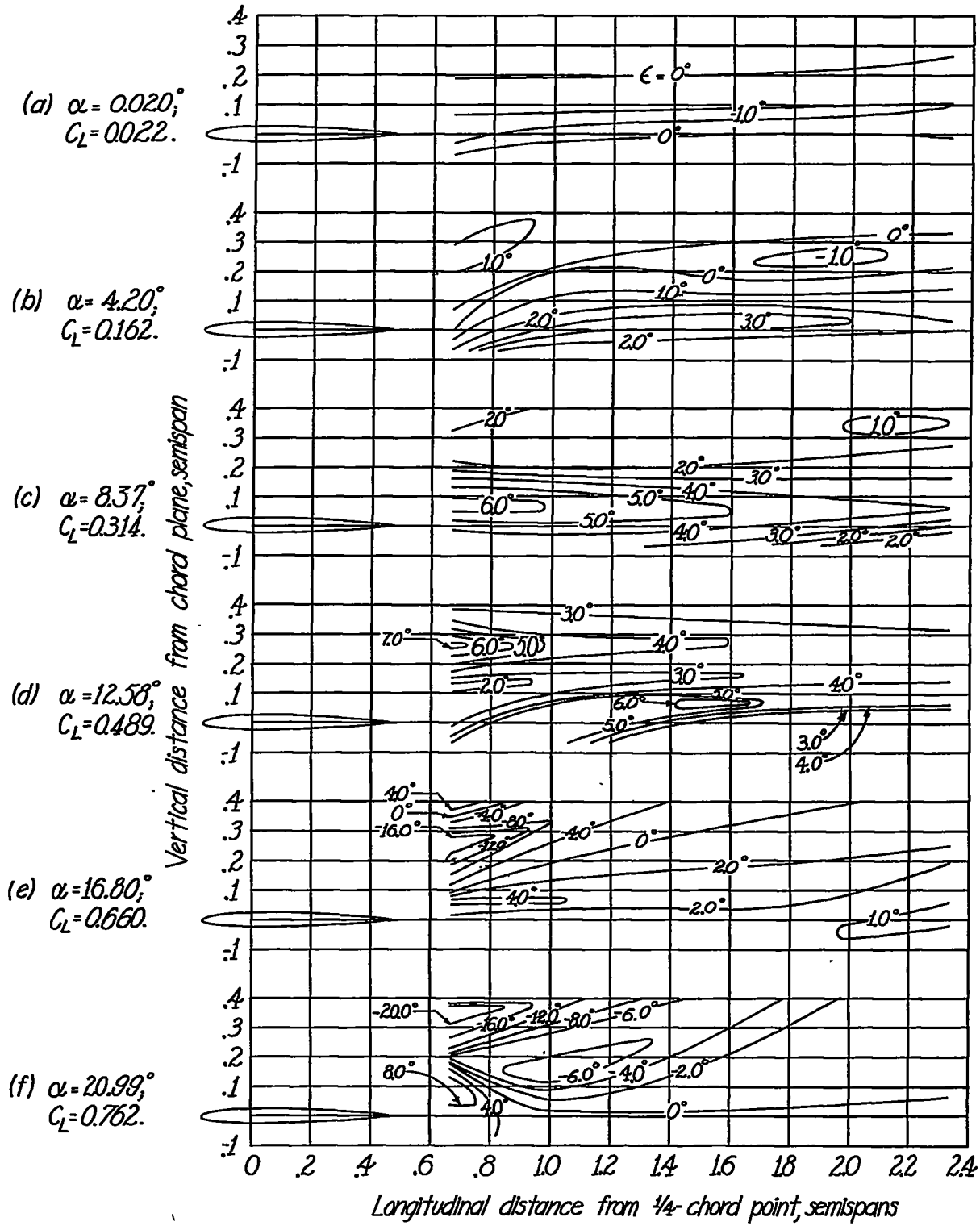

(a) Plane of symmetry.

Figure 23.- Downwash contours behind 60° sweptforward wing of 60-inch span. A = 3.

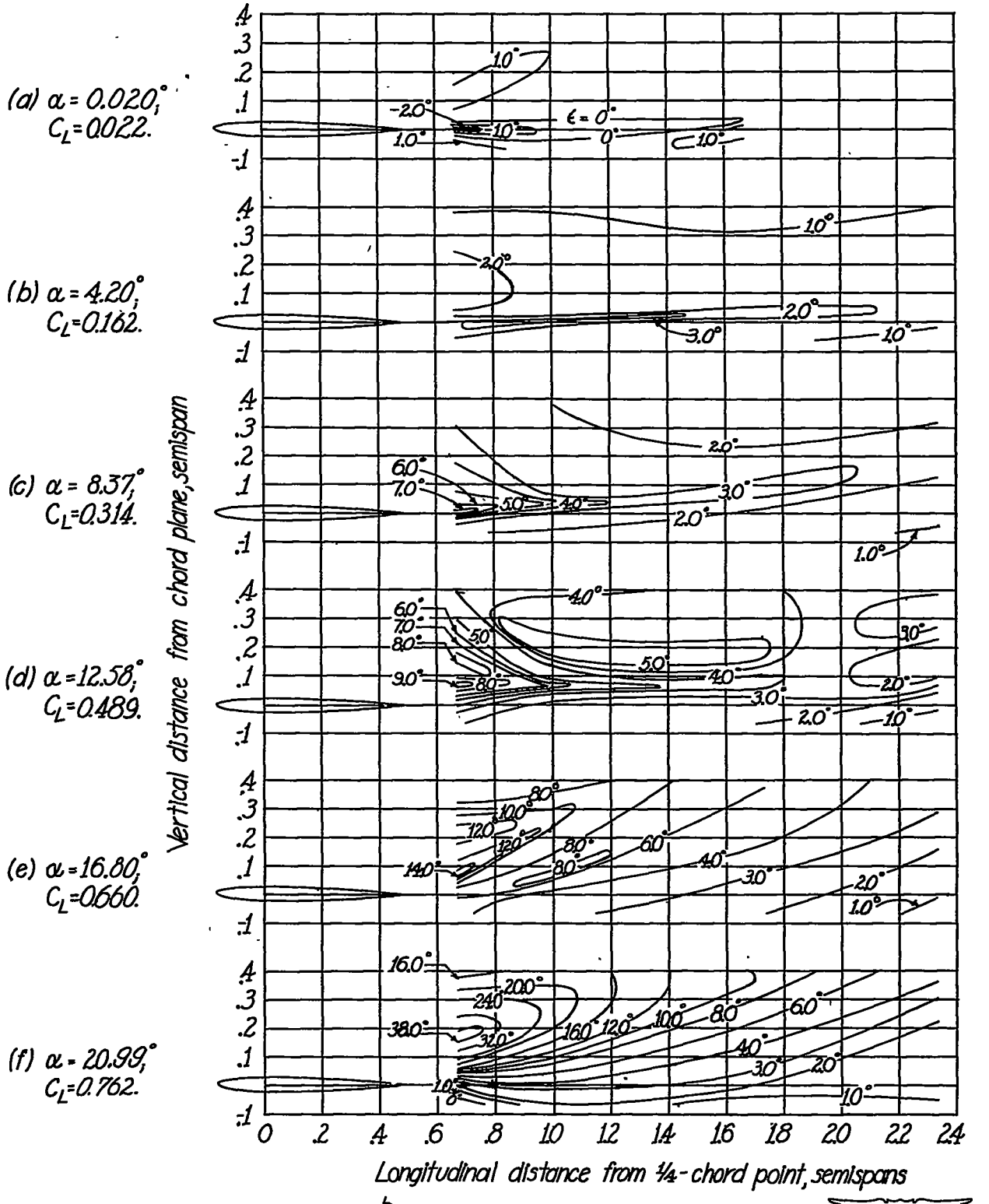

(b) $\frac{b}{6}$ spanwise station.

Figure 23.– Continued.

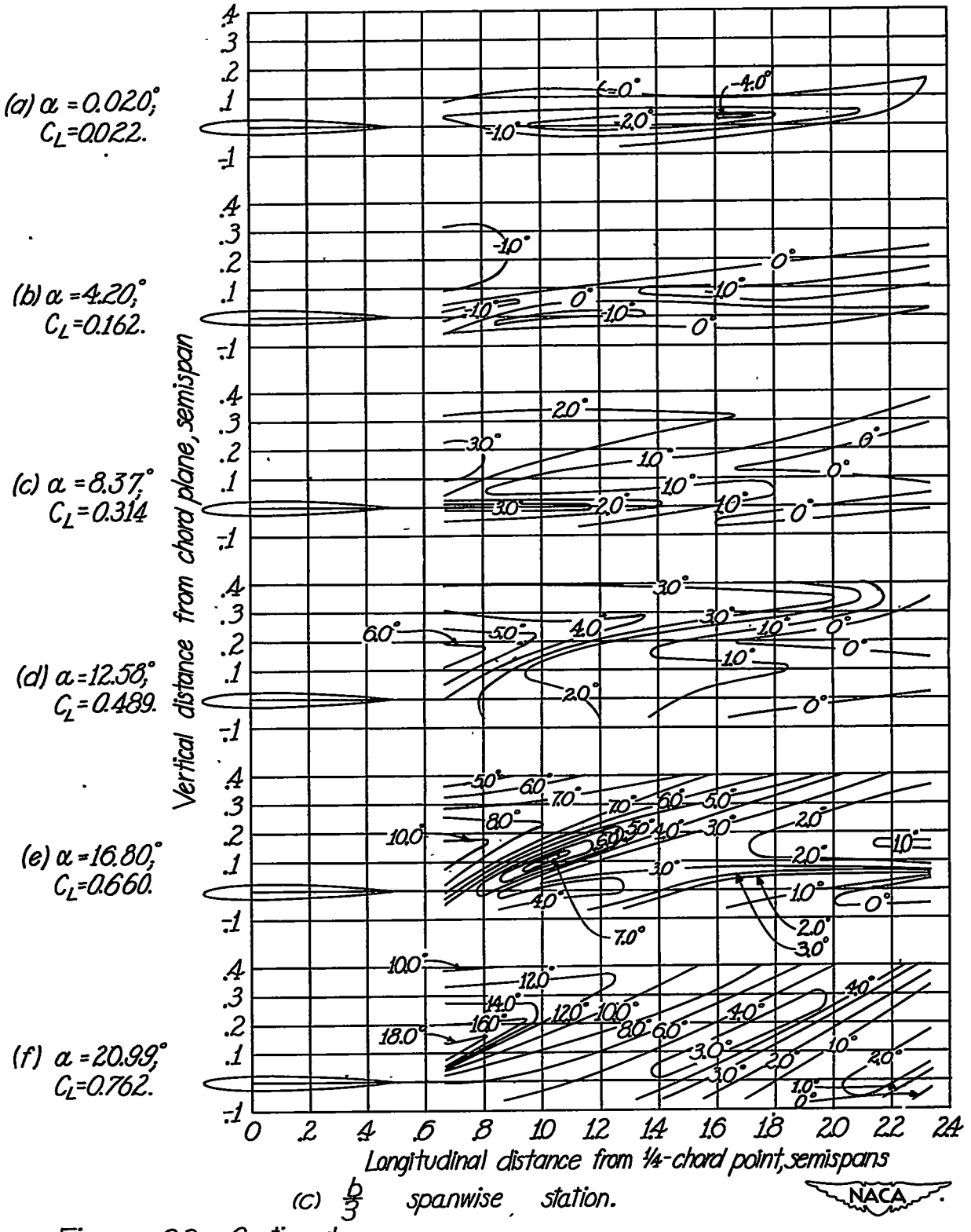

(c) $\frac{b}{3}$ spanwise station.

Figure 23.–Continued.

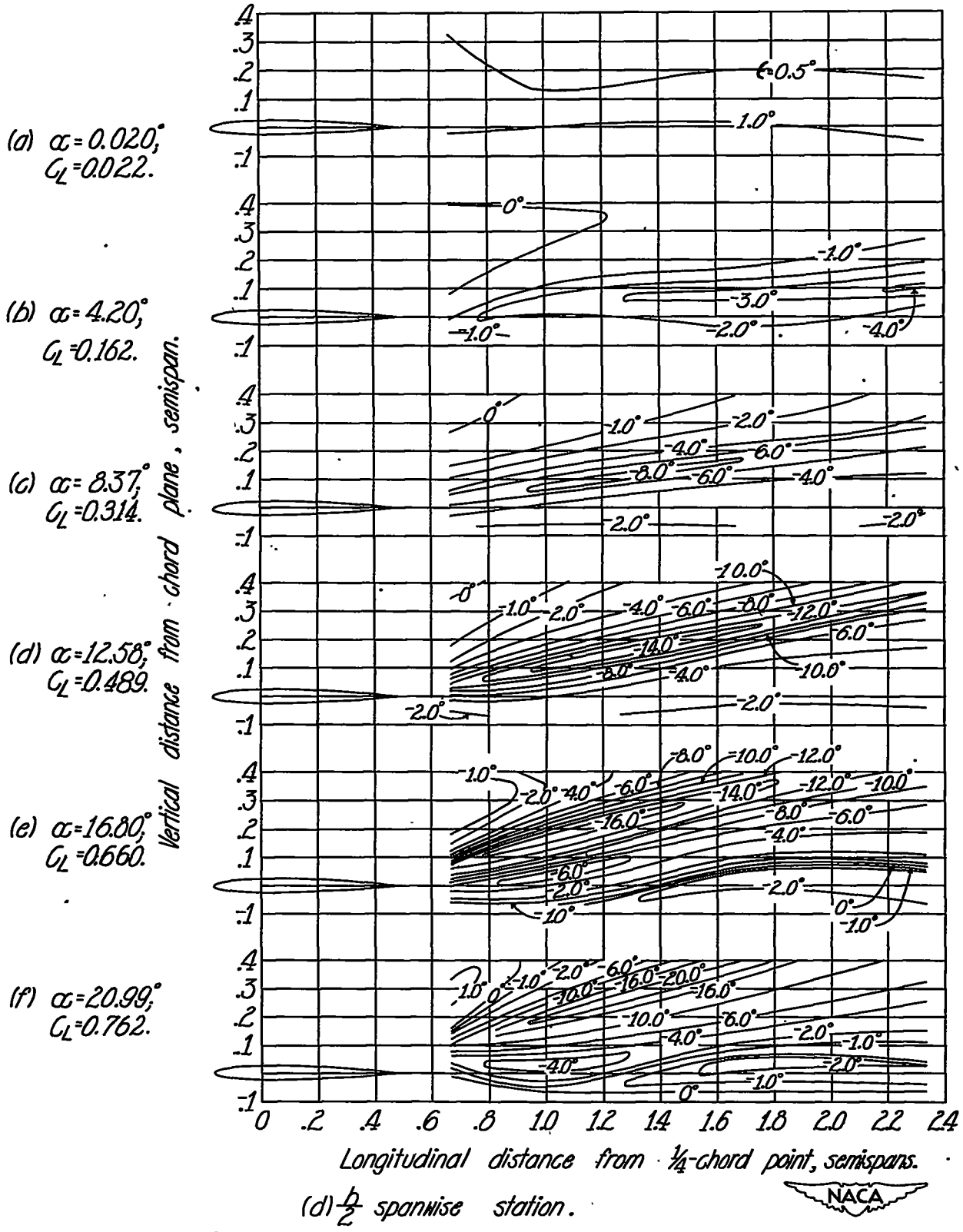

Figure 23.- Continued.

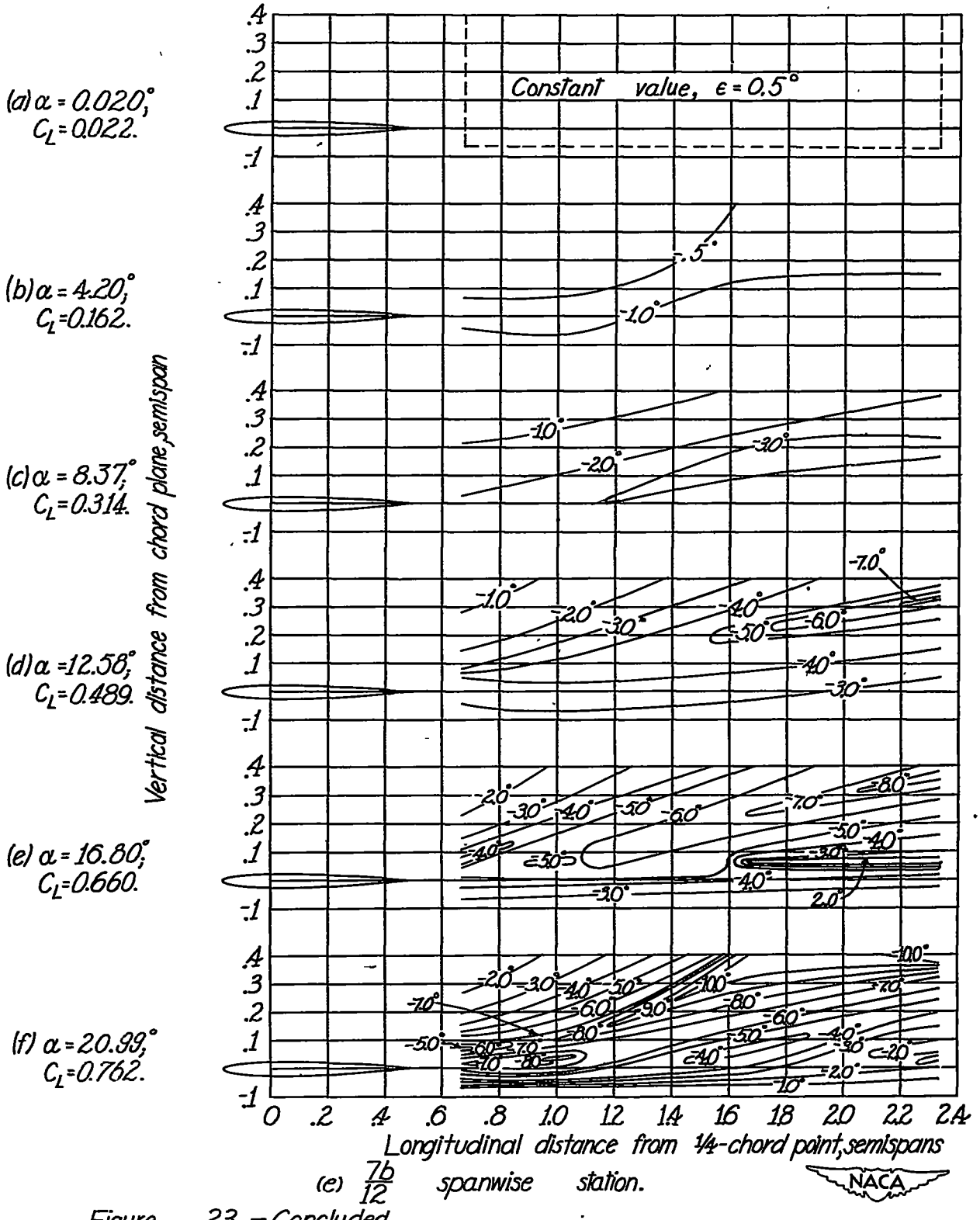

(e) $\frac{7b}{12}$ spanwise station.

Figure 23.—Concluded.

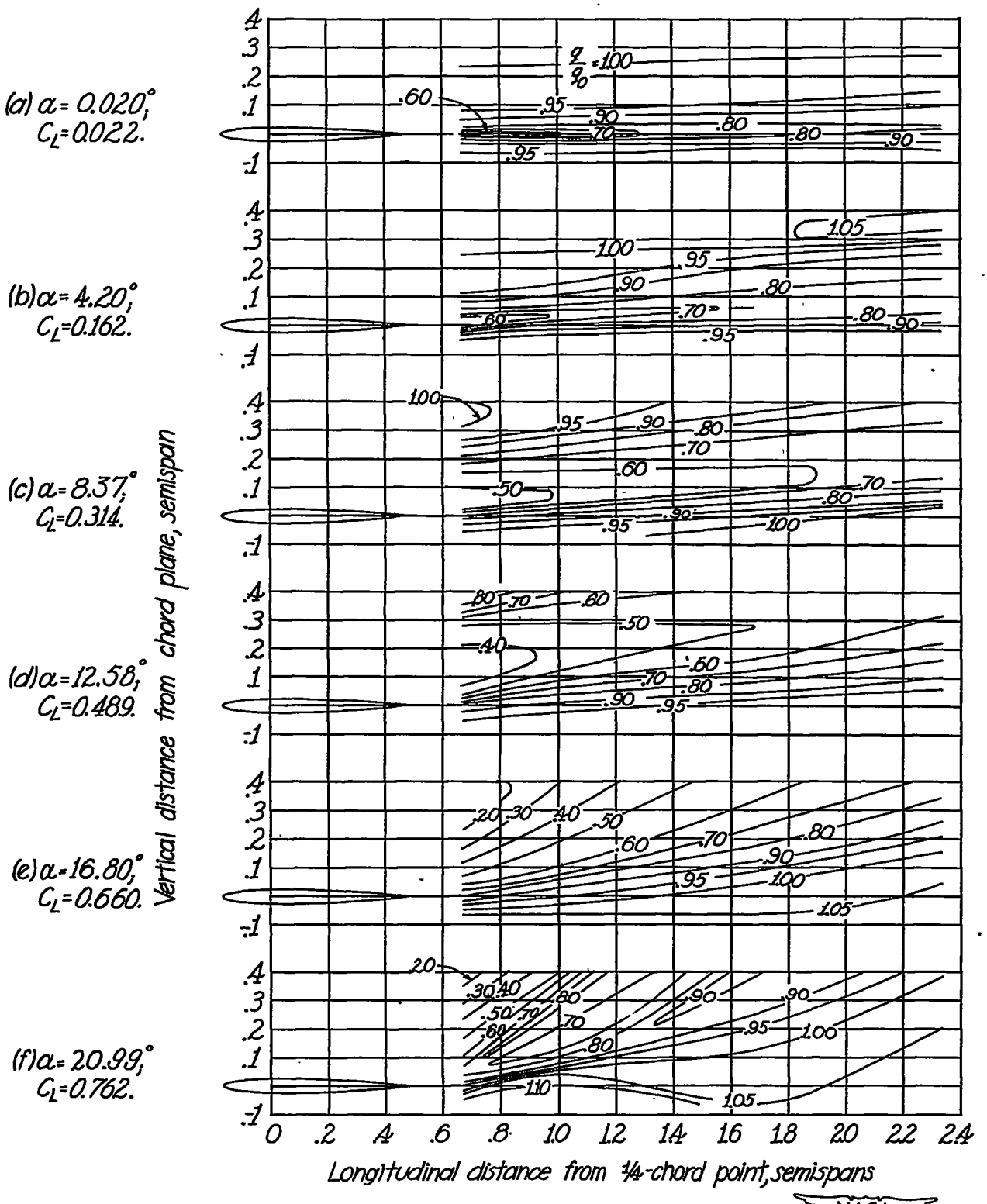

(a) Plane of symmetry.

Figure 24.- Dynamic-pressure-ratio contours behind 60° swept forward wing of 60-inch span. A = 3.

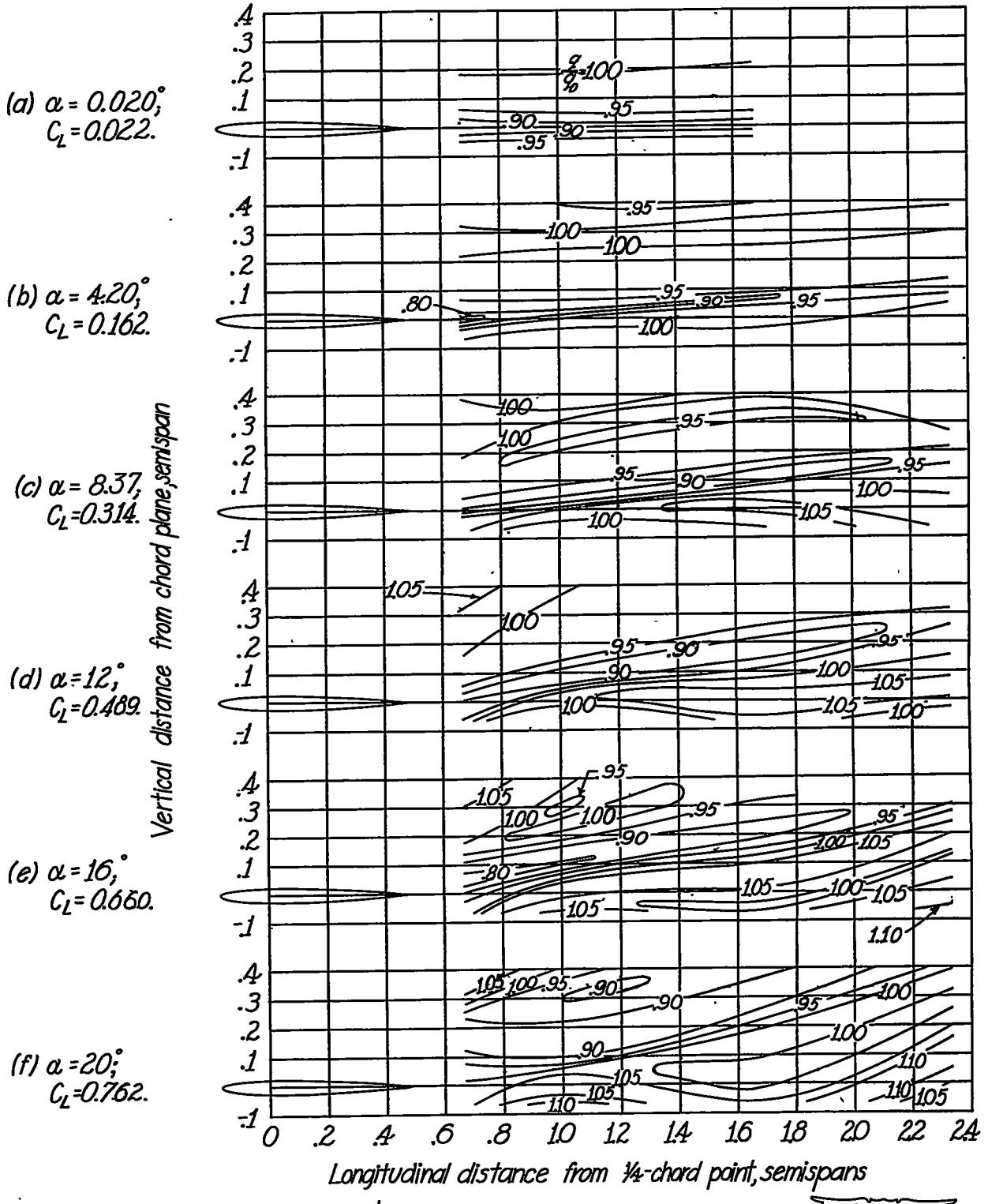

(b) $\frac{b}{6}$ spanwise station.

Figure 24.- Continued.

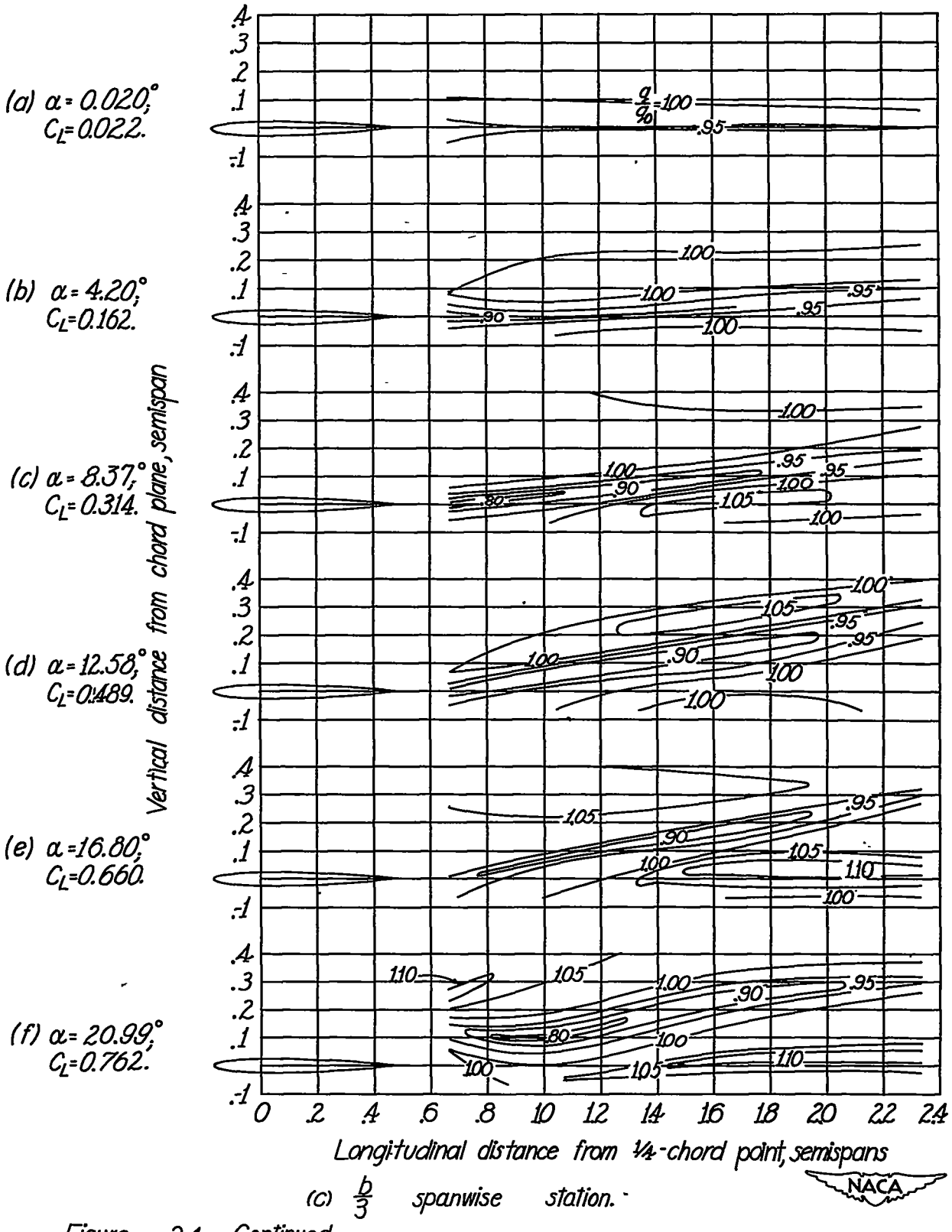

(c) $\frac{b}{3}$ spanwise station.

Figure 24.- Continued.

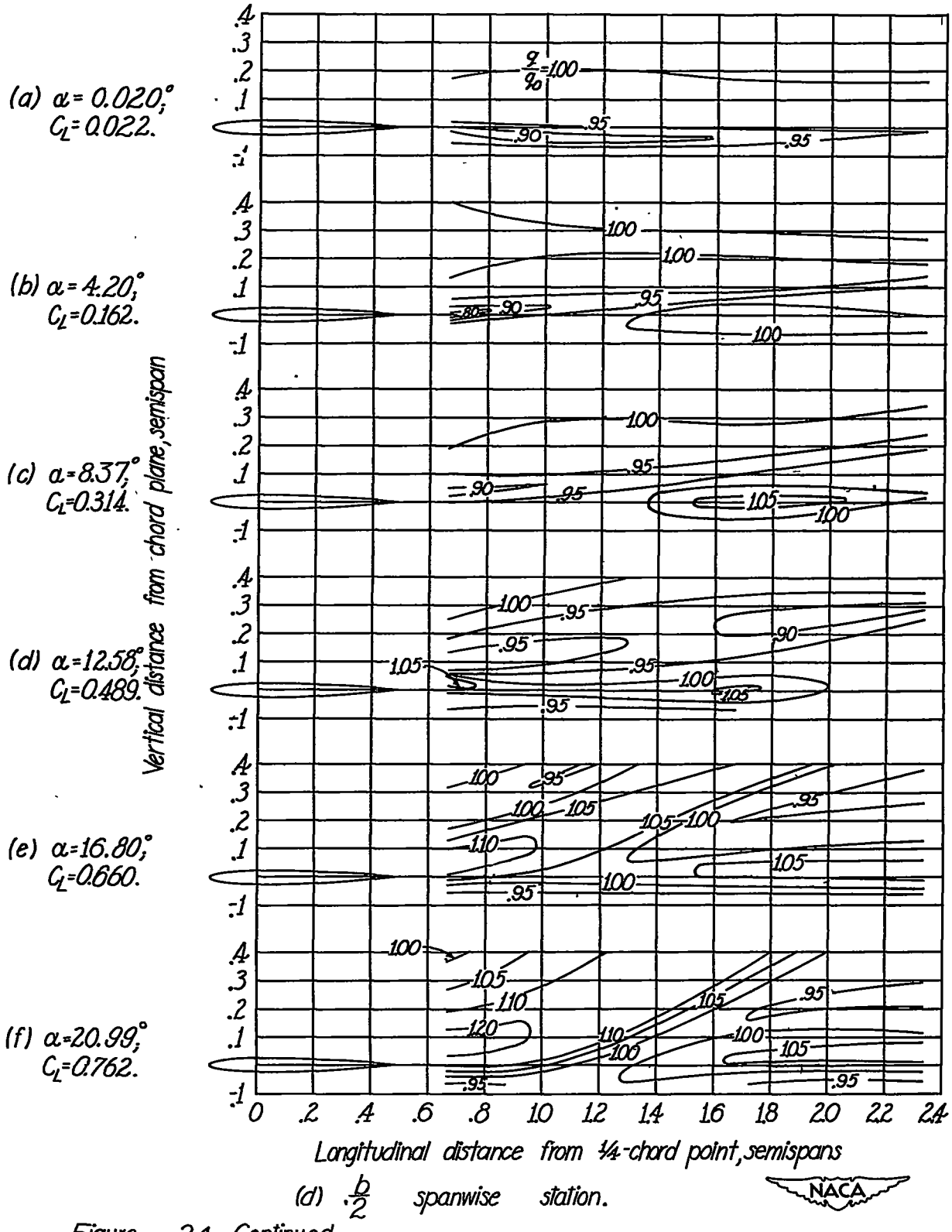

(d) $\frac{b}{2}$ spanwise station.

Figure 24.-Continued.

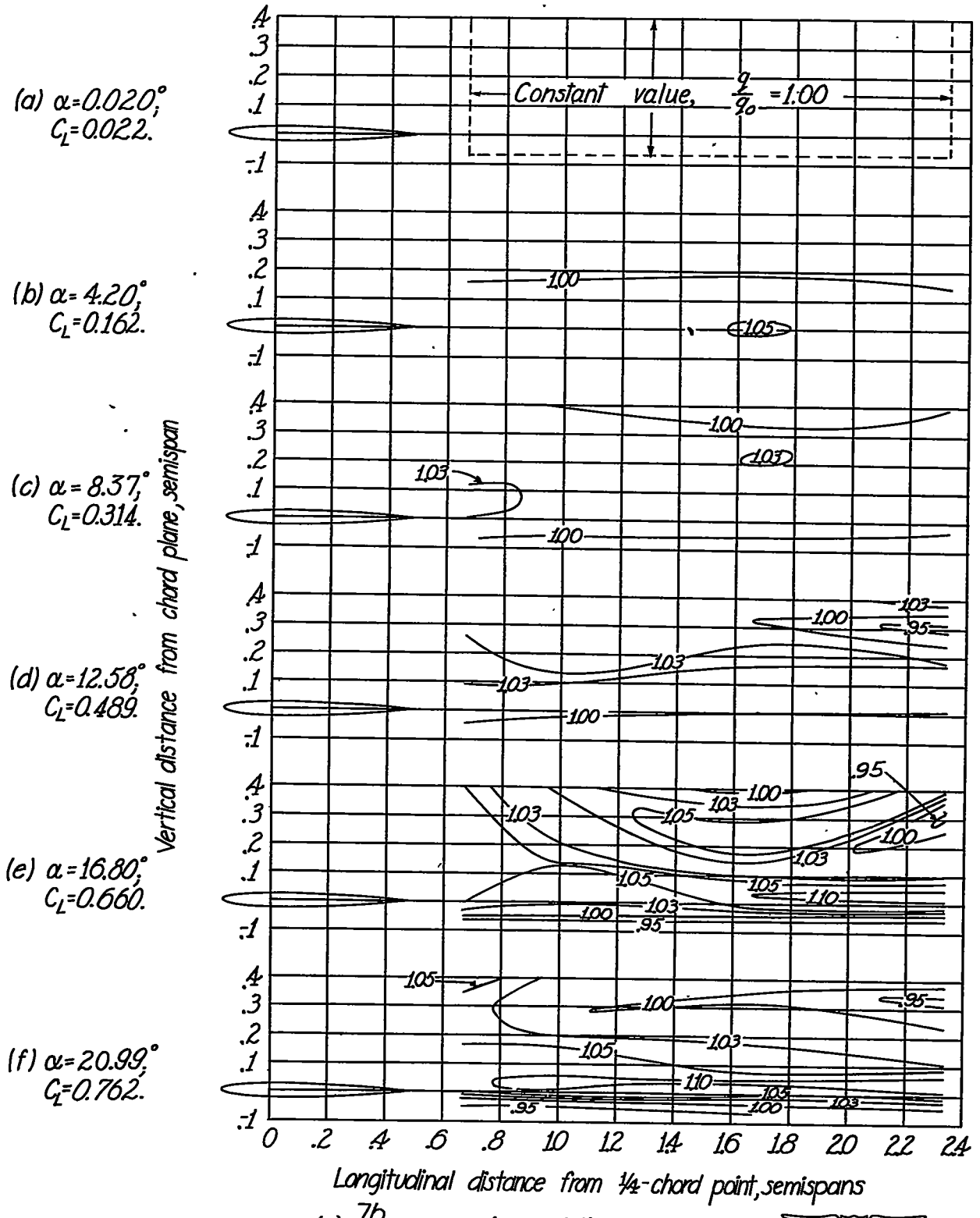

(e) $\frac{7b}{12}$ spanwise station.

Figure 24.- Concluded.

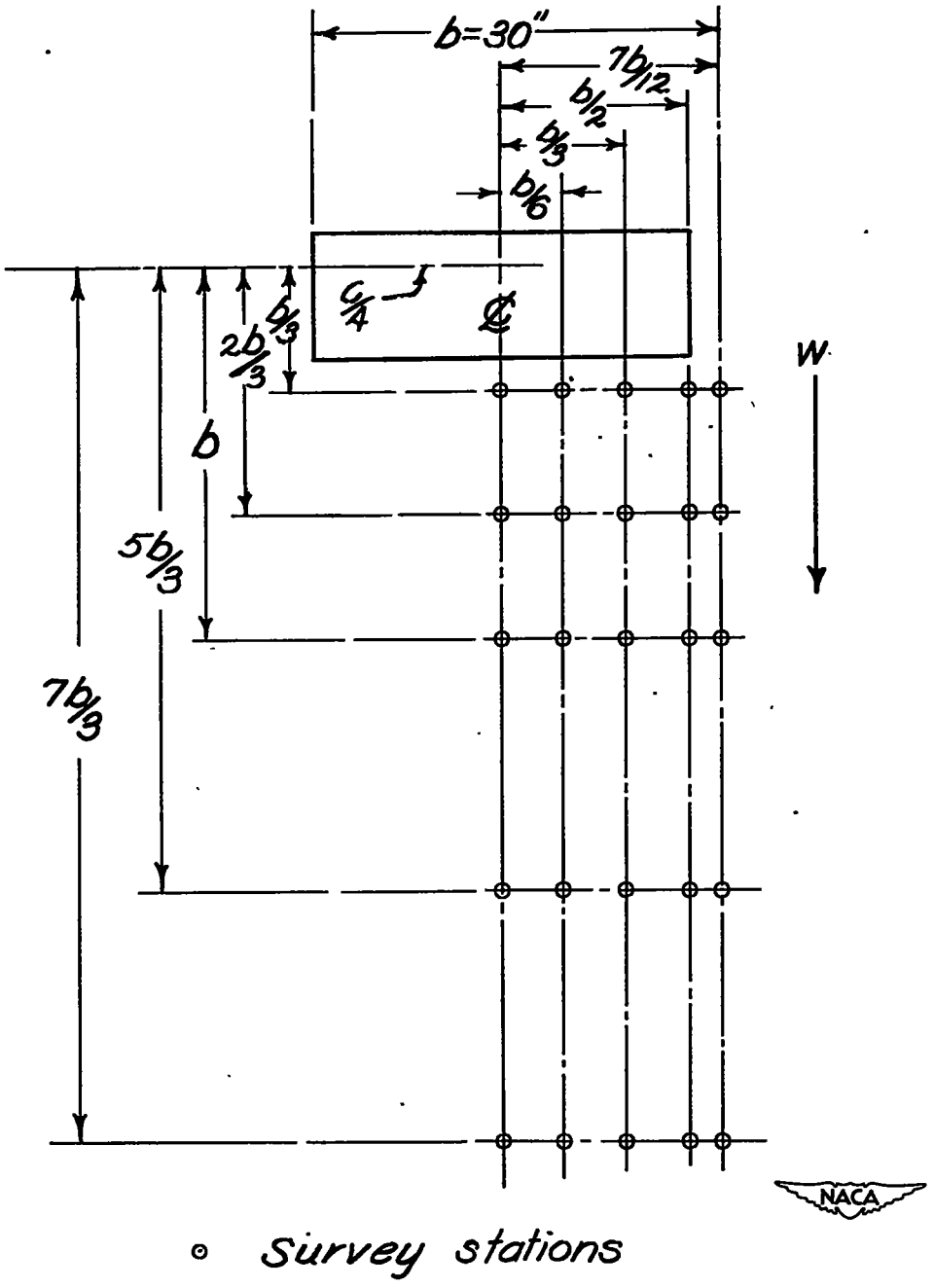

Figure 25.- Survey stations behind straight rectangular wing of 30-inch span. A=3.

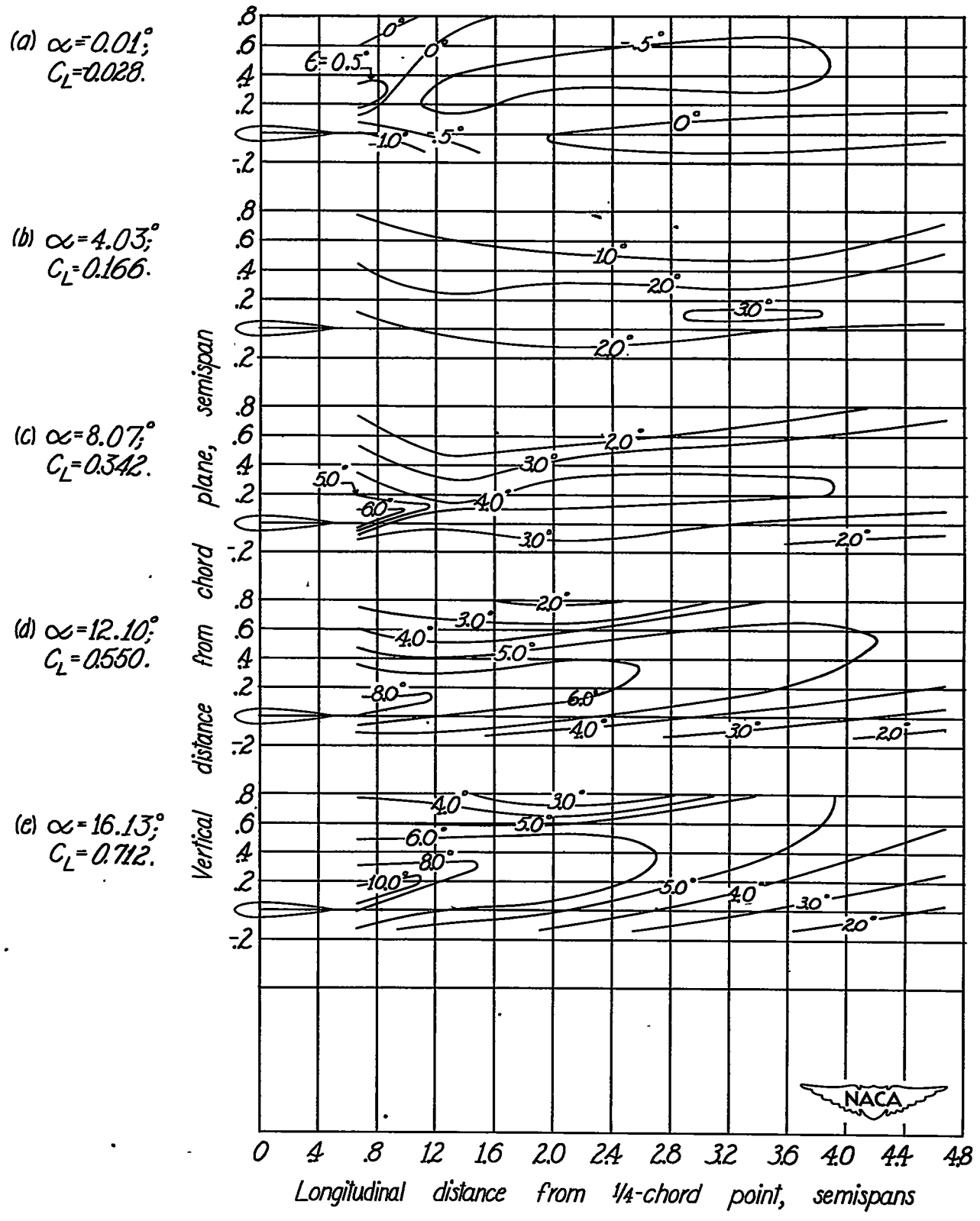

(a) Plane of symmetry.

Figure 26.- Downwash contours behind straight rectangular wing of 30-inch span. A=3.

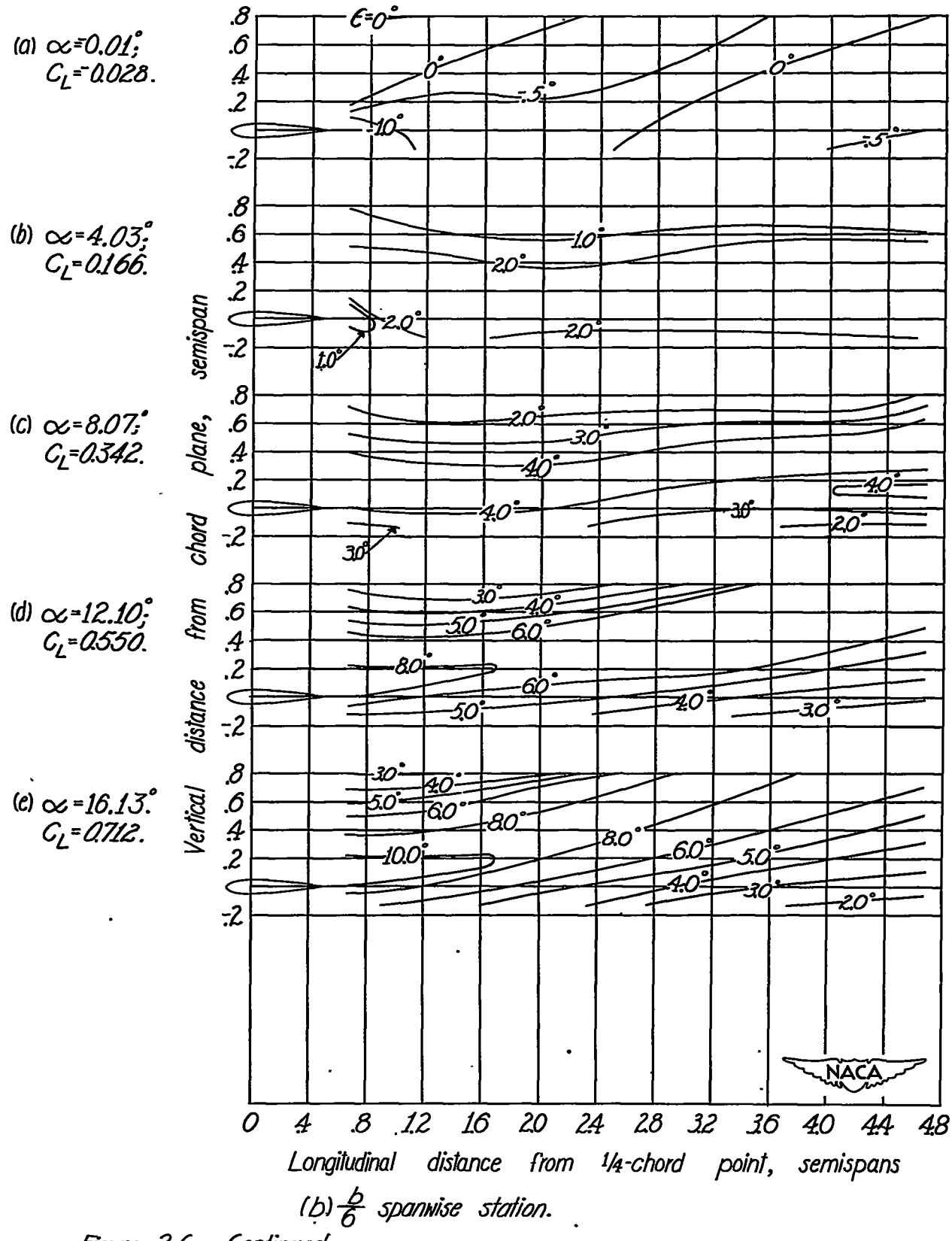

(b) $\frac{b}{6}$ spanwise station.

Figure 26.- Continued.

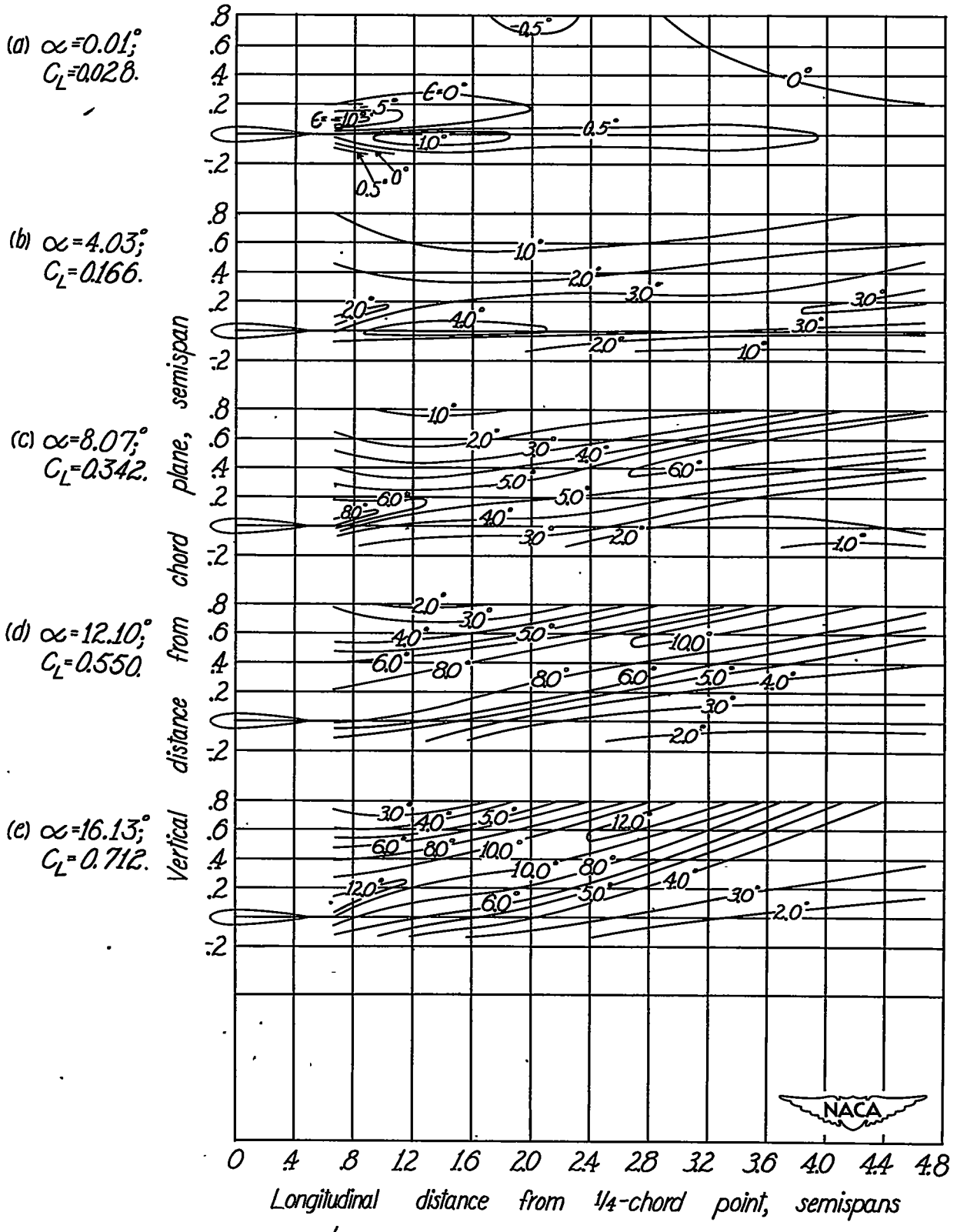

(c) $\frac{b}{3}$ spanwise station.

Figure 26.- Continued.

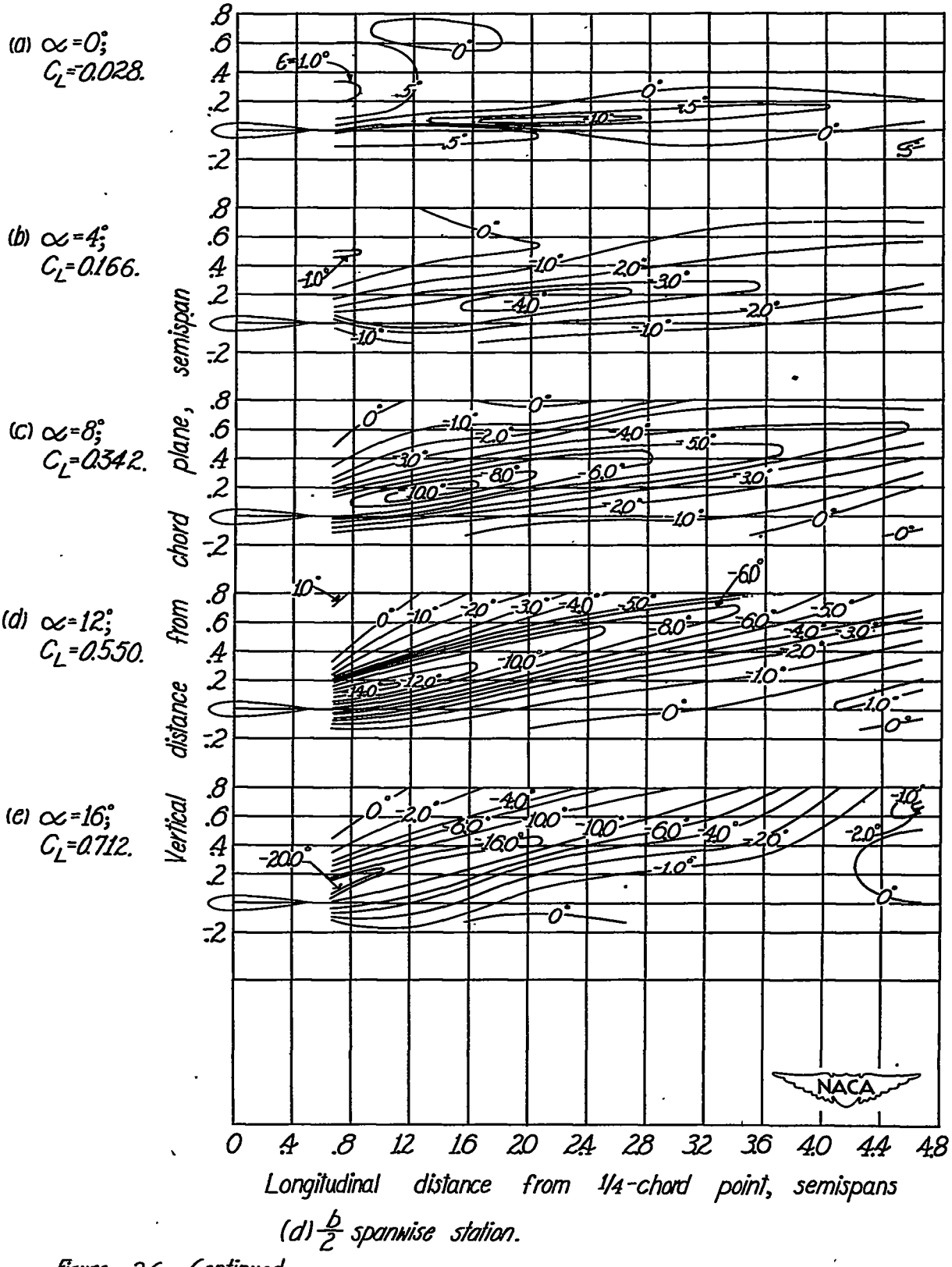

(d) $\frac{b}{2}$ spanwise station.

Figure 26.- Continued.

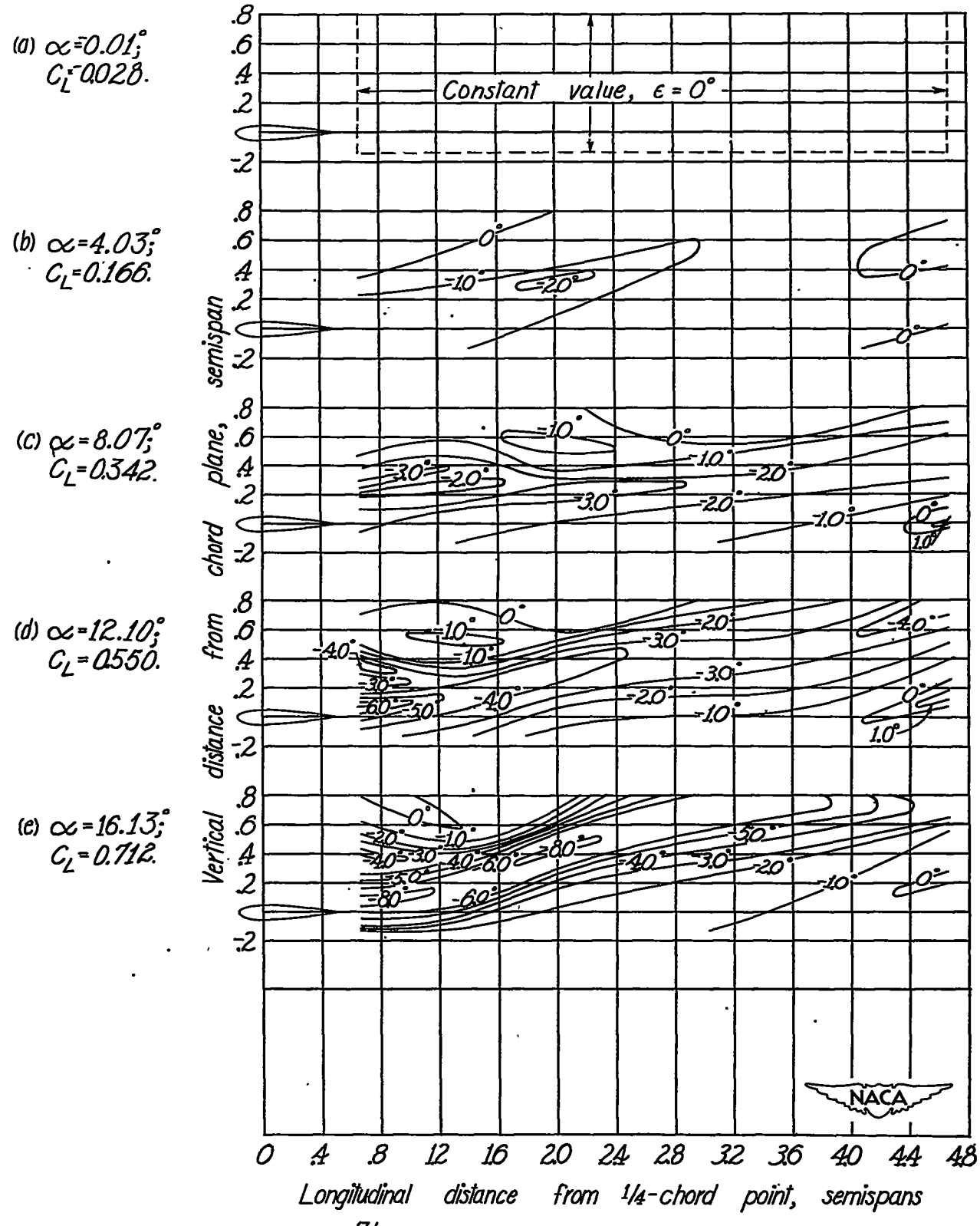

(e) $\frac{7b}{12}$ spanwise station.

Figure 26.- Concluded.

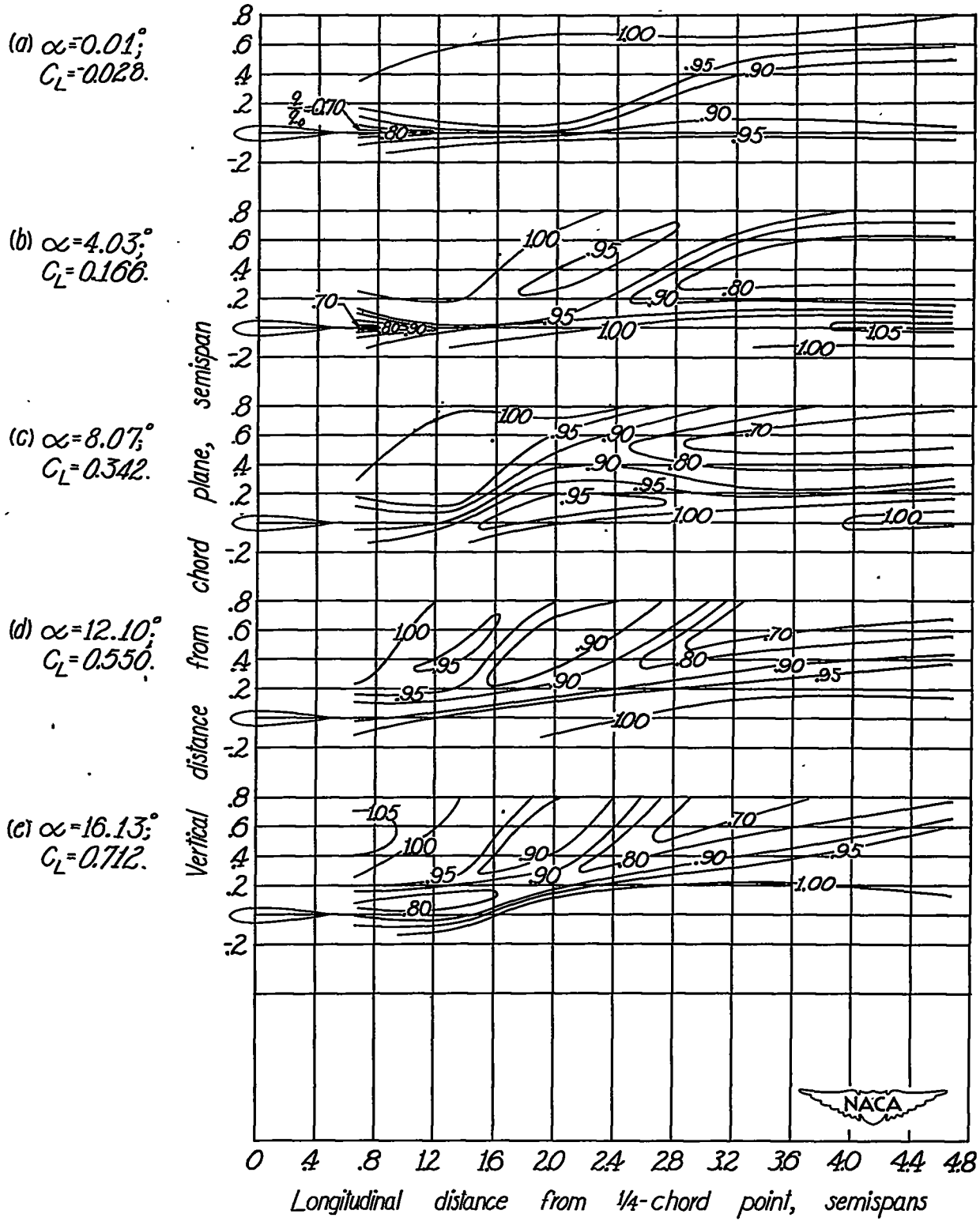

(a) Plane of symmetry.

Figure 27.- Dynamic-pressure-ratio contours behind straight rectangular wing of 30-inch span. A= 3.

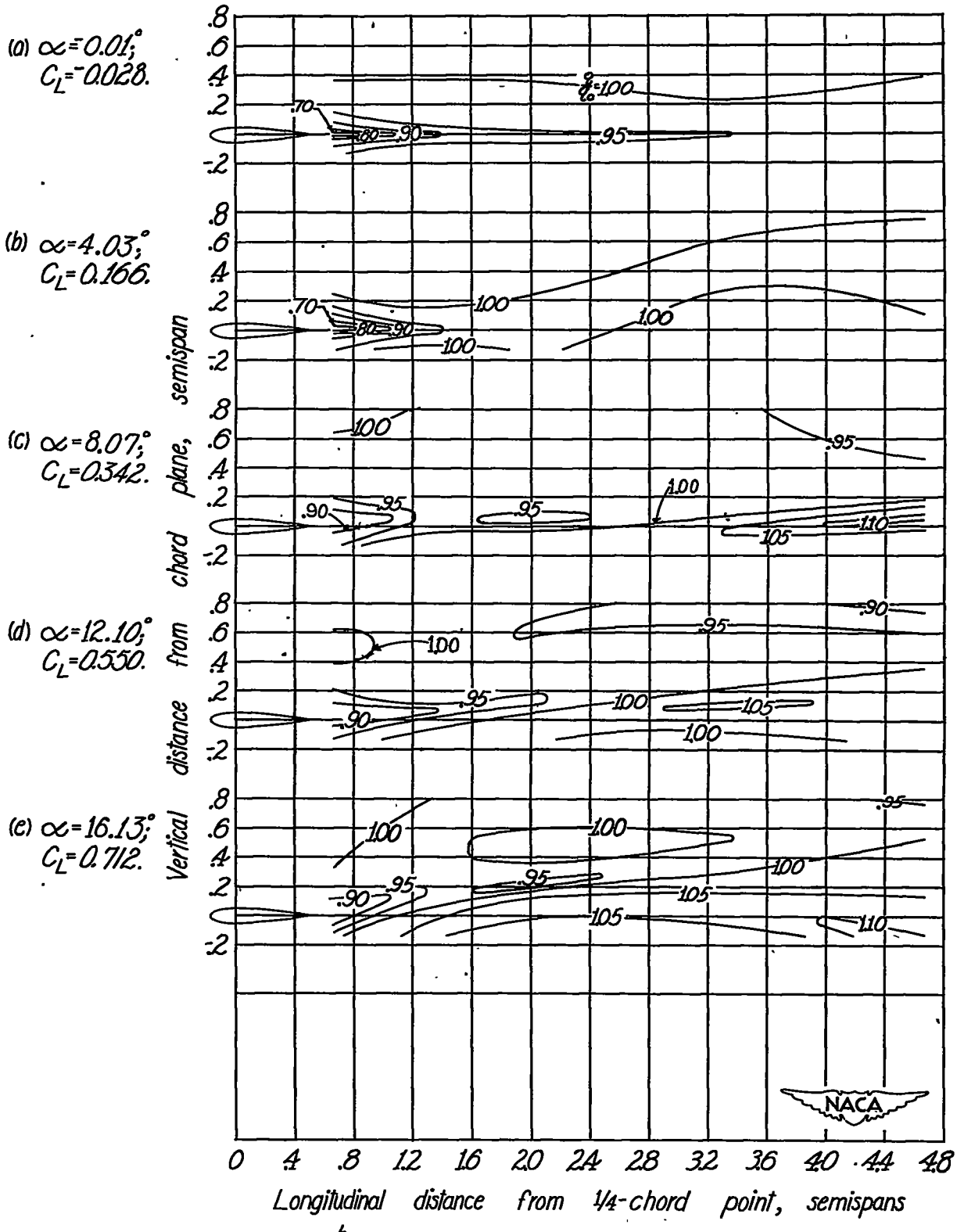

(b) $\frac{b}{6}$ spanwise station.

Figure 27.- Continued.

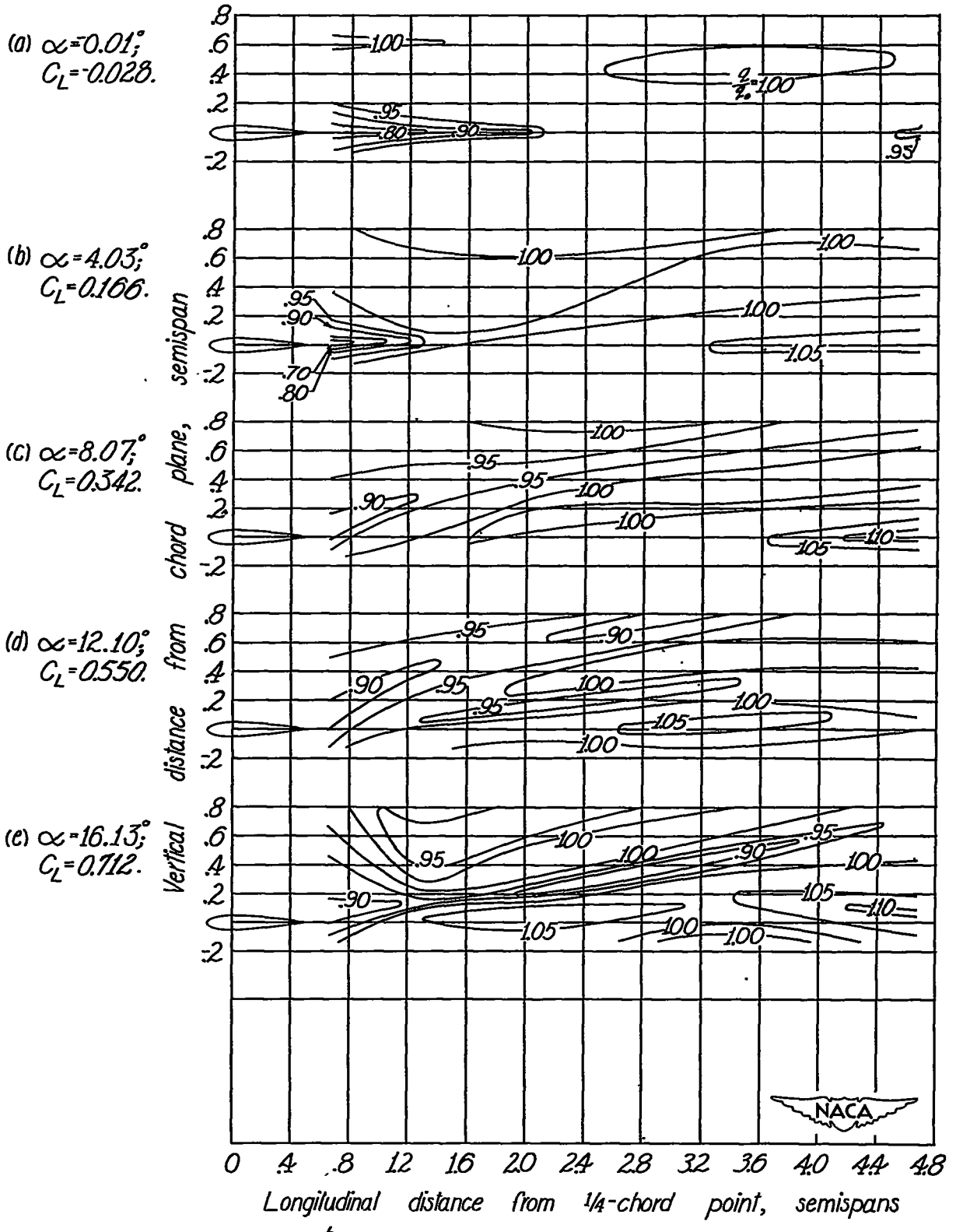

(c) $\frac{b}{3}$ spanwise station.

Figure 27.- Continued.

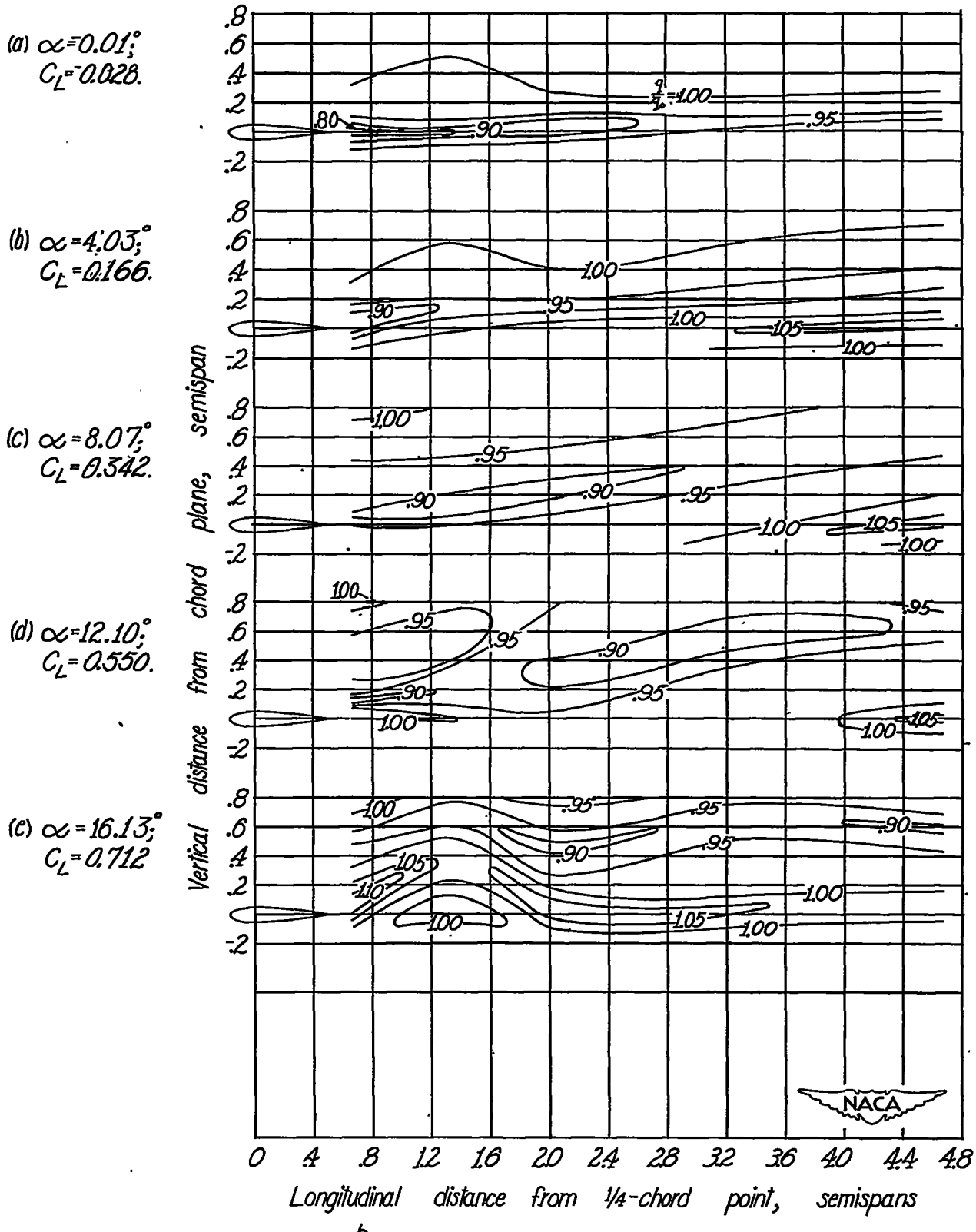

(d) $\frac{b}{2}$ spanwise station.

Figure 27.- Continued.

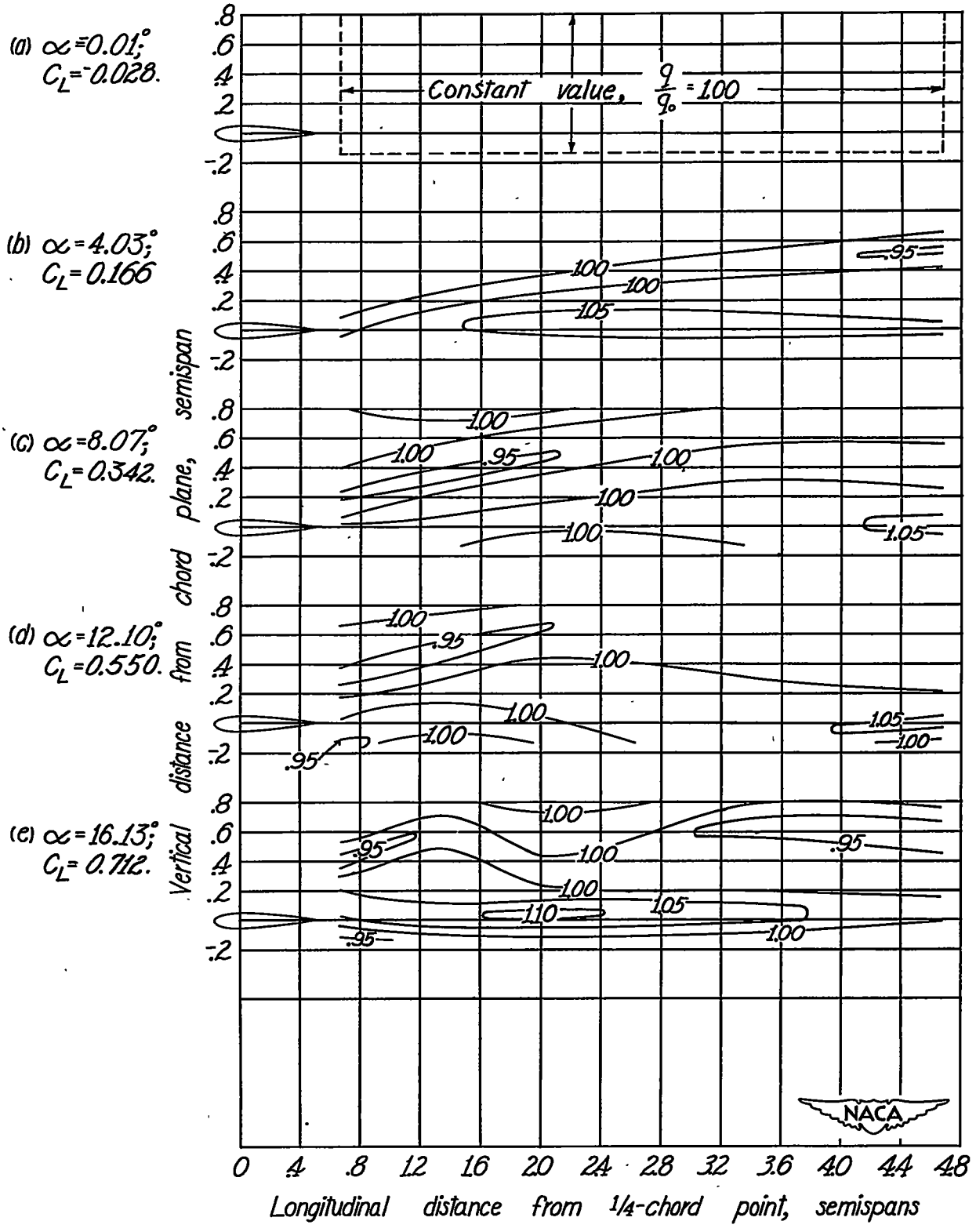

(e) $\frac{7b}{12}$ spanwise station.

Figure 27.- Concluded.

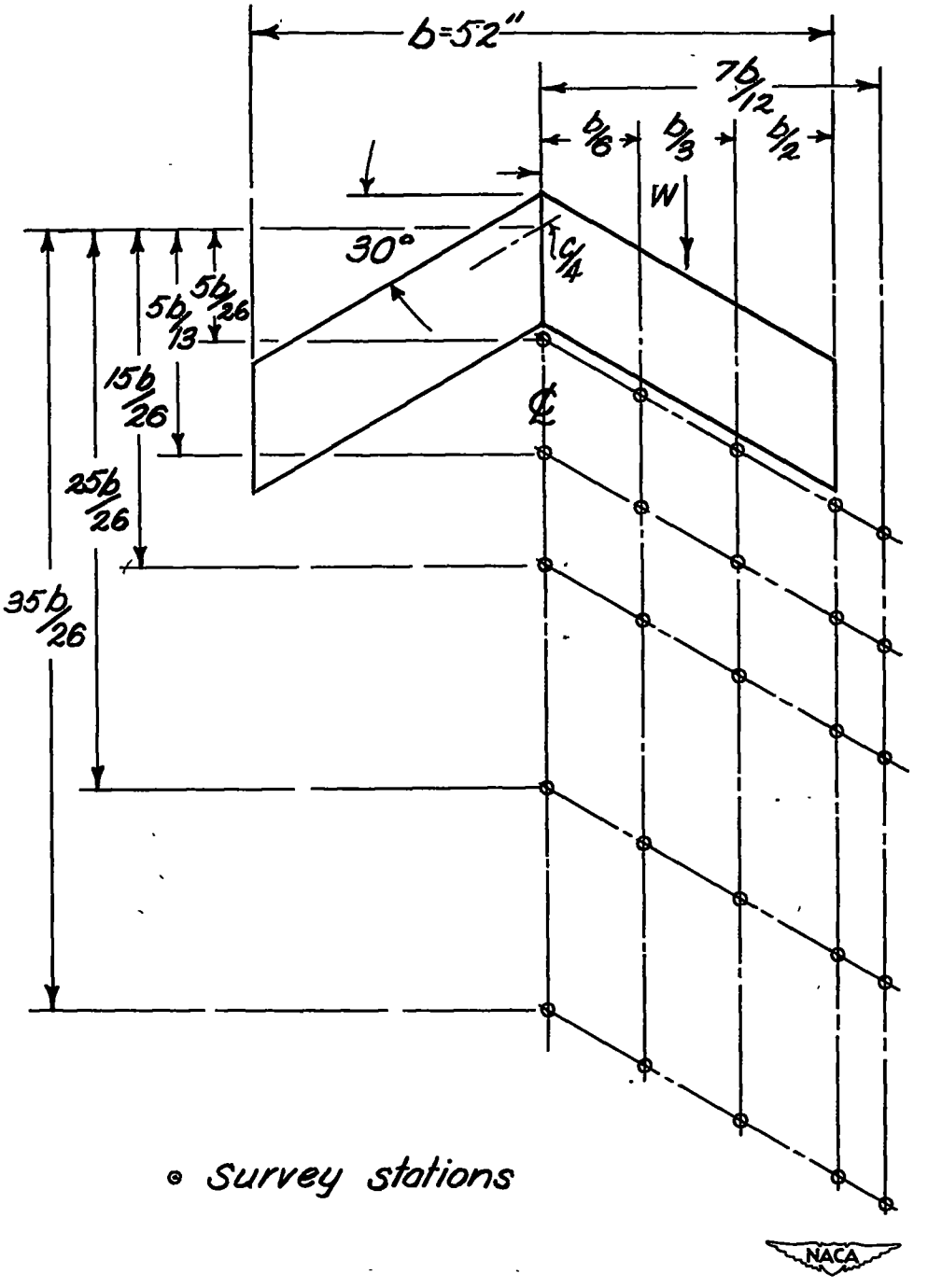

Figure 28.-Survey stations behind 30° sweptback wing of 52-inch span. A = 4.5.

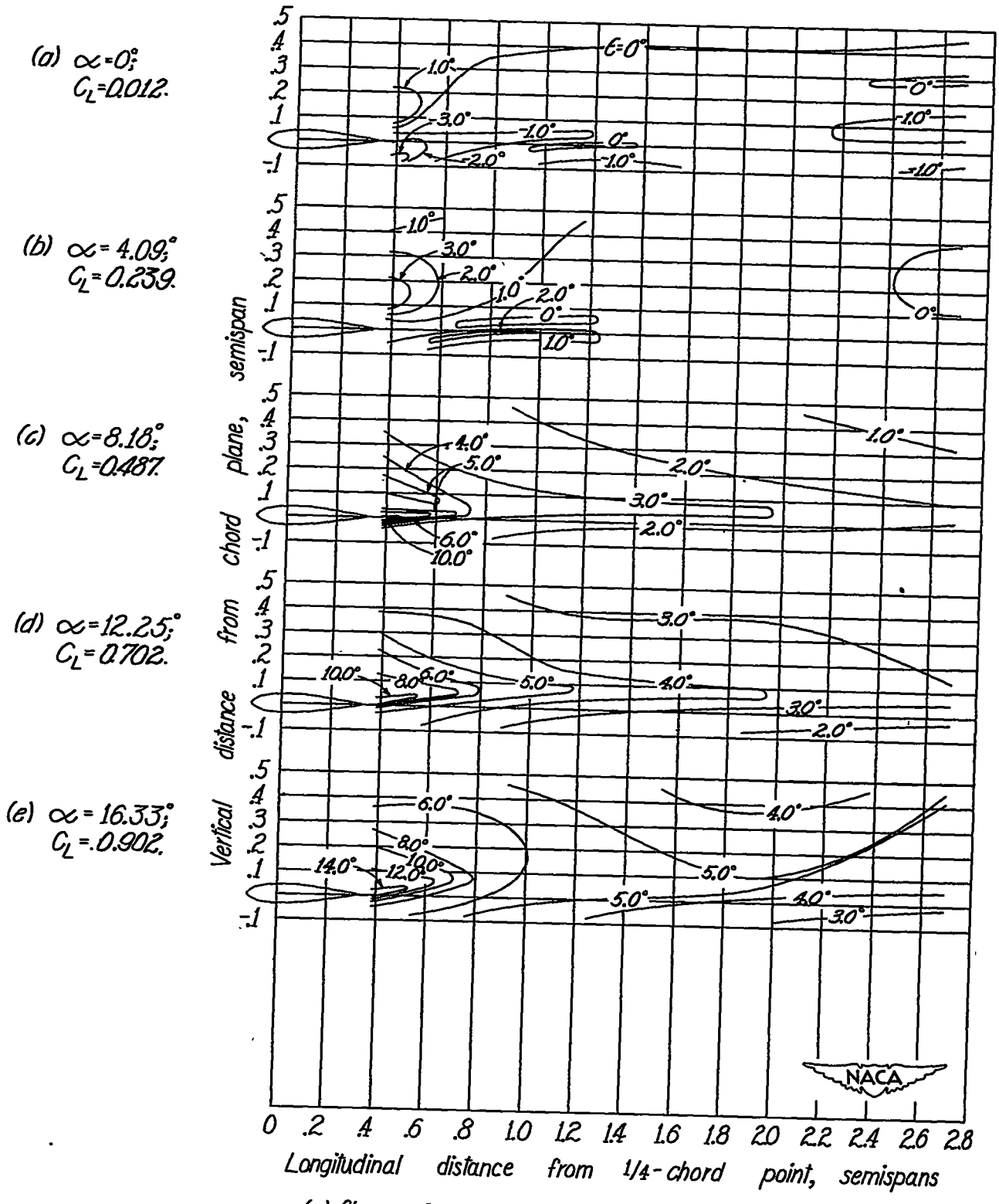

(a) Plane of symmetry.

Figure 29.- Downwash contours behind 30° sweptback wing of 52-inch span. A=4.5.

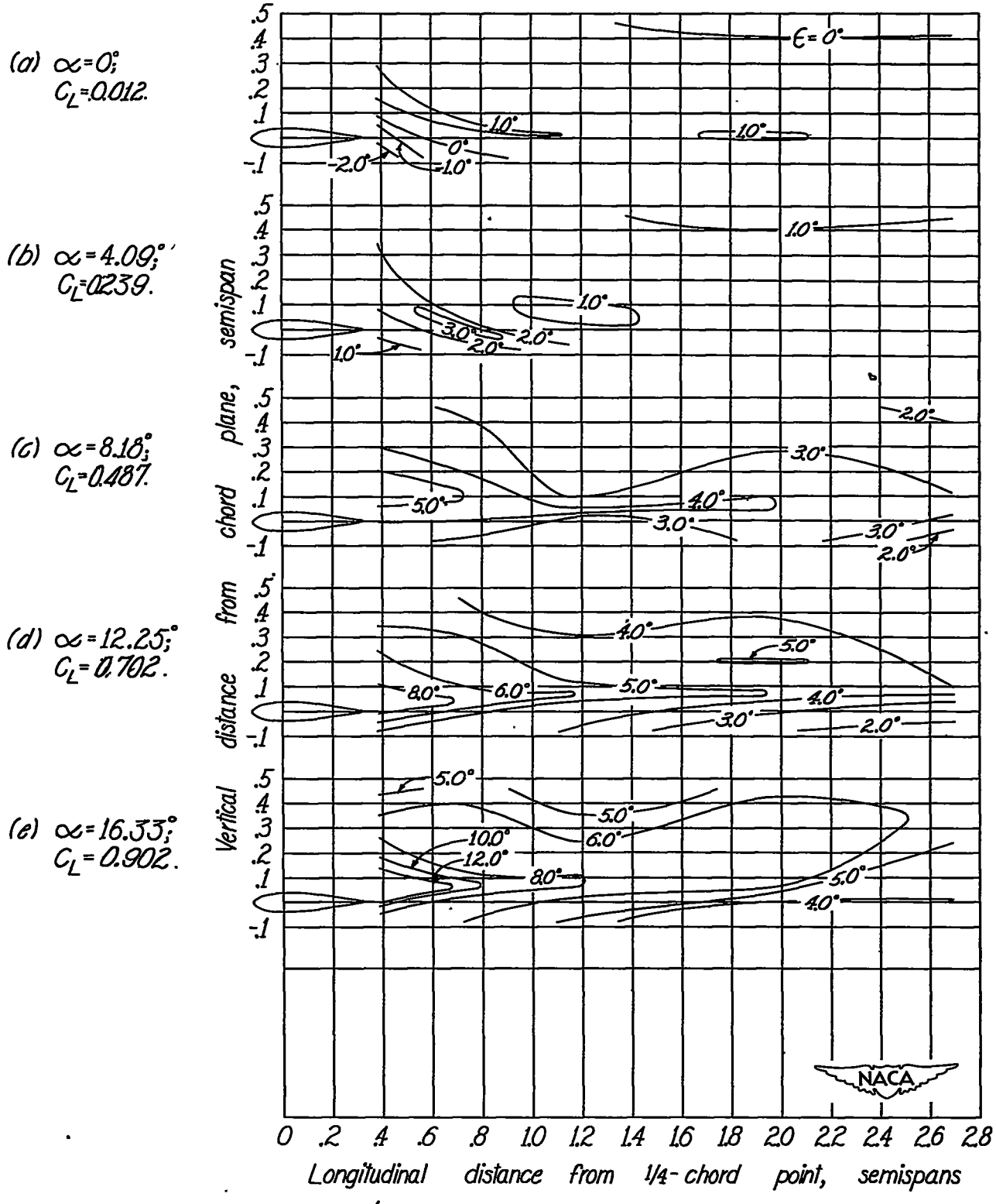

(b) $\frac{b}{6}$ spanwise station.

Figure 29. - Continued.

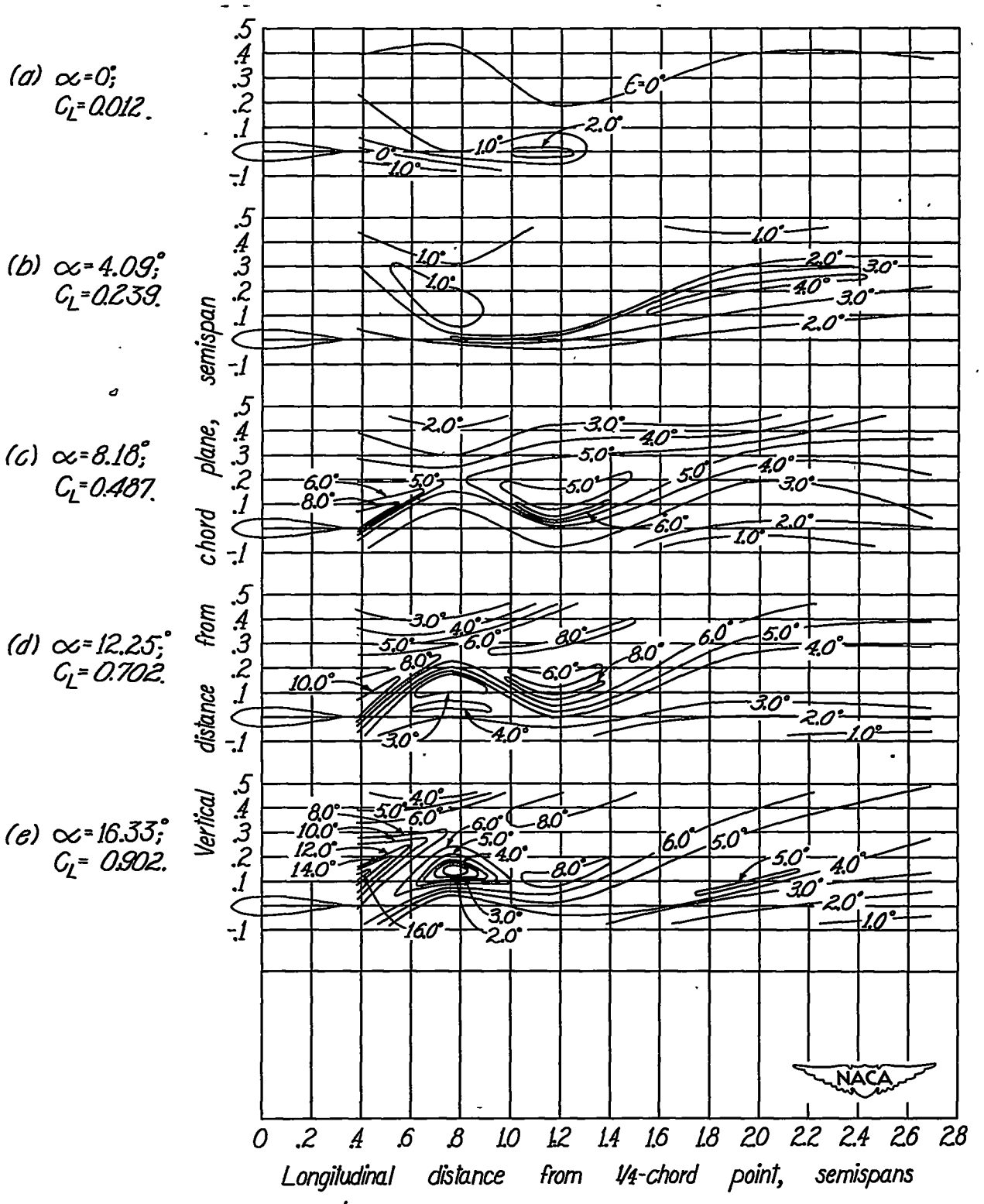

(c) $\frac{b}{3}$ spanwise station.

Figure 29. -Continued.

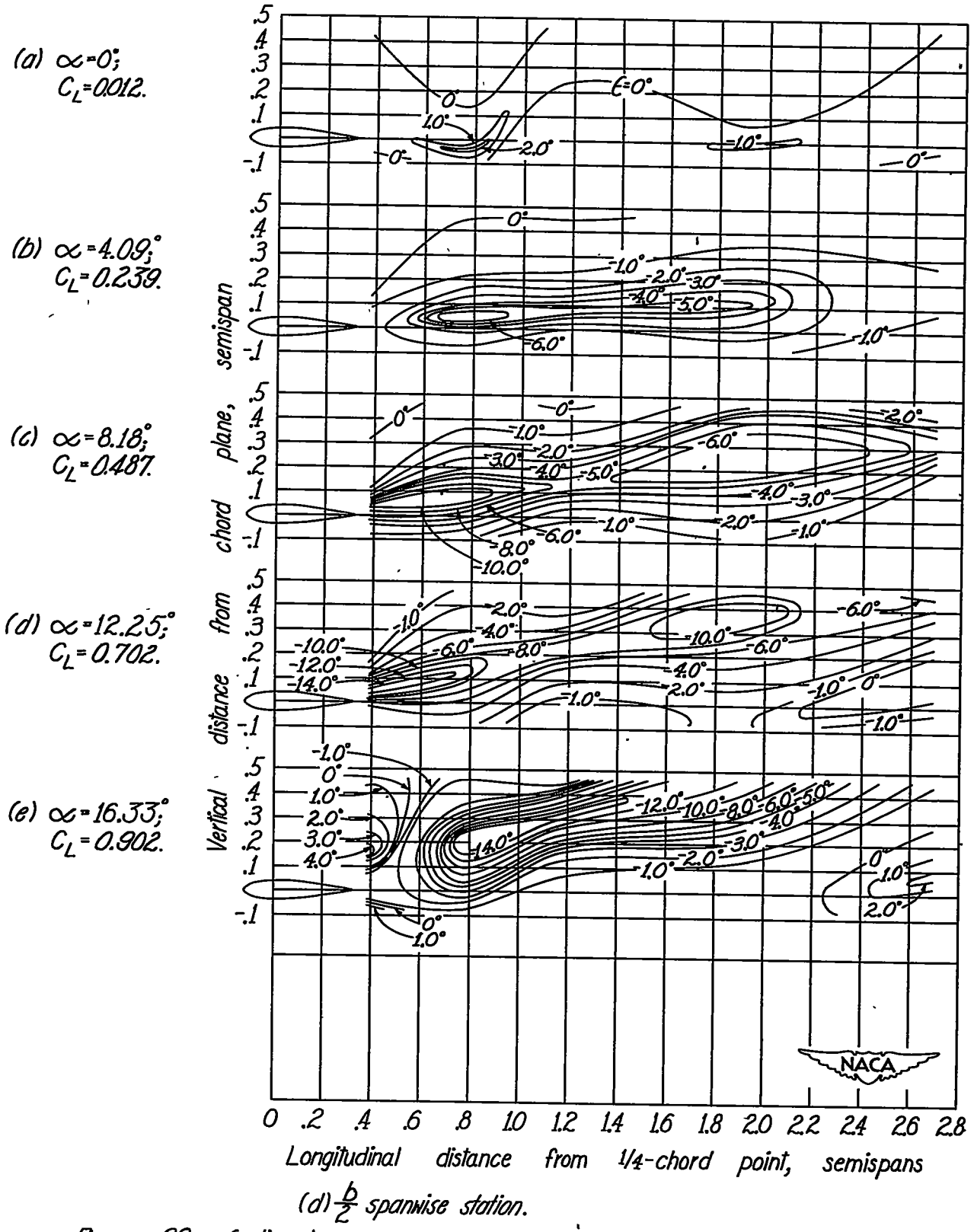

(d) $\frac{b}{2}$ spanwise station.

Figure 29. - Continued.

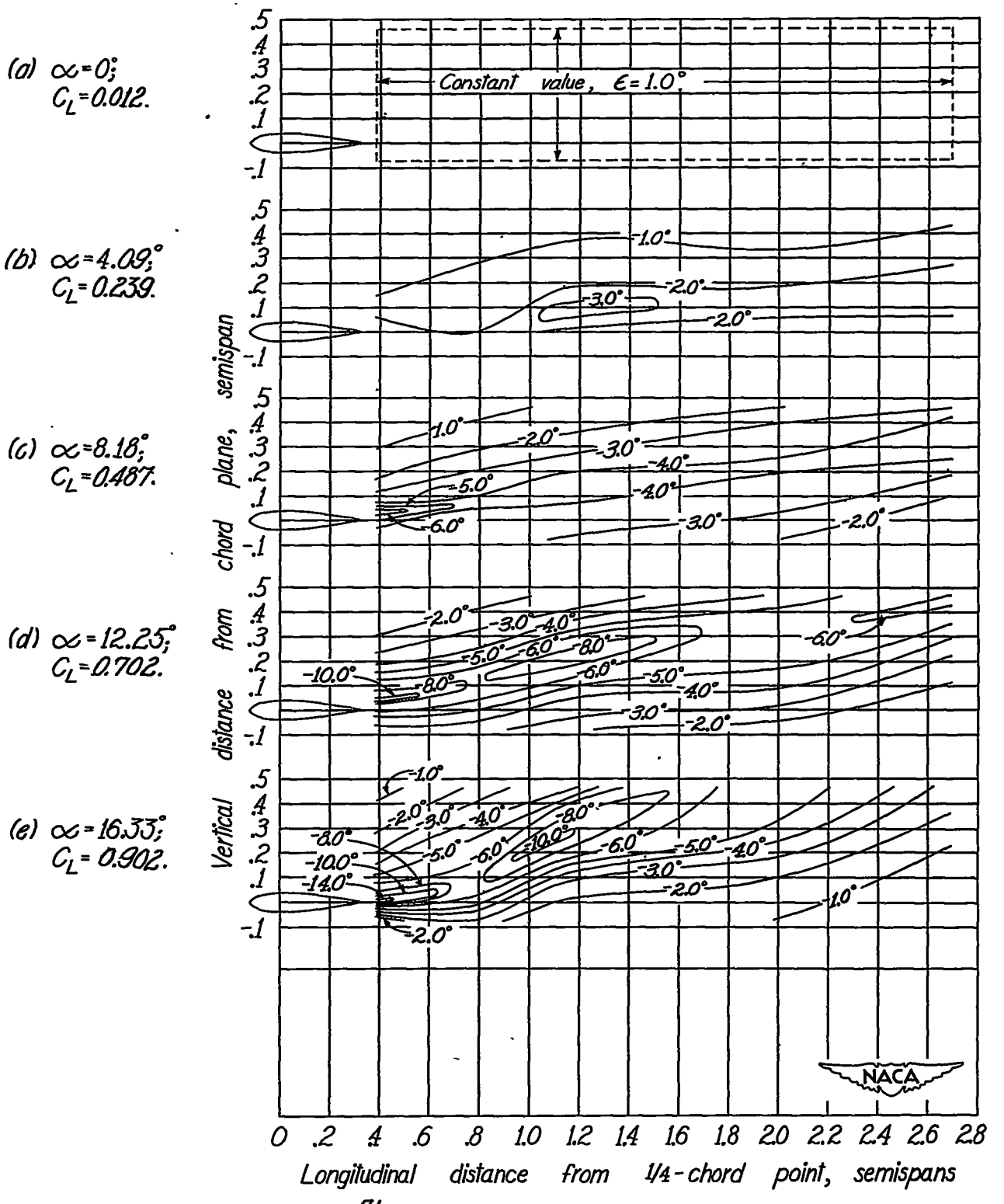

(e) $\frac{7b}{12}$ spanwise station.

Figure 29.- Concluded.

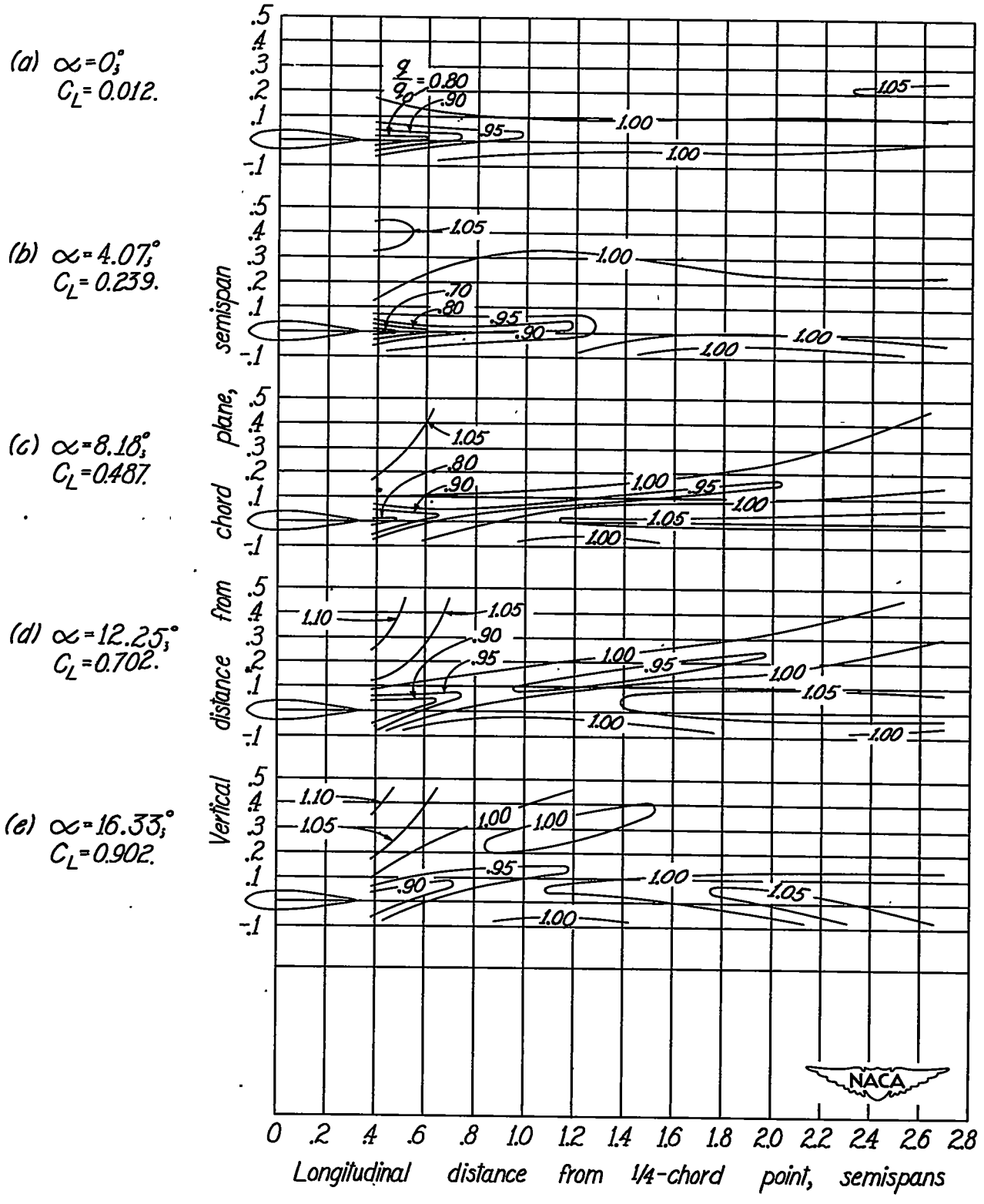

(a) Plane of symmetry.

Figure 30.- Dynamic-pressure-ratio contours behind 30° swept-back wing of 52-inch span. A=4.5.

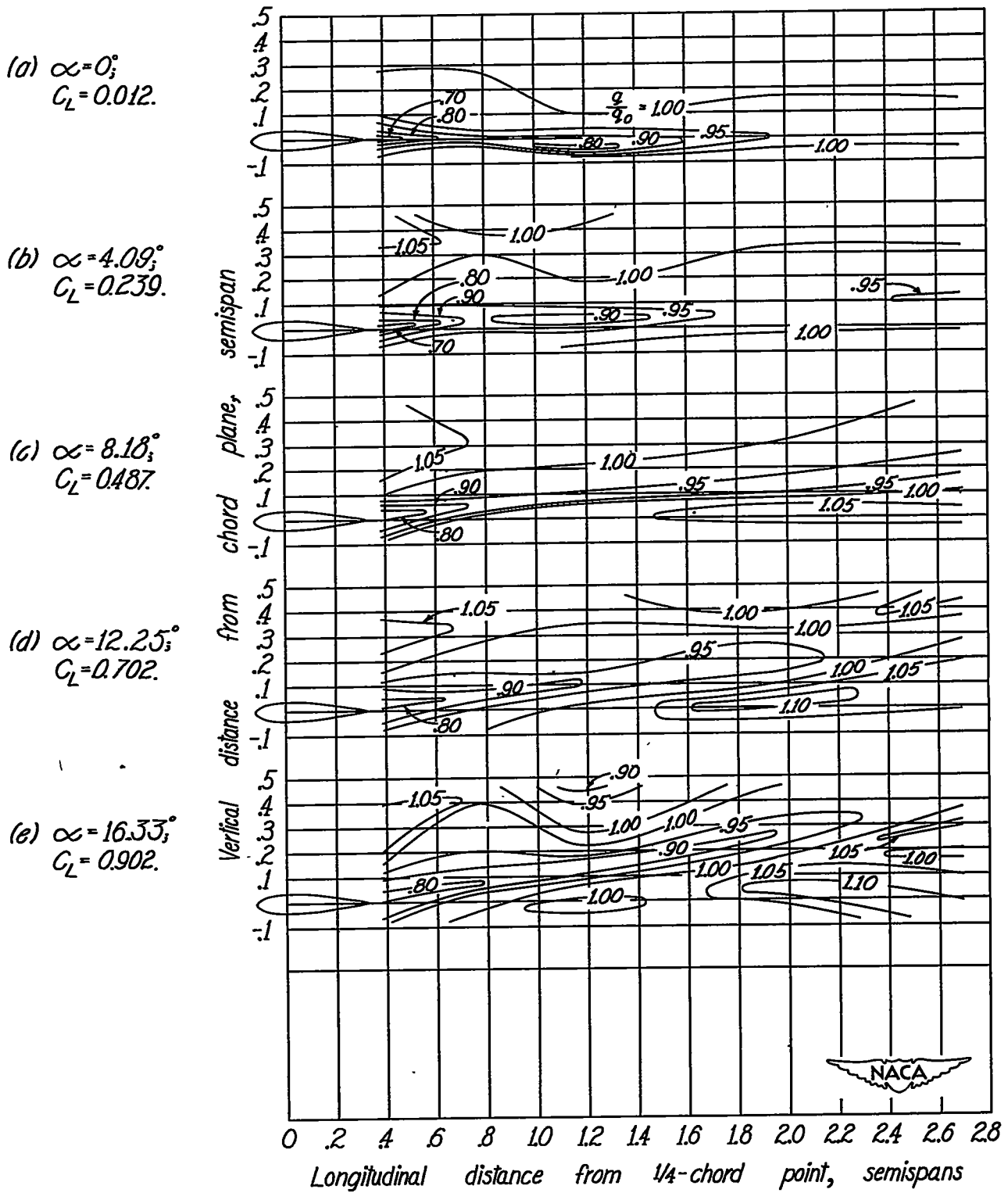

(b) $\frac{b}{6}$ spanwise station.

Figure 30.- Continued.

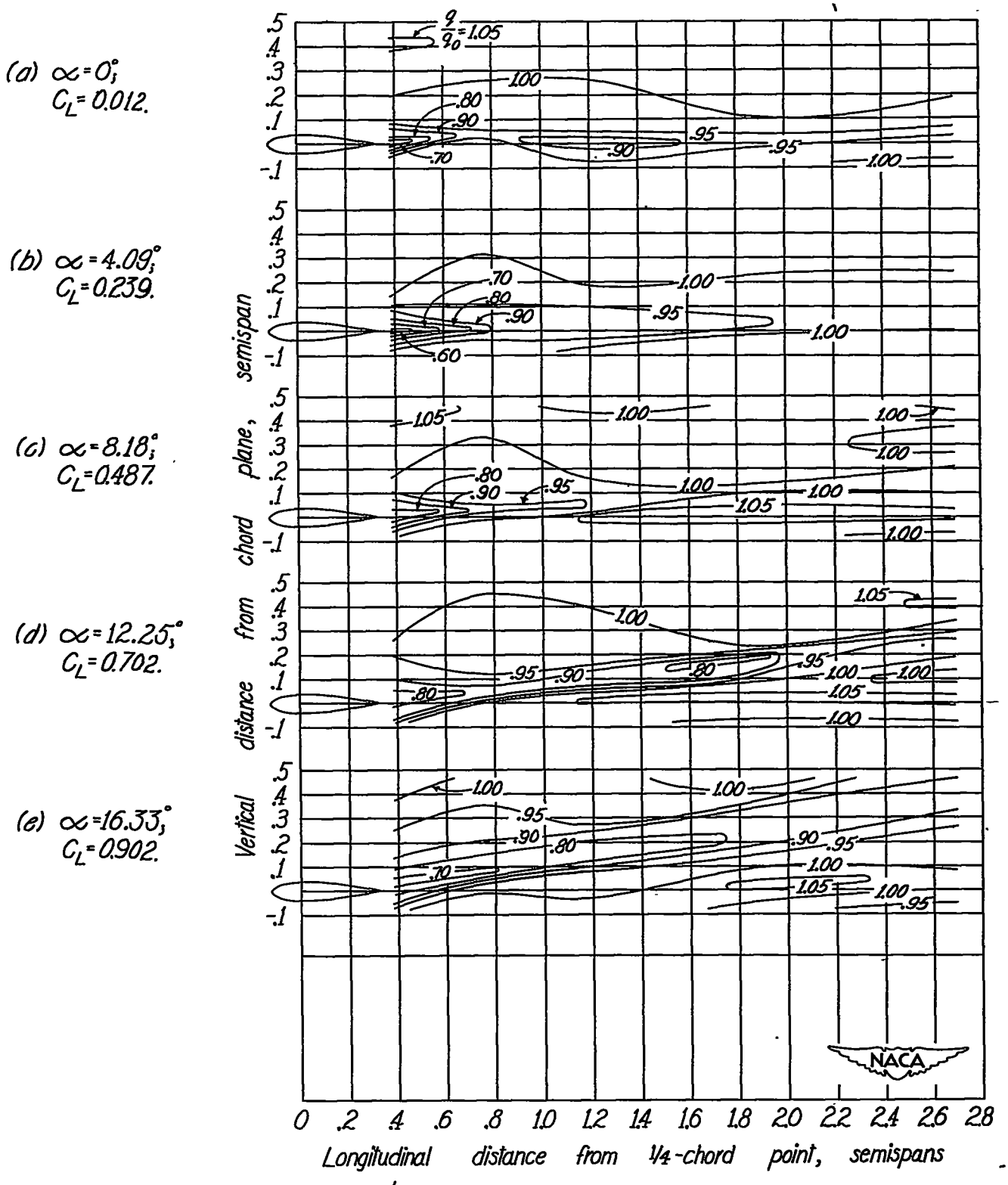

(c) $\frac{b}{3}$ spanwise station.

Figure 30.- Continued.

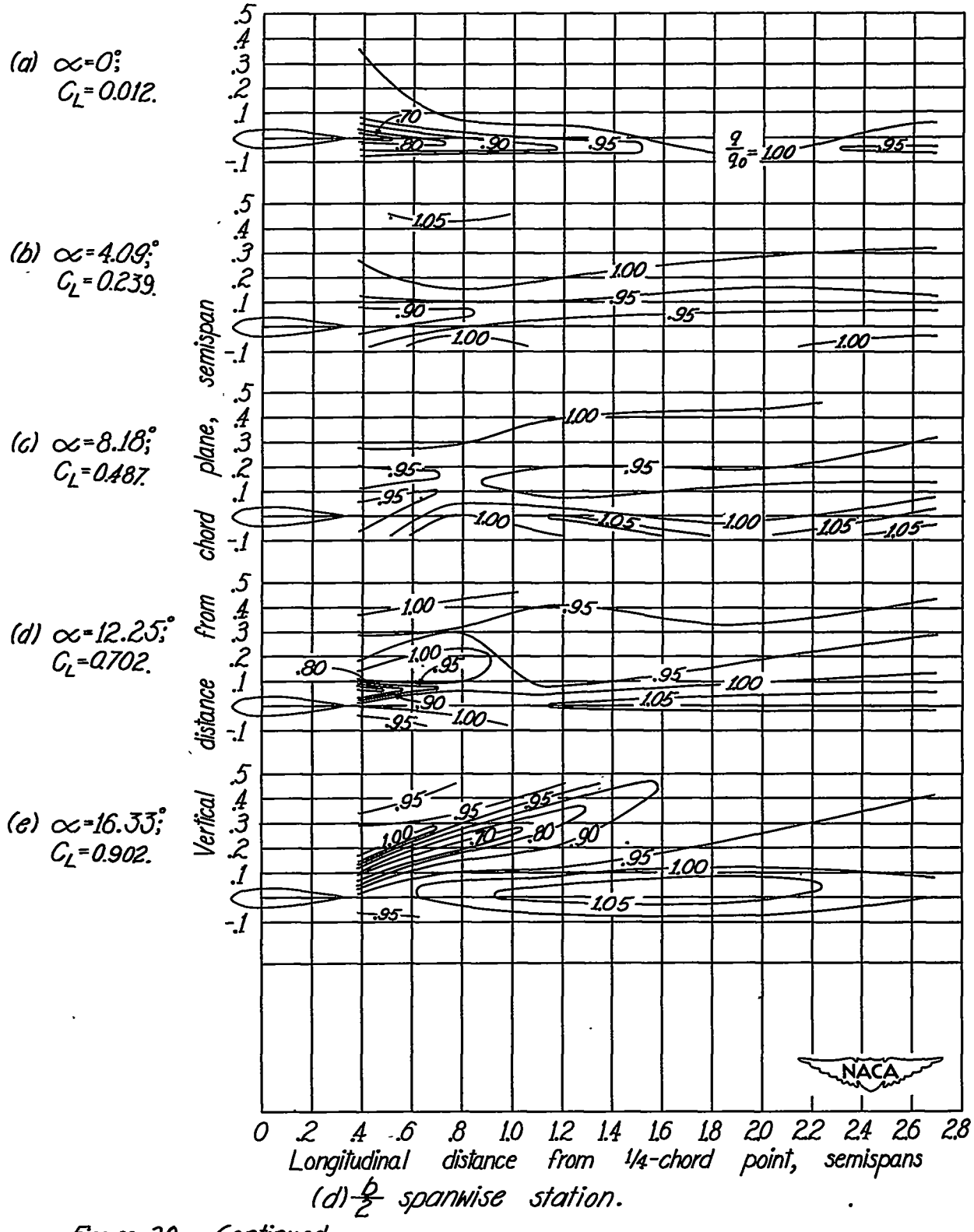

(d) $\frac{b}{2}$ spanwise station.

Figure 30.- Continued.

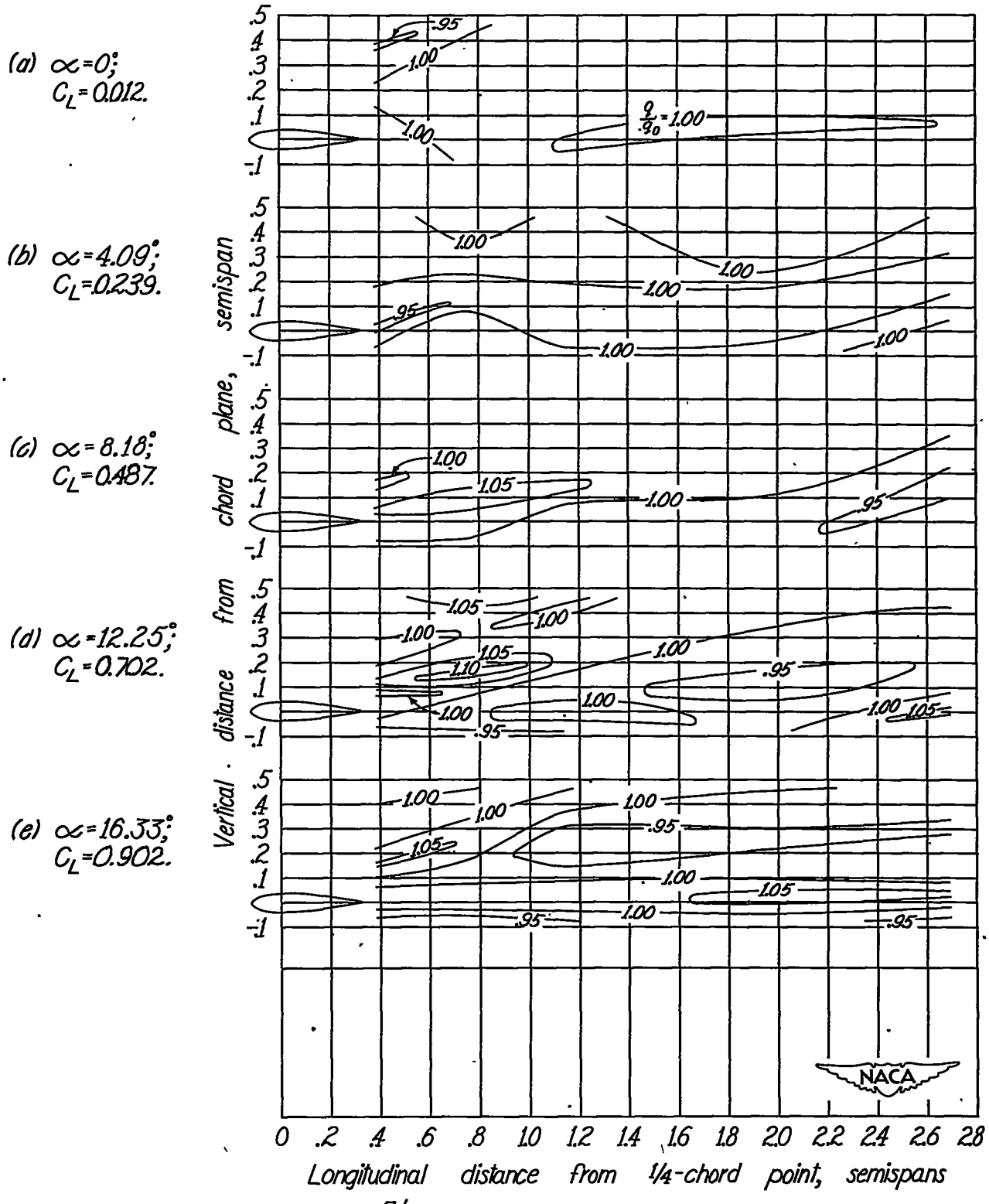

(e) $\frac{7b}{12}$ spanwise station.

Figure 30.- Concluded.

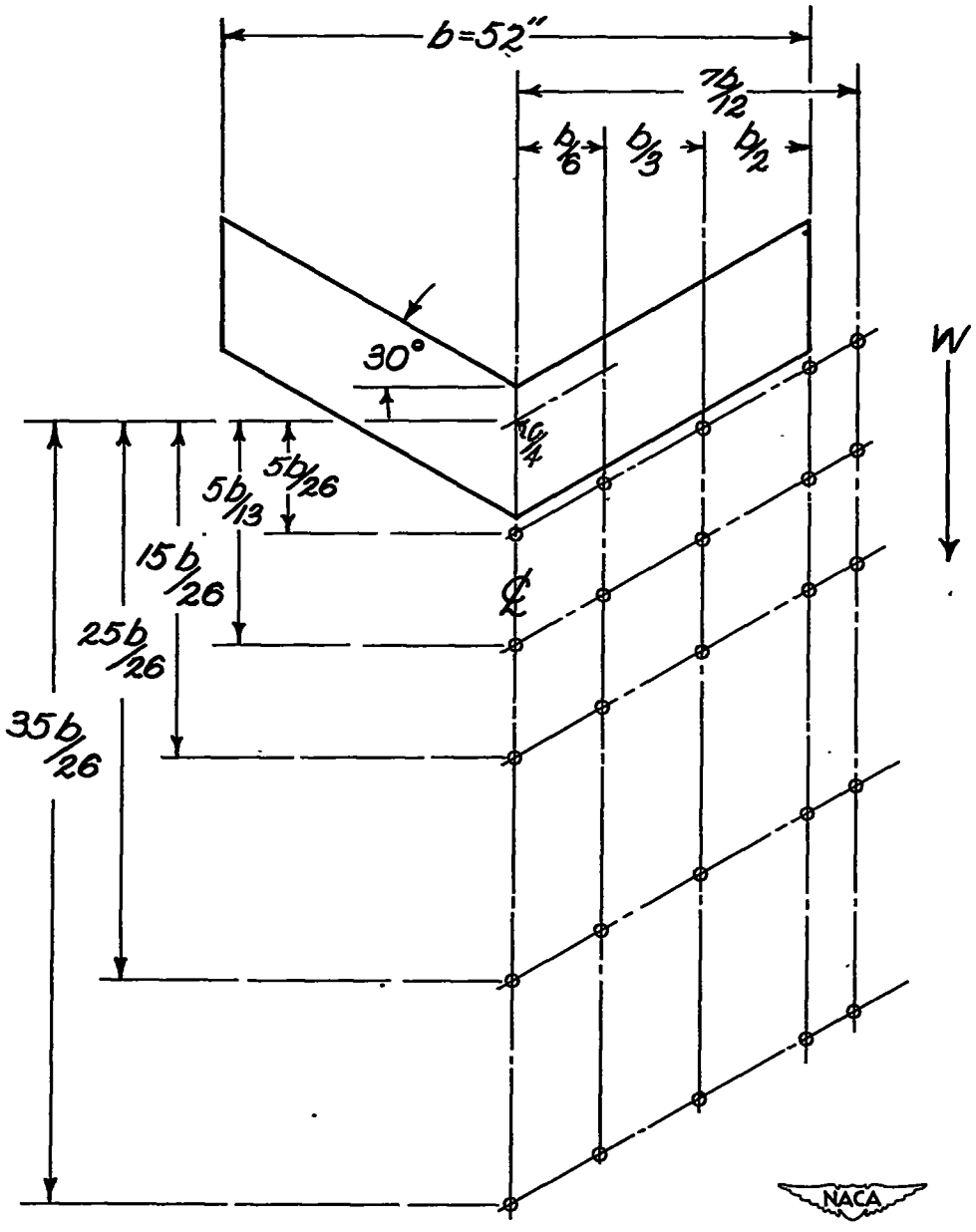

• Survey stations

Figure 31.- Survey stations behind 30° swept-forward wing of 52-inch span. A=4.5.

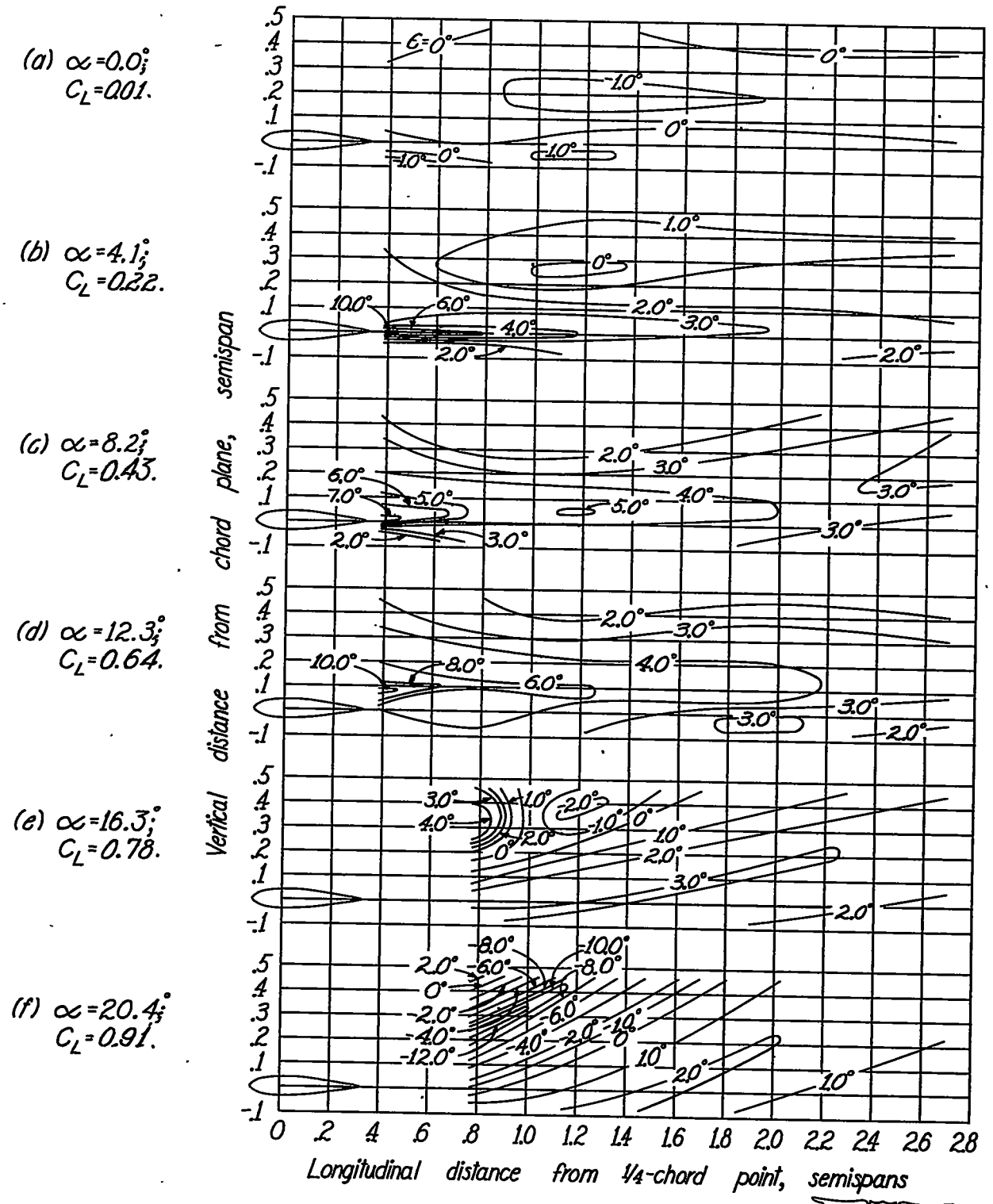

(a) Plane of symmetry.

Figure 32.- Downwash contours behind 30° sweptforward wing of 52 - inch span. A= 4.5.

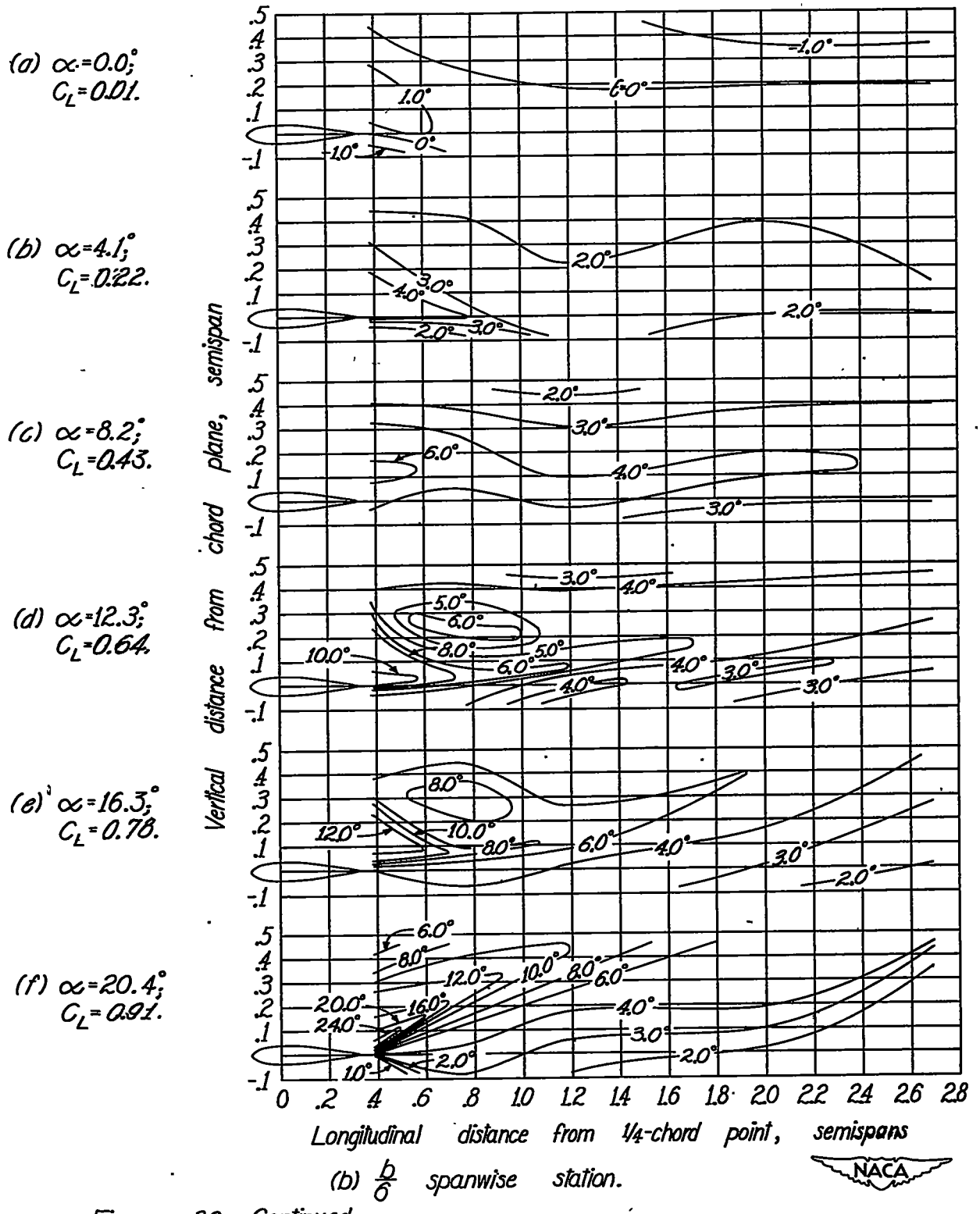

(b) $\frac{b}{6}$ spanwise station.

Figure 32.- Continued.

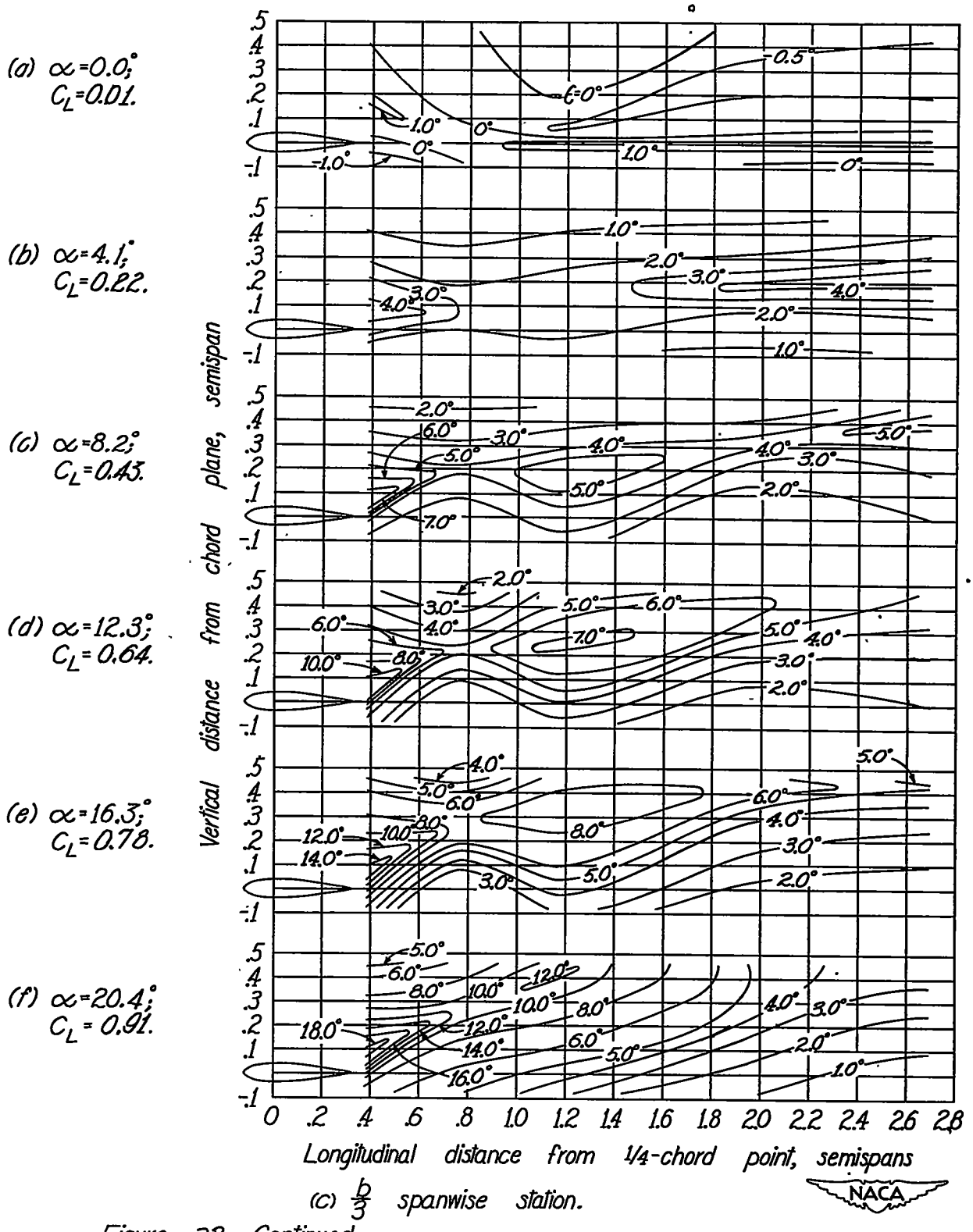

(c) $\frac{b}{3}$ spanwise station.

Figure 32.- Continued.

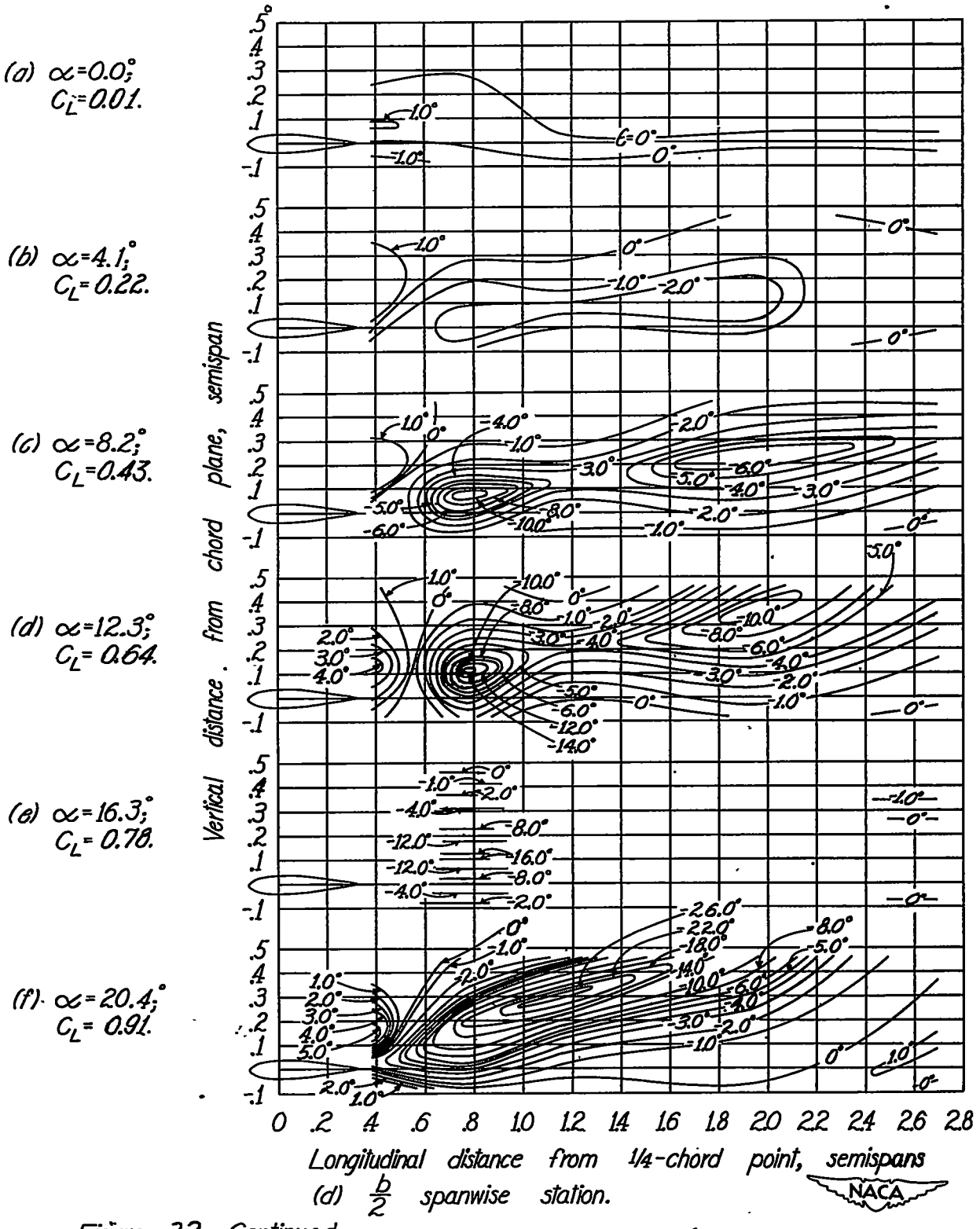

(d) $\frac{b}{2}$ spanwise station.

Figure 32.- Continued.

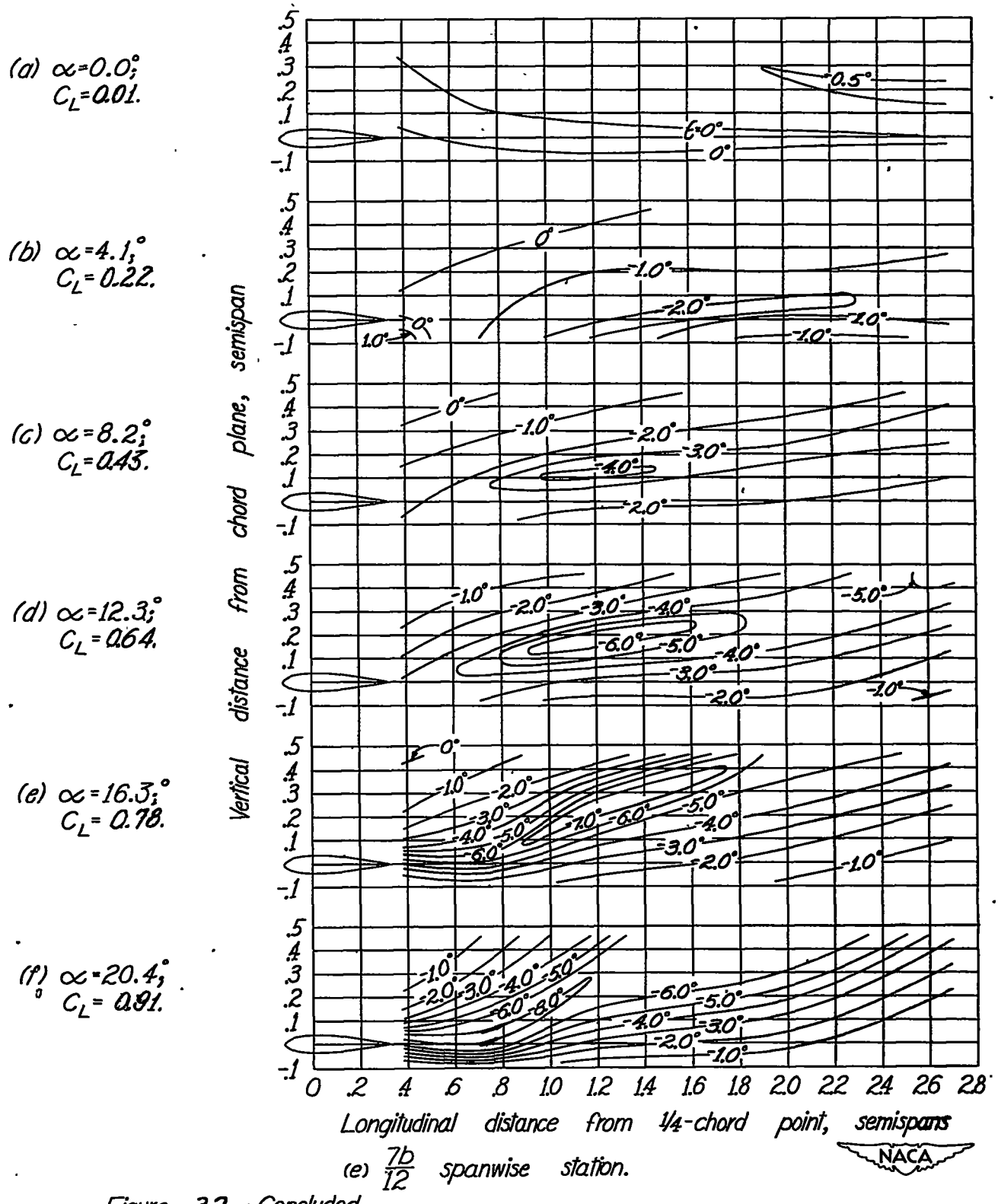

(e) $\frac{7b}{12}$ spanwise station.

Figure 32.- Concluded.

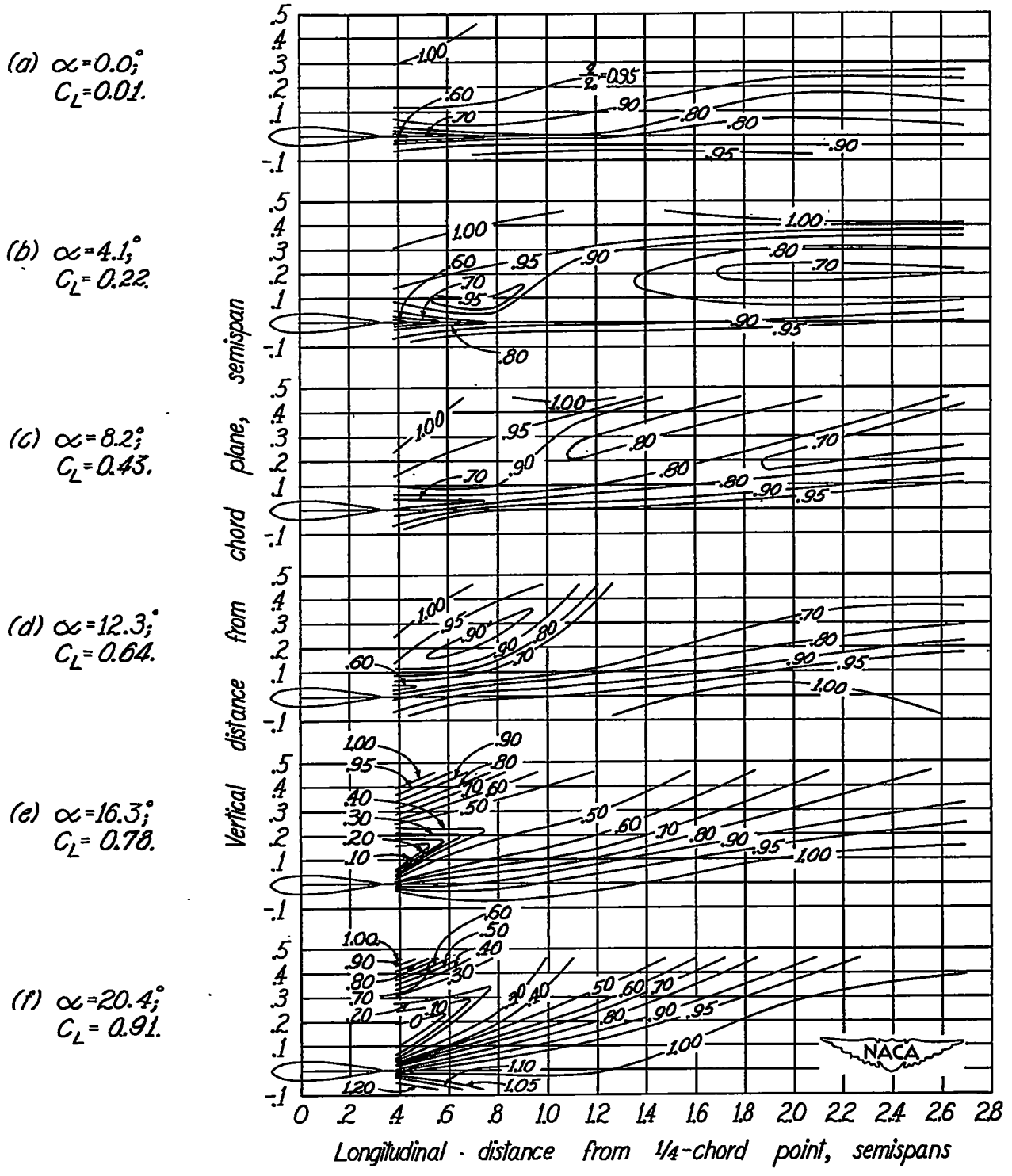

(a) Plane of symmetry.

Figure 33.- Dynamic - pressure - ratio contours behind 30° sweptforward wing of 52 - inch span. A=4.5.

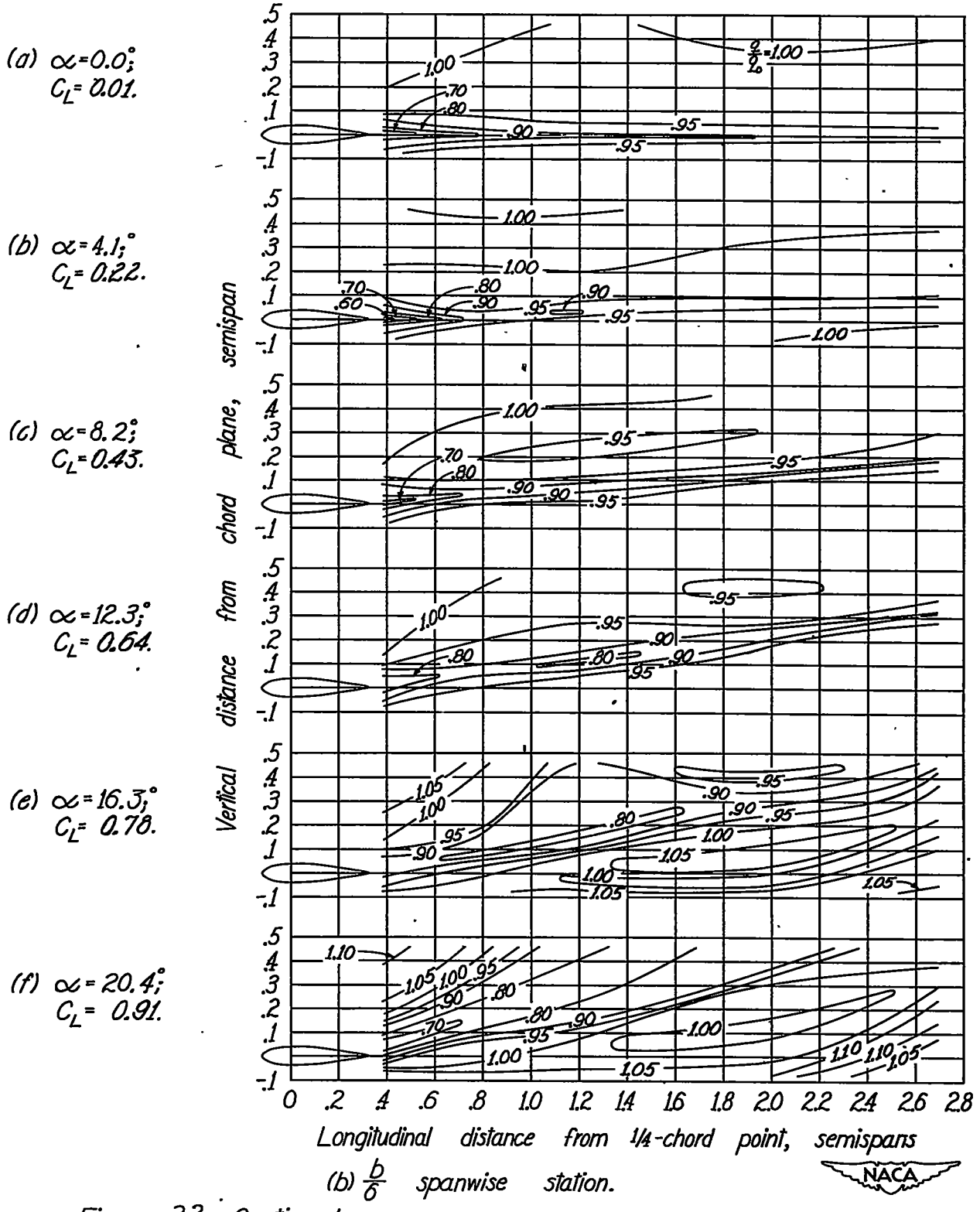

(b) $\frac{b}{6}$ spanwise station.

Figure 33.-Continued.

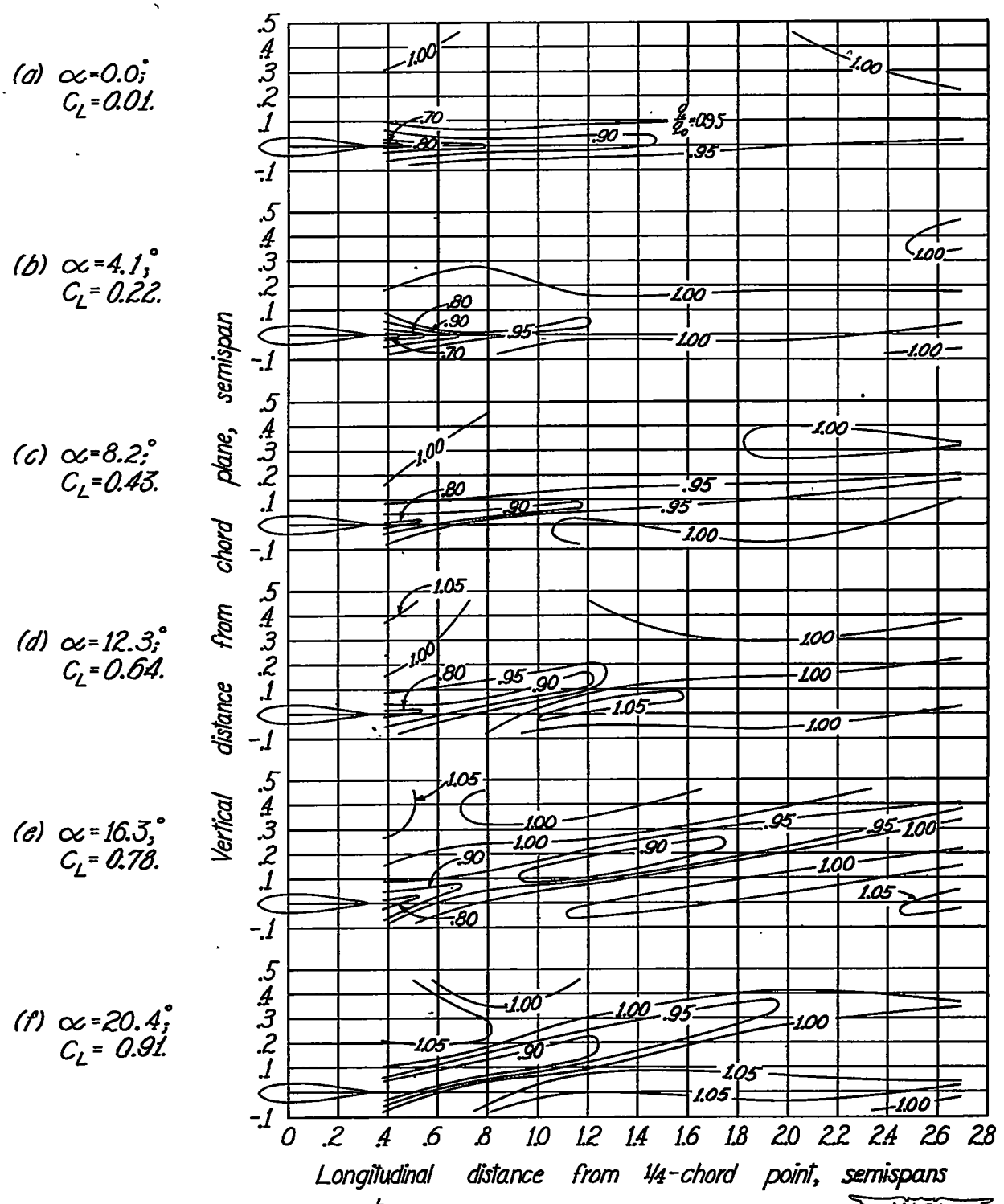

(c) $\frac{b}{3}$ spanwise station.

Figure 33.-Continued.

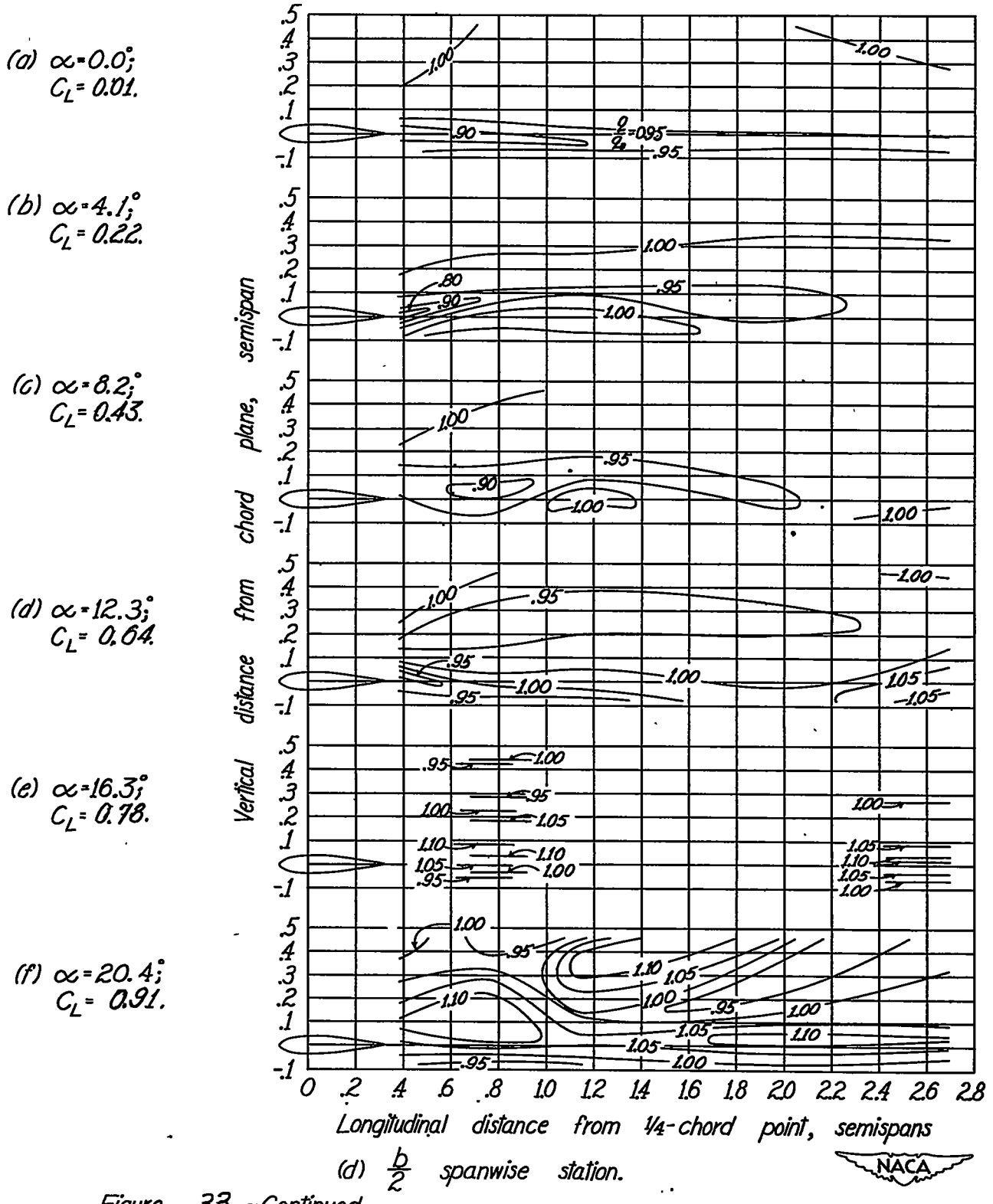

Figure 33.-Continued.

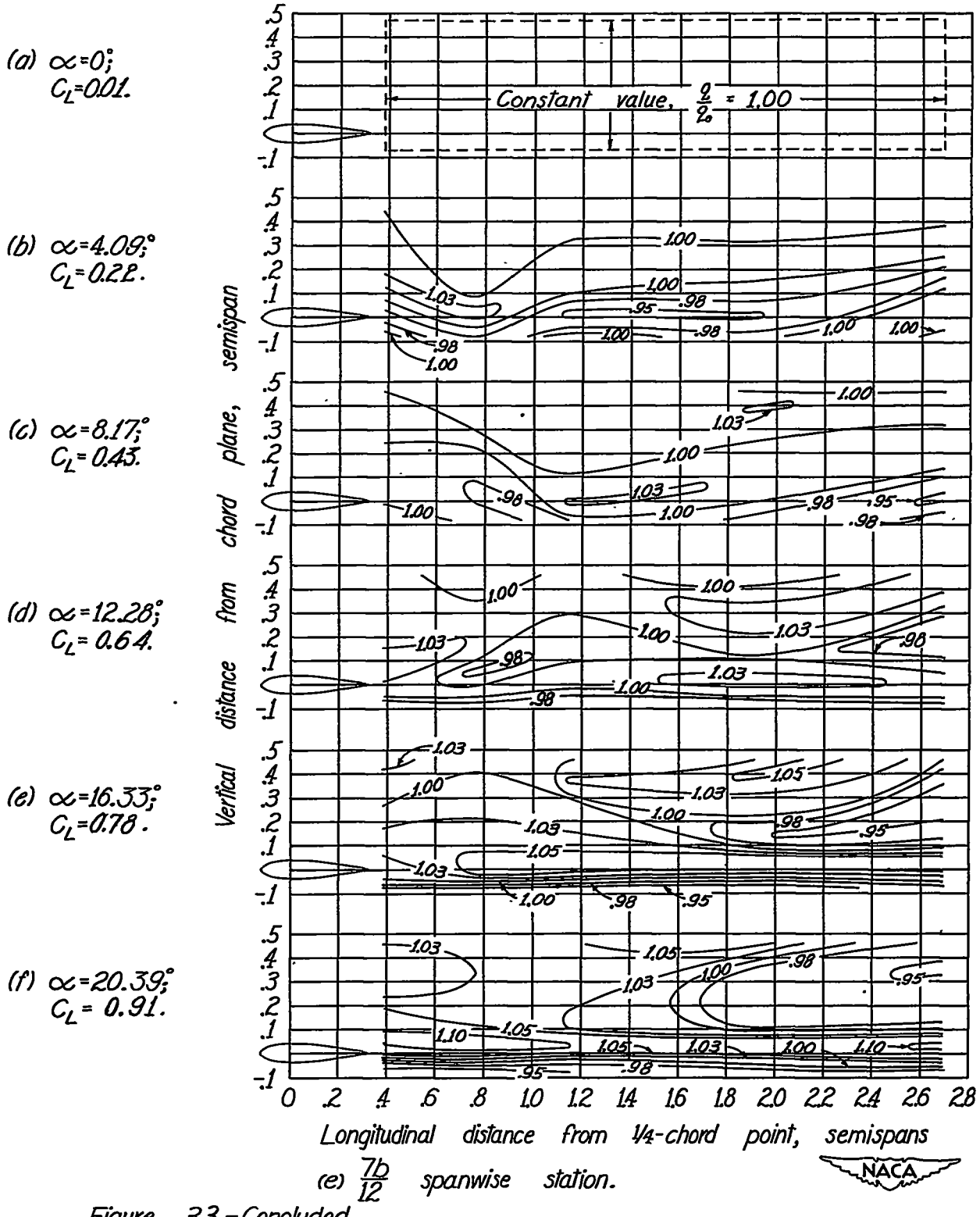

(e) $\frac{7b}{12}$ spanwise station.

Figure 33.-Concluded.

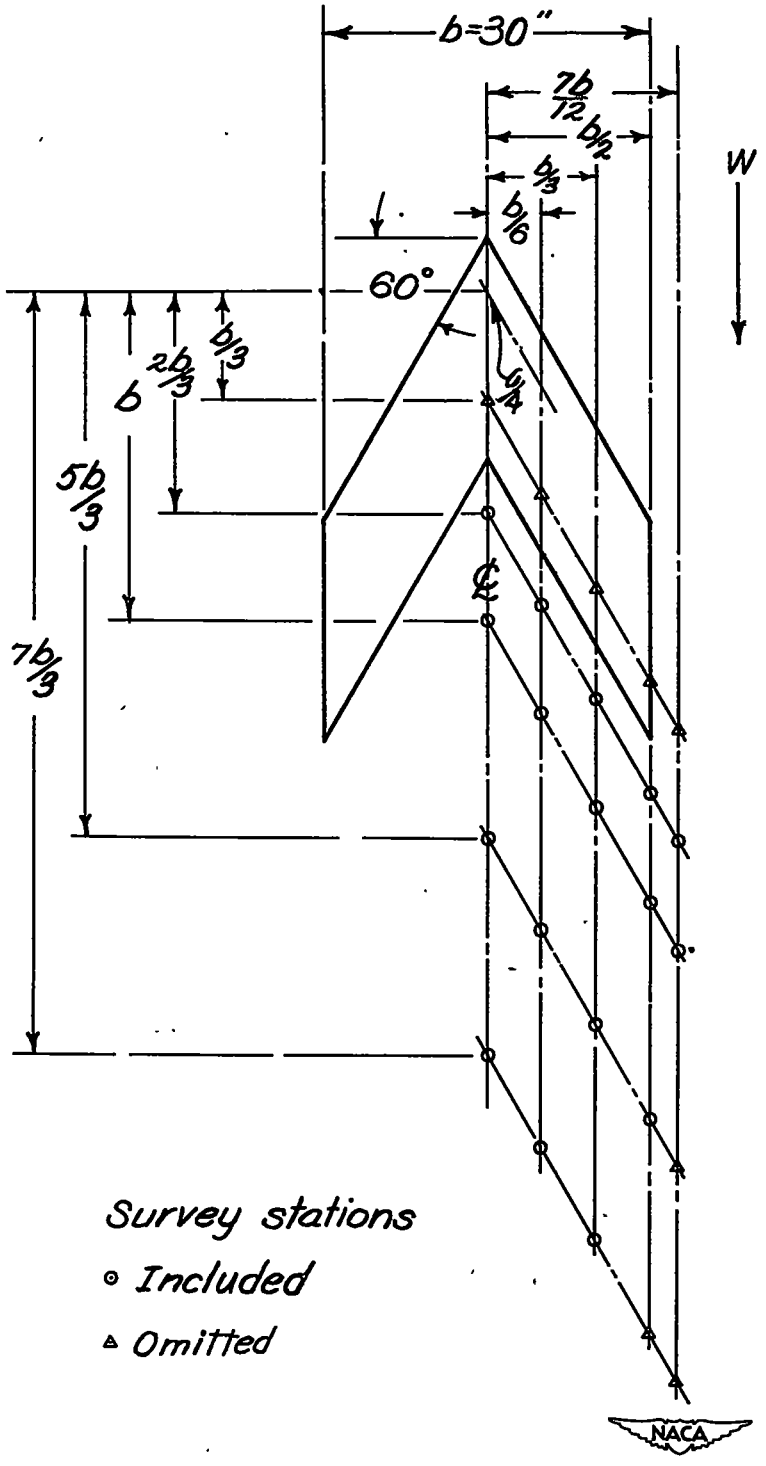

Figure 34.- Survey stations behind 60° sweptback wing of 30-inch span. A=1.5.

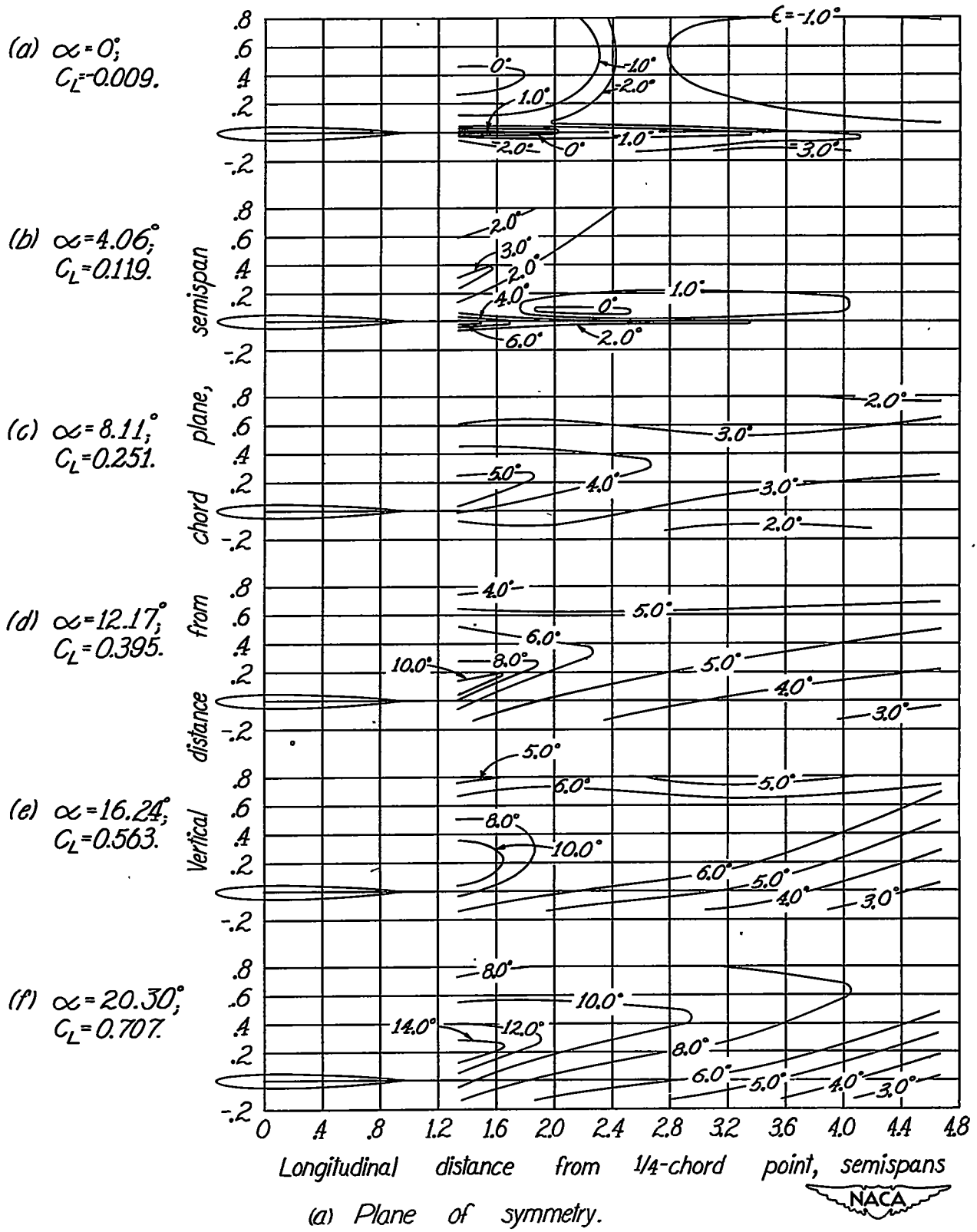

(a) Plane of symmetry.

Figure 35.- Downwash contours behind 60° sweptback wing of 30-inch span. A = 1.5.

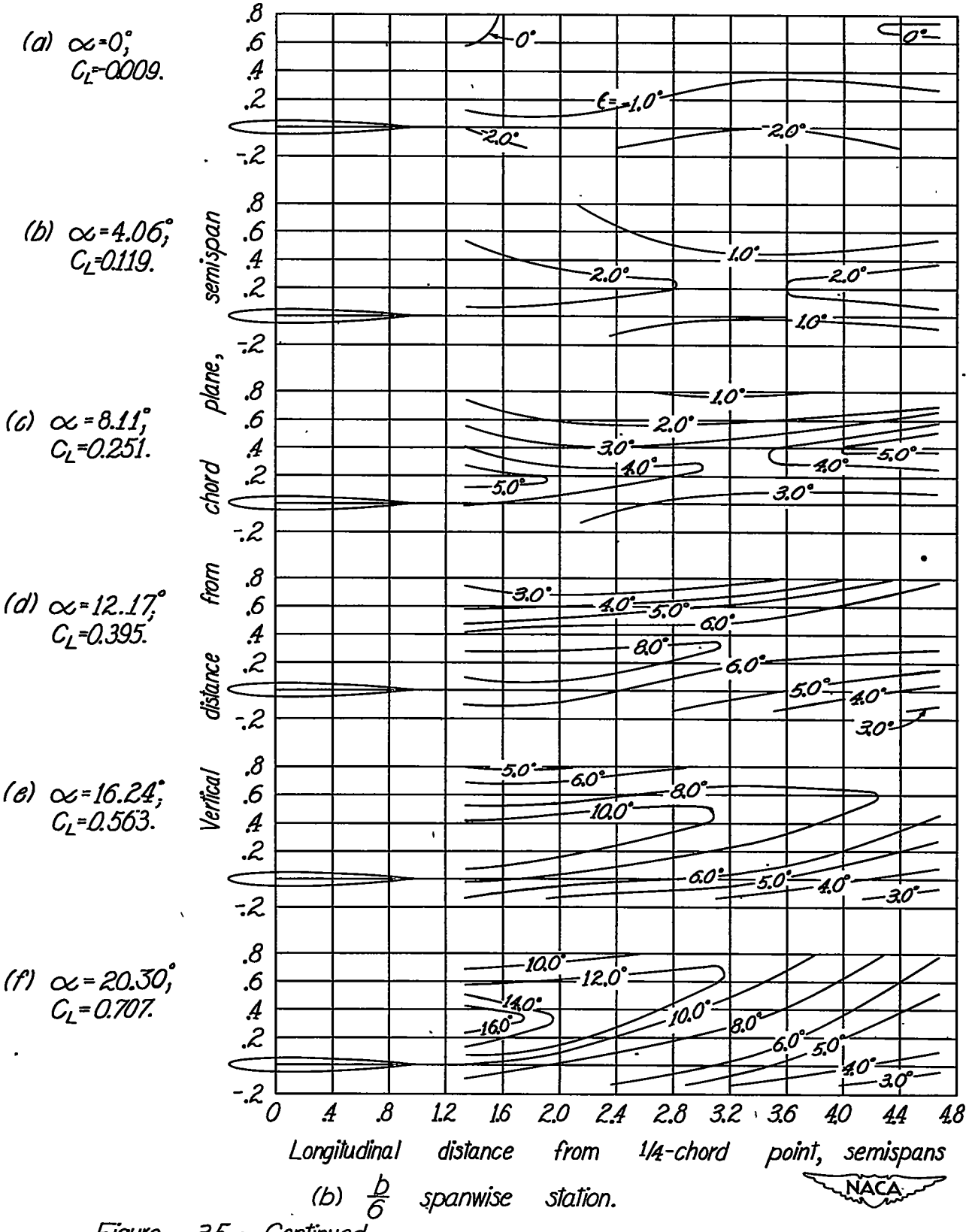

(b) $\frac{b}{6}$ spanwise station.

Figure 35.- Continued.

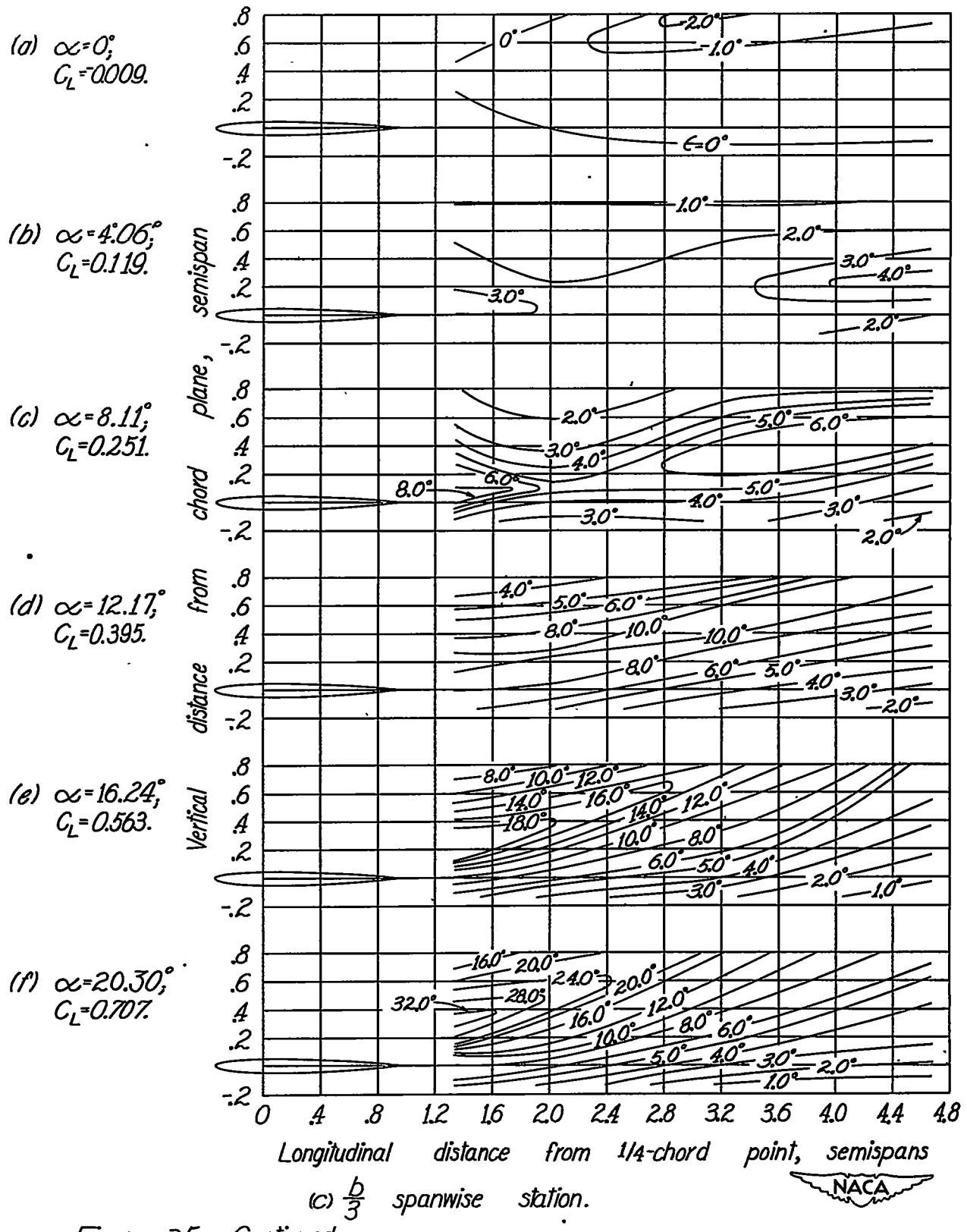

(c) $\frac{b}{3}$ spanwise station.

Figure 35.-Continued.

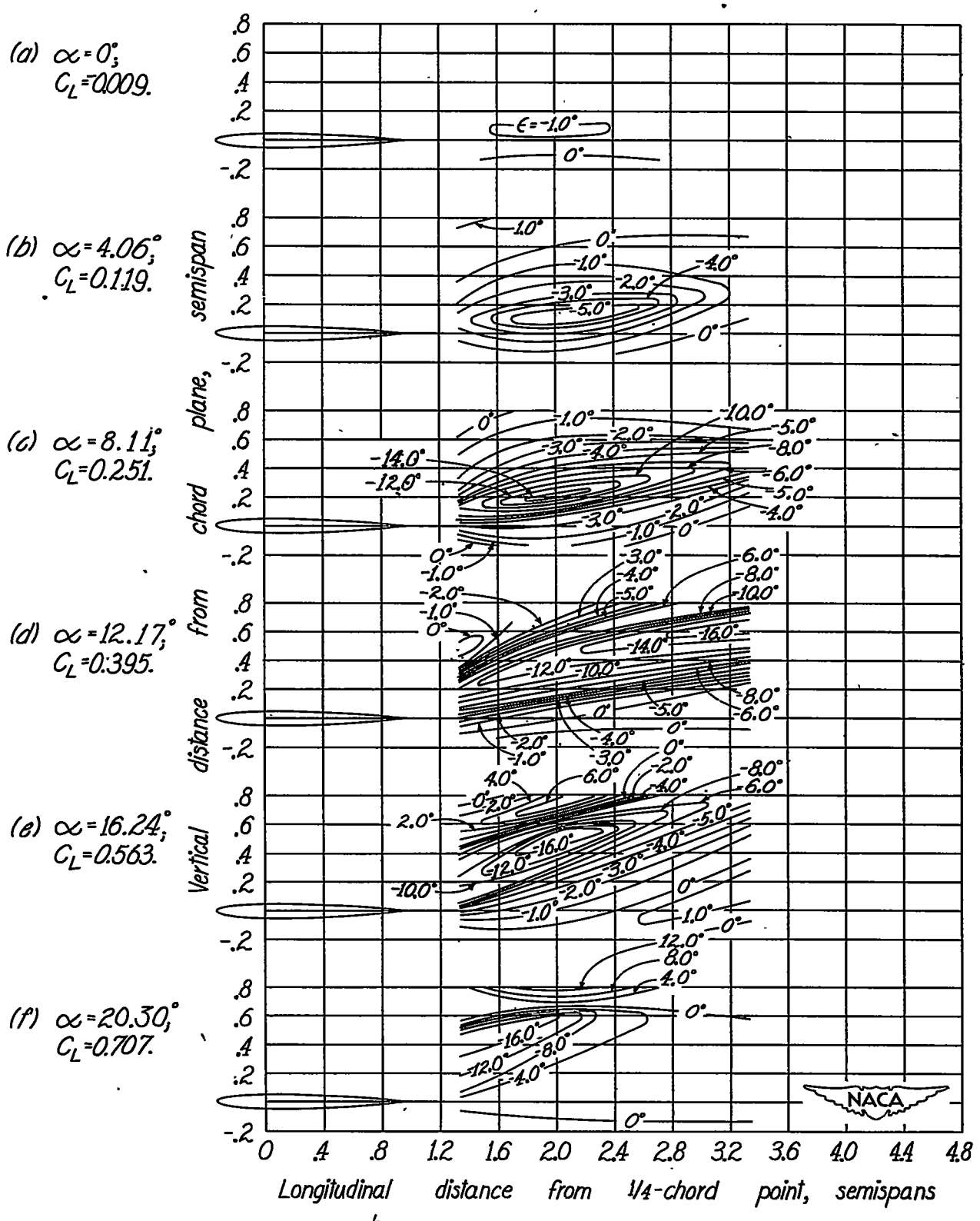

(d) $\frac{b}{2}$ spanwise station.

Figure 35.–Continued.

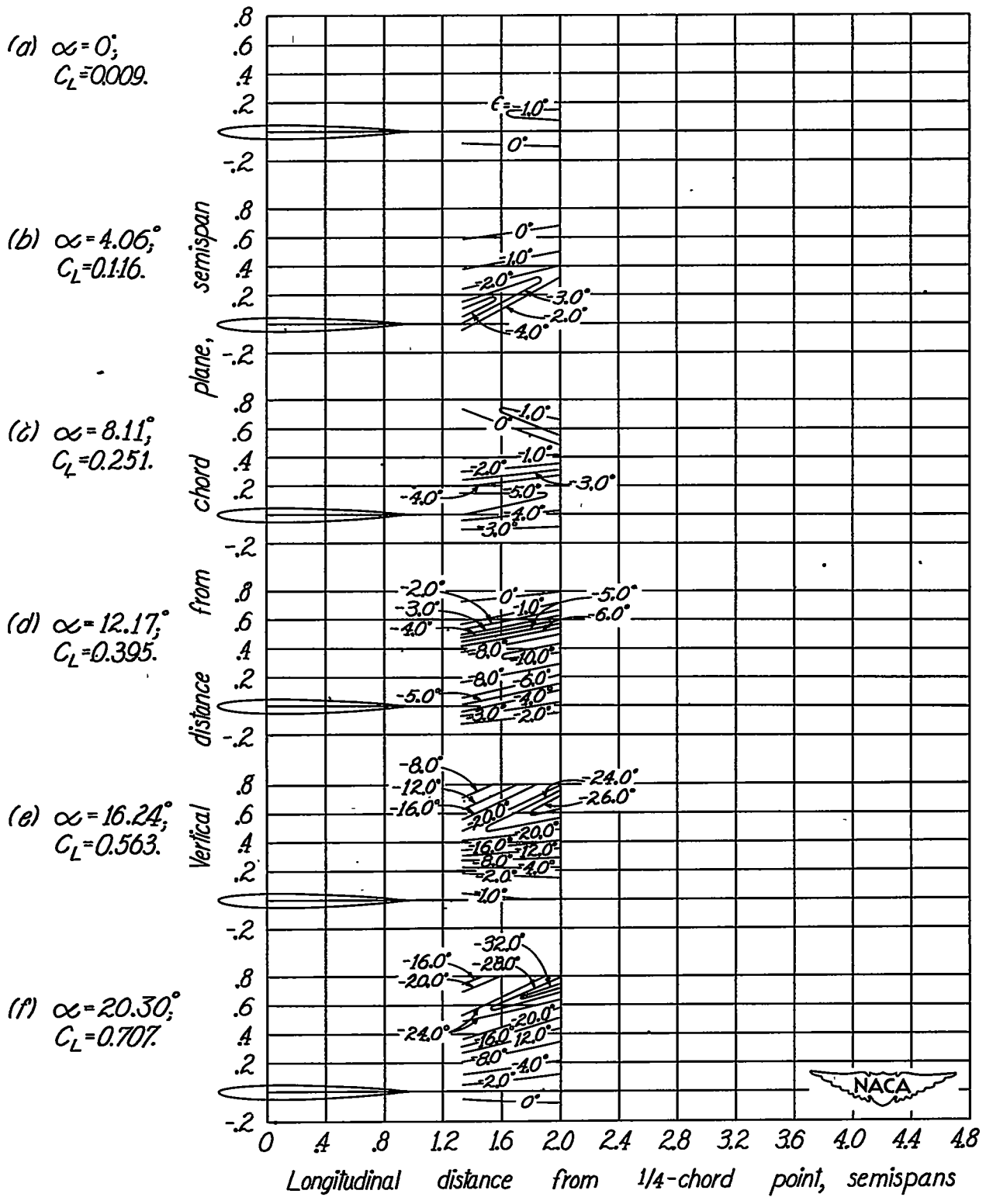

(e) $\frac{7b}{12}$ spanwise station.

Figure 35.- Concluded.

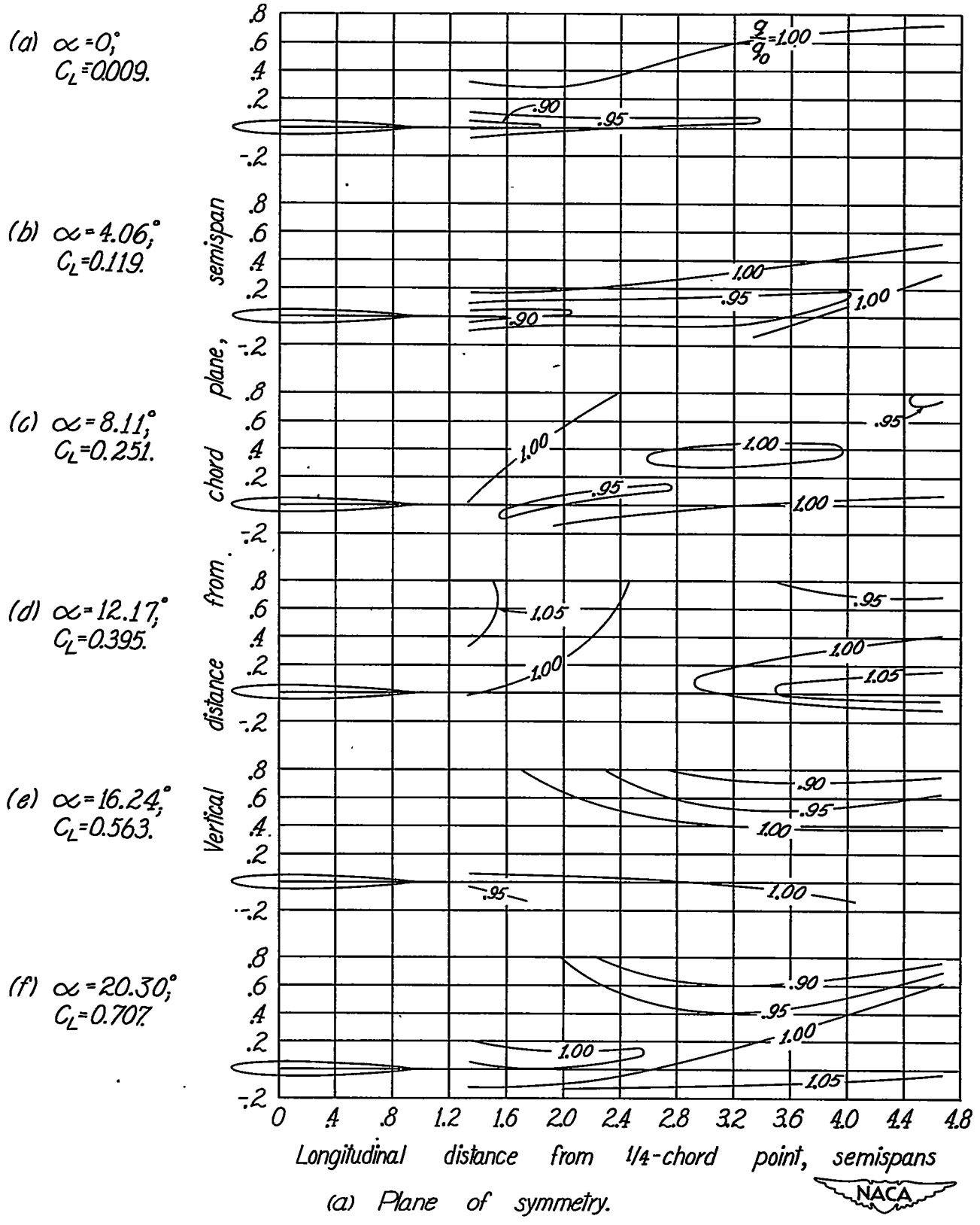

(a) Plane of symmetry.

Figure 36.- Dynamic-pressure-ratio contours behind 60° swept-back wing of 30-inch span. A=1.5.

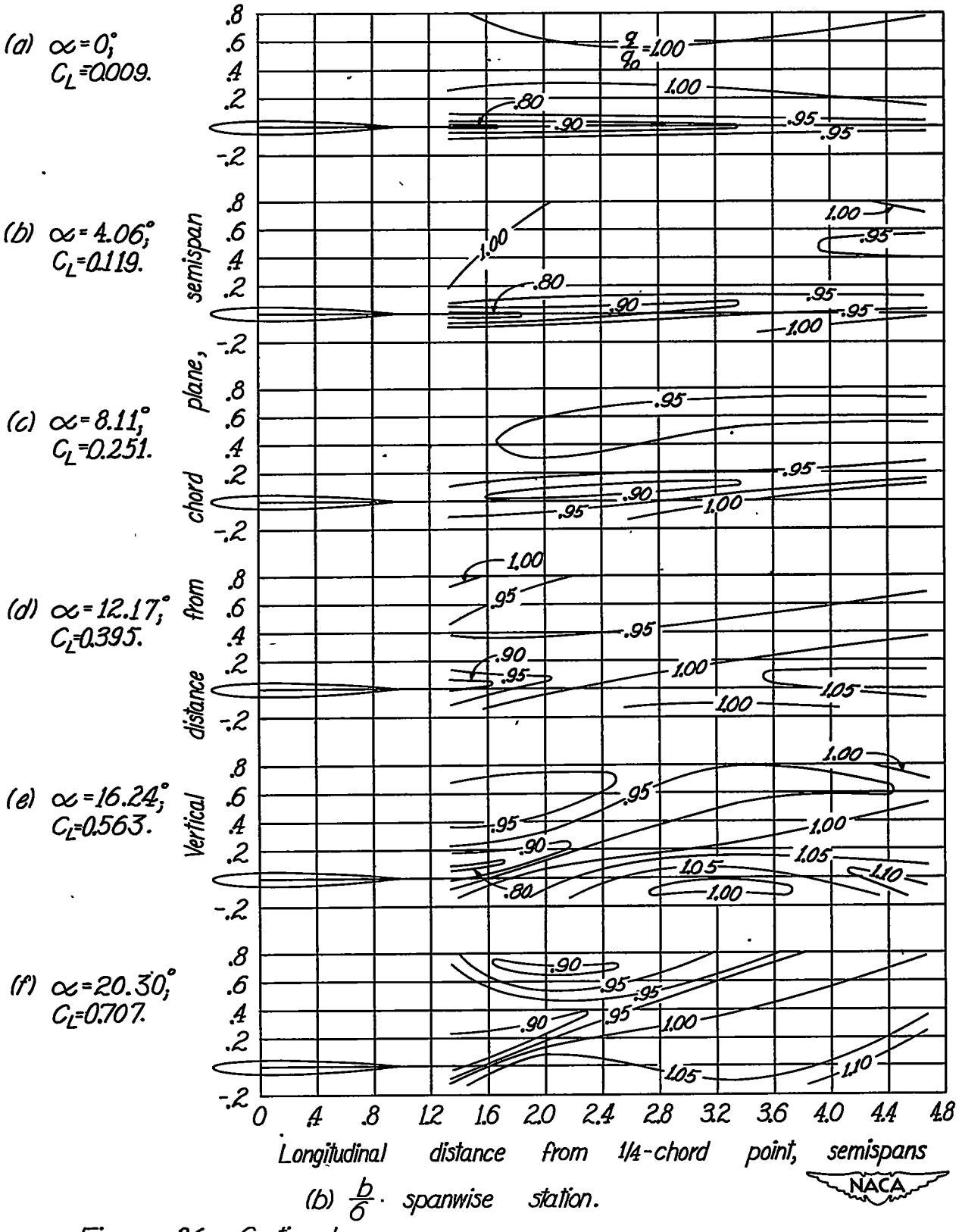

(b) $\frac{b}{6}$ · spanwise station.

Figure 36.–Continued.

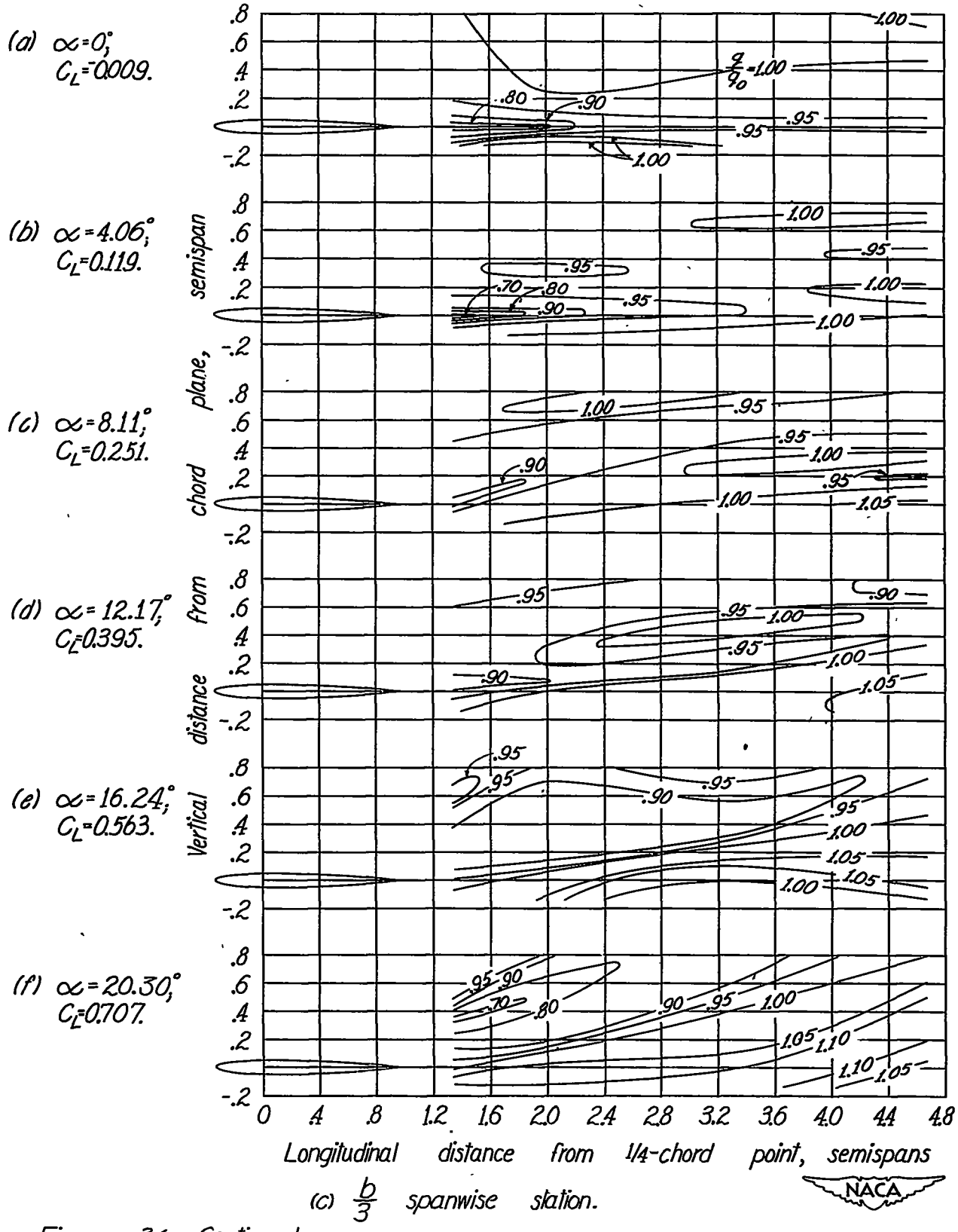

(c) $\frac{b}{3}$ spanwise station.

Figure 36.-Continued.

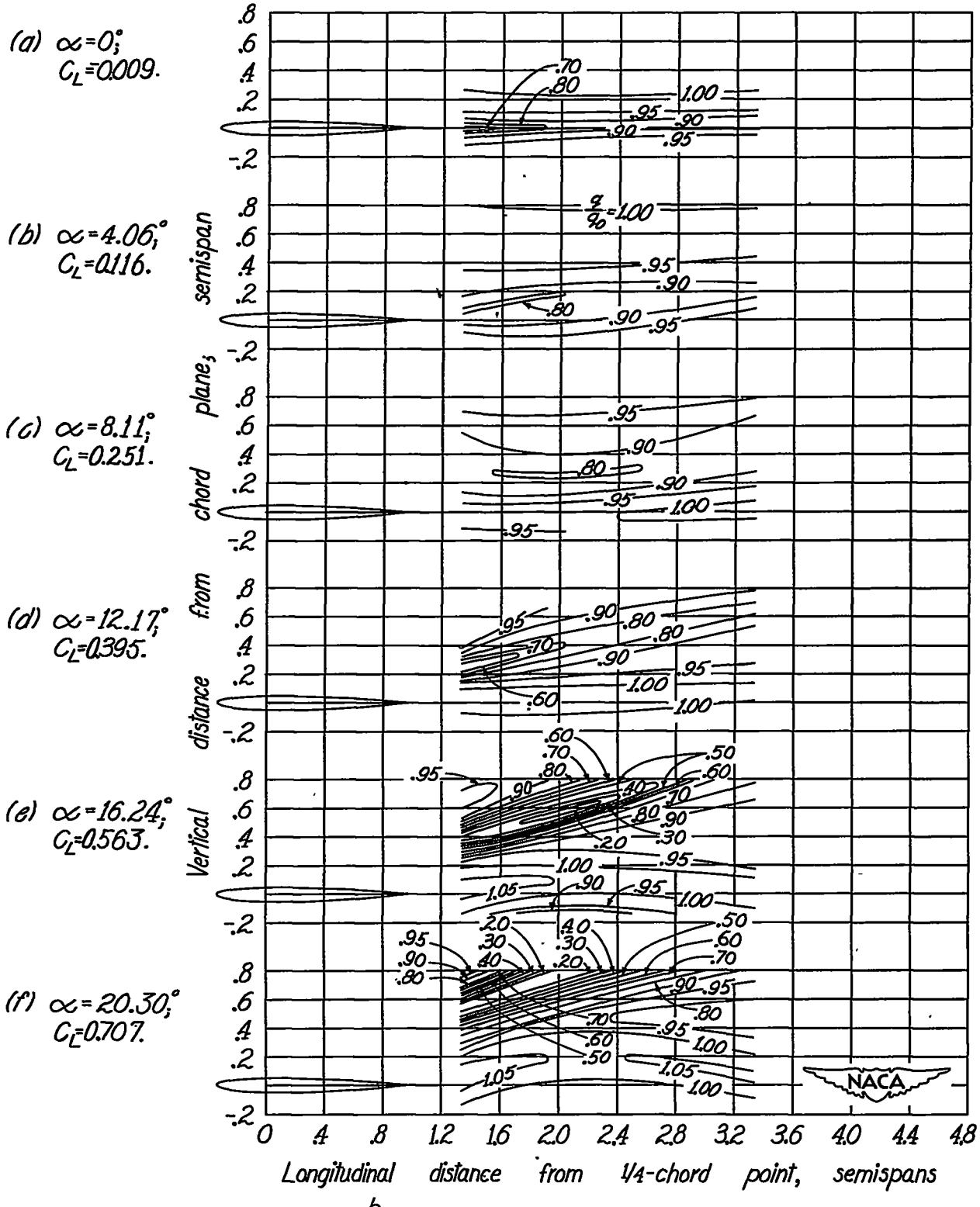

(d) $\frac{b}{2}$ spanwise station.

Figure 36.- Continued.

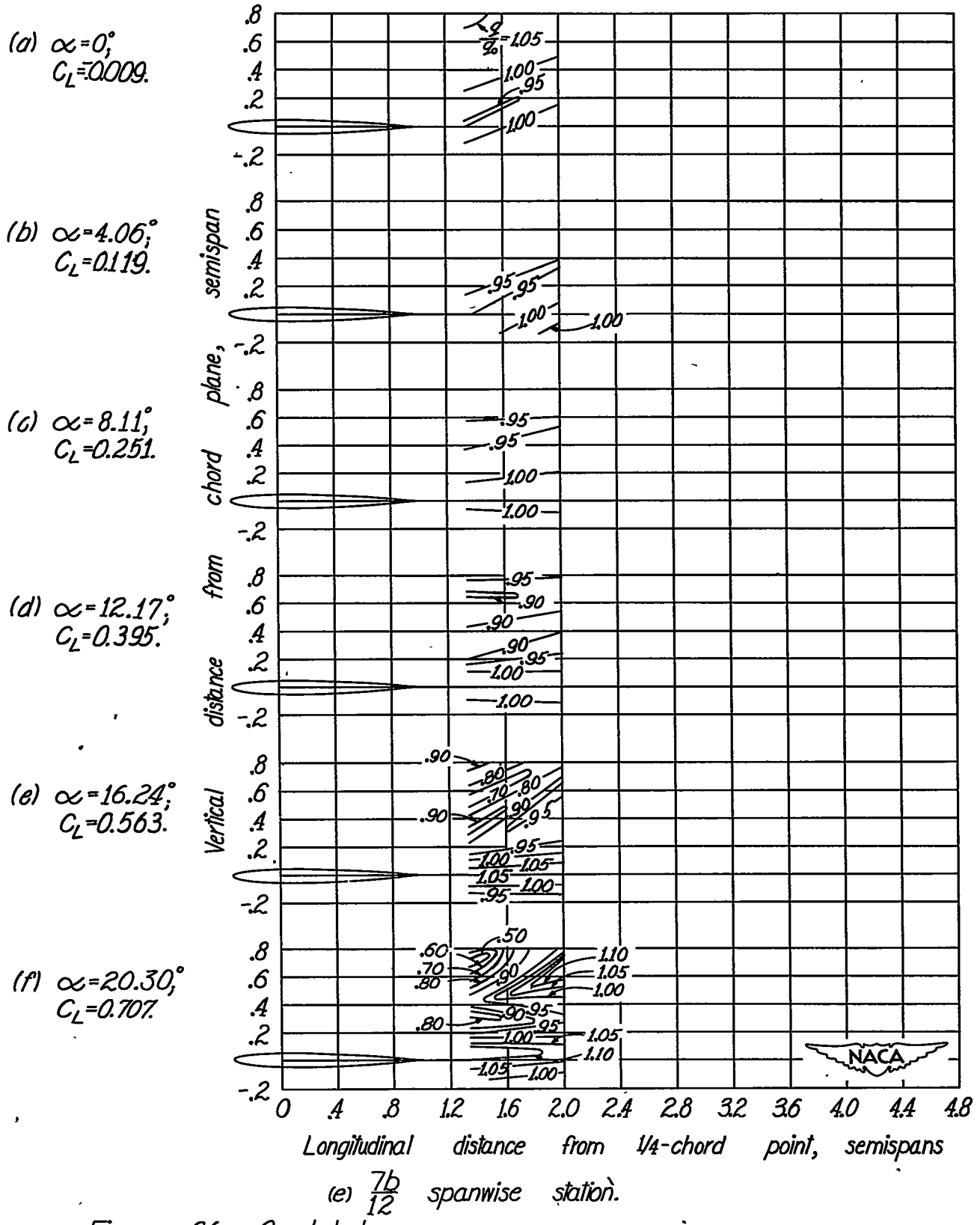

(e) $\frac{7b}{12}$ spanwise station.

Figure 36.—Concluded.

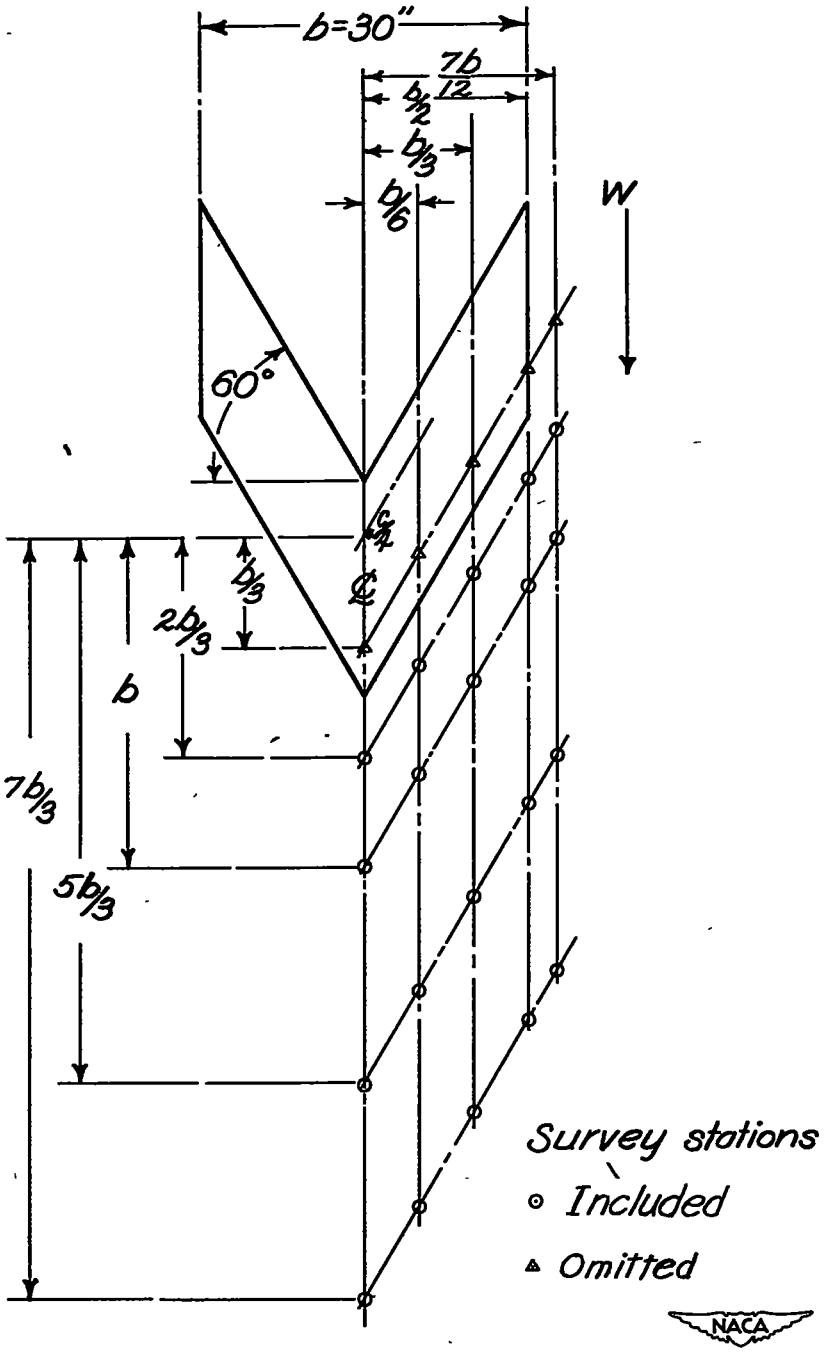

Figure 37.- Survey stations behind 60° sweptforward wing of 30-inch span. A=1.5.

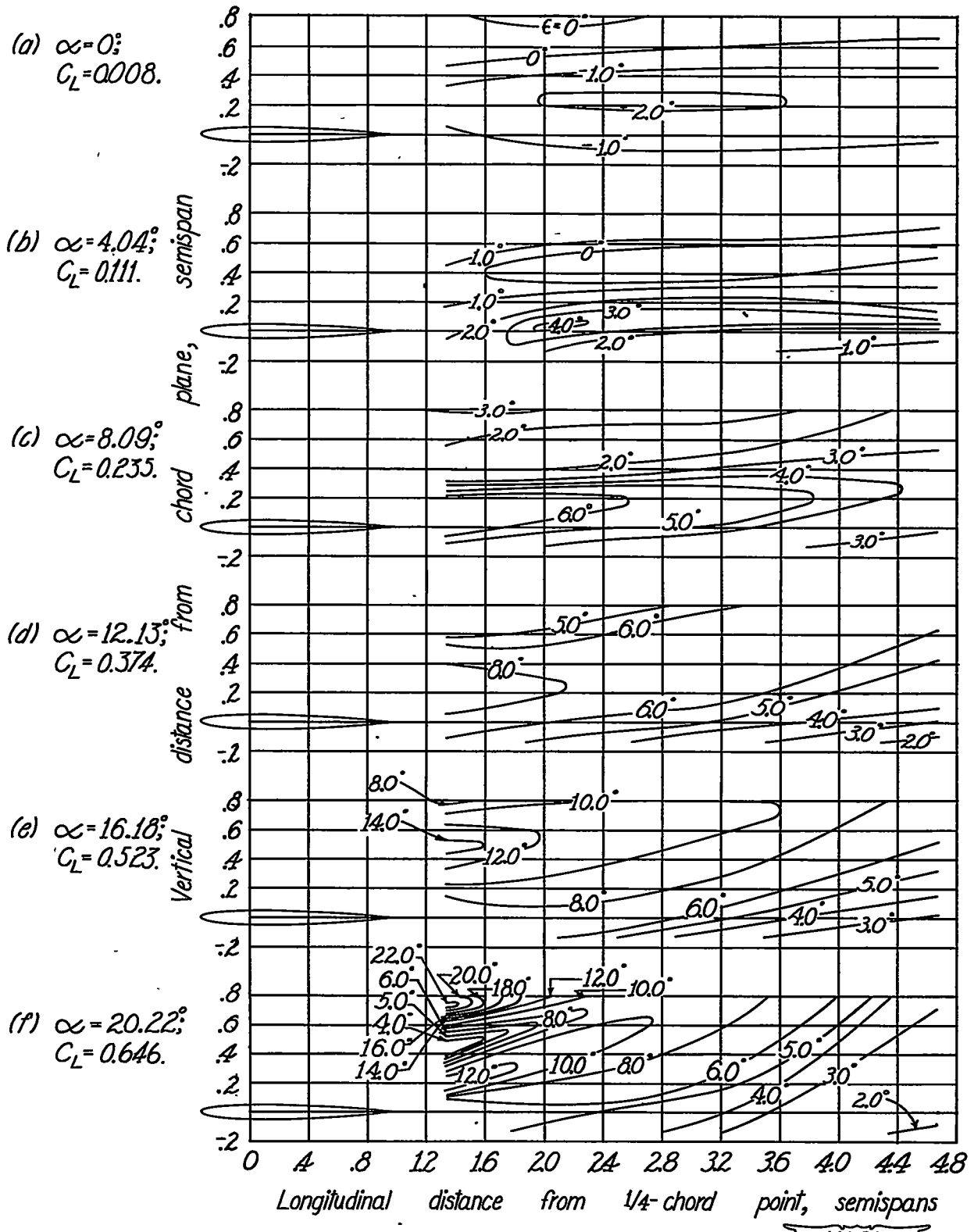

(a) Plane of symmetry.

Figure 38.- Downwash contours behind 60° sweptforward wing of 30-inch span. A=1.5.

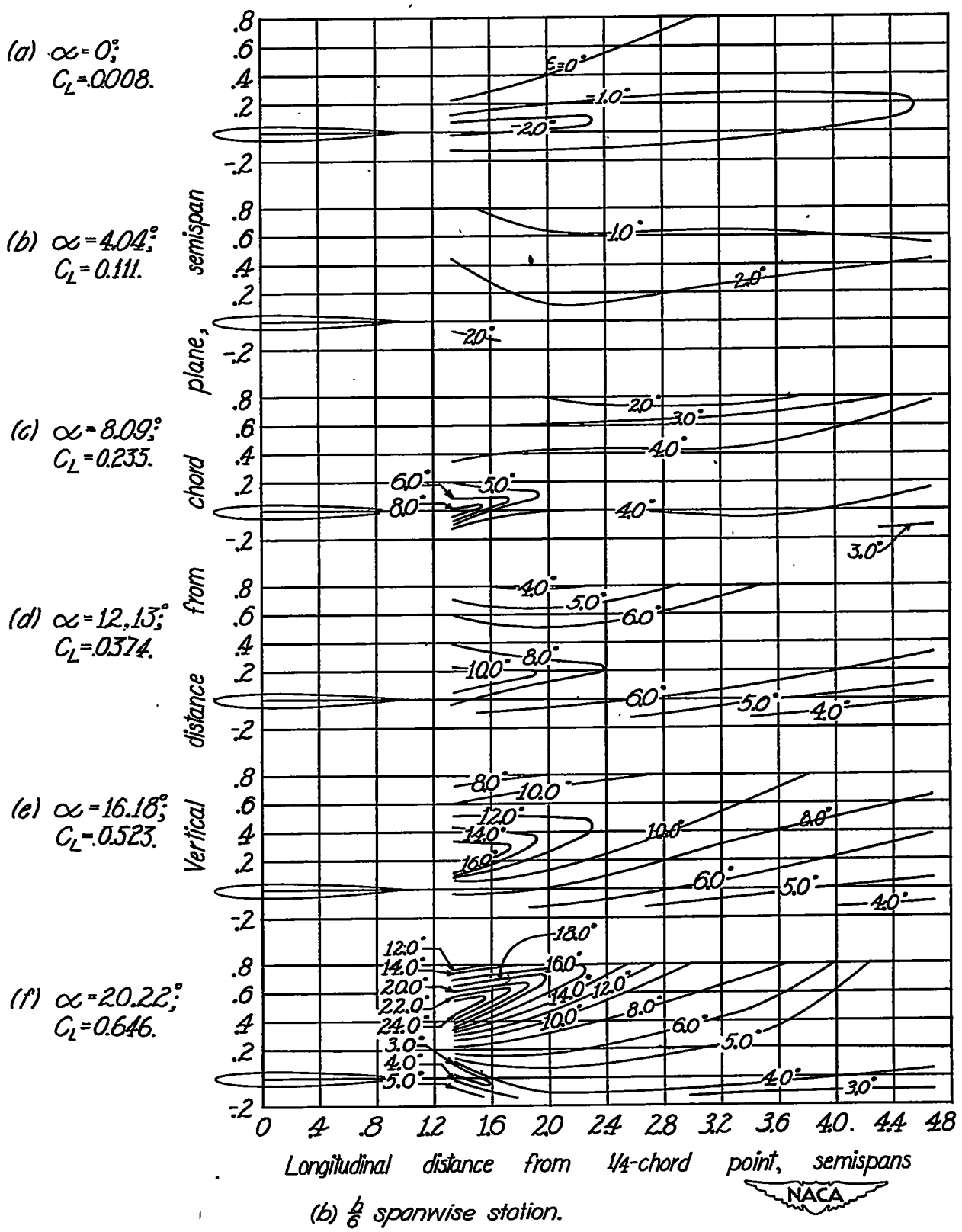

(b) $\frac{b}{6}$ spanwise station.

Figure 38.-Continued.

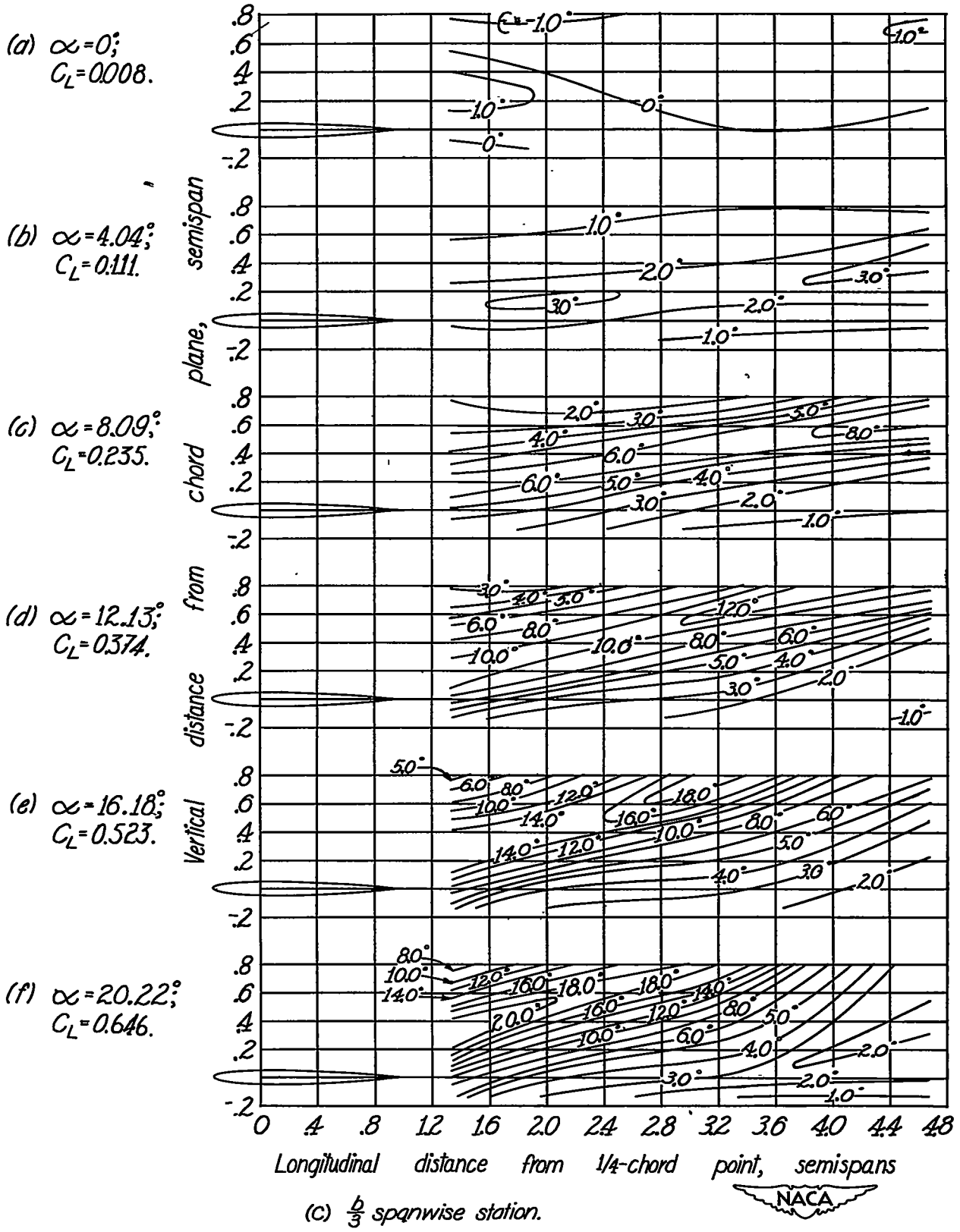

(c) $\frac{b}{3}$ spanwise station.

Figure 38.-Continued.

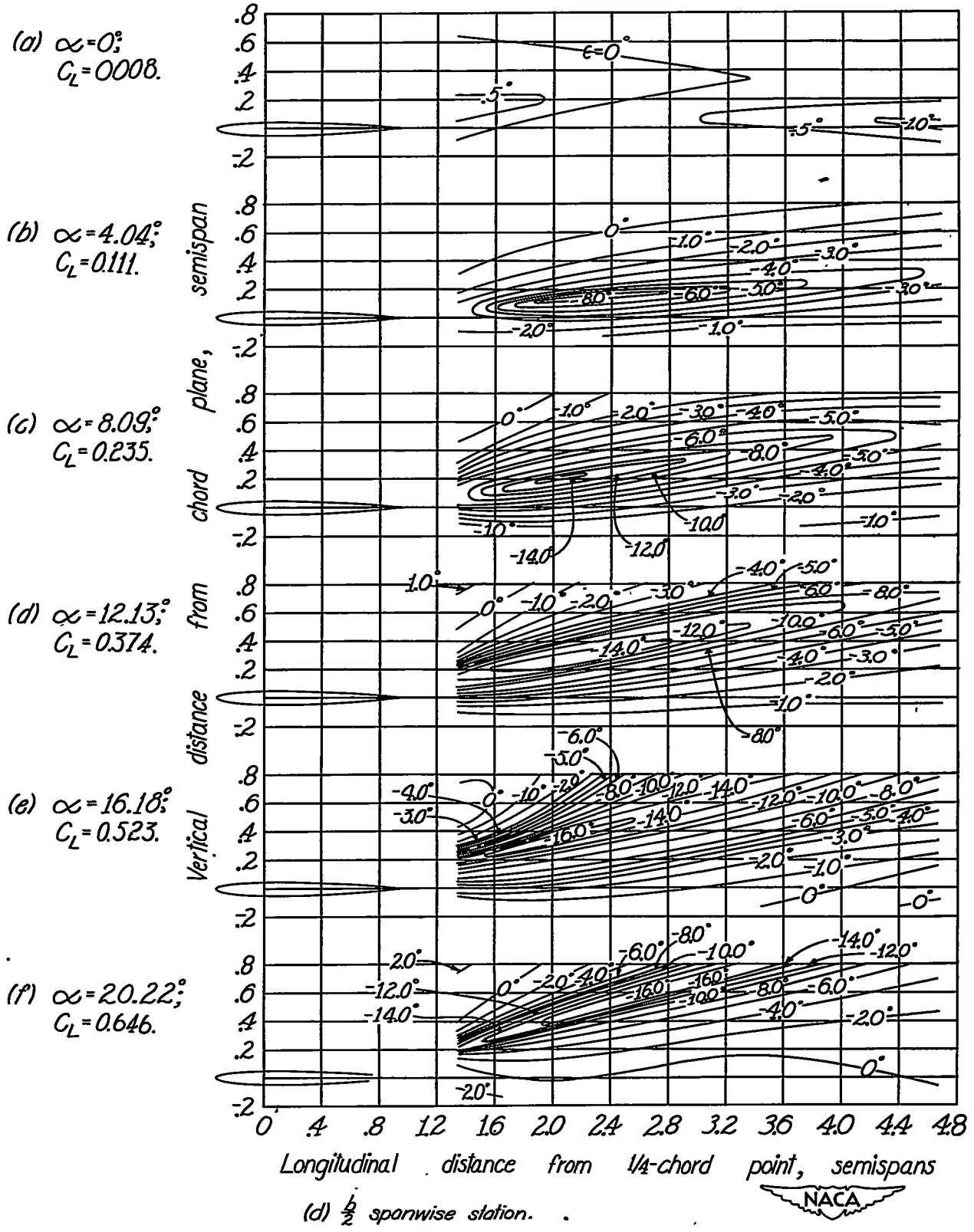

(d) $\frac{b}{2}$ spanwise station.

Figure 38.–Continued.

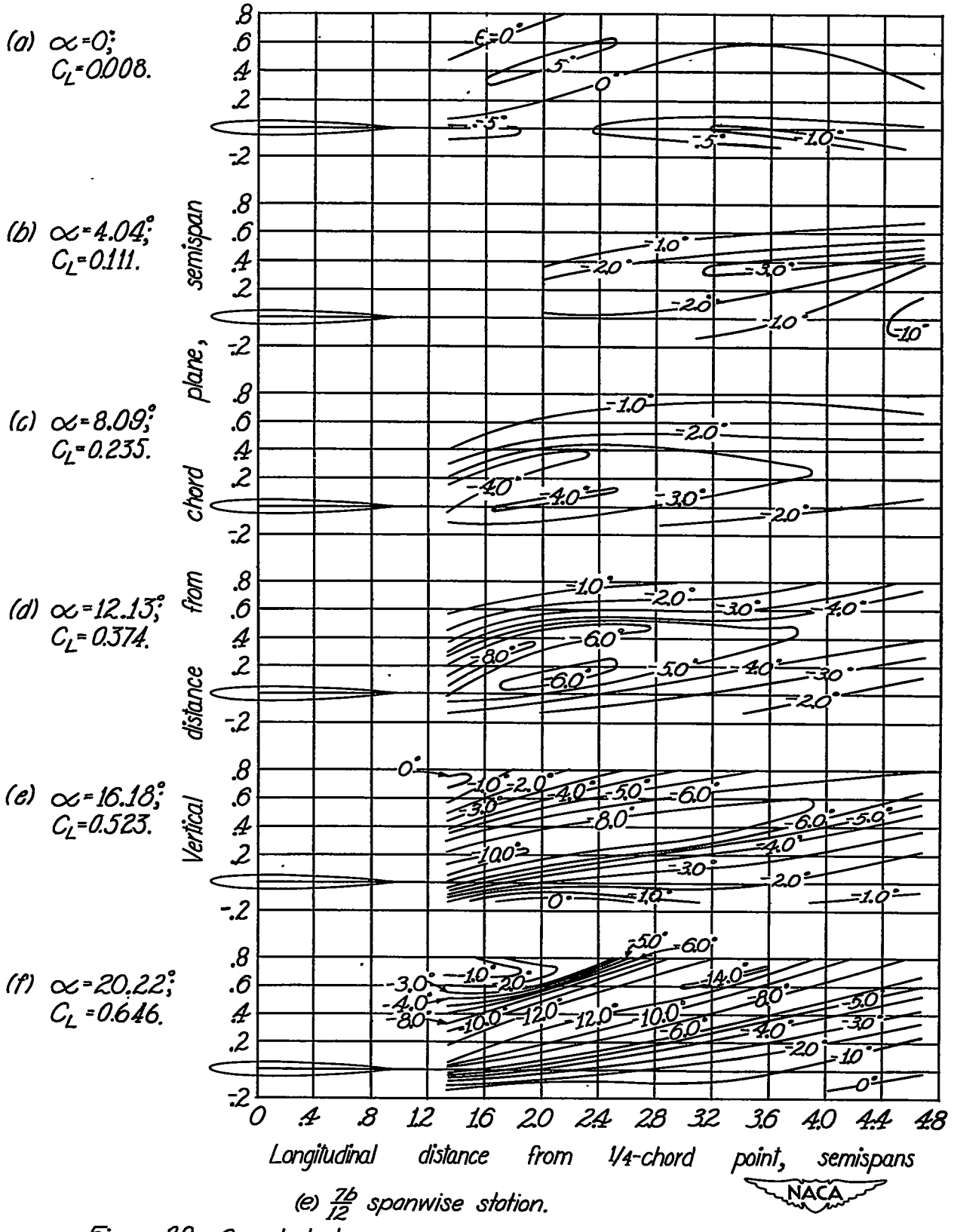

(e) $\frac{7b}{12}$ spanwise station.

Figure 38.- Concluded.

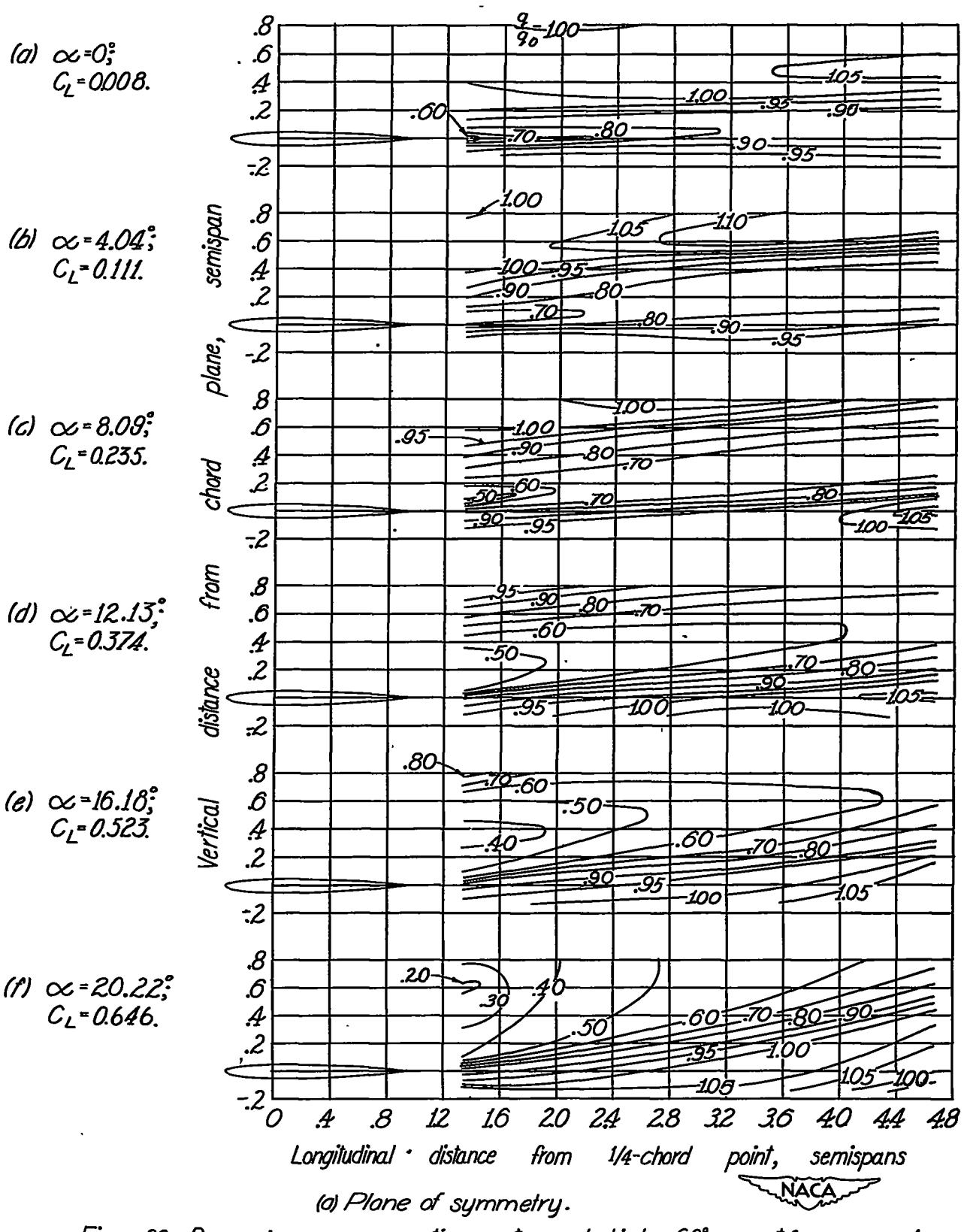

(a) Plane of symmetry.

Figure 39.- Dynamic-pressure-ratio contours behind 60° swept-forward wing of 30-inch span. A=1.5.

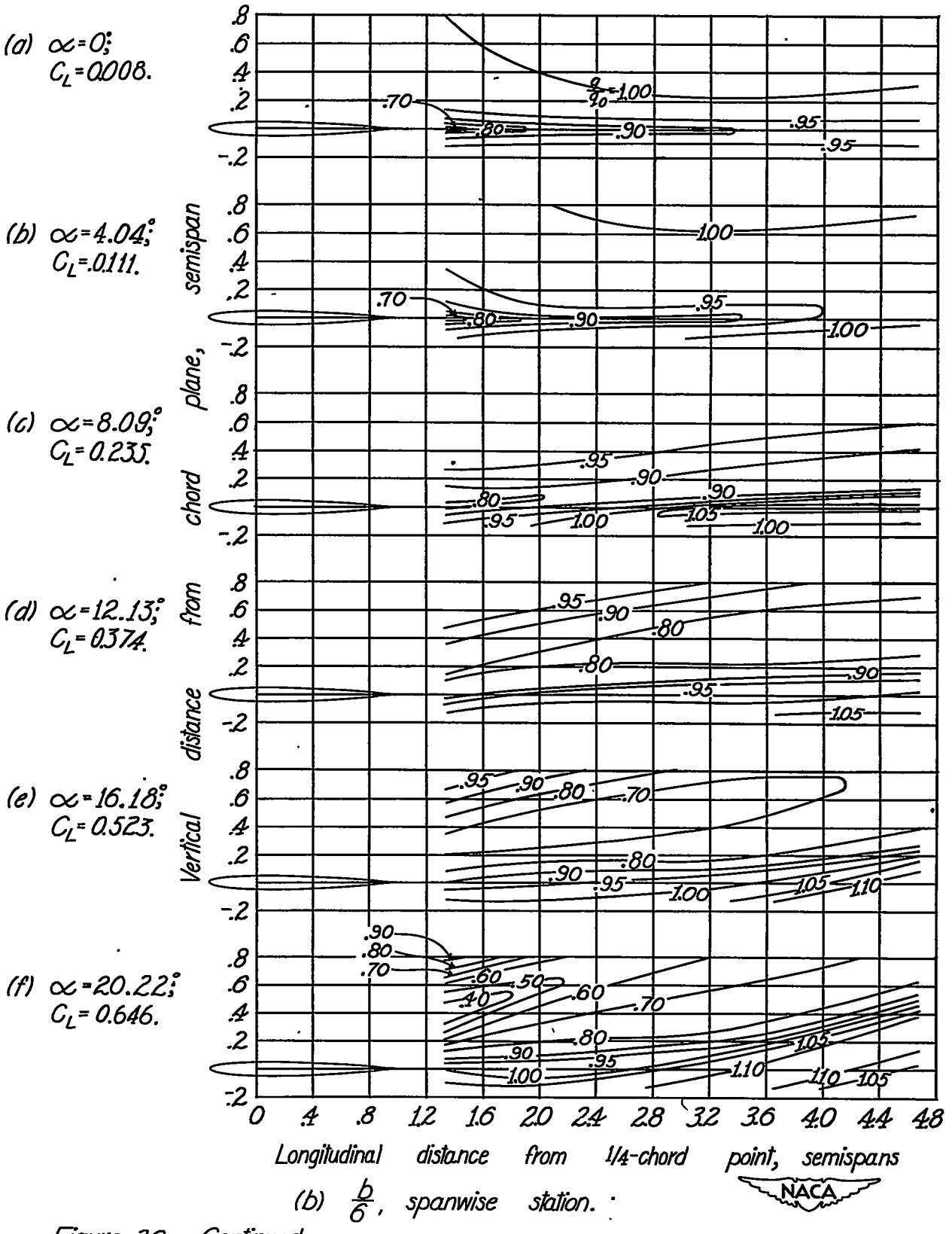

Figure 39.—Continued.

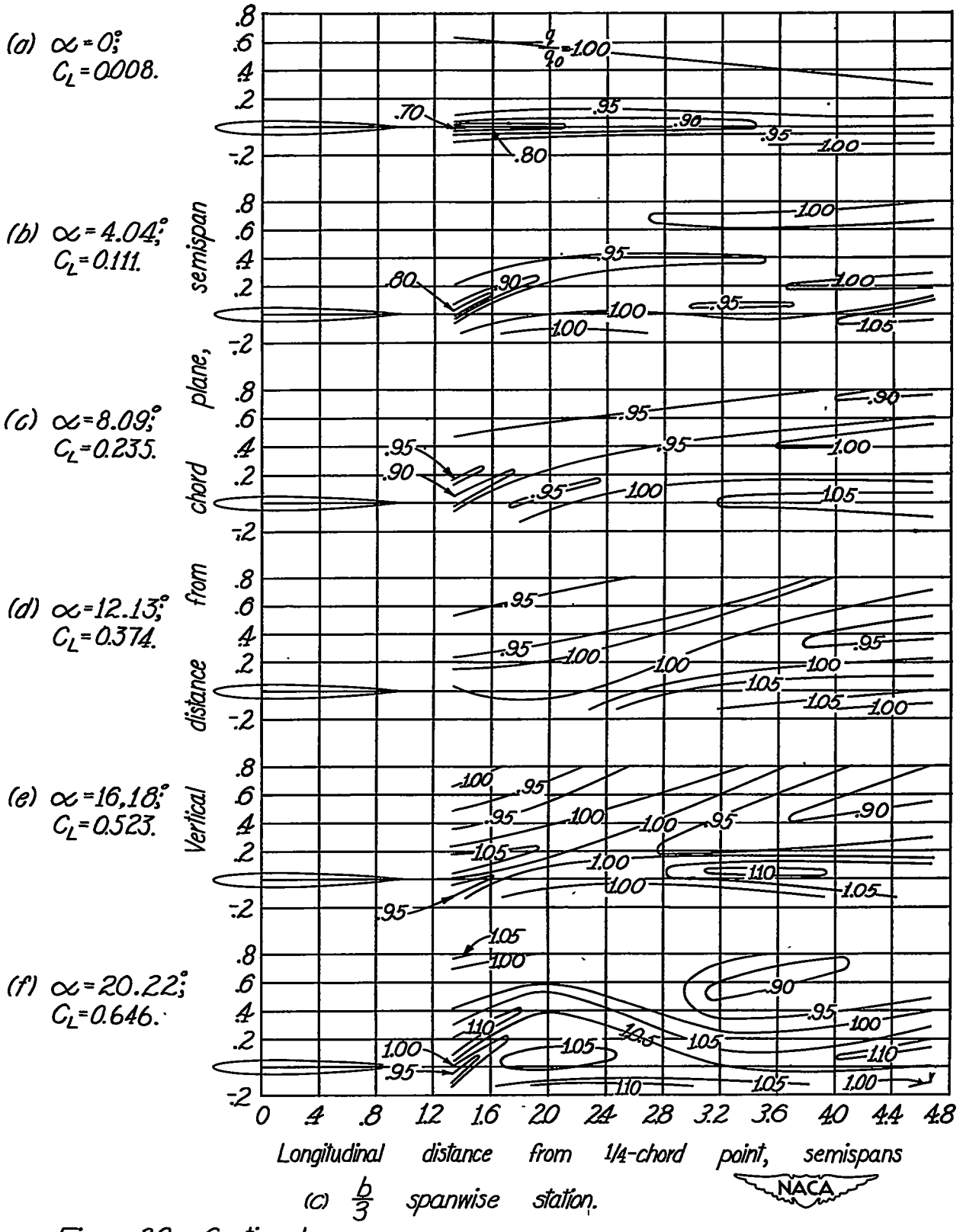

Figure 39.-Continued.

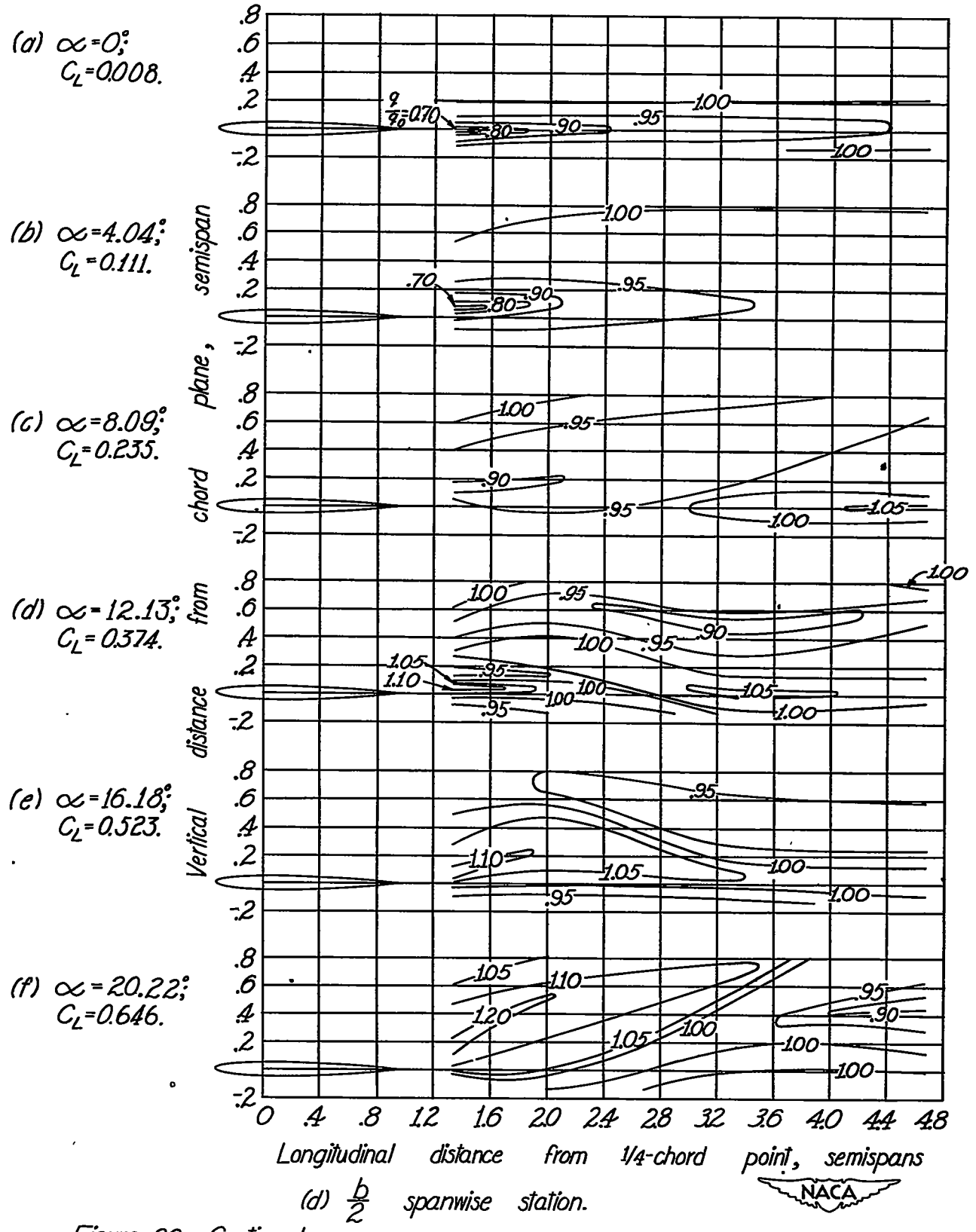

(d) $\frac{b}{2}$ spanwise station.

Figure 39.-Continued.

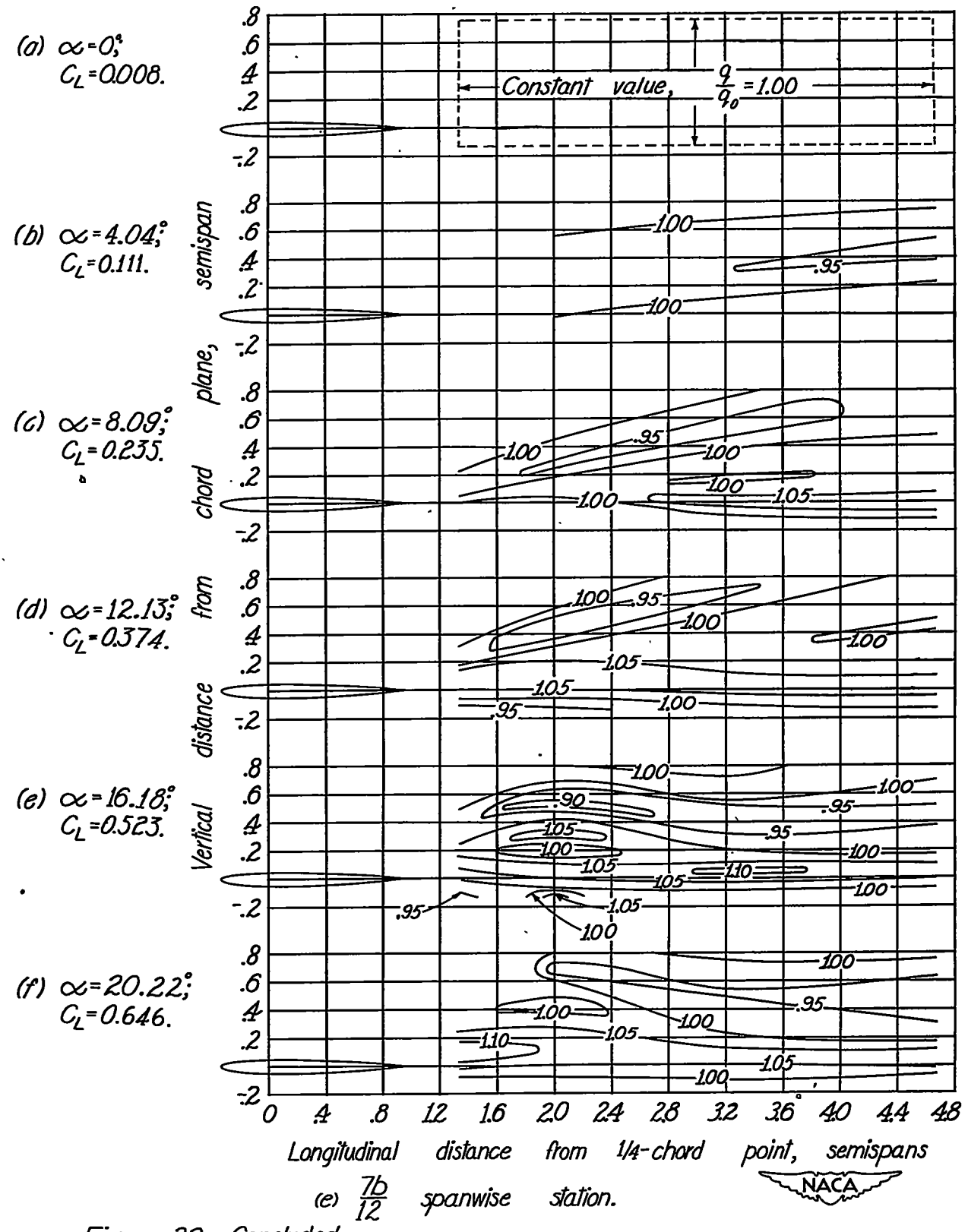

Figure 39.–Concluded.

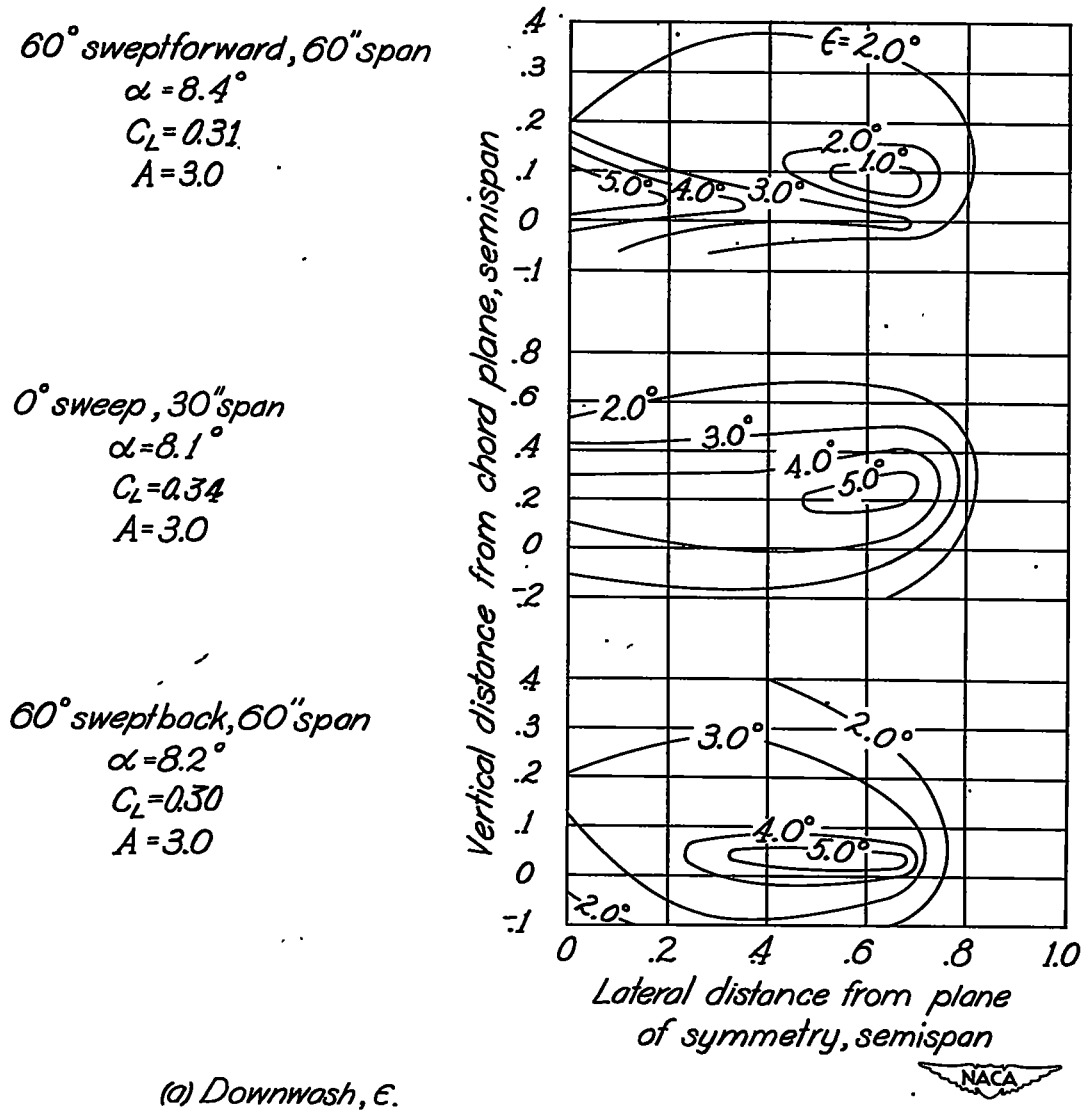

(a) Downwash, ε.

Figure 40.-Effect of sweep on the spanwise distribution of downwash and dynamic-pressure ratio behind wings of the same aspect ratio. Tail length, 1.0 semispan for 60-inch-span wings and 2.0 semispans for the 30-inch-span wings.

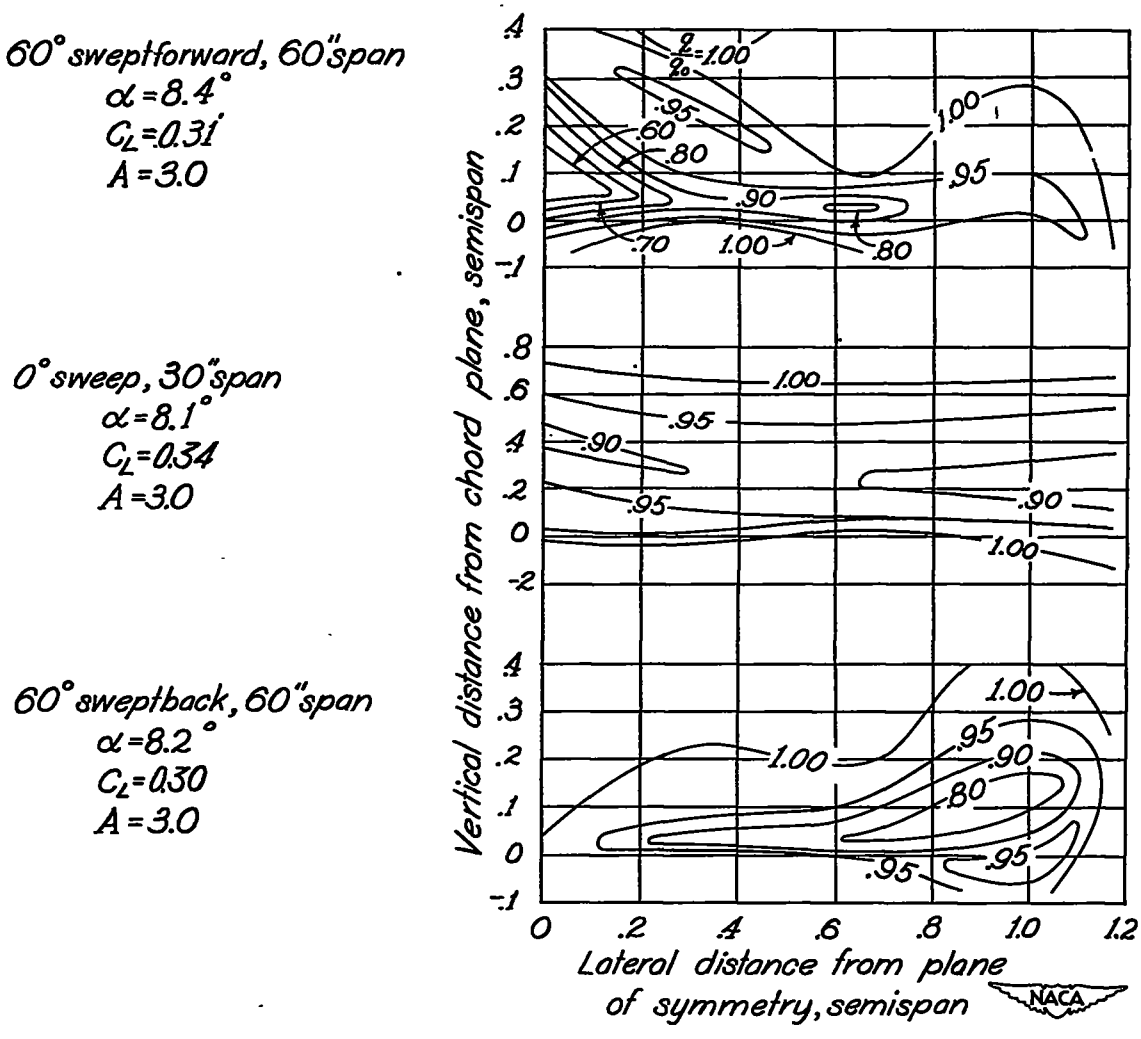

(b) Dynamic-pressure ratio, q/q_0.

Figure 40.- Concluded.

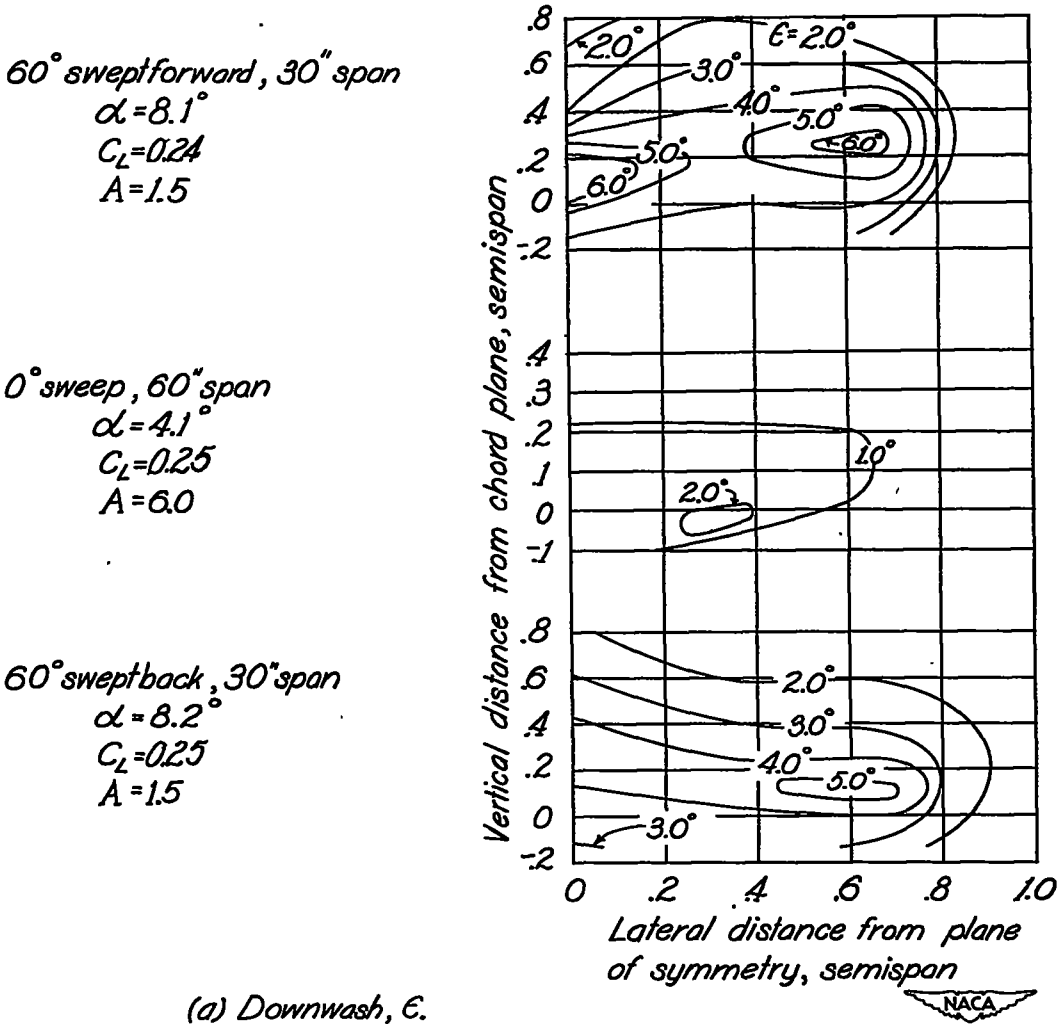

(a) Downwash, ε.

Figure 41.-Effect of sweep on the spanwise distribution of downwash and dynamic-pressure ratio behind wings of the same basic panel. Tail length, 1.0 semispan for 60-inch-span wings and 2.0 semispans for 30-inch-span wings.

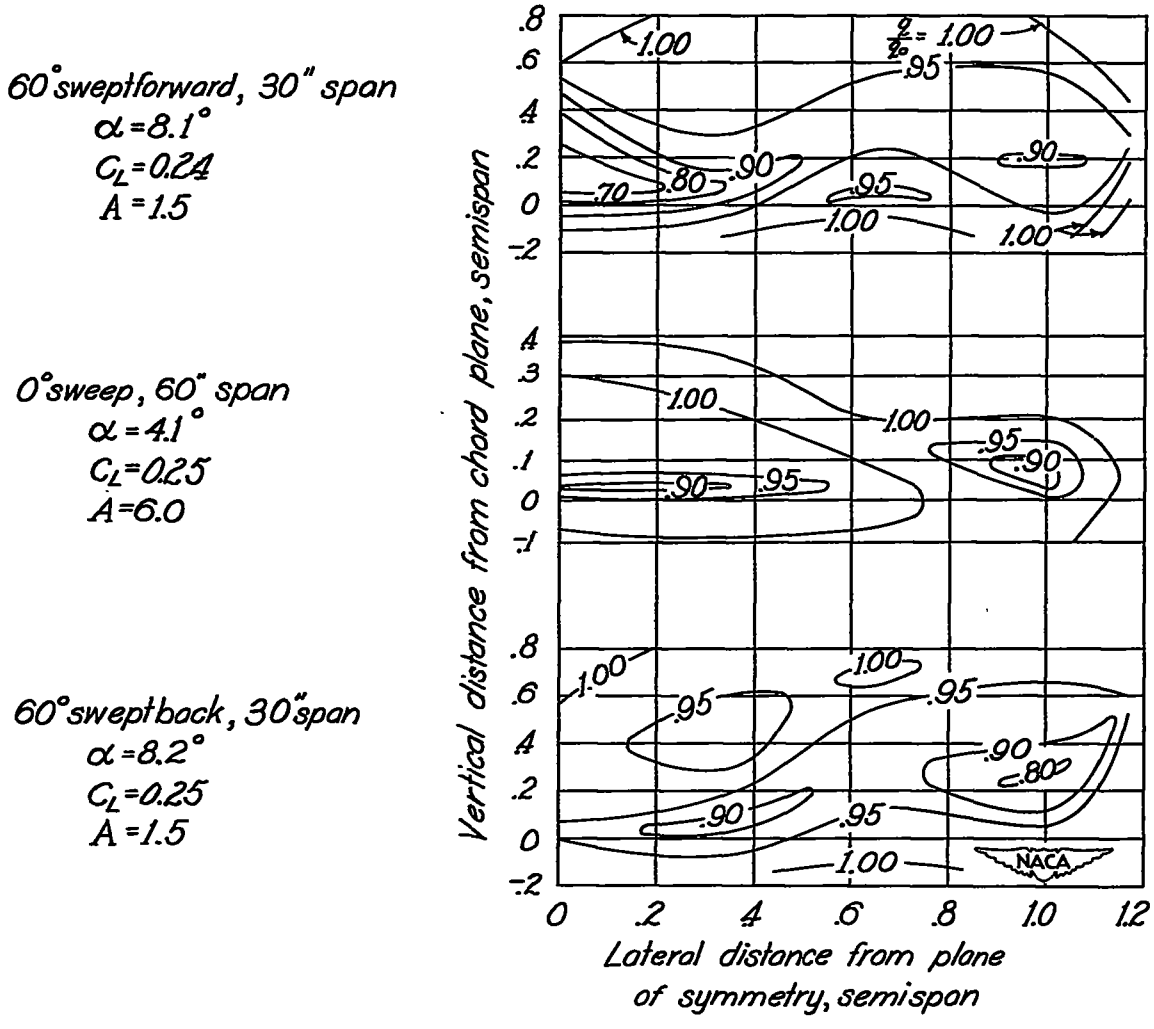

(b) Dynamic-pressure ratio, q/q_0.

Figure 41.- Concluded.

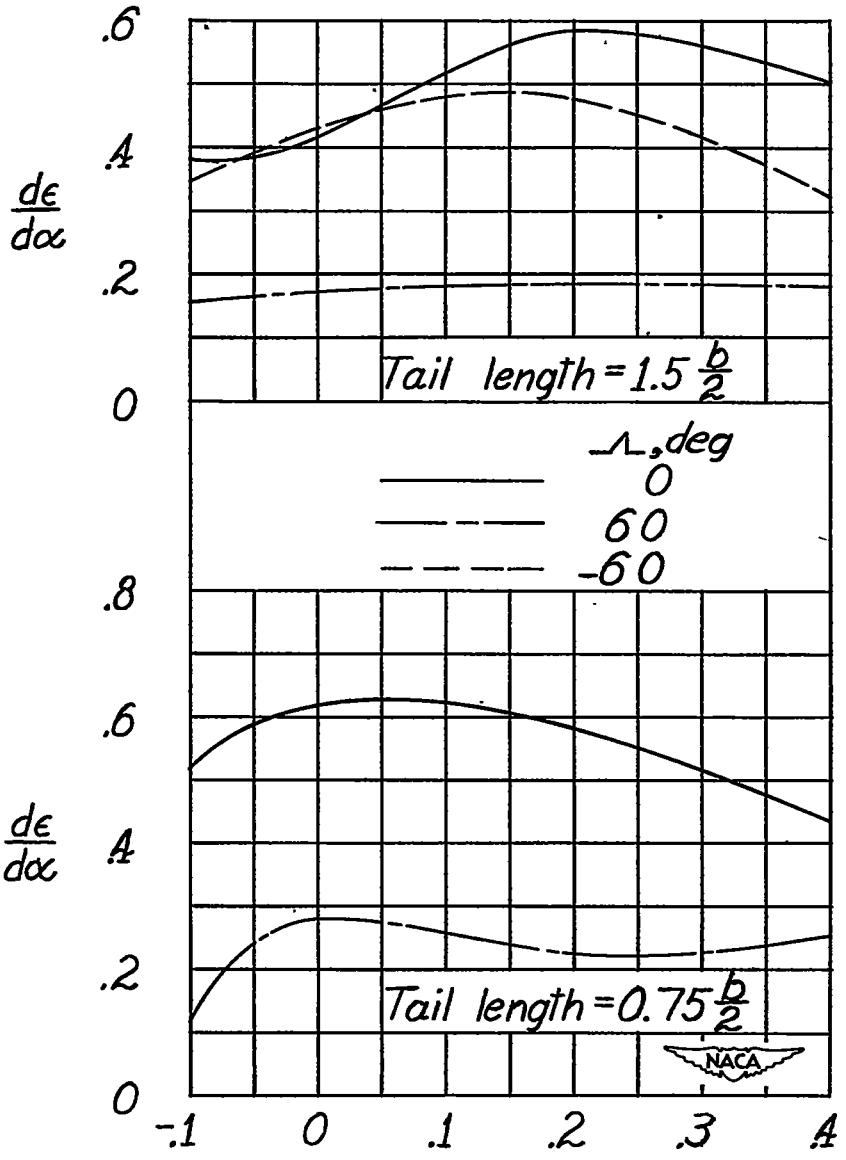

(a) Plane of symmetry; $\alpha \approx 8°$.

Figure 42.–Effect of sweep and tail position on the variation of downwash with angle of attack for the different swept wings of aspect ratio 3.

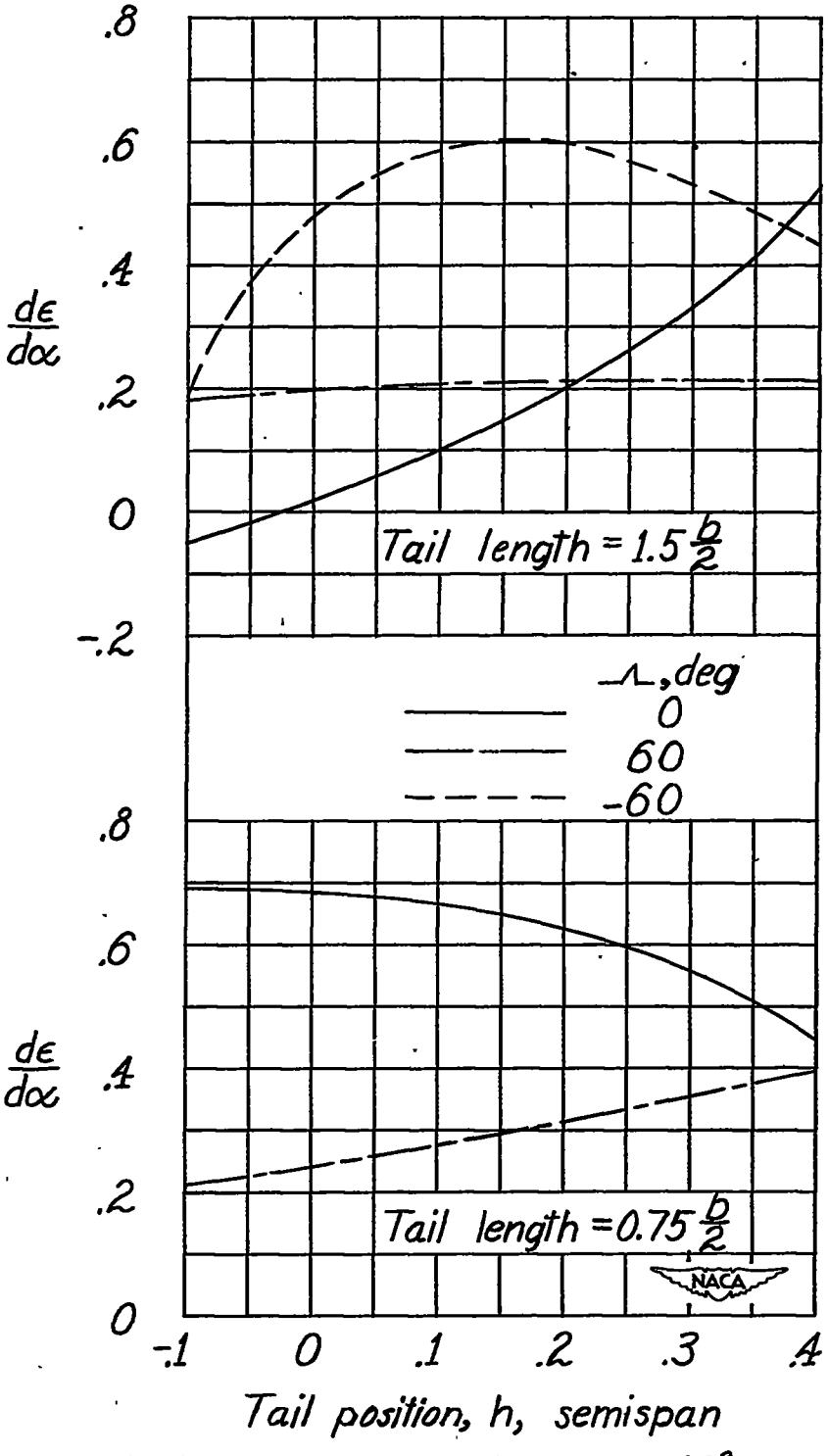

(b) Plane of symmetry; $\alpha \approx 16°$.

Figure 42.- Continued.

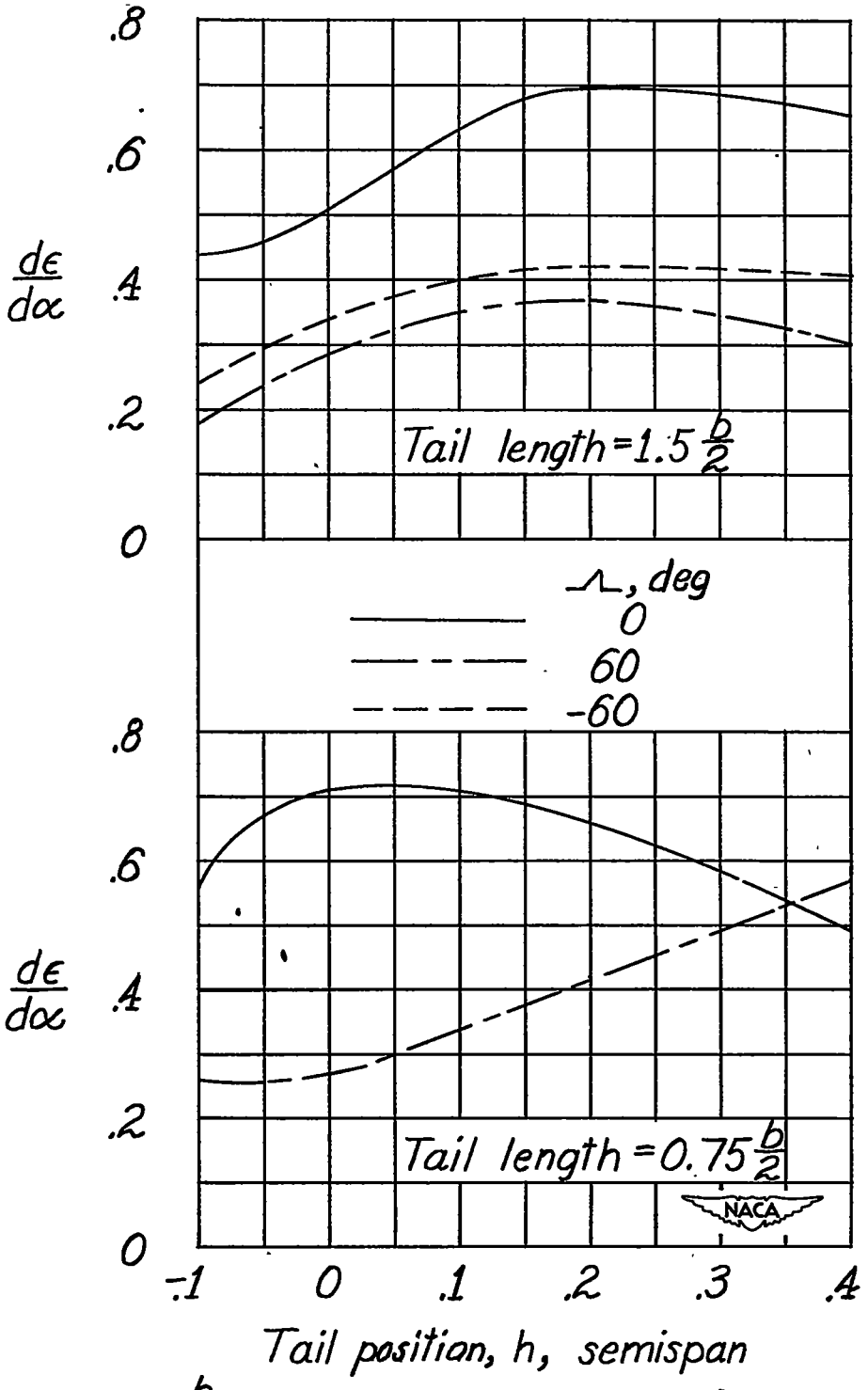

(c) $\frac{b}{6}$ spanwise plane; $\alpha \approx 8°$.

Figure 42.- Continued.

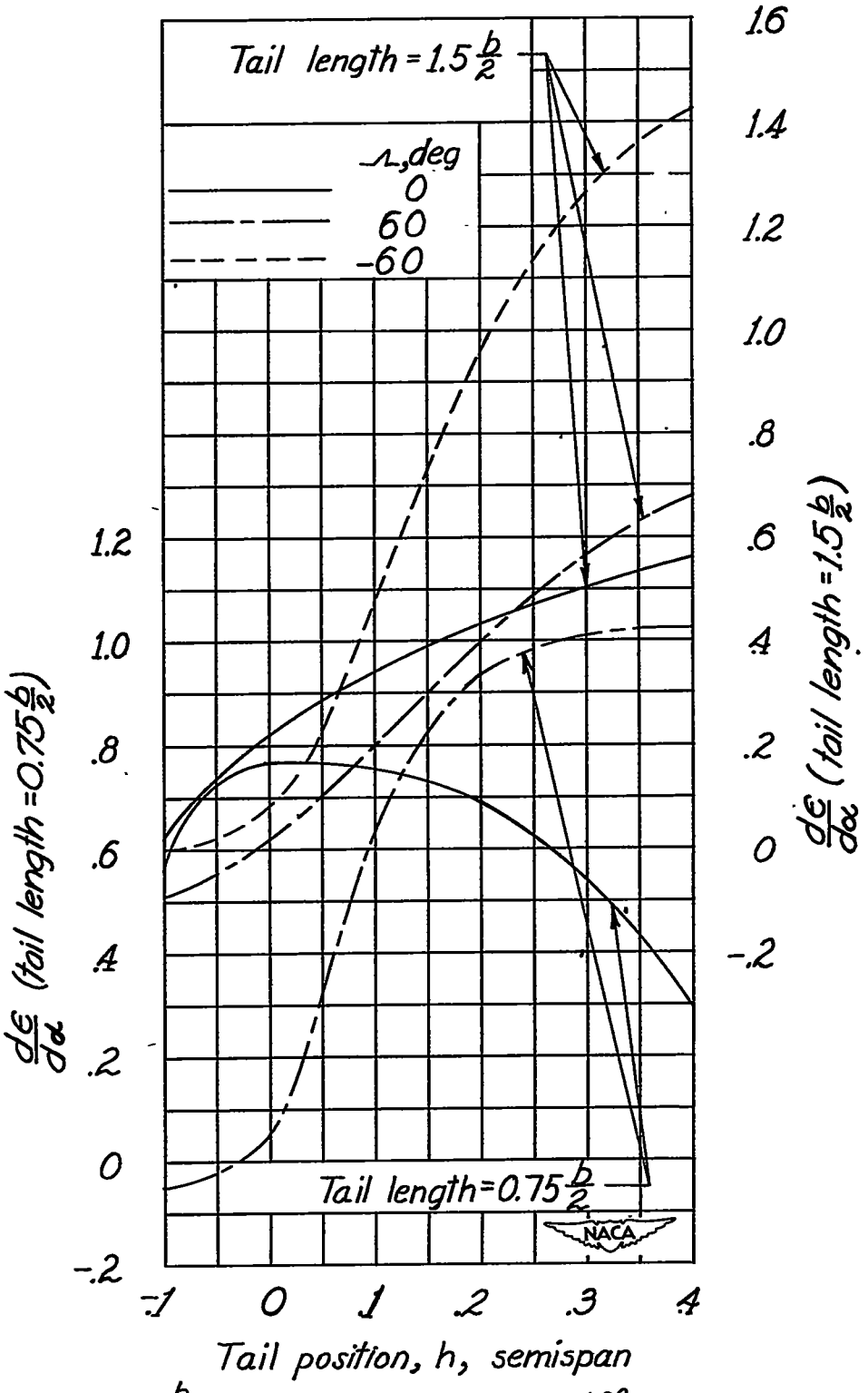

(d) $\frac{b}{6}$ spanwise plane; $\alpha \approx 16°$.

Figure 42.- Concluded.

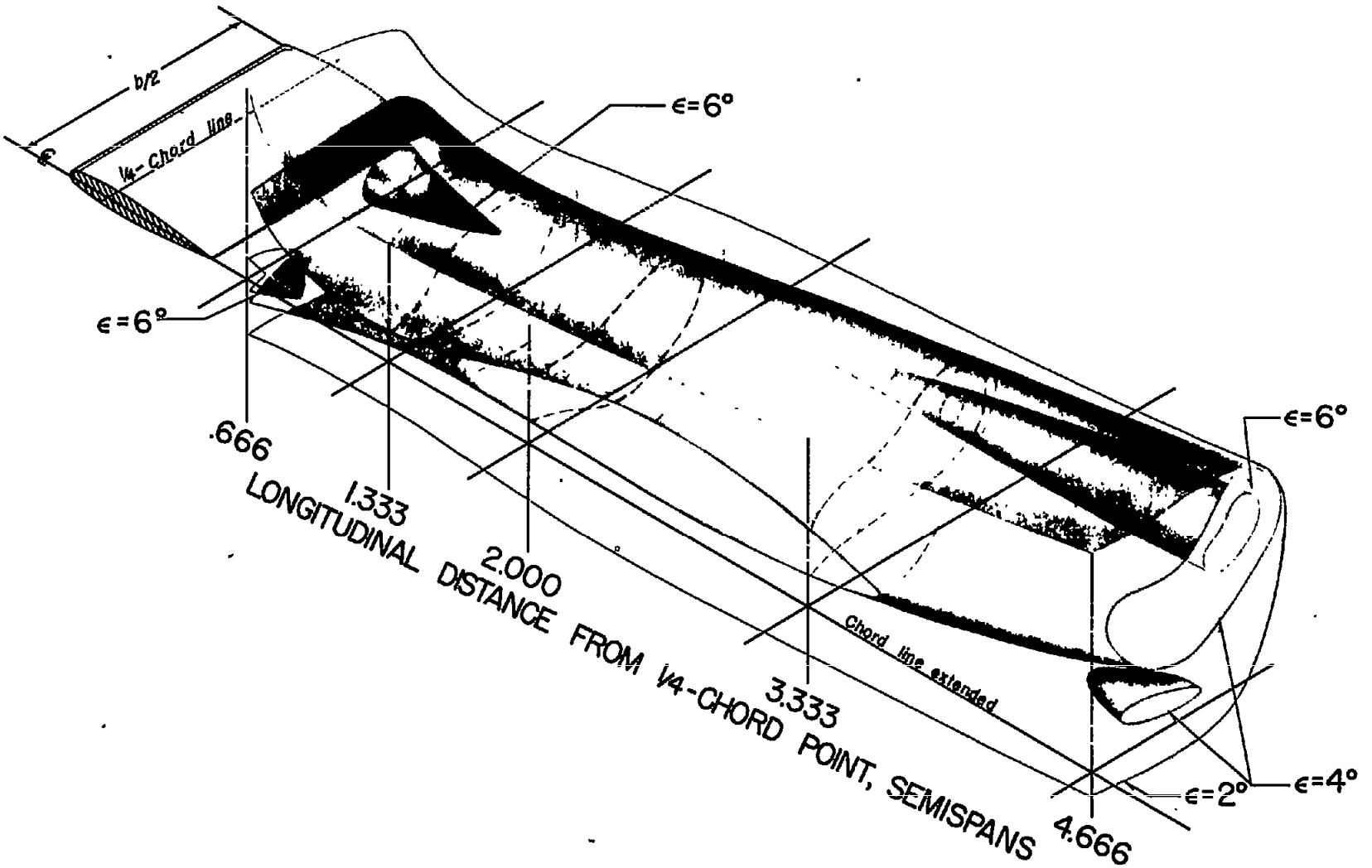

Figure 43.- Constant-downwash sheets behind 30-inch-span wing with 0° sweep. $\alpha = 8.07^{\circ}$; $C_L = 0.342$.

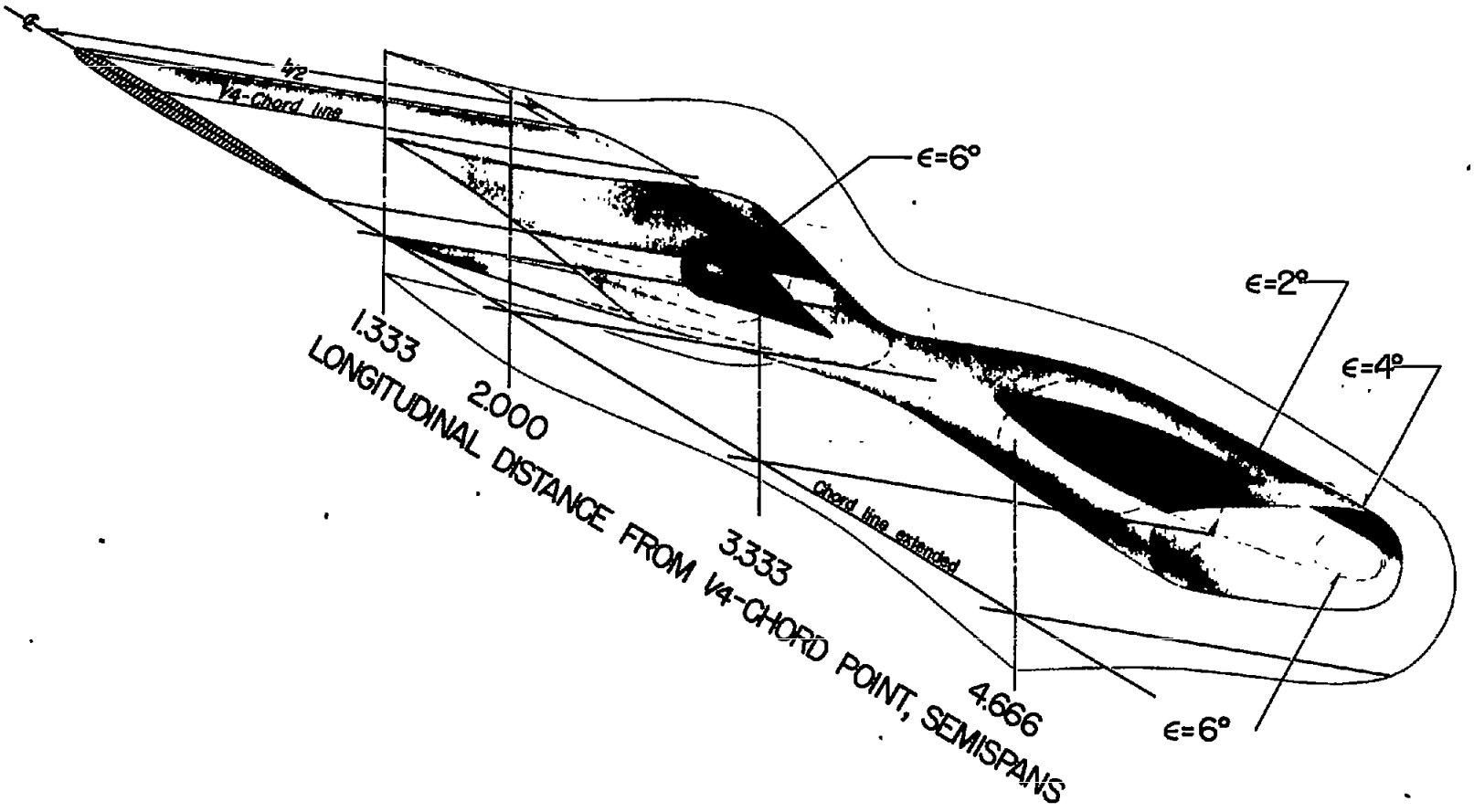

Figure 44.- Constant-downwash sheets behind 30-inch-span wing with 60° sweepback. $\alpha = 8.11^{\circ}$; $C_L = 0.251$.